# An investigation into the applicability of the Fourier transform to dispersive water waves and their short term prediction

James Ross Halliday

This thesis is submitted for the degree of Doctor of Philosophy to the University of Glasgow

Department of Electronics and Electrical Engineering

January 2007

## Abstract

After many years of slow but progressive development, the wave energy industry is on the cusp of breaking through the economic and technical barriers to full scale deployment of wave energy electrical generating devices. As the major obstacles in device design are solved, and with several devices in the water, the scope for increasing their efficiency through advanced control techniques is now becoming clearer. In some cases, it would be advantageous to integrate an advanced prediction of wave behaviour (of some tens of seconds into the future) into these control methods. Past research on wave prediction has focused on utilising the Fourier theorem to deconstruct wave records and then make predictions ahead in space, with published results indicating promise. However, predicting ahead in time has so far not been achieved. This thesis takes the Fourier theorem method of prediction to its logical conclusion by exploring its limitations in predicting over both time and space. A discussion as to why these limits should exist, and possible future work into the solution of the wave prediction problem, are also presented.

A review of current devices under development, and the history and emergence of the wave generating industry (which is a comparatively recent technology and still in its infancy), are also included as appendices to the main thesis in order to put the work into context.

...that night, lying there, I experienced a sense of shame, which those who swear by civilisation will certainly fail to understand, that civilised man can be the worst vermin of the whole earth. For wherever he comes, he destroys the wonderful equipose of Nature, and much as he bothers himself in his so-called arts, he is not even capable of repairing the damage he causes ...

Andreas Reischek // Yesterdays in Maoriland

# Acknowledgements

I would like to thank my family and my long suffering wife for putting up with the lost days caused by the writing of this thesis. Hopefully they will once again be able to get my attention and possibly more than five minutes worth of conversation without the topics of wave energy and FFTs cropping up.

On a serious note, I would like to thank my family for their support over the past 21 years of schooling and for their encouragement in keeping going. I would also like to thank the University of Glasgow and the University of Canterbury for hosting me during this time and providing much needed support and time to discuss my ideas. The technical staff, in particular Stuart McLean for putting together the wave flume for us, deserve a special mention.

A big thank you is due to my supervisors in Scotland and in New Zealand. Dr Dorrell in Glasgow was very generous in making the study of this thesis possible and for trusting me to work away from the confines of the University. For the many discussions and input into my papers and especially for keeping my train of thought on track to be focused on one single problem rather than trying to solve everything at once.

Dr Wood in Christchurch is deserving of a big thank you for making it possible to spend a fruitful time in the company of lateral thinking Kiwis and for allowing me to enjoy one of the most incredibly beautiful and determined countries in the world. The time in New Zealand taught me that literally nothing is impossible and hopefully I've managed to bring back with me some of the Kiwi attitude to life.

Thanks are also due to the EPSRC for funding this work and making the last three years possible. An additional special mention must be made to the wave energy group at the University of Edinburgh and especially Jamie Taylor for fielding all manner of wild and wonderful suggestions.

And, before I forget, thanks to Bella and Whisky, despite making a mess of the living room and eating most of the wallpaper, you've cheered me up no end.

# Contents

# List of Tables

# List of Figures

# Chapter 1

# Introduction

The development of new renewable energy generating devices has been gaining momentum over the last two decades. Wind energy generation has grown at an increasing rate through Europe and it is now a maturing industry with several standard turbine manufacturers, using a few set arrangements (such as the doubly-fed induction generator connected to the turbine via a gearbox, or a fixed-speed grid-connected cage-rotor induction generator also connected via a gearbox), dominating the market. Attention is now turning to marine energy generation via sea-wave or tidal energy. However, this industry is several decades behind the wind energy industry in terms of development.

Serious development of wave energy devices began in the mid 70s with Prof. Salter's Ducks. At this time there was a crisis in the Middle East and the cost of oil had soared. The western coasts of Europe receive some of the greatest concentrations of wave energy in the world, this is largely due to the predominantly Westerly travel of storms coming from the Atlantic. Prof. Salter's device aimed to capture this energy. Over the next ten years there was interest in wave energy from many countries and a variety of devices emerged to various stages of development. Unfortunately in the 80s, as oil prices came down and nuclear power proliferated, funding to development programmes was cut. For the next 10 year period few developments went ahead, with the exception of some academic work and a few demonstration installations. In the mid 90s public interest in renewable energy and a new found understanding of human impact on the environment led to the reinstatement of some funding for device developers. This has had an almost exponential effect on the number of devices currently being developed, these are document in Appendix B.

With the high number of devices under development various governments and the European Union have tried to bind together knowledge by publishing reports on common areas

where collaborative research would benefit the industry as a whole. This thesis is concerned with one element of this mixed research, namely the short-term prediction of sea waves.

This introductory chapter is split into three sections dealing with the origin of the problem tackled in this thesis, past studies in this area and the structure of the following report.

## 1.1 Problem genesis

The principles of energy extraction from sea waves come from the three basic motions: pitch, surge and heave. If a buoy is placed in the water pitching describes a rotation about its central point; surging is the movement of this point in a horizontal plane and heaving is the motion in a vertical plane. Several methods, peculiar to each device, exist to extract energy from each of these motions, these are detailed more fully in Appendices A and B.

For extraction of energy to take place it is common to couple a power take off (PTO) to one or more of these three motions. The PTOs on most devices are capable of being adjusted to achieve a maximum power extraction. A simple example is that of two platforms hinged by a hydraulic pump. As a wave passes, the two platform hinge will open and close causing the fluid in the pump to be moved. In a passive setup, as is used at present, the complex impedance of the joint is set to an average value and whatever shape and amplitude of wave that arrives will work against this. If you were able to vary the complex impedance on a wave by wave basis it would be possible to extract more energy from each wave increasing the output of the device. For this to work a short-term prediction of wave amplitude and shape is required.

This principle was recognised in a recent report from the European Wave Energy Thematic Network, published in March 2003 [1]. It examined in detail the progress being made in wave and tidal devices and found that a strand of potential research common to all devices was the requirement of a short term prediction of wave elevation at the device interface, as discussed above.

At the present time several devices have made it from the drawing board to full scale testing (see Appendix B). Much of the current testing of devices has been in ensuring the survival of these devices and the verification that their power take off (PTO) systems are capable of generating electricity to the grid.

The next step, as recognised by the EWEN report and device developers, is for the development of PTOs to reach maximum economic extraction levels in a variety of sea states. To this end the prediction of wave behaviour may assist in allowing the complex

impedance of devices PTOs to be set on a wave by wave basis. For this to take place a method for the short term prediction of wave behaviour that is cost effective needs to be developed.

## 1.2 Previous studies

The study of short term wave prediction has not been widely reported in the scientific literature. In the field of offshore engineering, where this topic would naturally lie, interest has been mainly in predicting the probable occurrence of extreme wave events. This type of prediction is important to the oil, gas and shipping industries as it ultimately governs the cost of large civil projects, e.g. oil rigs and new shipping vessels. This information is, however, of interest to wave device developers in ensuring device survival, but not in the precise control of PTOs.

The studies that concern the short term prediction of waves have focused largely on predicting forces at a distance from the recorder rather than directly making a prediction of surface elevation. The following papers are representative of current research.

### 1.2.1 Naito and Nakamura

This Japanese study [2] involved a wave tank with a simple wave device model. The wave amplitude was measured at a small distance away from the device and at the device itself. This measured data was then used to create a transfer function for the device and for the propagation of the waves by using a Fourier decomposition and imposing causality. The results presented for the extracted power of the device show good correlation to the incident wave field. However, there is little data on the experimental equipment (i.e., the tank dimensions) and the possible limits to their method are absent.

### 1.2.2 Belmont

Belmont has, over several years, studied the short term prediction problem [3]. He has claimed that predictions up to 30 sec ahead in time are possible. The prediction model he puts forward is based on the Fast Fourier Transform (FFT) of wave records taken either at a fixed point or over a fixed time.

The claim made for a prediction 30 sec ahead may be debatable as it makes use of the FFT method (the prediction in time using this method is proved later in this thesis not to

be very accurate). The wave model and prediction method also places very strict limits on the type of wave-field that can be predicted, namely a very narrow swell spectrum with little to no local sea state. Personal communication with various specialists in this area indicate that, in Scottish waters, this situation will rarely occur.

The conclusions of the research also point to the use of a fixed time prediction being more accurate than fixed point. A fixed point measurement is that taken from a wave buoy. A fixed time measurement is a sampled wave elevation taken over a stretch of ocean surface. The fixed point method requires specialised measurement equipment which brings its own technical difficulties (non-uniform sampling and wave shadowing). The equipment proposed by Belmont must be sited at approximately twice the height of the highest wave crest above the sea surface. This may be a reasonable proposition for an on-shore device but in the offshore environment it would be prohibitively expensive.

### 1.2.3 Skourup and Sterndorff

This second order model [4] was developed in Denmark with a view to improving the description of wave kinematics at crests when considering loading forces on offshore structures. The model was developed by splitting the complex time series into superposed first and second order series. The second order series were presented as the sub and super harmonics of the first order series. An FFT was initially taken to provide estimates for the first order components. The second order series were then derived from this step and the reconstruction compared to the original. If the match was not sufficiently accurate then the iteration process continued.

Numerical comparisons for second order Stokes waves showed good correlation. In real water the model was tested at a scale of 1:10 with a maximum wave amplitude of 2 m over a range of regular waves covering one full spectrum. The prediction was made over a distance of 15 m with no prediction ahead in time. Additional tank testing of this method was undertaken by the Pelamis device team [5], who achieved prediction results to 70 m with good results.

### 1.2.4 Voronovich, Holmes and Thomas

A preliminary study of wave prediction [6] was undertaken at the University of Cork which was based on the linear decomposition of wave elevation time series using the Fourier method. The Fourier coefficients in the series were then used with standard linear wave equations

(Chapter 2) to propagate the wave field to a distant point. The spectrum used in generating the wave-fields is relatively sparse, containing between 3 and 5 frequencies. The prediction distance was 12 m without a prediction over time and returned promising results.

### 1.2.5 Sulisz and Paprota

This is a recent study investigating the propagation and evolution of linear and non-linear wave packets [7]. The explanatory figures in the study report are ambiguous; however, it can be assumed that the FFT of the time series from the first wave sensor was used to provide initial conditions for a boundary value problem which was then solved for other sensors placed at more distant locations. The maximum prediction distance was 8 m. An element of prediction-over-time was suggested in the text but this was not followed in the report.

### 1.2.6 Zhang

Zhang's work is the most extensive study found in the literature review. His first study [8] repeated the technique of iteratively decoupling the higher order wave interactions from the first order free waves. The method utilised two decomposition methods, applying one where the frequencies of the wave vectors under consideration were close together, and an alternative method when they were further apart. Again, the foundation of the method was the FFT of a measured time series. Laboratory comparisons [9] showed good results for both linear and non-linear wave-fields to a distance of 8 m.

In his second study [10], Zhang extended the technique and applied his methodology to directional seas. By using three point measurements (i.e. acceleration, pitch and roll angles from a wave buoy) a directional spectrum can be fitted (Chapter 4) and the first order wave vectors can be calculated. Zhang's iterative procedure was then used to fit the second-order effects. Laboratory test results [11] yielded satisfactory predictions to a distance of 22 m. Real sea testing was conducted using pressure sensors on an offshore oil platform where predictions to 59.4 m were achieved.

### 1.2.7 Discussion

All of the above studies have shown good prediction results in comparison to numerical and laboratory testing. However, none of these studies indicated the limitations of the methodologies proposed. At this point the question arises as to where the predictions diverge from the true values. A second important issue is why these studies do not deal with the

prediction in time. A third point to note is that all of these studies have used fixed point measurements in their experiments, whereas the most appropriate method available to device developers is the wave buoy, which will move in the water.

In this thesis an exploration of the Fast Fourier Transform, when applied to a dispersive wave prediction, is proposed. The limitations of the method are found for both the time and distance cases and explanations are given based on the results obtained. Additional methodologies will also be proposed to enhance the predictions, and an examination of the possible measurement devices will be given.

## 1.3 Thesis structure

This thesis is split into the following chapters. The early chapters progress through the background information necessary to understand the implications of the wave prediction problem, before the experiments are introduced and discussed.

1. **Introduction** A brief review of the applicable literature is given here and the formulation of the problem presented in this thesis is described.

2. **Basic wave theory** This introductory chapter outlines simple wave theory to allow for the development of further concepts.

3. **Wave generation, spectra and simulation** This chapter describes the generation and mathematical representation of waves. The chapter concludes with an explanation of the modelling assumptions made and the equations used in time series generation.

4. **Measurement technology** An overview of the available measurement technologies, and a discussion concerning operational choices for offshore wave farms, is put forward in this chapter.

5. **Spectral analysis** This chapter gives a discussion of the spectral techniques used throughout this thesis.

6. **Experiments** A chronological discussion of the experiments, both computational and laboratory based, undertaken during this study, is developed in this chapter.

7. **Discussion** An examination of the results returned in the experimental chapter, which provides an explanation and discussion of their implications, is described here.

**8. Future work** This is a brief chapter presenting possible future research avenues.

**9. Conclusion** This chapter links together all the previous chapters, and reviews the work and draws conclusions.

**A. A brief history of the wave industry** An appendix is included here in order to place the wave industry into the context of modern energy studies and how it has advanced from the early stages of device design to almost the brink wave farm commissioning.

**B. Device design index** A comprehensive list of past and present device designs is included here as an appendix for completeness.

**C. Publications** Facsimiles of published works resulting from this study.

# Chapter 2

# Basic Wave Theory

This chapter aims to develop the basic theory of wave behaviour and to put forward some of the mathematical concepts utilised in other areas of this thesis. The majority of this chapter is derived from chapter 2 of [12] with additional information drawn from other sources ([13], [14] and [15]).

## 2.1 The basic wave equations

In this section a simple travelling wave is put forward and the dimensions for describing its structure and behaviour are given. After this, the Airy equations are presented and the justification for their use is discussed.

### 2.1.1 Intuitive definitions

A one dimensional sinusoid is the starting point for many wave theories and for sea wave prediction it is no different. A simple time-varying wave is:

$$\zeta(t) = a\sin(\omega t) \tag{2.1}$$

This describes a basic time-oscillating quantity such as the displacement of the ocean's surface from rest, $\zeta(t)$. The frequency of the wave $\omega$ is related to the time period $T = \frac{2\pi}{\omega}$, with the amplitude given by $a$.

This definition can be extended in the spatial $x$ dimension to produce a travelling wave by including, in the frequency term, the wave number $k = \frac{2\pi}{\lambda}$:

$$\zeta(x,t) = a\sin(kx - \omega t) \tag{2.2}$$

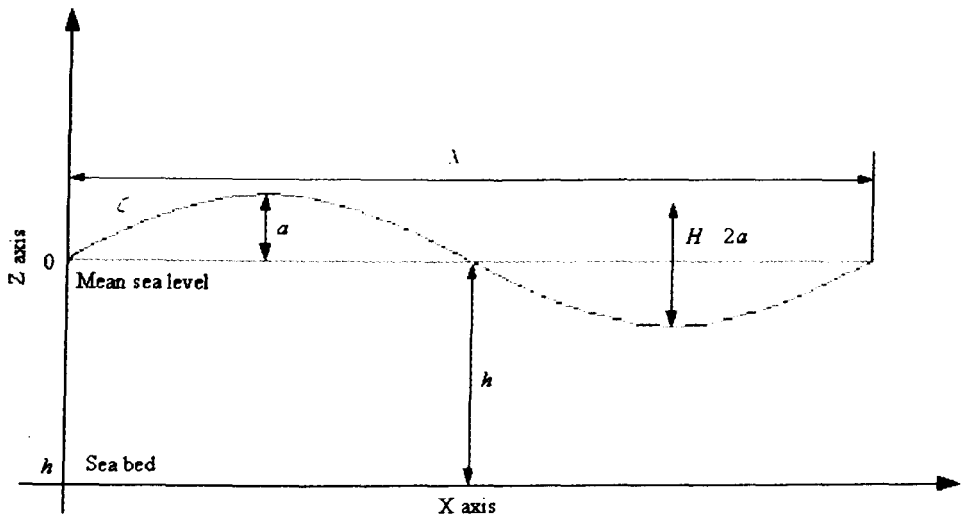


Figure 2.1: Showing the dimensions of a simple wave

where $\lambda$ is the wavelength. The inclusion of the wave number makes this a progressive wave travelling with a celerity (speed) of $c = \frac{\lambda}{T} = \frac{\omega}{k}$ in a positive $x$ direction. This type of waveform is common in electromagnetic and acoustic applications.

For electromagnetic waves the relationship between the frequency $\omega$ and wave number $k$ is a linear one

$$\omega = ck \tag{2.3}$$

where $c$ is the speed of light. A gravity wave on water is dispersive and has the relationship

$$\omega = \sqrt{gk} \tag{2.4}$$

where $g$ is the acceleration due to gravity. This equation is valid for a wave travelling over deep water. As a rough guide the depth of water is considered deep when $h > \frac{\lambda}{4}$, where $h$ is the depth of the water.

Due to its dispersive nature, as the frequency of the wave decreases, the wavelength and phase velocity increase so that lower frequency waves travel faster than higher frequency ones. This leads to the definition of a group velocity $c_g$ when considering a spread of wave frequencies. Since the phase velocity changes with individual wavelength, $c_g$ is not equal to any particular wave velocity $c_p$ in the group. As an example if two wave trains of slightly different wavelengths are superimposed to produce a beating wave then the envelope, which carries the energy, travels at the group velocity. Fig. 2.2 shows this for two waves of almost the same frequency, the arrows indicate the wave group progressing over distance. In deep water a rough guide to the group velocity is

$$c_g = c_p/2 \tag{2.5}$$

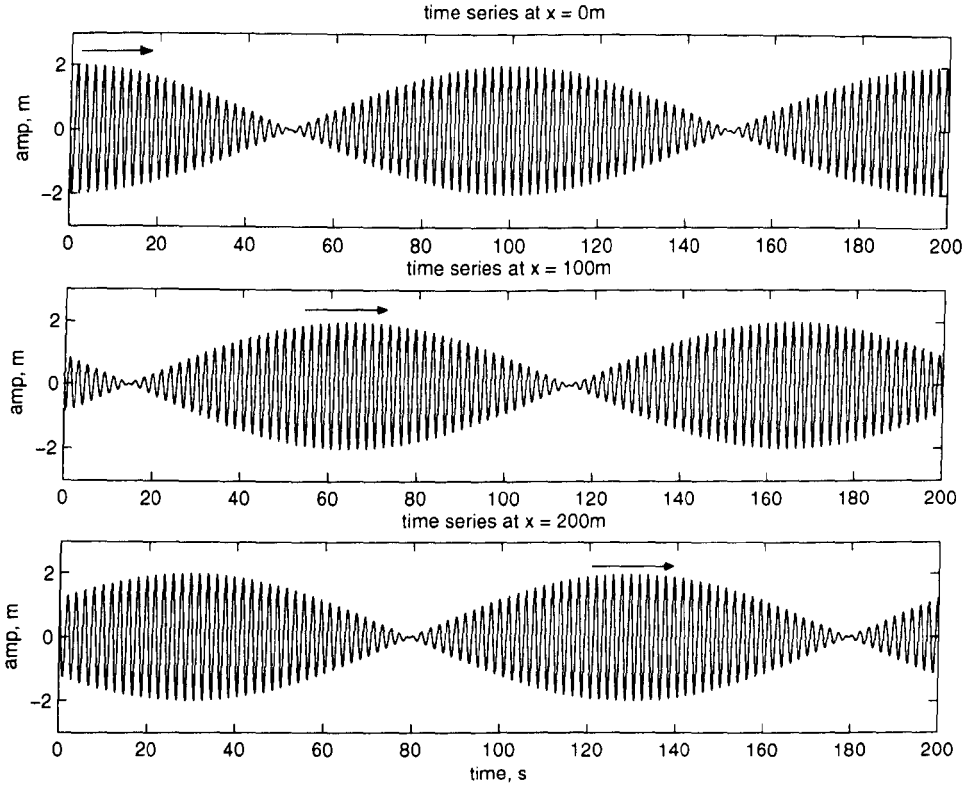


Figure 2.2: Group velocity of two superposed waves

In a mixed sea state where different frequencies are present at both the upper and lower ranges an average $c_g$ is derived from the statistical properties of the sea state.

Fig 2.1 shows the basic dimensions of a simple dispersive wave as already discussed. These are: the amplitude $a$ (the height from the mean sea level to the crest of the wave), the wavelength $\lambda$ (the distance between two successive peaks or troughs), the wave height $H$ (the height from the trough to the peak) and the depth $h$ (the distance from the seabed to the mean water surface). $\zeta$ is the surface elevation and a positive value of $k$ will cause the wave to progress from left to right along the positive x-axis with a velocity (celerity) of $c$.

So far the surface elevation only has been discussed. In many situations, the motion of the water particles below this level are of interest. The particles on the surface describe a circular orbit, as progress is made deeper into the water column ($z$ negatively increasing) the amplitude of these circular orbits decrease, this is shown in the left of Fig. 2.3. If the $x$ and $z$ displacements of a particle are $\chi$ and $\zeta$ from its rest position:

$$\chi = a\exp(kz)\cos(kx - \omega t - \phi) \tag{2.6}$$

$$\zeta = a\exp(kz)\sin(kx - \omega t - \phi) \tag{2.7}$$

where an additional phase term $\phi$ has been introduced.

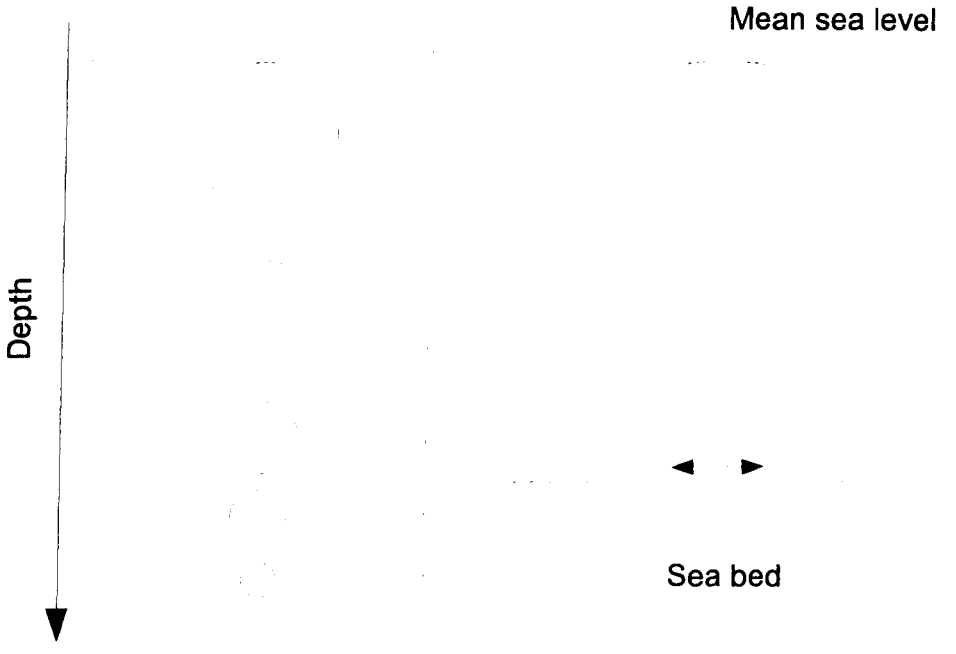


Figure 2.3: Particle orbits for deep and shallow water

The particles move forward in the wave crests and backward during the troughs. This motion decreases in amplitude below the waves until it reaches a point where the water becomes still. This effect is commonly experienced by divers who, upon entering a rough sea, will be pushed and pulled backwards and forwards until they have attained enough depth to be away from influence of the surface waves. Two further equations of use are: the velocity of the water particles round their circular orbit:

$$v_0 = \frac{2\pi a \exp(kz)}{T} \tag{2.8}$$

and the pressure fluctuation measured by a fixed sensor at a depth $z$:

$$p = \rho g a \exp(kz) \sin(kx - \omega t - \phi) \tag{2.9}$$

The values of the particle displacement, particle velocity and pressure decrease rapidly with depth. This result limits the extent to which bottom-mounted pressure sensors can be used to record wave behaviour. In particular, the resolution of these devices is affected by the depth of water in which they are placed.

It can be noted that with increasing wavelength and amplitude, the effect of a passing wave train will be experienced to a greater depth. An example of this would be the destruction of coral reefs during tropical storms. Normal sea conditions exert little force on coral reefs as wave amplitudes are usually small, but in storm conditions wavelengths are long and

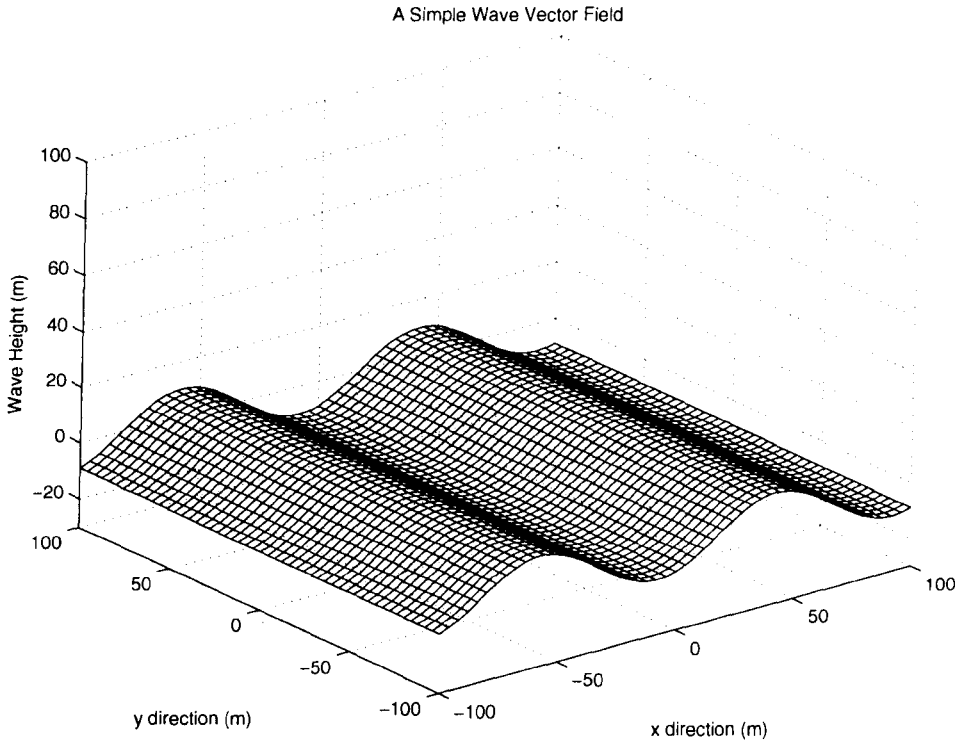


Figure 2.4: Simple long crested wave train

amplitudes are high so the energy present in the waves is great and they are able scour the coral from the sea bed.

The final modification to the simple wave equation is to vectorise the wave, i.e. include the direction of travel $\theta$ of a wave-train with respect to the x-axis so that

$$\zeta(x, y, t) = a \exp(kz) \sin(lx + my - \omega t - \phi) \tag{2.10}$$

where $l = k \cos\theta$ and $m = k \sin\theta$. An example of a long crested wave train with $\lambda = 100$ m and $\theta = 0^o$ is shown in Fig. 2.4.

### 2.1.2 Airy waves

So far the motion of a surface wave has been explained in terms of a travelling wave created by the circular motion of water particles. This is an oversimplification of the natural process. A fuller theory for describing the generation and propagation of ocean surface waves is complex and will not be given in its entirety here. However, the following is a summarised version of that appearing in Dean and Dalrymple [16] and will suffice in detail for the upcoming discussion.

### Equation formulation

In order to reach manageable solutions that can be easily worked with, certain assumptions about the fluid in which the waves are travelling must be made. First of all the fluid must be incompressible and since the density of sea water is relatively constant this property will hold true. This is known as the continuity of mass

$$\nabla \cdot \bar{u} = 0 \tag{2.11}$$

where $\bar{u}$ is a vector of the three dimensional particle velocity and $\nabla$ is the gradient operator. In terms of the velocity potential $\phi$

$$\nabla \cdot \nabla\phi = 0 \tag{2.12}$$

At all points throughout the fluid the velocity potential must satisfy the Laplace equation

$$\nabla^2\phi = \frac{\partial^2\phi}{\partial x^2} + \frac{\partial^2\phi}{\partial y^2} + \frac{\partial^2\phi}{\partial z^2} = 0 \tag{2.13}$$

A further assumption made is that the fluid particles are irrotational.

$$\Delta \times \bar{u} = 0 \tag{2.14}$$

which leads to the existence of a stream function also conforming to the Laplace equation:

$$\nabla^2\psi = \frac{\partial^2\psi}{\partial x^2} + \frac{\partial^2\psi}{\partial y^2} + \frac{\partial^2\psi}{\partial z^2} = 0 \tag{2.15}$$

Eq. 2.13 is a second order differential equation and is termed the governing equation. In order to solve the governing equation some boundary conditions must be given, Fig. 2.5 shows these conditions for

$$\nabla^2\phi = 0, \quad 0 < x < \lambda, \quad -h < z < \zeta \tag{2.16}$$

At the seabed, which is assumed horizontal, the bottom boundary condition (BBC) is

$$-\frac{\partial\phi}{\partial z} = 0 \quad \text{on } z = -h \tag{2.17}$$

which essentially states that flow everywhere to the sea bed is tangential and no fluid will cross this boundary.

At the free surface, $\zeta$, two conditions must hold. The kinematic free surface boundary condition (KFSBC) is

$$-\frac{\partial\phi}{\partial z} = \frac{\partial\zeta}{\partial t} - \frac{\partial\phi}{\partial x}\frac{\partial\zeta}{\partial x} \quad \text{on } z = \zeta(x,t) \tag{2.18}$$

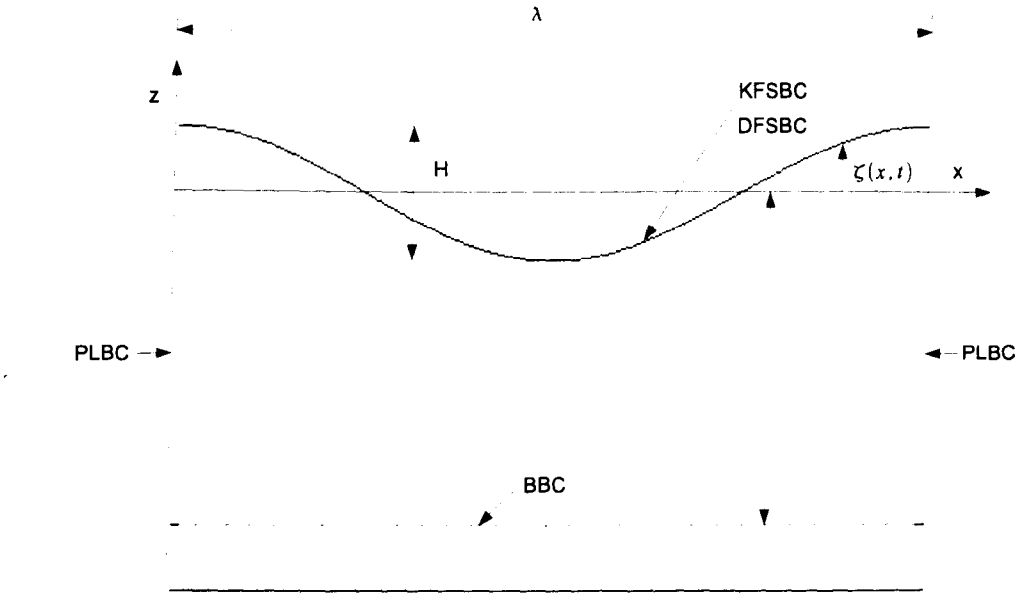


Figure 2.5: Boundary conditions for the Airy equations

This is similar to the BBC and states that no fluid shall cross this boundary and that fluid will flow tangentially to the free surface, $\zeta(x,t)$.

The second condition is the dynamic free surface boundary condition (DFSBC), which, when the pressure at the free surface is taken as the gauge, $p_\zeta = 0$ becomes

$$-\frac{\partial\phi}{\partial t} + \frac{1}{2}\left[\left(\frac{\partial\phi}{\partial x}\right)^2 + \left(\frac{\partial\phi}{\partial z}\right)^2\right] + g\zeta = C(t) \tag{2.19}$$

This is an application of the Bernoulli equation to the free surface and dictates that the pressure at any point on the surface boundary is a constant. In more complicated instances where the pressure distribution over a surface is known, the equation can be adapted to couple the pressure field to the wave system allowing the waves to become forced.

The final conditions that must be obeyed are the periodic lateral boundary conditions (PLBC) which apply in both space and time:

$$\begin{aligned} \phi(x,t) &= \phi(x+\lambda,t) \\ \phi(x,t) &= \phi(x,t+T) \end{aligned} \tag{2.20}$$

This ensures that the solution repeats itself in time and space and that it can be extended to describe a progressive wave train.

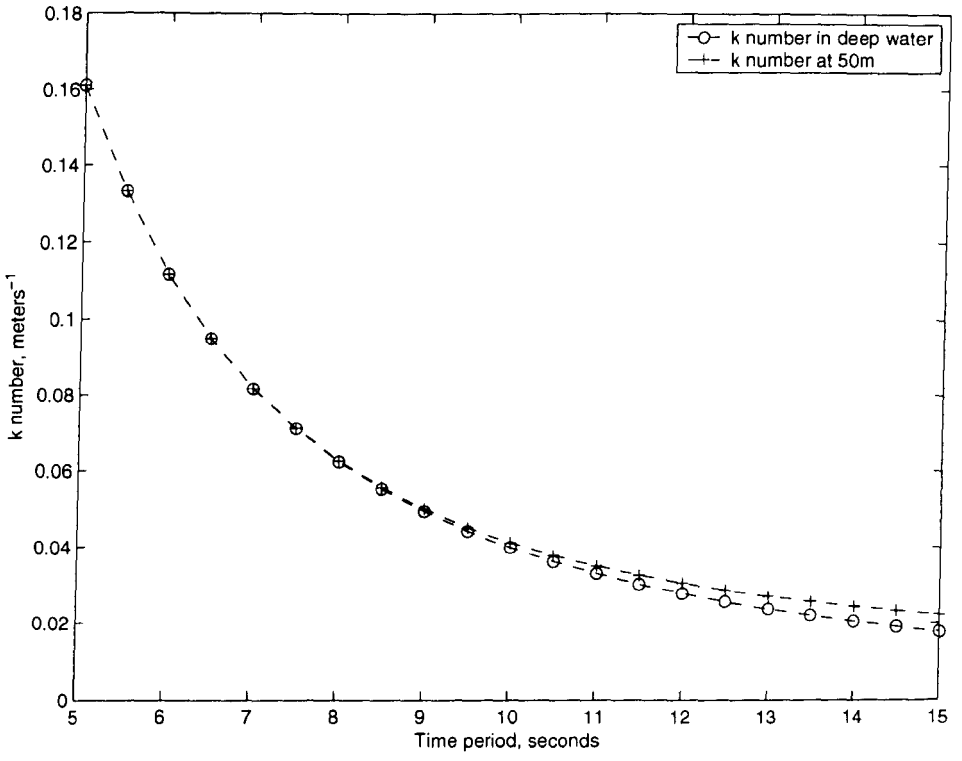


Figure 2.6: Comparison of $k$ at 50 m contour and deep water

### Solution

The full solution to this problem is given in, [16]. A first order solution to these equations was given by Airy [17] in 1845 and will form the basis of much of the work put forward here. The $x$ and $z$ particle elevations for a small-amplitude wave in water of depth $h$ are

$$\chi = a\frac{\cosh k(z+h)}{\sinh kh}\cos(kx - \omega t - \phi) \tag{2.21}$$

$$\zeta = a\frac{\sinh k(z+h)}{\sinh kh}\sin(kx - \omega t - \phi) \tag{2.22}$$

where $h$ is measured from the sea bed and is taken as positive, $z$ is measured from the mean sea elevation and is negative with increasing depth as was shown in Fig. 2.1.

The phase velocity $c_p$ of the wave is now given by

$$c_p = \sqrt{\frac{g}{k}}\tanh kh \tag{2.23}$$

and the group velocity as

$$c_g = \frac{1}{2}c_p\left(1 + \frac{2kh}{\sinh 2kh}\right) \tag{2.24}$$

These basic equations are all in terms of the local wave number $k$. In practice the data available is usually the period $T$ or the frequency $f$. As the phase velocity $c_p = \lambda/T = \omega/k$,

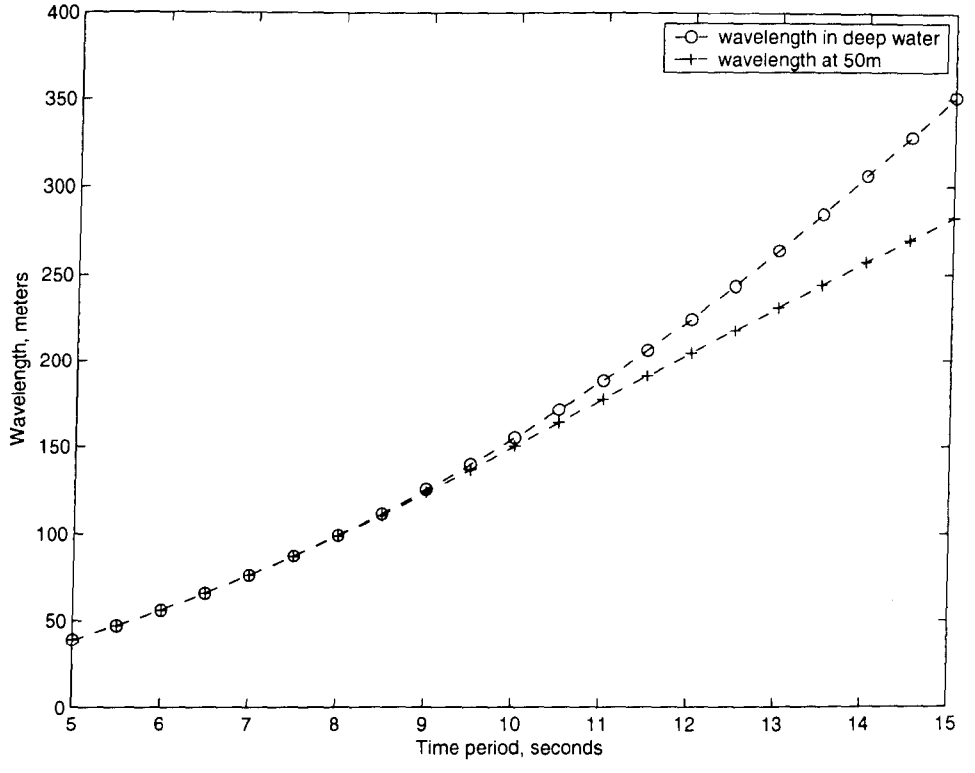


Figure 2.7: Comparison of wavelength at 50 m contour and deep water

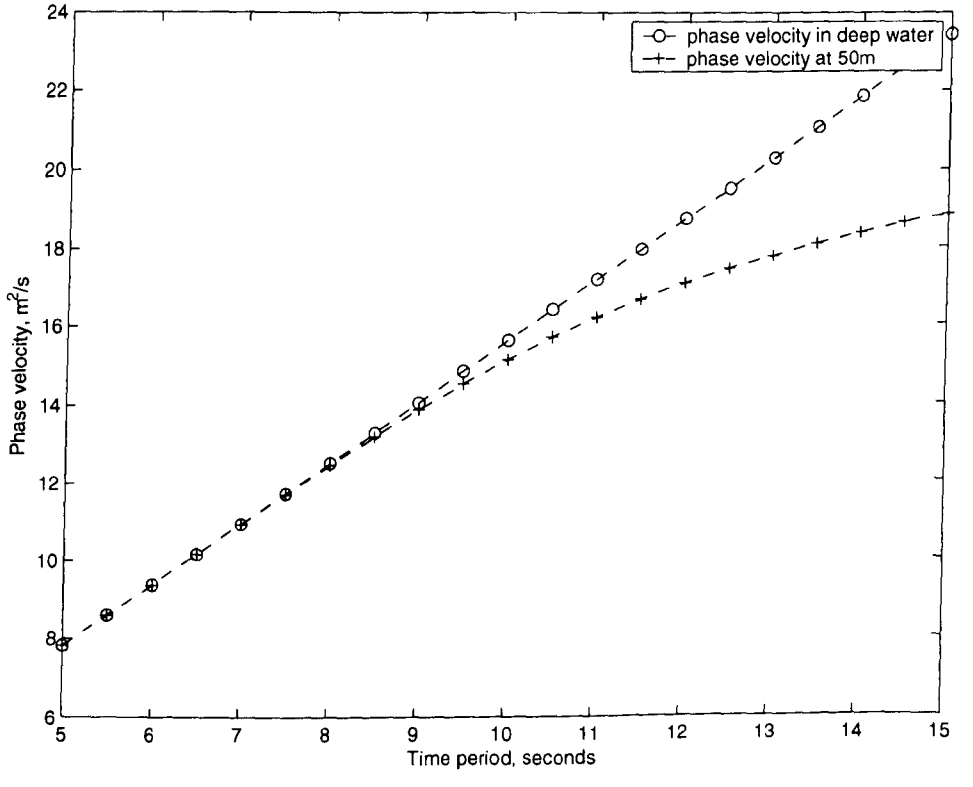


Figure 2.8: Comparison of phase velocity at 50 m contour and deep water

| Periodic term | | Deep water | | | 50 m | | |
|---|---|---|---|---|---|---|---|
| freq (Hz) | Time (s) | $k$ ($m^{-1}$) | $\lambda$ (m) | $c_p$ (m/s) | $k$ ($m^{-1}$) | $\lambda$ (m) | $c_p$ (m/s) |
| 0.2 | 5 | 0.161 | 39.0327 | 7.8065 | 0.161 | 39.0327 | 7.8065 |
| 0.16667 | 6 | 0.1118 | 56.2072 | 9.3679 | 0.1118 | 56.2056 | 9.3676 |
| 0.14286 | 7 | 0.0821 | 76.5042 | 10.9292 | 0.0822 | 76.4629 | 10.9233 |
| 0.125 | 8 | 0.0629 | 99.9238 | 12.4905 | 0.0631 | 99.5615 | 12.4452 |
| 0.11112 | 9 | 0.0497 | 126.4661 | 14.0518 | 0.0503 | 124.8286 | 13.8698 |
| 0.1 | 10 | 0.0402 | 156.131 | 15.6131 | 0.415 | 151.2983 | 15.1298 |
| 0.0909 | 11 | 0.0333 | 188.9185 | 17.1744 | 0.0353 | 178.1325 | 16.1939 |
| 0.08334 | 12 | 0.0279 | 224.8286 | 18.7357 | 0.0307 | 204.8328 | 17.0694 |
| 0.07693 | 13 | 0.0238 | 263.8614 | 20.297 | 0.0272 | 231.1809 | 17.7831 |
| 0.07143 | 14 | 0.0205 | 306.0168 | 21.8583 | 0.0244 | 257.1158 | 18.3654 |
| 0.06667 | 15 | 0.0179 | 351.2947 | 23.4196 | 0.0222 | 282.6475 | 18.8432 |

Table 2.1: The effect of depth on wavelength, $k$ number and phase velocity

then

$$\omega^2 = gk \tanh(kh) \tag{2.25}$$

In the ideal case, this equation would be used to calculate $k$ from $T$ or $f$ but, as it cannot be inverted it must be solved numerically using iteration techniques (this can be very computationally expensive when a wide range of frequencies is considered). It can be seen that the wave number will vary as the wave-train passes over a sea bed of variable depth.

### The effect of depth

Table 2.1 gives a range of time periods with associated wave numbers, wavelengths and velocities for deep water and 50 m depth. Figs. 2.6, 2.7 and 2.8 illustrate the various parameters against time period at these two depths. The 50 m contour is regularly quoted as an ideal depth for installing wave energy conversion devices.

It can be seen that in deep water, where $\tanh kh \to 1$, the approximation $\omega^2 = gk$ is valid. As the water depth decreases then the longer wavelengths will begin to experience drag from the bottom. This means that the water particles (which were previously travelling in circular orbits) will encounter friction with the sea bed and their orbits will become elliptical, this process is shown to the right of Fig. 2.3. The effect of this is to slow down the phase velocity of the wave and to some extent cause the wave amplitude to increase. The effect of this can

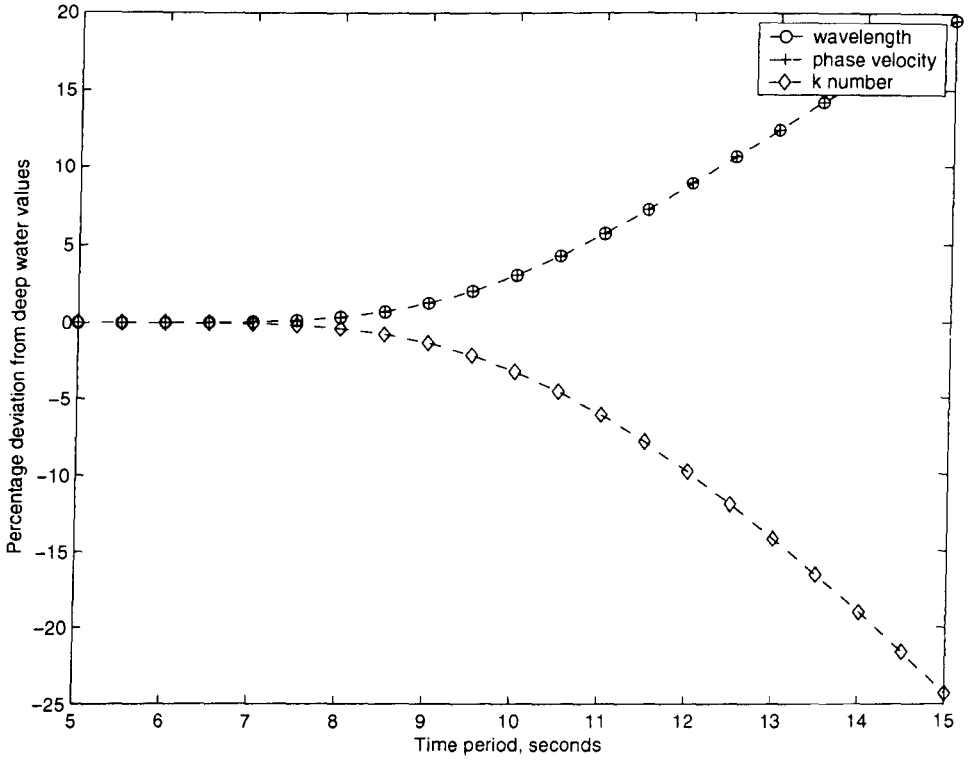


Figure 2.9: Percentage deviation between deep water and 50 m results

be seen on any shallow sloping beach where the waves increase in height as they approach the shore before eventually breaking.

For offshore wave devices at the 50 m contour the full Airy equations should be utilised. At longer wavelengths, the water in which the devices would be typically situated is too shallow for the deep water approximation to strictly hold true. The percentage deviations from the deep water values increase for periods greater then 7 s (see Fig. 2.9). One of the most important results in terms of wave prediction is that the phase velocity changes as the waves enter shallower water. This change in velocity will alter the distance travelled by the wave in a set time period.

### 2.1.3 Pressure as a variable

Discussed in the analysis of the deep water equations, pressure is sometimes used as a measurement variable and is also affected by the depth of water at which it is taken. The Airy equation relating pressure fluctuation $p$ at a depth $h$ is given by

$$p = \rho g a \frac{\cosh k(z+h)}{\cosh kh} \sin(kx - \omega t - \phi) \tag{2.26}$$

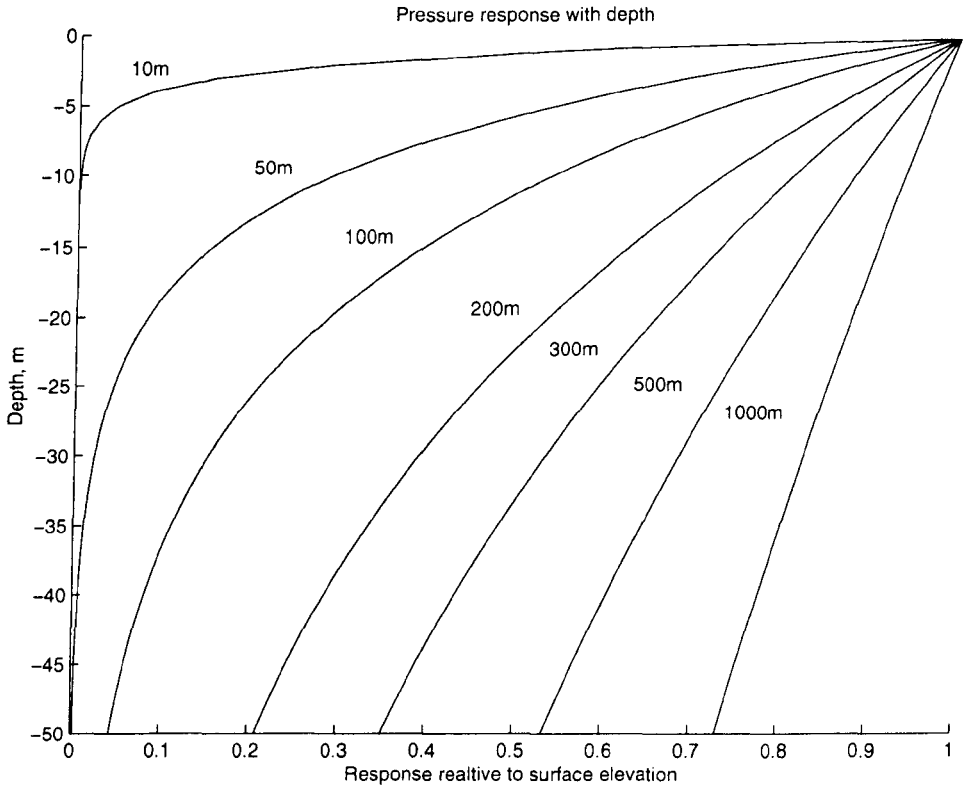


Figure 2.10: Pressure attenuation for a range of wavelengths

For deep water, as $h \rightarrow \infty$, the pressure at depth $z$ becomes

$$p = \rho g a e^{kz} \sin(kx - \omega t - \phi) \tag{2.27}$$

From this, the relative falloff in pressure fluctuation with depth is

$$R(k, z) = e^{kz} \tag{2.28}$$

Which, as stated previously, leads to resolution difficulties if pressure sensors are sited in deep water. Fig. 2.10 shows the attenuation due to depth for a range of wavelengths. For longer wavelengths (i.e. 500 m and 1000 m) the pressure attenuation at 50 m depth will be less than 50 % of its surface value, but for wavelengths less than this the falloff will be considerably greater.

### 2.1.4 Superposition

An important concept to be addressed is that of superposition. In a linear first order system many inputs can be added together and processed to reach a cumulative output that would be the same as if each input had been processed separately then summed after the output.

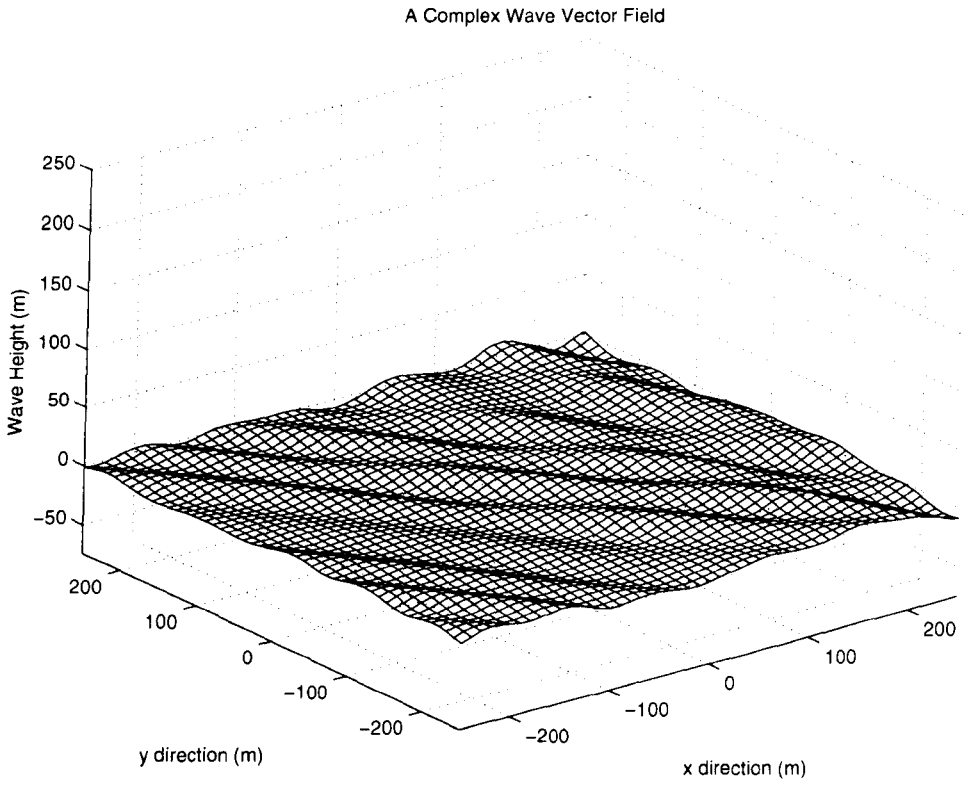


Figure 2.11: Superposition of many wave trains, with a North East swell present

Since small-amplitude Airy waves are linear they can be added to produce a more complex sea state.

The simple periodic wave as described by Eq. 2.22 of this section with constant amplitude can only be generated in a laboratory wave tank and will never occur naturally. In a wave system generated by the wind (Chapter 3), the heights of successive waves and the elevation along wave crests will vary. For most purposes this situation can be adequately described by the linear superposition of a great number of different wave trains. This is because the small amplitude equations are linear, so that the resultant elevation can be described by

$$\zeta = \zeta_1 + \zeta_2 + \zeta_3 + \ldots \zeta_n \tag{2.29}$$

So, from Equation 2.7:

$$\zeta = \sum_n a_n \exp(k_n z) \sin(l_n x + m_n y - \omega_n t - \phi_n) \tag{2.30}$$

where the components $n$ are densely distributed in frequency and direction

$l_n = k_n \cos\theta_n$

$m_n = k_n \sin\theta_n$

and $\theta_n$ is the direction of travel of the n$^{th}$ component.

An example of such a superposition is shown in Fig. 2.11 for a mixed sea state with a dominant North Easterly swell.

### 2.1.5 Assumptions made

The following lists the assumptions made in formulating the first order theory for small amplitude waves, [15].

1. The wave shapes are sinusoidal.
2. The wave amplitudes are very small compared with wavelength and depth.
3. Viscosity and surface tension are ignored.
4. The Coriolis force and vorticity, which result from the Earth's rotation, are ignored.
5. The depth of the water is considered uniform, and the seabed is flat.
6. The waves are not constrained or deflected by land masses.
7. That real three-dimensional waves behave in a way that is analogous to a two-dimensional model.

## 2.2 The wave spectrum

The wave spectrum is one of the key components in describing a wave field. This concept is used for generating realistic wave fields from which to construct predictions. The following sections set out the theory for introducing this concept. Further information on wave spectra and their generation can be found in Chapter 3. Detailed information on Fourier theory and spectral analysis will be given in Chapter 5.

### 2.2.1 The omnidirectional spectrum

If the elevation of the sea surface is measured above the origin of the co-ordinate system $(x = 0, y = 0)$ then Eq. 2.30 looses dependency on $x$ and $y$ and reduces to

$$\zeta(t) = \sum_n a_n \sin(\omega_n t - \phi_n) \tag{2.31}$$

squaring this

$$\zeta^2(t) = \sum_n \sum_m a_n a_m \sin(\omega_n t - \phi_n) \sin(\omega_m t - \phi_m)$$

and using trigonometric identities

$$\zeta^2(t) = \sum_n \sum_m \frac{1}{2} a_n a_m \{\cos[(\omega - n - \omega_m)t + (\phi_n - \phi_m)] - \cos[(\omega - n + \omega_m)t + (\phi_n - \phi_m)]\} \tag{2.32}$$

allowing $n = m$, and taking the long term average, while removing the oscillatory parts:

$$E = \overline{\zeta^2(t)} = \sum_n \frac{1}{2} a_n^2 \tag{2.33}$$

This shows that the variance of the sea-surface elevation equals the sum of the variances of its component wave-trains. Since the variance is proportional to the average energy per unit area of the sea surface, the total energy of the wave system is just the sum of the energies associated with individual wave-trains. This is a property of linear systems where the component sinusoids have random phases.

If the output of a wave recording device is filtered to select only those frequencies on the right-hand side of Eq. 2.31 with frequencies in the range $f - \Delta f/2$ to $f + \Delta f/2$, giving a variance $\Delta E$, then a function $S(f)$ can be defined by

$$S(f) = \Delta E / \Delta f \tag{2.34}$$

$S(f)$ will remain finite as $\Delta f \to 0$ and from this it can be seen that

$$E = \int_0^\infty S(f) df \tag{2.35}$$

$S(f)$ is called the "omnidirectional spectral density function", and has units of $\mathrm{m}^2/\mathrm{Hz}$. An example is given in Fig. 2.12.

In practise it is not possible to continuously sample the sea surface elevation and an estimate has to be made for a finite period of time/space, this is denoted as $\hat{S}(f)$. This estimated spectrum will contain some element of random variability and is discussed in Chapter 5.

### 2.2.2 Spectral moments

Some useful definitions and statistical results can be expressed in terms of the spectral moments of the spectral density function $S(f)$. The concept of a moment is taken from mechanics where it is used to describe the turning effect of forces applied to various objects. A common application is the calculation of the moment for rotating a beam fixed at a central point. The opposite of this force will restore the equilibrium. In this application, if

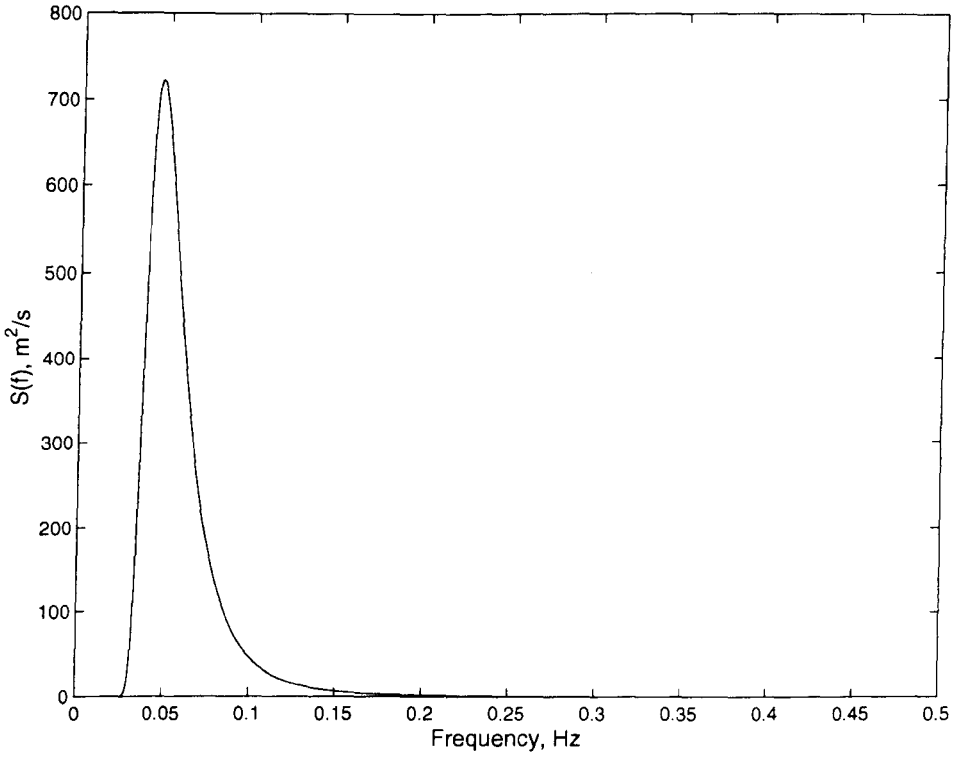


Figure 2.12: An omnidirectional spectrum for wind speed of 30 m/s

the omnidirectional spectrum is represented as a two dimensional laminar shape, then the first spectral moment is the balance point along the ordinate when the laminar shape is vertical (i.e., as shown in Fig. 2.12).

In general the $n^{th}$ spectral moment is given by

$$m_n = \int_0^\infty f^n S(f) df \tag{2.36}$$

and it can be seen that the zero-moment is

$$\begin{aligned} m_0 &= \int_0^\infty S(f) df \\ &= \text{total variance ("energy") of the wave spectrum} \\ &= \overline{\zeta^2} \end{aligned} \tag{2.37}$$

A common use of the zero-moment is to define the significant wave height where

$$H_{m0} = 4\sqrt{m_0} \tag{2.38}$$

The next few moments can be used to describe the spectral characteristics of ocean waves. The first moment $m_1$ determines the mean wave frequency and mean wave period, hence

$$\overline{\omega} = \frac{m_1}{m_0} \tag{2.39}$$

and

$$\overline{T} = \frac{2\pi}{\overline{\omega}} = 2\pi\frac{m_0}{m_1} \tag{2.40}$$

An alternative estimate of the mean frequency (period) is called the average frequency of up-crossing of the mean level $\overline{\omega}_0$ (average period $\overline{T}_0$). This gives:

$$\overline{\omega}_0 = \sqrt{\frac{m_2}{m_0}} \tag{2.41}$$

and

$$\overline{T}_0 = \frac{2\pi}{\overline{\omega}_0} = 2\pi\sqrt{\frac{m_0}{m_2}} \tag{2.42}$$

In addition to the moments $m_n$, the central moments $\overline{m}_n$ can also be used. These are defined as

$$\overline{m}_n = \int_0^\infty (\omega - \overline{\omega})^n S(\omega) d\omega \tag{2.43}$$

Thus:

$$\overline{m}_0 = m_0 \tag{2.44}$$

$$\overline{m}_1 = m_1 - \overline{\omega} m_0 = 0 \tag{2.45}$$

$$\overline{m}_2 = m_2 - \frac{{m_1}^2}{m_0} \tag{2.46}$$

The central moment $\overline{m}_2$ is a measure of the concentration of the spectral wave energy around frequency $\overline{\omega}$. In other words an indication as to whether the spectra is narrow or wide band.

### 2.2.3 The directional spectrum

If, instead of using Equation 2.31, the full equation including directional terms (Eq 2.30) was used, then the same result would be reached, i.e.,

$$E = \overline{\zeta^2(t)} = \sum_n \frac{1}{2} a_n^2 \tag{2.47}$$

If it was now possible to filter in the directional wave-trains, i.e., those travelling between $\theta + \Delta\theta/2$ and $\theta - \Delta\theta/2$ in addition to filtering in terms of frequency, then by analogy to Eq 2.34, the directional spectral density function $S(f, \theta)$ can be defined by

$$S(f, \theta) = \frac{\Delta E}{\Delta f \Delta\theta} \rightarrow \frac{d^2 E}{df d\theta} \tag{2.48}$$

It is usual to define $S(f, \theta)$ as the product of the omnidirectional spectrum $S(f)$ and a normalised directional distribution $G(\theta)$, therefore:

$$S(f, \theta) = S(f) G(\theta) \tag{2.49}$$

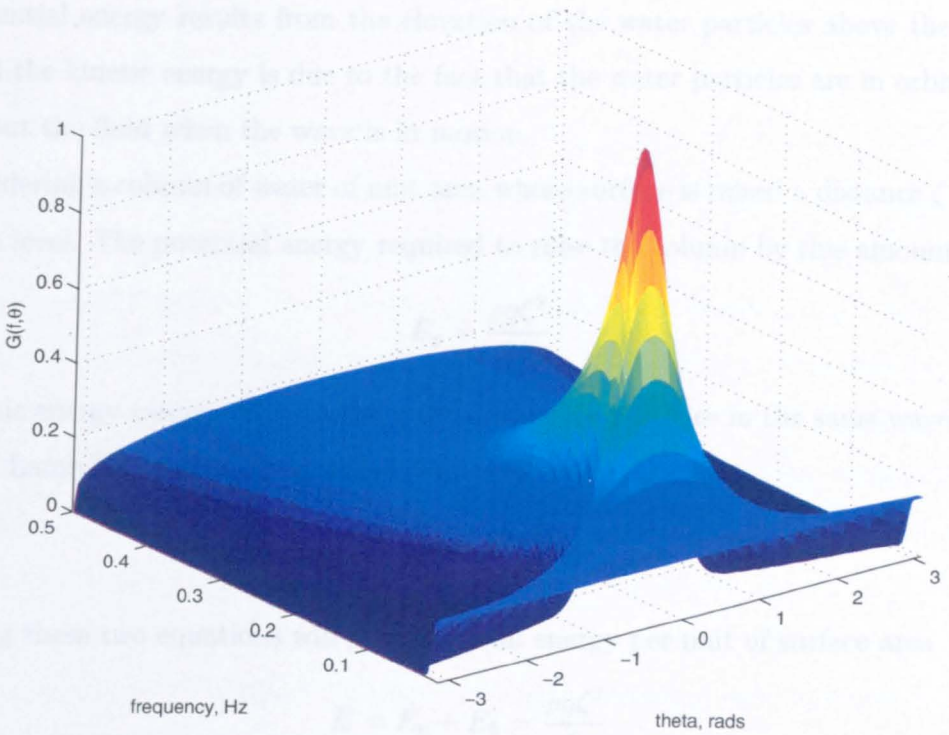


Figure 2.13: Full $G(\theta, f)$ for a 30 m/s wind

so that

$$\int_0^\infty G(\theta) d\theta = 1 \tag{2.50}$$

In fact $G(\theta)$ varies with frequency and will therefore be represented by $G(\theta, f)$. An example of a full directional spectrum is shown in Fig. 2.13. A full description of the directional spectra and its various formulations is given in Chapter 3.

## 2.3 Energy and power

The transmission and transformation of energy is a fundamental process in the progression and dispersion of ocean surface waves. The concept of the wave spectrum and the development of oceanic scale models of wave behaviour are based on tracking the energy balance from inception to dispersal. Energy is important to many processes because it cannot disappear; for example, if a transformation is made from the frequency domain to the time domain the energy present before the transform should equal the energy present after. If it is found that the energy does not balance then there must be an error in the transformation process.

The total energy in a wave can be broken down into potential energy and kinetic energy.

The potential energy results from the elevation of the water particles above the mean sea level and the kinetic energy is due to the fact that the water particles are in orbital motion throughout the fluid when the wave is in motion.

Considering a column of water of unit area whose surface is raised a distance $\zeta$ above the mean sea level. The potential energy required to raise the column by this amount is

$$E_p = \frac{\rho g \zeta^2}{16} \tag{2.51}$$

The kinetic energy associated with the motion of water particles in the same wave has been shown by Lamb [18] and Dean and Dalrymple [16] to be

$$E_k = \frac{\rho g \zeta^2}{16} \tag{2.52}$$

Combining these two equations will give the total energy per unit of surface area

$$E = E_p + E_k = \frac{\rho g \zeta^2}{8} \tag{2.53}$$

This equation is a function of surface elevation only and neither the depth of water nor the frequency of the wave will affect the energy present. This shows that the energy in the wave is split equally between the potential energy and kinetic energy. In deep water the energy is usually contained within half a wavelength of the surface, [14].

There is a simple analogy that can be made here between the flow of energy in a wave system and the flow of energy in an A.C. electrical power system. In a wave, the kinetic energy is cycling energy due to the motion of the water particles. To a first order this does not cause the transfer of energy from one system point to another, i.e, it is not a power flow and cannot be utilized as an energy source. However, energy can propagate from one point of the system to another in the form of a flow of sea waves, which is a flow of potential energy. This is a power flow component.

This is analogous to real power in an A.C. power system, which is the flow of energy from one point of the system to another (and similarly for the flow of potential energy in a sea wave). Additionally the reactive power, which is the cycling of energy around the system with no net power flow from one point to another (this cycling occurs twice per voltage cycle and is associated with the cycling between stored magnetic field energy in inductive components and stored electric field energy in capacitive components). This raises the point that only 50% of the energy in the deep sea system can be converted into usable energy, and to do this, then a wave energy converter should be a matched load. If the wave system has a characteristic impedance, then the wave converter should have an impedance that is

the complex conjugate of this characteristic impedance to obtain maximum sea wave energy extraction.

However this analogy may not be entirely true as certain devices will extract potential and kinetic energy from the waves raising the energy extraction to greater than 50%. For example a point absorber will extract the potential energy by following the heave but a device akin to the Pelamis or wave dragon will extract some kinetic energy also.

The power, or energy flux, contained in a wave is a multiple of the energy per unit area times the velocity at which this energy is travelling. For an omni-directional single frequency wave this is simply the phase velocity of the wave, $c_p$. For a real situation where many waves are present the group velocity, $c_g$ must be considered. This can also be termed the energy transport [13] and in a similar vein a mass transport can also be defined. In an ideal situation the wave particles will travel in a perfect circle and remain always in the same mean position. In reality they will be continually displaced by a small distance over time this is known as the Stokes drift and this is equivalent to the mass transport of water particles due to the incident wave field.

To show the calculation for a full sea state, the definition of $S(f)$ in Eq. 2.34, gives

$$S(f)\Delta f = \sum \frac{1}{2} a_n^2 \tag{2.54}$$

where the sum is taken over those component wave trains whose frequencies lie in the range $f - \Delta f/2$ and $f + \Delta f/2$. Thus, using Eq. 2.53, for a given spectrum, the total energy per unit area of the sea surface is

$$\begin{aligned} E &= \rho g \int S(f) df = \rho g m_0 \\ E &= \rho g (H_s^2/16) \end{aligned} \tag{2.55}$$

where $H_s$ is the significant wave height (given later in Eq. 2.58). For a unidirectional wave system, the power transported per metre of crest length is

$$P = \rho g \int c_g(f) S(f) df \tag{2.56}$$

If a directional spectrum is considered, then this formula gives the power being transported across a fixed circle of unit diameter.

For deep water, using Eq. 2.36, this becomes

$$\begin{aligned} P &= \frac{\rho g^2}{4\pi} \int f^{-1} S(f) df \\ &= \frac{\rho g^2}{4\pi} m_{-1} \end{aligned} \tag{2.57}$$

## 2.4 Height and period parameters

As has been previously stated, when discussing the properties of spectral moments, having general parameters to describe a complex wave field is very useful. The moments as already highlighted can be combined to present generalised height and time parameters. The follow is taken almost entirely from Tucker, [12], as alternate reference material did not in general deal with this subject in as much detail.

### 2.4.1 From time histories

Some of the parameters derived from a time history are shown below

$h_z$ is the range of elevation between two zero-upcrossings of the mean water level

$h_{cm}$ is the height of a crest above the mean water level

$h_{tm}$ is the depth of a trough below mean water level

$h_c$ is the difference in level between a crest and the succeeding trough

$t_z$ is the time interval between two successive up-crossings of the mean water level

$t_c$ is the time interval between two successive crests.

$T_z$ is the mean value of $t_z$ over the length of a particular time-history

In practice, $h_c$ and $t_c$ are not commonly derived from time-history records, and interest is given over more to the zero-crossing parameters.

In early work on wave prediction, the term "Significant wave height" was applied to the highest one third of zero-upcross waves. This is the average crest-to-trough height of the highest one third of waves and was chosen as being close to the wave height reported by visual observers aboard vessels. However no relationship was ever found to relate this parameter to the other more fundamental wave parameters and its use is now largely historical.

The parameter now in general use and also called the "Significant wave height", which is denoted as $H_s$ or $H_{m0}$ and is defined by

$$H_{m0} = 4\sqrt{m_0} \tag{2.58}$$

where $m_0$ is the variance of sea surface elevation and comes from the zeroth spectral moment. The value of $H_{m0}$ can be derived by the manual Tucker-Draper method [19].

| Symbol | Title | Description | Moment definition | Value (s) |
|---|---|---|---|---|
| $T_E$ | Energy Period | Total wave power in deep water $= \frac{\rho g^2}{4\pi} T_E m_0$ | $m_{-1}/m_0$ | 12.51 |
| $T_1$ or $\bar{T}$ | Mean period | 1/average frequency of the spectrum | $m_0/m_1$ | 11.27 |
| $T_2$ or $T_z$ | Zero-crossing period | The average period of the zero-upcross waves | $m_2/m_0$ | 10.38 |
| $T_I$ | Integral period | The $T_z$ of the integral of the record | $m_{-2}/m_0$ | 13.00 |
| $T_M$ or $T_p$ | Modal period or peak period | The period at which $S(f)$ has its highest value | None | 14.60 |
| $T_{pc}$ | Calculated peak period | Approximation to the modal period | $m_{-2}m_1/m_0^2$ | 15.00 |

Table 2.2: Wave period parameters for an 18.6m/s Pierson-Moskowitz spectrum

The individual values of $h_z$ and $t_z$ within a particular wave record are found to be related to each other. In general, a higher value for $h_z$ means a longer $t_z$. The majority of these parameters are of interest in the forecasting of extreme wave behaviour and not for general concern in the prediction of waves. However, they can prove useful in quick checks to determine if prediction and simulation results are approximately correct. Table 2.2 gives various wave period parameters for a 18.6 m/s Person-Moskowitz spectra, this is a widely used spectral formulation in Ocean Engineering and is defined later in Chapter 3.

### 2.4.2 From omni-directional spectra

A first step in analysing a wave record is to take its FFT and then to construct its spectrum. The sea-state parameters are generally computed at this time and stored with the spectrum. It is common for the spectral moments from $m_{-2}$ to $m_4$ to be calculated and from these moments, the "spectral" values of $H_{m0}$ and $T_z$. $T_p$ is also often recorded, it is defined as $1/f_p$ where $f_p$ is the peak of the spectrum. As the low-frequency limit of significant wave energy is approximately $0.03Hz$ [12], the integration for the moments usually extends from the lowest frequency estimate which includes this, to a high frequency limit which, in the case of wave buoy measurement, is often taken as just below the heave resonance. In some

instances, a "Phillips tail" can be added above the high frequency limit to replace the lost part of the spectrum (as described in Chapter 3). In cases where the wind speed is low, the energy of the spectrum will tend to fall into the higher frequency range. This data is generally lost when selecting the upper limit for calculating the spectral moments, but it must also be noted that the response of the measuring device in the low wind scenario is likely to be corrupted.

$H_{m0}$ as defined in Section 2.4.1, is in almost universal use as the height parameter but a whole range of other period parameters are also utilised in papers published over the past 50 years.

From communications theory, Rice [20], with random noise signals, showed that for a Gaussian signal

$$T_z = \sqrt{(m_0/m_2)} \tag{2.59}$$

$$T_c = \text{mean value of } t_c = \sqrt{(m_2/m_4)} \tag{2.60}$$

A large amount of existing theory dealing with ocean surface waves treats the problem in probabilistic terms. With much of the existing research focused on extreme wave height prediction for use in civil engineering projects where storm limits are required.

Certain problems exist with parameters that are dependent on negative or higher order moments, primarily through raising the frequency term to high powers, which will tend to favour high frequencies. At the higher frequencies the signal will tend to be dominated by noise terms which are amplified and skew the results. During the course of this study the parameters that are dependent on moments from 0 through to 2 have been most stable and are in agrement with the theoretical values given by Tucker [12] and replicated here in Table 2.2.

### 2.4.3 Wind speed to wave height

Table 2.3 is taken from [15] and shows how wind speed is related to significant wave height. It also relates these values to the Beaufort Wind Scale which is more often heard in the general context of television or radio weather forecasting.

| Beaufort Number | Name | Wind Speed (mean) m/s | km/hr | Significant wave height $H_{m0}$ |
|---|---|---|---|---|
| 0 | Calm | 0.0–0.2 | 0.0–0.72 | 0 |
| 1 | Light air | 0.3–1.5 | 1.08–5.4 | 0.1–0.2 |
| 2 | Light breeze | 1.6–3.3 | 5.76–11.88 | 0.3–0.5 |
| 3 | Gentle breeze | 3.4–5.4 | 12.24–19.44 | 0.6–1.0 |
| 4 | Moderate breeze | 5.5–7.9 | 19.8–28.44 | 1.5 |
| 5 | Fresh breeze | 8.0–10.7 | 28.8–38.52 | 2.0 |
| 6 | Strong breeze | 10.8–13.8 | 38.88–49.68 | 3.5 |
| 7 | Near gale | 13.9–17.1 | 50.04–61.56 | 5.0 |
| 8 | Gale | 17.2–20.7 | 61.92–74.52 | 7.5 |
| 9 | Strong gale | 20.8–24.4 | 74.88–87.84 | 9.5 |
| 10 | Storm | 24.5–28.4 | 88.2–102.24 | 12.0 |
| 11 | Violent storm | 28.5–32.7 | 102.6–117.72 | 15.0 |
| 12 | Hurricane | $> 32.7$ | $> 118$ | $> 15$ |

Table 2.3: Comparing Beaufort number to wind speed and wave height

# Chapter 3

# Wave Generation, Spectra and Simulation

The generation and propagation of waves across the surface of any body of water is a complicated process that is at yet not fully understood by modern science. In order to make engineering approximations for the prediction of wave behaviour, information on the growth and evolution of wave fields is necessary. In this chapter, the present state of knowledge is briefly described as well as the manner in which oceanography and ocean engineering choose to represent the processes. The linearisation and approximations required to run a simulation of wave behaviour in near to real time are then presented and the model structure discussed.

## 3.1 Wave generation by wind

The subject of this section has been widely covered in the literature and a full treatise on the theory is not required. The following overview is based on Tucker [12] with additional information from Townson [14] and Brown et. al. [15]. For a full account of the mechanisms involved in the generation and propagation of wave energy see Komen et. al. [21] or Massel [22].

As with many physical processes the analysis of the generation and propagation of a wave considers the conservation and movement of energy between different mediums. The ultimate source of this energy is the sun. The energy from the sun differentially warms the earth and causes areas of low and high pressure. The formation of storms and winds follow. The energy has been transformed from solar to wind energy. The mechanism for the transfer

of this energy to the waves is still under debate but it can best be summed up as an energy balance equation.

### 3.1.1 The energy balance equation

The process of wave generation can be initially described using two examples: waves on a small stretch of water such as a loch and storm-force waves as generated by a hurricane.

First, consider a wind passing over the surface of a loch. On a calm day the water will be still. With a slight breeze the surface will be deformed by capillary waves, largely sustained by surface tension. On a gusty day small waves will have formed and on a day when high winds are blowing true gravity waves will have developed and will be running up onto the shore. The wave will develop in magnitude across the loch and break onto the shore facing the oncoming wind.

A second, more extreme case, is to consider a hurricane blowing in the Caribbean. Winds in excess of 64 knots will feed energy into the wave system over a prolonged period of time, developing seas with significant wave heights greater than 15 m. This wave energy will remain in the system until it has been dispersed. If the storm is mainly blowing in an easterly direction then the waves can leave the Caribbean basin and progress across the Atlantic eventually meeting a land mass several days later to break on its shores.

Although these are simplified accounts, the above examples include all the elements of the wave equation. The equation has to account for the input energy, the energy dissipation and the change in stored energy with time and space. Hence:

$$\frac{\delta E}{\delta t} + (c_g + U_d)\frac{\delta E}{\delta x} = W + I + D \tag{3.1}$$

where $E$ is the spectral density of energy per unit area at a frequency $\omega$ and position $x$, $c_g$ is the group velocity at $\omega$, $U_d$ is the speed of the wind-driven current, $W$ is the rate of energy transfer from the wind, $I$ is the rate of non-linear transfer among the frequency components, and $D$ is the rate of energy dissipation. In the real sea, $U_d$ is small compared to $c_g$ over the range of interest and the equation reduces to

$$\frac{\delta E}{\delta t} + c_g\frac{\delta E}{\delta x} = W + I + D \tag{3.2}$$

In a fully-developed sea, i.e., one in which the energy input from the wind is balanced against the energy dissipated in the waves, the equation becomes $W = I + D$. This is because the first term on the left-hand side indicates a changing sea state with time while the second left-hand term indicates a changing sea-state with respect to distance.

### 3.1.2 Wind input $W$

As indicated in the previous section it is the winds which blow continuously over the surface of the sea that are the source of ocean waves. When a wind blows across a hard surface, it generates turbulence. On a dry dusty day this turbulence can be seen by observing the vortexes or mini-whirlwinds that form. This is caused by patterns of alternating high and low pressure. These patterns can be resolved into harmonic components travelling in different directions at different speeds. Although not a true solid surface, the surface of the sea is much more dense than air so friction is developed between the two layers and so turbulence is generated. Some of the pressure pattern harmonics will have the correct wavelength and velocity to resonate with the water waves, i.e., they are travelling with the same velocity as the phase velocity of the wave, and with the same wavelength, and therefore it can transfer energy to it. This method was first put forward by Phillips [23] and is sufficient to deal with linear growth, although for well developed waves of longer wavelength and higher amplitude an interactive mechanism is required where the pressure differences on the sea-surface are driven by the waves themselves.

A theory was put forward by Miles [24] and modified by Janssen [25] to explain how this occurs. What is required is for a high pressure to develop on the upwind side of the wave where the water level is dropping, and a lower pressure on the downwind slope where the water is rising. These pressures will then do work on moving the water particles and feed energy into the wave. It can be thought of as the same process that creates and moves sand dunes along a beach.

Inside a water wave, if the force due to the linear acceleration is integrated up a vertical column, it just balances the change in weight of a column due to a change in surface elevation, leaving a constant pressure at the water surface. For a wave travelling under still air, the air particle movements are the reverse of the water particle movements in the wave, and the dynamic and static pressures add instead of subtracting. If an air pressure sensor was floated on top of the wave then the change in air pressure would be $2\rho_a g H$, where $\rho_a$ is the density of air and $H$ is the wave height. Since it is in phase with the wave profile there is no energy exchange between the two mediums.

For a phase change to exist and for energy transfer to occur there must be friction between the two layers. Relaxing the still air condition and allowing a following wind to blow, a turbulent boundary layer is created therefore inducing a phase shift giving the correct conditions for energy transfer from the wind to the wave. This process will occur when the

wind speed exceeds the phase velocity of the wave.

Snyder et al [26] took measurements of air pressure over waves under active generation which produced a formula for the wind input $W$, which is the work done on the waves by the wind at a vector wave number $\mathbf{k}$ where, for $U_5 \cos\theta > c_p$:

$$W(\mathbf{k}) = \frac{\delta E(\mathbf{k})}{\delta t} = 0.2\frac{\rho_a}{\rho_W}\left\{\frac{U_5}{c_p}\cos\theta - 1\right\} \tag{3.3}$$

However, for $U_5 \cos\theta < c_p$ then

$$W(\mathbf{k}) = 0 \tag{3.4}$$

For Eq. 3.3:

$W(\mathbf{k})$ is the rate of energy input per unit area per unit range of $\mathbf{k}$

$E(\mathbf{k})$ is the rate of spectral density of the waves in terms of energy per unit area per unit range of $\mathbf{k}$

$U_5$ is the wind speed at a height of 5 m

$\theta$ is the angle between the wind direction and the direction of wind travel

$\rho_a$ is the air density

$\rho_W$ is the water density

$c_p$ is the phase velocity of the waves with wave number $\mathbf{k}$

$\omega = 2\pi f$

The equation shows that for high wind speeds, the wind feeds energy into the waves over a wide range of wave directions, but as the wind speed approaches the phase velocity the range of wave directions that can be added to narrows. This results in directional spreading where energy is widely distributed for higher frequencies but concentrated in a narrow directional range for lower frequencies. Formulas utilising this behaviour will be given later in this Chapter.

### 3.1.3 Non-linear interactions I

During the 1970s there was much interest in developing models for statistically predicting wave behaviour on an oceanic scale. A key part of this was developing an understanding of how the energy present in a wave system can be transferred between different frequencies,

e.g., why does the energy present at a system source at the higher frequencies (i.e., the centre of a storm) translate to a low frequency swell that arrives on distant shores?

The assumption of linearity and superposition will no longer hold for steep waves such as those found in developing wave systems. But, this non-linearity is generally weak, so a linear superposition of sinusoidal waves can be initially assumed to investigate how the nonlinearities cause interactions.

Starting with the component surface elevations $\zeta_1, \zeta_2, \ldots, \zeta_n$, the second-order nonlinearities produce terms that are multiples of these, i.e., in general terms

$$\zeta_{nm} = K_{nm}\zeta_n\zeta_m \tag{3.5}$$

where $K_{nm}$ is a factor which can be calculated from hydrodynamic analysis

If $\zeta_n$ and $\zeta_m$ have vector wave numbers $\mathbf{k}_n$ and $\mathbf{k}_m$ and frequencies $\omega_n$ and $\omega_m$, then substituting the relevant wave equations and multiplying out shows that $\zeta_{nm}$ consists of two components, one with a vector wave number $\mathbf{k}_{nm}(+) = \mathbf{k}_n + \mathbf{k}_m$ and a frequency $\omega_{nm}(+) = \omega_n + \omega_m$, and the other with a wave number $\mathbf{k}_{nm}(-) = \mathbf{k}_n - \mathbf{k}_m$ and a frequency $\omega_{nm}(-) = \omega_n - \omega_m$. For second order interactions there are no cases where $\mathbf{k}_{nm}(+)$ and $\omega_{nm}(+)$ obey the dispersion relationship for a free wave, and the same is true for the difference components. Hence, all second-order components are tied waves and cannot build up by resonant interactions.

This being said, Hasselmann [27] showed that for third order interactions, certain combinations of vector wave numbers can produce resultant components which do obey the dispersion relationship and which are therefore capable of building up by resonance. He further went on to show that energy could be transferred from one part of the wave spectrum to another. In particular energy from the higher frequencies is transferred to the lower frequencies, extending the low frequency range of the wave. With the JONSWAP spectrum (Section 3.2.2) it is also possible for energy from the mid-part of the spectrum to be moved to higher frequencies. The breaking of waves may also account for much of the energy transfer during the early stages of growth from higher to lower frequencies. Komen [21] expands upon this concept.

### 3.1.4 Dissipation of energy $D$

The second balancing force of $W = I + D$ is the energy that is dissipated. The two most important processes in deep water wave analysis are losses due to molecular viscosity and

wave breaking. However, inshore, the processes of shoaling and refraction also become important as can be observed in the SWAN model [28].

### Loses due to viscosity

The theory of molecular viscosity and its effects have been long known (Lamb [18]). For lightly damped waves, viscous attenuation causes the amplitude to decay with time but has little affect on other aspects of a waves behaviour, such as frequency. For the light damping condition to hold the proportional energy loss per cycle should be small which is the case for the wavelengths of interest.

Viscosity is a linear phenomenon, so that, for a given wavelength, the shear forces generated are proportional to the wave amplitude, and the energy loss due to the amplitude squared. If a spatially-uniform wave-train is generated then allowed to decay, the rate of loss would therefore be

$$\frac{dE(t)}{dt} = \frac{-E(t)}{\tau_e} \tag{3.6}$$

where $\tau_e$ is a constant with the dimension of time. Solving the first order differential equation for $E(t)$ will give

$$E(t) = E_0 \exp(-t/\tau_e) \tag{3.7}$$

or, in terms of amplitude:

$$A(t) = A_0 \exp(-t/\tau_a) \tag{3.8}$$

Lamb gives the formula for $\tau_a$ as

$$\tau_a = \frac{\lambda^2}{8\pi\nu} \tag{3.9}$$

where $\lambda$ is wavelength and $\nu$ is kinematic viscosity.

Viscosity is only really a serious problem if dealing with short wavelengths, (much less than 0.5 m), or for wave-trains that are being tracked over a great distance or a long time. For example, a wavelength of 25 m will need to travel 16400 km to decay to $1/e$ of its initial value. The width of the Pacific Ocean, for comparison, is 17600 km at the equator.

### Energy loses due to whitecapping

For the range of the spectrum that we are interested in the more dominant method of energy loss is whitecapping. This occurs when the amplitude of the wave has exceeded its physical maximum imposed by $H_b = 0.14\lambda$. Whitecapping is seen as white foam forming at the peak of the wave as it begins to break and the water becomes aerated. If the wave has grown

exceedingly high then the centre of gravity of the upper wave, that above the mean sea level, will overtake the centre of gravity of the lower part of the wave causing it to topple over. This process is more commonly seen as breaking waves at the shoreline.

Theoretical treatment is difficult, but models for computerised wave prediction make use of adjustment factors in the standard wave spectra to approximate the process into something akin to real life. Hasselmann [29] proposed a formula based on the integral wave steepness parameter

$$\hat{\alpha} = \frac{m_0 \bar{\omega}^4}{g^2} \tag{3.10}$$

where $\bar{\omega} = 2\pi \bar{f} = 2\pi m_1/m_0$ and $m_n$ is the $n^{th}$ spectral moment.

Komen, Hasselmann and Hasselmann [30] examined the energy balance requirements to produce the Pierson-Moskowitz spectrum (Section 3.2.2), and concluded that they got the best results by using

$$S_{Dis}(\mathbf{k}) = -3.33 \times 10^{-5} \left(\frac{\omega}{\bar{\omega}}\right)^2 \bar{\omega} \left(\frac{\hat{\alpha}}{\alpha_{PM}}\right)^2 E(\mathbf{k}) \tag{3.11}$$

Where,

$S_{DiS}(\mathbf{k})d\mathbf{k}$ is the rate of energy dissipation per unit area of the sea-surface from a range of vector wave number $d\mathbf{k}$.

$\alpha_{PM}$ is the value of $\hat{\alpha}$ calculated for the Pierson-Moskowitz spectrum.

$E(\mathbf{k})$ is the spectral density in vector wave number terms.

Eq. 3.11 can be restated in terms more commonly used as:

$$S_{DIS}(\omega, \theta) = -3.33 \times 10^{-5} \left(\frac{\omega}{\bar{\omega}}\right)^2 \bar{\omega} \left(\frac{\hat{\alpha}}{\alpha_{PM}}\right)^2 E(\omega, \theta) \tag{3.12}$$

Note that $\hat{\alpha}$ is proportional to the wave energy and $S_{DIS}$ is proportional to $H_{m0}^4$. Whitecapping therefore gives a tight control over the amplitude of a wave, reinforcing the assumption made with regard to the maximum height before breaking $H_b = 0.14\lambda$.

### 3.1.5 Time line

Having given definitions for the terms involved in the energy transfer of a developing sea state, mention must be given to the time line of evolution and the terms applied.

#### Fully developed sea

The simplest state to describe is the fully developed sea. The size of waves is governed both by the wind speed and the unobstructed distance over which the wind has been blowing,

known as the fetch. Provided the fetch is extensive, and the wind has been blowing at a constant velocity an equilibrium state in the energy balance equation is reached (as discussed earlier where $W = I + D$). In this balancing condition the size and shape of the waves do not change.

#### Young sea

A young sea occurs before the equilibrium condition for a fully developed sea is reached. This happens at the start of a storm when the waves are gradually gaining in height and energy is being transferred between different frequencies of the spectrum.

#### Swell sea

This occurs after the wave-field has left its source area and the local wind is no longer contributing. The higher frequencies of the fully developed spectrum gradually feed their energy into the lower ranges resulting in waves of lesser amplitude but longer wavelength. This is generally what you see arriving at the coast and what wave device developers are looking for.

#### Real sea

A real sea will in general consist of several swell seas and a locally generated young sea depending on local conditions. For the west coast of Scotland, swells can arrive from storms in the Southern Ocean, the Caribbean, the North West Atlantic and the seas around Iceland. In addition to this, a local young sea will almost always be present. If a storm begins to form in the local area then a fully developed sea can be produced and mask the presence of any swell seas that are arriving.

## 3.2 Spectral representation of wave fields

Further exploration of wave generation theory leads to the need for dimensional analysis techniques. Although the underlying principles of wave generation are understood, the mathematics cannot be succinctly stately.

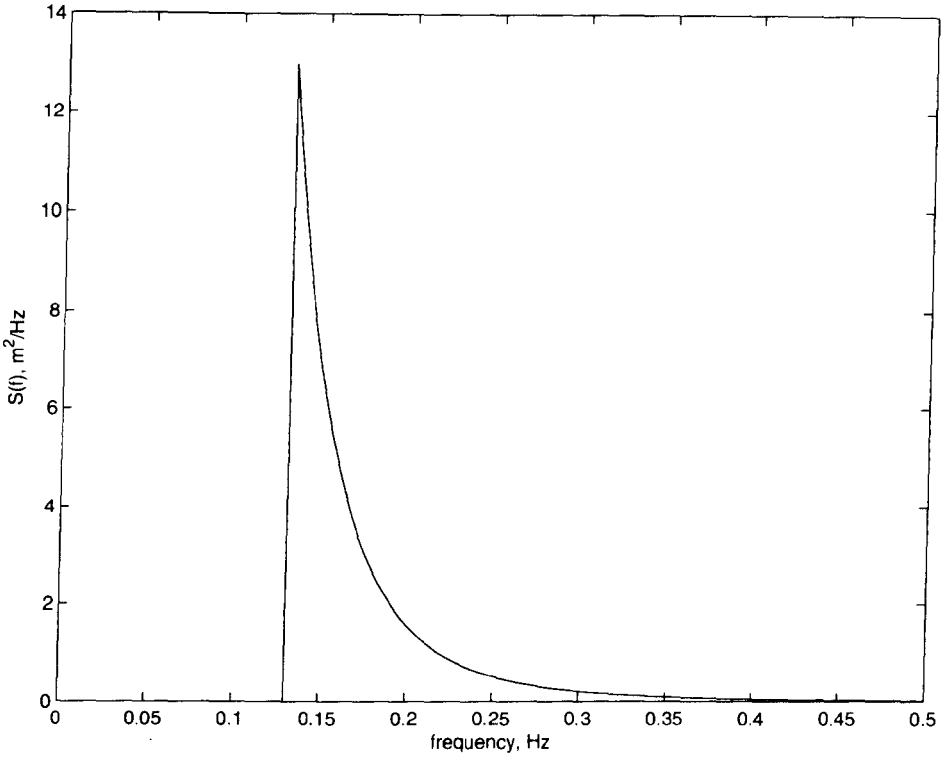


Figure 3.1: Phillips spectrum for a 12 $ms^{-1}$ wind

### 3.2.1 Similarity theorems

Consideration of the energy balance equation and the concepts developed in the previous sections suggests that a saturation point will be reached for the upper frequencies where the spectrum will be governed by the local physical parameters of spectral density $S(\omega)$, the densities of air $\rho_a$ and water $\rho_w$, gravity $g$ and frequency $\omega$. Taking the densities of air, water and gravity as constant, Phillips [31] suggested that the saturated spectrum should follow the form of:

$$S(\omega) = \alpha g^2 \omega^{-5} \tag{3.13}$$

A simple spectral formula can be derived from this

$$S(f) = \alpha g^2 (2\pi)^{-4} f^{-5} \text{ for } f > f_0 \tag{3.14}$$

$$= 0 \text{ for } f < f_0 \tag{3.15}$$

where

$$\text{peak frequency } f_0 = g/2\pi U_{10} \tag{3.16}$$

$\alpha = 0.0081$ is an empirical constant and $U_{10}$ is the wind speed at 10 m. Fig. 3.1 shows a plot of the spectrum. It is only defined above the peak frequency since the formula does not account for the lower frequency effects.

Massel [22] gives several other formulations for the basic saturation spectrum involving the variation of $\alpha$ and arguments that the saturation limit should decay as $\omega^{-4}$. The more common approach is to follow the argument put forward by Kitaigorodskii [32] (original paper in Russian).

The spectrum of interest is normally limited by the fetch over which a steady wind has been blowing. This adds the fetch $X$ and the wind speed $u$ to the basic Phillips equation so that

$$S(\omega) = g^2\omega^{-5}F\left(\frac{u\omega}{g}, \frac{gX}{u^2}\right) \tag{3.17}$$

where

$$u\omega/g = \tilde{\omega} = \text{dimensionless frequency} \tag{3.18}$$

$$gX/u^2 = \tilde{x} = \text{dimensionless fetch} \tag{3.19}$$

and $F$ is an unknown but universal function. Putting the equation in this form means that for any spectra measurements taken in a locally-generated sea, $\omega^5 S(\omega)/g^2$ plotted against $\tilde{\omega}$ for any value of $\tilde{x}$, will result in the same basic shape.

### 3.2.2 General spectra

While Phillips and Kitaigorodskii carried out the initial investigations for analysis of the upper reaches of spectral saturation, real experiments were required to correctly define the spectra for the most energetic part of the spectra below the peak frequency. In common with all the proposed spectra is a set of power functions which are multiplied by an exponential function. A general form for the spectral density function is:

$$S(\omega) = A\omega^{-p}\exp\left[-B\omega^q\right], \tag{3.20}$$

in which $A, B, p$ and $q$ are free parameters.

The following are some of the spectra in use.

#### The Pierson-Moskowitz spectrum

This spectrum represents a fully developed sea where the phase speed is equal to the wind speed and the spectrum is saturated. Using field data, Pierson and Moskowitz [33] proposed that

$$S(\omega) = \alpha g^2\omega^{-5}\exp\left[-B\left(\frac{g}{\omega U_{19.5}}\right)^{-4}\right] \tag{3.21}$$

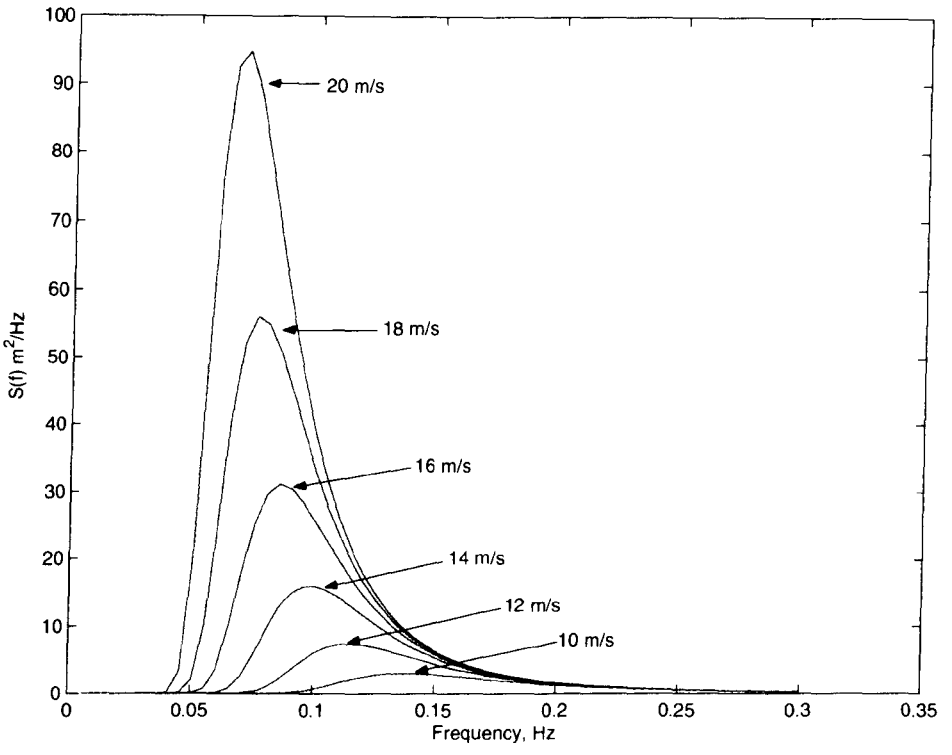


Figure 3.2: The Pierson Moskowitz spectra for wind speeds 10 to 20 $ms^{-1}$

where $\alpha = 8.1 \times 10^{-3}$ and $B = 0.74$ are empirically-derived parameters. The one variable in the equation is the wind speed $U_{19.5}$ at an elevation of 19.5 m above the sea surface. This was the elevation of the measurement equipment during the experiment; however it can be changed to other heights (Tucker [12]). Most other formulae take the wind speed at a height of 10 m and a simple relationship is $U_{10} = 0.93U_{19.5}$. Fig. 3.2 shows the Pierson-Moskowitz spectra for a range of wind speeds. The increase of energy density, and thus significant wave height, with wind speed is clearly seen here. It is common when simulating a wave-field to work with these spectra as an initial trial.

A form of Eq. 3.21 in terms of the frequency of the spectral peak $\omega_p$ is useful in formulating other spectra and is given by

$$S(\omega) = \alpha g^2 \omega^{-5} \exp\left[-\frac{5}{4}\left(\frac{\omega}{\omega_p}\right)^{-4}\right] \tag{3.22}$$

An alternate form in terms of spectral peak frequency $f_p$ is also given here:

$$S(f) = \alpha g^2 (2\pi)^{-4} f^{-5} \exp\left[-\frac{5}{4}\left(\frac{f_p}{f}\right)^{4}\right] \tag{3.23}$$

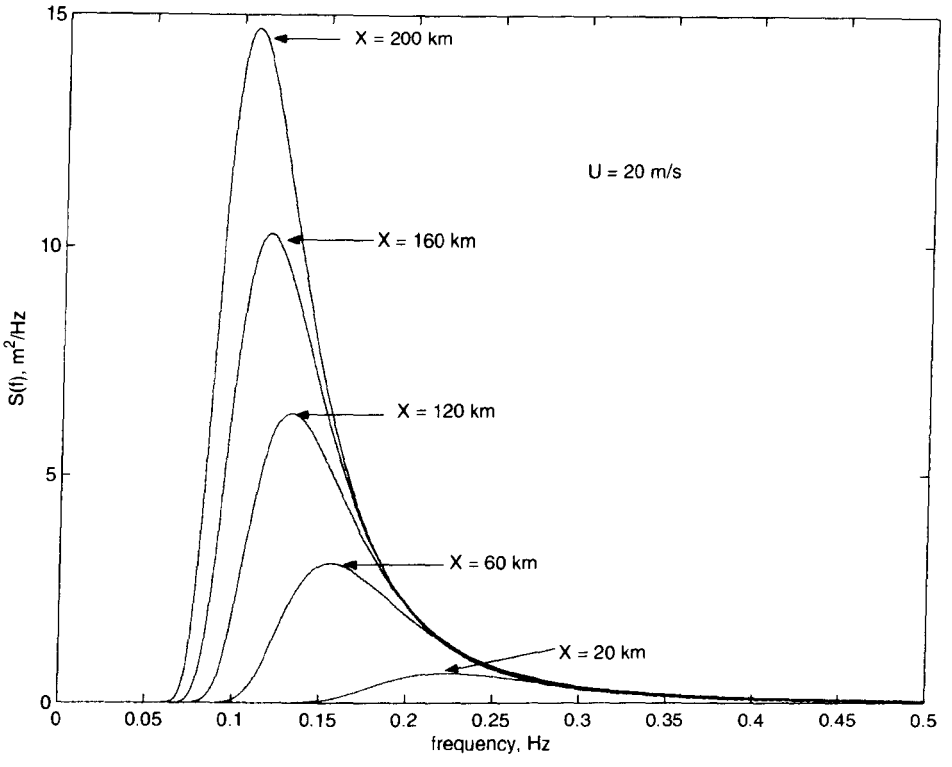


Figure 3.3: JONSWAP spectra for fetches 20 200km

### The JONSWAP spectrum

Using a large-scale measurement experiment carried out in 1968 and 1969 (the Joint North Sea Wave Project - JONSWAP), the shape of a spectrum when related to fetch was considered and a modification to the Pierson-Moskowitz spectrum was proposed (Hasselmann et al. [34]).

$$S(\omega) = \alpha g^2 \omega^{-5} \exp\left[-\frac{5}{4}\left(\frac{\omega}{\omega_p}\right)^{-4}\right] \gamma^{\delta} \tag{3.24}$$

in which

$$\delta = \exp\left[-\frac{(\omega - \omega_p)^2}{2\sigma_0{}^2 \omega_p{}^2}\right] \tag{3.25}$$

and

$$\sigma = \sigma_a \text{ for } \omega < \omega_p \text{ or } \omega = \omega_p \tag{3.26}$$

$$\sigma = \sigma_b \text{ for } \omega > \omega_p \tag{3.27}$$

$$\gamma = 3.3 \tag{3.28}$$

$$\alpha = 0.076 \left(\frac{gX}{U^2}\right)^{-0.22} \tag{3.29}$$

$$\omega_p = 7\pi \left(\frac{g}{U}\right) \left(\frac{gX}{U^2}\right)^{-0.33} \tag{3.30}$$

As can be seen, the first term on the right-hand side of Eq. 3.24 is identical to the Pierson-Moskowitz spectrum (Eq. 3.22). The second term on the right-hand side given in detail in Eq. 3.25 is a peak enhancement factor which raises the peak of the spectrum according to the fetch distance. It is designed to simulate the development of a wind sea before it is fully developed. In this spectrum $\alpha$ and $\omega_p$ are now dependent on fetch.

Fig. 3.3 shows examples of the spectrum for a wind speed of 20 m/s and fetches of 20 km to 200 km. The development of the spectrum with distance more closely mirrors the natural evolution of a spectrum than the Pierson-Moskowitz, with the density of the spectrum increasing with distance and the width of the peak narrowing over greater fetch. Wind speed has a similar effect.

In taking the JONSWAP spectrum to a long fetch case, it should ideally result in the Pierson-Moskowitz formulation. Instead it retains its enhanced peak. Several attempts have been made to resolve this and other inconsistencies, these are detailed in Tucker [12] and Massel [22].

#### Swell and additional spectra

Alternative formulations to the JONSWAP and Pierson-Moskowitz spectra have been proposed using different data sets and are given in Massel [22]: Donelan, Wallops, Krylov, Davidian and TMA. Of use in the prediction of waves for wave energy devices is the swell spectrum proposed by Davidan (translation in Massel [22]). In contrast to the Pierson-Moskowitz and JONSWAP spectra, where the waves are forced, when the wind speed drops the waves begin to attenuate and become free waves. The wind can still sustain saturation at the higher frequencies but, for lower frequencies, the energy tends to the lower range and reduces the non-linear effects. The proposed spectrum has the form:

$$S(\omega) = 6m_0(\omega_p)^{-1}\left(\frac{\omega}{\omega_p}\right)^{-6}\exp\left[-1.2\left(\frac{\omega}{\omega_p}\right)^{-5}\right] \tag{3.31}$$

### 3.2.3 Directional spectra

So far the wave spectrum has been considered as omnidirectional. In a real situation the spectrum also shows directional spreading which can be represented as many superposed wave-trains travelling in different directions. The energy transfer that occurs between the wind and the wave system ensures that energy around the peak frequency is concentrated about the mean direction in which the wind is blowing. For higher and lower frequencies the energy is more spread out in all directions.

Knowledge of the directional spectrum is more sparse than that of the point spectrum due to the limitations in instrumentation (for a discussion see Chapter 4). The common method for defining a directional spectrum $S(f,\theta)$ is to fit a directional spreading function $D(\theta,f)$ to a recorded point spectrum $S(f)$ so that

$$S(f,\theta) = S(f)D(\theta,f) \tag{3.32}$$

provided that

$$\int_0^\infty \int_{-\pi}^{\pi} D(f,\theta) = 1 \tag{3.33}$$

The total energy in the point spectrum will remain unaffected, but will be given to wave vectors travelling in different directions.

Several formulations for the directional spreading function exist and are given in the following sections. Information on the extraction of directional spectra from measurements and the formulation of spectral harmonics are detailed in Chapter 4.

### The cosine-power models

Pierson et al. [35] made the first historical attempt to model the directional spreading of wave energy by proposing that

$$D(\theta) = \frac{2}{\pi}\cos^2\theta, \text{ for, } -\frac{\pi}{2} \leq \theta \leq \frac{\pi}{2} \tag{3.34}$$

As a first approximation it was reasonable but it neglected energy spreading in directions normal to the wind and it was assumed to apply equally to all frequency components.

From field studies conducted with a pitch and roll buoy, Longuet-Higgins et al. [36] proposed an extended formula such that

$$D(\theta,s) = \frac{s^{2s-1}}{\pi}\frac{\Gamma^2(s+1)}{\Gamma(2s+1)}\left|\cos\left(\frac{\theta-\theta_m}{2}\right)\right|^{2s}, \quad -\pi \leq \theta \leq \pi \tag{3.35}$$

where $\theta_m$ is the main peak frequency direction, $s$ is a function of frequency and $\Gamma$ is a gamma function given by:

$$\Gamma(x) = \int_0^\infty t^{x-1}\exp^{-t}dt \tag{3.36}$$

Several formulations for the spreading parameter $s(f)$ have been proposed. In common with all the formulations is that $s(f)$ is large at the spectral peak and smaller as it moves to lower and higher frequencies. In most experiments the parameter was found to be asymmetric decreasing faster on the lower frequency side.

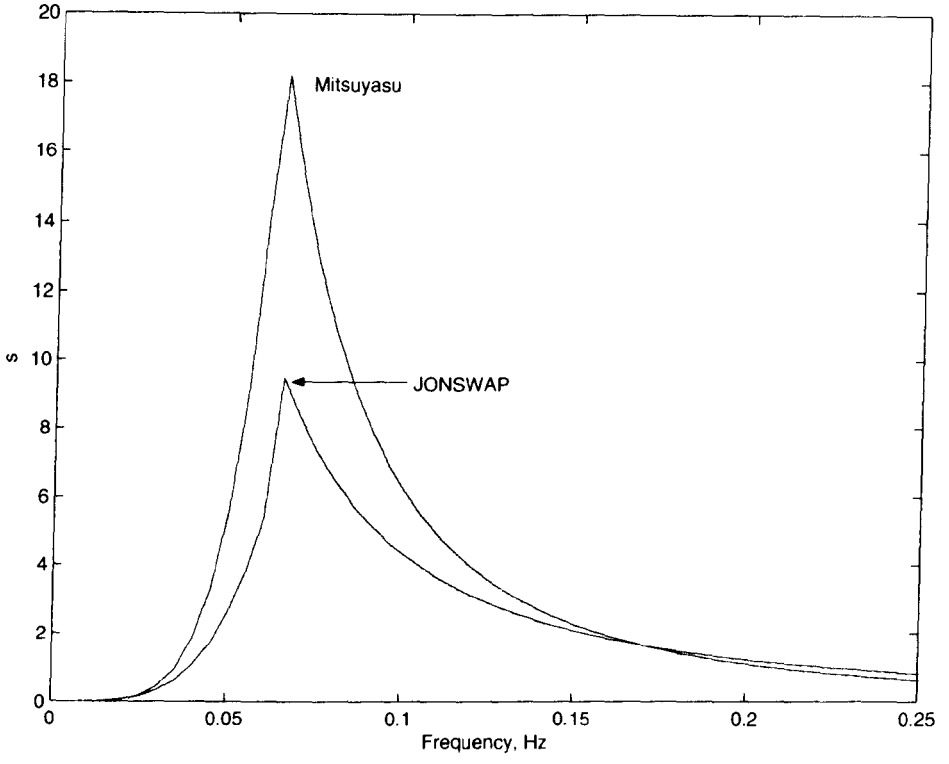


Figure 3.4: Mitsuyasu and JONSWAP spreading factors for $U_{10} = 20$ m/s

Mitsuyasu et al. [37] proposed the following based on cloverleaf buoy data:

$$\begin{aligned} \frac{s}{s_p} &= \left(\frac{f}{f_p}\right)^5 \quad \text{for } f < f_p \\ \frac{s}{s_p} &= \left(\frac{f}{f_p}\right)^{-2.5} \quad \text{for } f > f_p \end{aligned} \tag{3.37}$$

where $f_p$ is the frequency at the peak of the spectrum and $s_p$ is the value of $s$ at the spectral peak given by

$$s_p = 11.5 \left(\frac{U_{10}}{c_p}\right)^{-2.5} \tag{3.38}$$

$U_{10}$ is the wind speed at a height of 10 m and $c_p$ is the phase speed at the spectral maximum $c_p = g/2\pi f_p$.

As a result of the JONSWAP experiment Hasselmann et al. [38] proposed an additional form for a developing sea:

$$\frac{s}{s_p} = \left(\frac{f}{f_p}\right)^{\mu} \tag{3.39}$$

in which for $f < 1.05 f_p$:

$$\begin{aligned} s_p &= 6.97 \\ \mu &= 4.05 \end{aligned}$$

or, for $f > 1.05 f_p$

$$\begin{aligned} s_p &= 9.77 \\ \mu &= -2.33 - 1.45\left(\frac{U_{10}}{c_p} - 1.17\right) \end{aligned}$$

Obtaining plots of the two spreading functions is complicated by the apparently conflicting methods of calculating the peak spectral frequency $f_p$ for a wind speed of 20 m/s at 10 m elevation. Massel [22] using the wind speed at 19.5 m for a P-M spectrum, $U_{19.5} = U_{10}/0.93$, and the condition that

$$\frac{U_{19.5} f_p}{g} = 0.13 \tag{3.40}$$

obtains a peak spectral frequency of 0.0593 Hz.

Tucker [12] (p.p. 100) gives the definition of peak spectral frequency as

$$f_p = \frac{0.877 g}{2\pi U_{19.5}} \tag{3.41}$$

and obtains a figure of 0.0637 Hz. Later in the same text (p.p. 200), while demonstrating the properties of Mitsuyasu's spreading function, the definition is given as

$$f_p = \frac{0.88 g}{2\pi U_{10}} \tag{3.42}$$

which results in $f_p = 0.0687$ Hz. Replacing $U_{10}$ with $U_{19.5}$ will give the 0.0637 Hz result.

Alternatively, according to Mitsuyasu's original paper, the non-dimensional frequency is defined in terms of the wind speed at a 10 m elevation and a fetch $X$. Choosing a very large fetch (500 km), to approximate to a fully developed spectrum, the following results:

$$\begin{aligned} \frac{2\pi f_p U_{10}}{g} &= 18.8\left(\frac{gX}{U_{10}^2}\right)^{-0.33} \\ f_p &= \frac{18.8 g}{2\pi U_{10}}\left(\frac{gX}{U_{10}^2}\right)^{-0.33} \end{aligned} \tag{3.43}$$

Unfortunately this does not asymptotically approach a fully developed state until the fetch is exceedingly large.

On closer examination Massel [22] appears to have made a rounding error in Eq. 3.77 (his text). In checking the original Pierson paper [33] the equation should read

$$\frac{U_{19.5} f_p}{g} = 0.14 \tag{3.44}$$

and on substituting for $U_{19.5} = U_{10}/0.93$ a peak spectral frequency of 0.639 Hz is found.

To correct Tucker [12] on p.p. 200, a factor of 0.8184 relating to a wind speed at 10 m as stipulated by Mitsuyasu must be used in place of the 0.88 given. This results in

$$\frac{U_{10}}{c_p} = 0.8184 \tag{3.45}$$

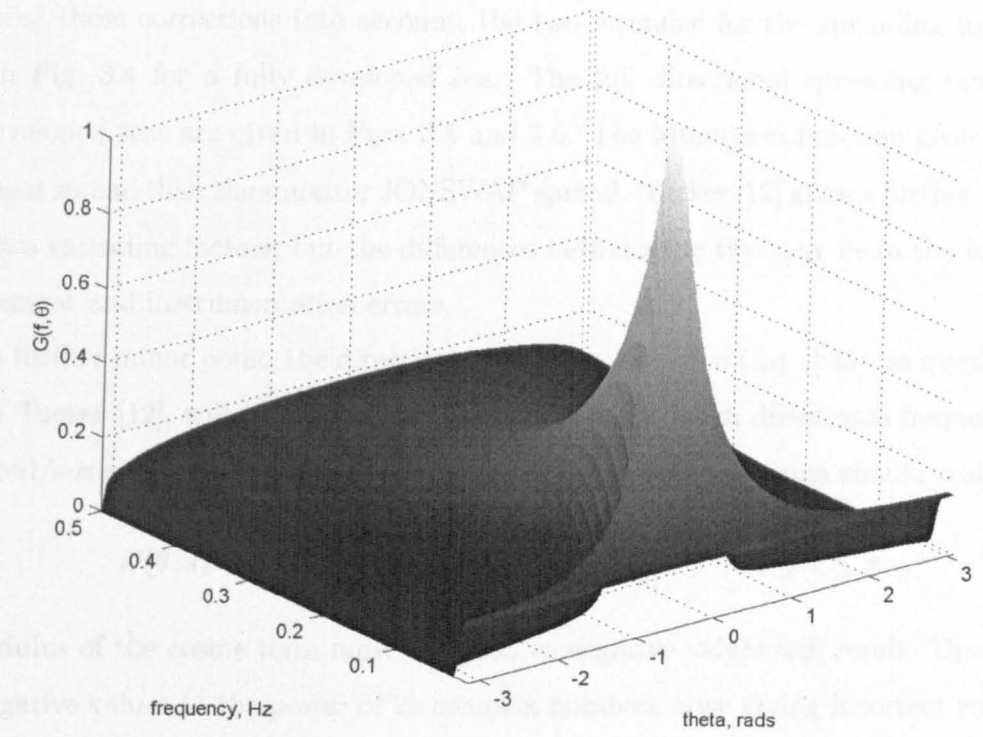


Figure 3.5: The directional spreading function using Mitsuyasu as the spreading factor

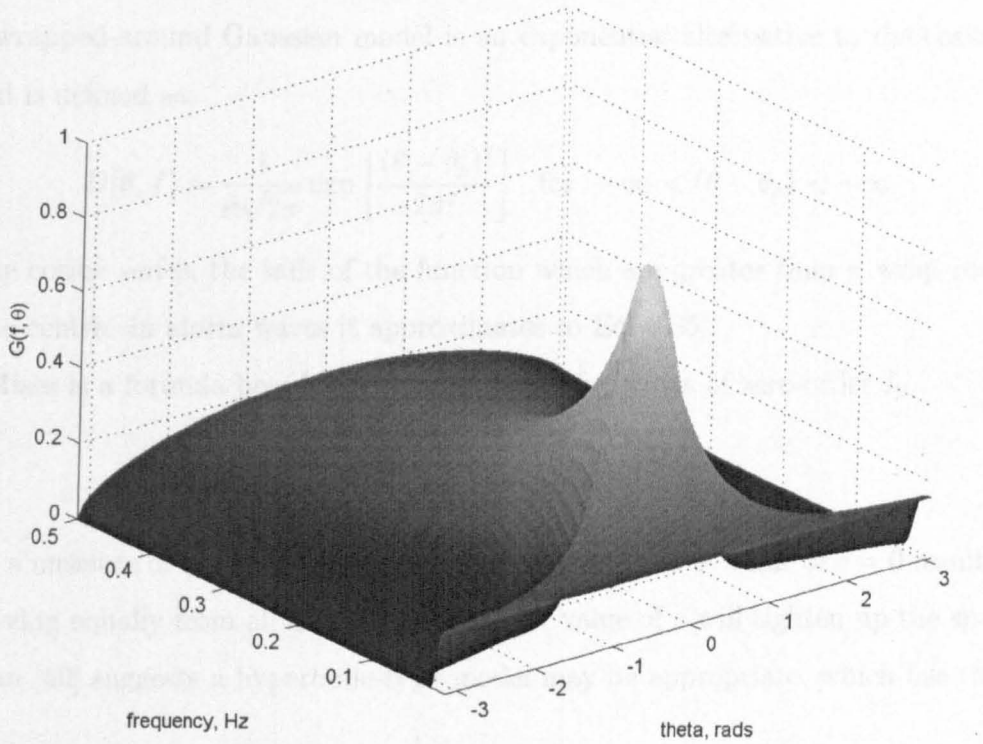


Figure 3.6: The directional spreading function using JONSWAP as the spreading factor

giving a peak spectral frequency of 0.639 Hz which matches the corrected Massel formula.

Taking these corrections into account, the two formulae for the spreading function are given in Fig. 3.4 for a fully developed sea. The full directional spreading functions for fully developed seas are given in Figs. 3.5 and 3.6. The Mitsuyasu function gives a sharper directional spread than the squatter JONSWAP spread. Tucker [12] gives a further discussion of the two spreading factors, but the differences between the two may lie in the methods of measurement and instrumentation errors.

As a further minor point, the directional spreading equation (Eq. 3.35), as quoted several times in Tucker [12], will return erroneous results when a mean directional frequency other than 0 rad/s is used. Returning to Cartwright [39] the correct formula should read

$$D(\theta, s) = \frac{s^{2s-1}}{\pi} \frac{\Gamma^2(s+1)}{\Gamma(2s+1)} \left| \cos\left(\frac{\theta - \theta_m}{2}\right) \right|^{2s}, \quad -\pi \leq \theta \leq \pi \tag{3.46}$$

The modulus of the cosine term must be taken or negative values will result. Upon raising these negative values to the power of $2s$ complex numbers arise giving incorrect results.

### Alternate spreading models

The following are given very briefly as they are not utilised in the experiments, but for comprehensive coverage and references see Massel [22].

The wrapped-around Gaussian model is an exponential alternative to the cosine power series and is defined as:

$$D(\theta, f) = \frac{1}{\sigma\sqrt{2\pi}} \exp\left[\frac{(\theta - \theta_p)^2}{2\sigma^2}\right] \quad \text{for } -\infty < (\theta - \theta_p) < +\infty \tag{3.47}$$

Unlike the cosine series, the tails of the function which are greater than $\pi$ wrap round and add to the centre. In storm waves it approximates to Eq. 3.35.

Von Mises is a formula based on modified Bessel functions of zero-order $I_0$.

$$D(\theta, f, c) = \frac{1}{2\pi I_0(c)} \exp[c\cos(\theta - \theta_p)] \tag{3.48}$$

where $c$ is a measure of concentration about the spectral peak. A value of $c = 0$ results in the waves arriving equally from all directions. A higher value of $c$ will tighten up the spectrum.

Donelan [40] suggests a hyperbolic type model may be appropriate, which has the form

$$D(\theta, f) = \frac{1}{2}\beta \cosh^{-1}[\beta(\theta - \theta_p)] \tag{3.49}$$

## 3.3 Wave modelling and time series simulation

As a pretext for developing prediction routines for ocean waves a selection of wave records from real measuring devices would have been ideal. Unfortunately this data was not available for this study. This lack of data is largely due to the costs involved in siting wave measurement devices and the sometimes commercial nature of the data returned. There are also technical difficulties involved in siting two devices in close proximity that are picked up on in Chapter 4. Instead, wave records had to be simulated from the spectra given in the previous section using the linear superposition of plane wave vectors. The method for this simulation, as well as input and output files, are presented below.

### 3.3.1 The wave modelling equations

For a simulation of wave records to take place within a reasonable period of time it was decided that a linear assumption should be made and that the superposition of many wave vectors would not result in serious errors. An additional assumption was made in that the waves would be propagating over an even bottomed surface and wave breaking effects could be ignored. Therefore Eq. 3.50 can be used for modelling:

$$\zeta(x,y) = \sum_{n=1}^{N}\sum_{m=1}^{M} a_n \sin(k_n x \cos\theta_m + k_n y \sin\theta_m - \omega_n t - \phi_n) \tag{3.50}$$

where the input parameters are obtained from a separate wave-field file, and the output $\zeta(x,y)$ is calculated for $(x,y)$ points, which is also given as a separate file. The model is broken down into these sections to allow for maximum flexibility and repeatability of tests. For example, the wave-field and the output file can be retained while the main modelling equations are changed and new outputs compared to old. Similarly, the position of output sensors can be changed and the experiment repeated. In particular, a sensor setup can be tested for a range of input values.

### 3.3.2 Model outputs

The wave model gives its outputs in two separate forms: an animation to visualise the wave-field and a time series for individual data points.

Fig. 3.7 shows a screen capture of the wave model output using a full directional spectrum as input with a mean direction of $0^o$ and wind speed $U_{10}$ of 18.6 m. A problem occurs with the definition of the direction of wind direction. Oceanographers work with compass angles

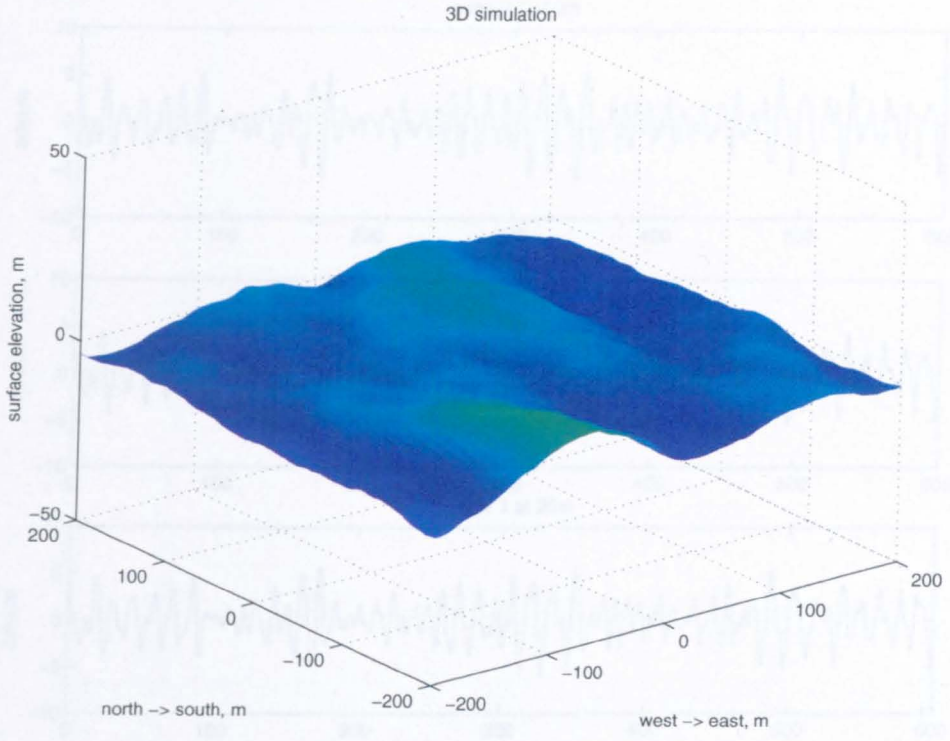


Figure 3.7: Screen grab of animated wave model output

i.e. $0^o$ being due north and the angle increasing clockwise. Mathematically it is simpler to work in a cartesian co-ordinate system with $0^o$ being directed along the positive x-axis and the angles increasing anticlockwise towards the positive y-axis. For the prediction problem it is simpler to think of everything in terms of the cartesian system as complications with the re-scaling of axes can easily lead to errors. If real wave data had became available it would have had to have been re-organised to fit the cartesian system and any results again transformed back to the compass system.

The other output available is in terms of a time series which is generated for a set of x-y points and given in a separate file. This is provisionally termed a wave staff file as it mirrors the data that would be recorded by a fixed wave staff or wave gauge (Chapter 4). This method is faster than making the full calculations for the animated model. It also allows the flexibility of being able to obtain a wave record for any point you desire. Fig 3.8 shows three examples of the time series produced by this method.

### 3.3.3 Input wave-field files

In order to run the wave model a file containing wave vector details is required. Three levels of complexity in the generation of this file exist.

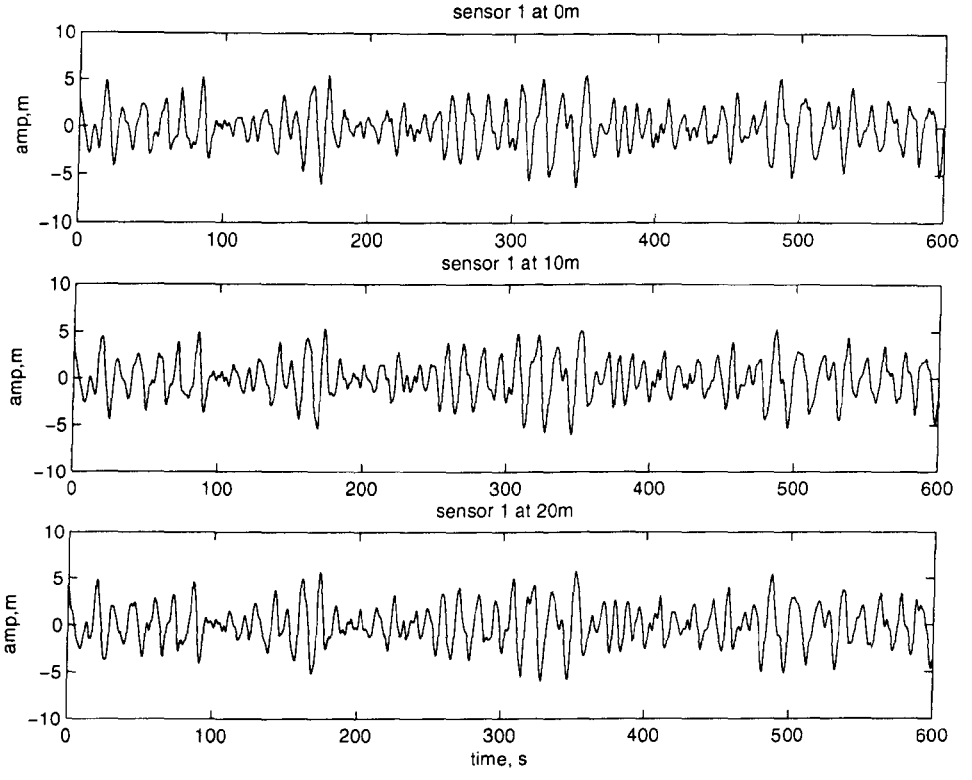


Figure 3.8: Three time series taken at 10 m intervals

### Manual input

This is the simplest input case where the desired wave frequency, amplitude and direction of propagation are given as the input to a text file. The information from this file is used to generate the additional wave vector parameters using the following equations.

$$\omega = 2\pi f \tag{3.51}$$

$$T = 1/f \tag{3.52}$$

$$\lambda = \frac{gT^2}{2\pi} \tag{3.53}$$

$$k = 2\pi/\lambda \tag{3.54}$$

$$c_p = \omega/k \tag{3.55}$$

A correction is made to the $k$, $c_p$ and $\lambda$ parameters based on a value for depth. As indicated in Chapter 2, the depth of water over which the waves are propagating affects the shape of the wave as dictated by the dispersion relationship (Eq. 2.25). The correction to the parameters is brought about through an iteration loop. These parameters are subsequently written to a separate text file to be used as inputs to the wave model.

The primary purpose of this file is for testing various routines where a single wave in a

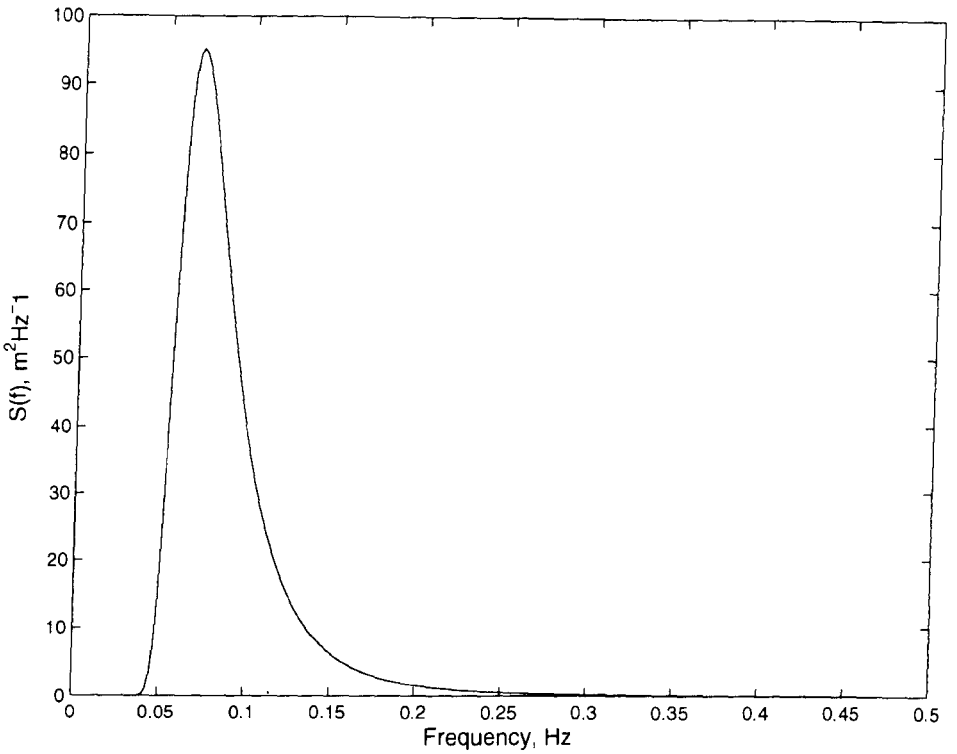


Figure 3.9: Pierson-Moskowitz spectrum for a 18.6 $ms^{-1}$ wind

prescribed direction is required. An example would be in the diagnostic testing of directional wave buoy code where a single frequency wave vector can be used to check the correlation between two time series.

### Omnidirectional input

In order to make the simulation of wave behaviour more realistic the spectra discussed in Section 3.2.2 must be simulated. Any of the spectra may be used but only the Pierson-Moskowitz formulation is available at this time (Eq. 3.56) where

$$S(f) = \alpha_{PM} g^2 (2\pi)^{-4} f^{-5} exp\left[-\beta(f_0/f)^4\right] \tag{3.56}$$

In addition to the wind speed and direction, the required number of frequency terms between 0 and 0.5 Hz is also needed. The upper limit of 0.5 Hz is chosen here as wave measurement devices are seldom able to return useful results above this limit (Tucker [12]). With this information the frequency step $\Delta f$ can be calculated. The frequency information is then adjusted so that each frequency is given at the centre of a frequency band of width $\Delta f$.

An example of a Pierson Moskowitz spectrum with 100 frequency components is given

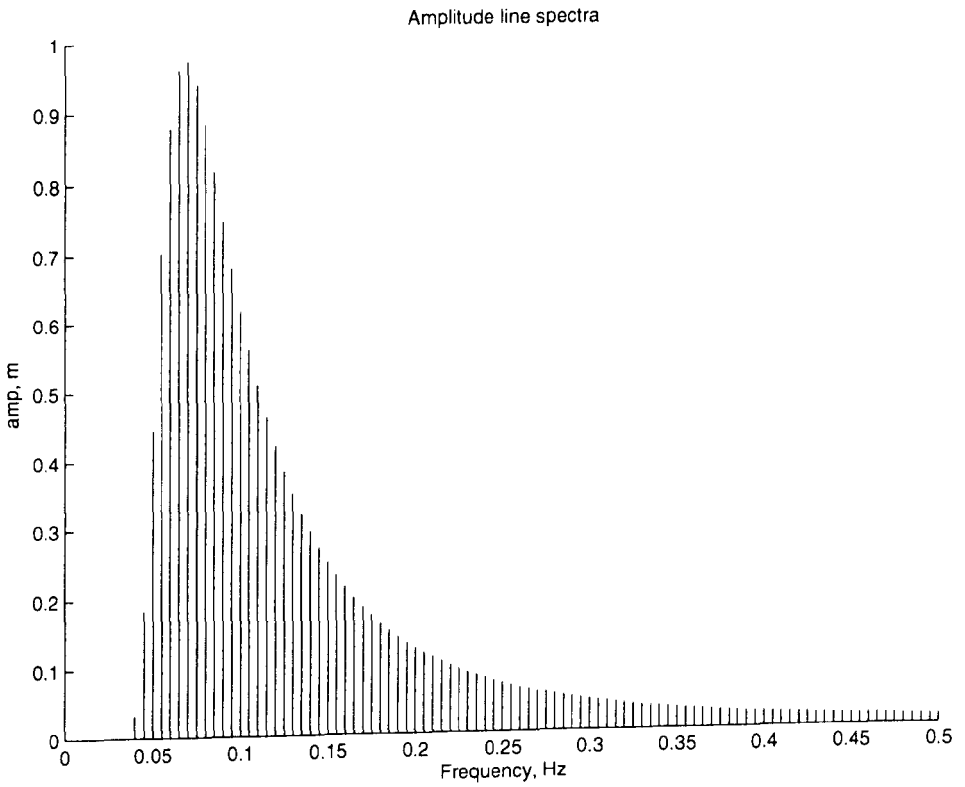


Figure 3.10: Amplitude line spectrum for a simulated P-M spectrum

in Fig. 3.9. To convert the spectrum values into amplitudes Eq. 3.57 is used:

$$a(f) = \sqrt{S(f)2\Delta f} \tag{3.57}$$

The line amplitude spectrum is shown in Fig. 3.10. The shape closely matches that of the original P-M spectrum.

Using the amplitude, frequency and wind direction parameters, the same equations that were used for the manual input file are invoked to produce the output file of wave vectors. Additionally, a random phase component is also calculated with a value between $\pm\pi$ for each wave vector. An example of this spectrum as simulated is shown in Fig. 3.11. To provide a means of comparing the spectral characteristics of the wave records, the spectral moments of the input spectra (Eq. 3.58) are calculated from $m^{-2}$ to $m^4$ and stored along with some time period characteristics where:

$$m^n = \sum^{M} f(m)^n S(f(m)) m \Delta f \tag{3.58}$$

Unfortunately, for discrete spectra, only the lower moments can accurately be calculated so that the significant wave height $H_{m0}$, integral period $T_I$ and energy period $T_E$ are the parameters available for comparison.

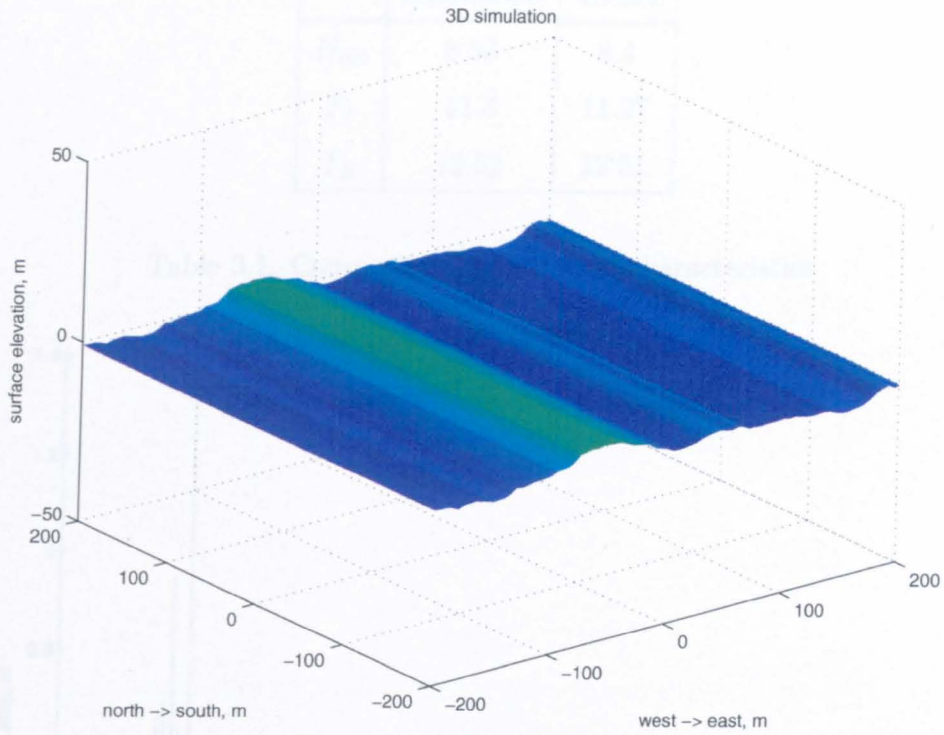


Figure 3.11: Animation screen for an omni wave file

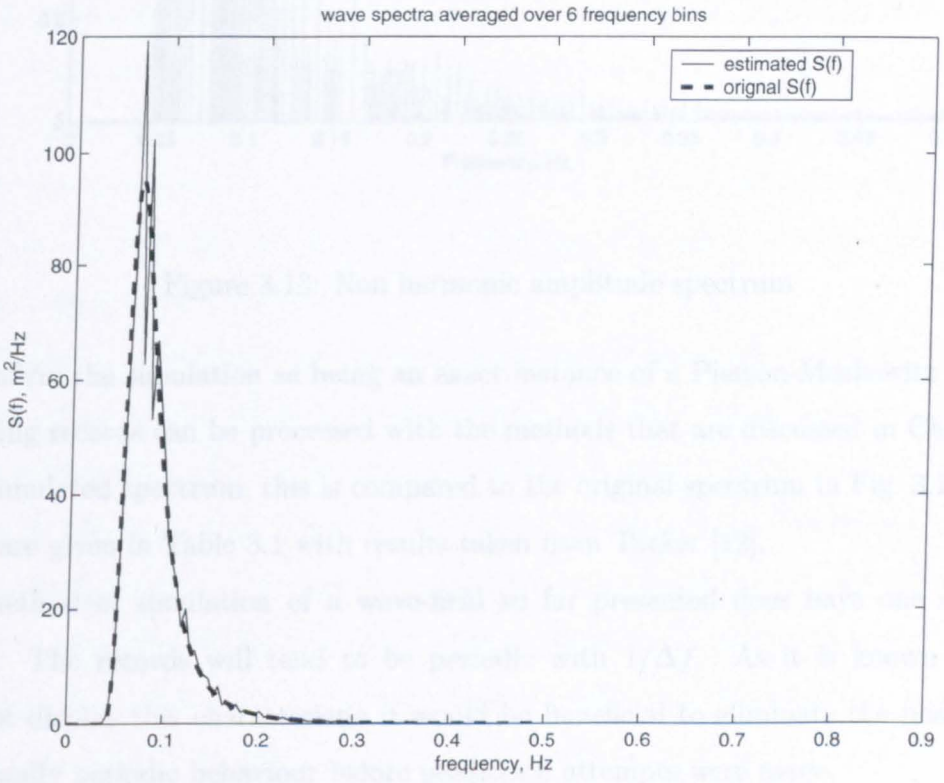


Figure 3.12: Comparison of simulated spectrum to the original.

| | Simulation | Tucker |
|---|---|---|
| $H_{m0}$ | 8.53 | 8.4 |
| $T_l$ | 11.3 | 11.27 |
| $T_E$ | 12.52 | 12.51 |

Table 3.1: Comparison of statistical characteristics

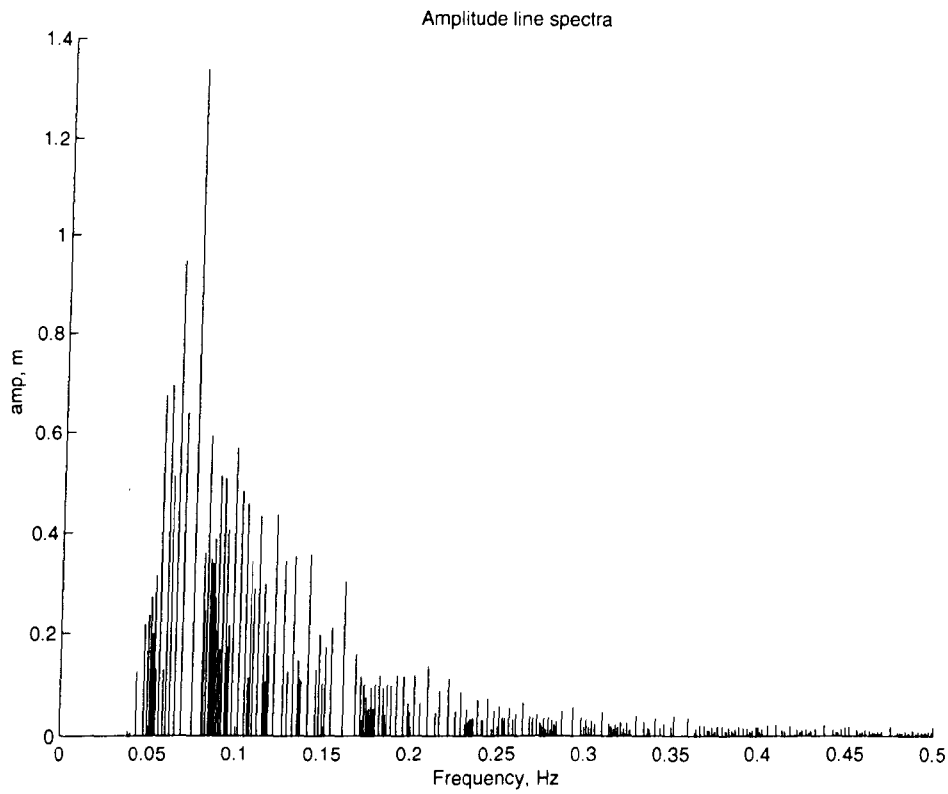


Figure 3.13: Non harmonic amplitude spectrum

To confirm the simulation as being an exact instance of a Pierson-Moskowitz spectrum, the resulting records can be processed with the methods that are discussed in Chapter 5 to give the simulated spectrum, this is compared to the original spectrum in Fig. 3.12 and the moments are given in Table 3.1 with results taken from Tucker [12].

The method of simulation of a wave-field so far presented does have one significant drawback. The records will tend to be periodic with $1/\Delta f$. As it is known that real seas do not display this characteristic it would be beneficial to eliminate the possibility of unintentionally periodic behaviour before prediction attempts were made.

Instead of using wave vectors spaced at $n\Delta f$ a random spacing would hopefully eliminate the periodic nature of the final records. For example, 99 uniformly distributed random

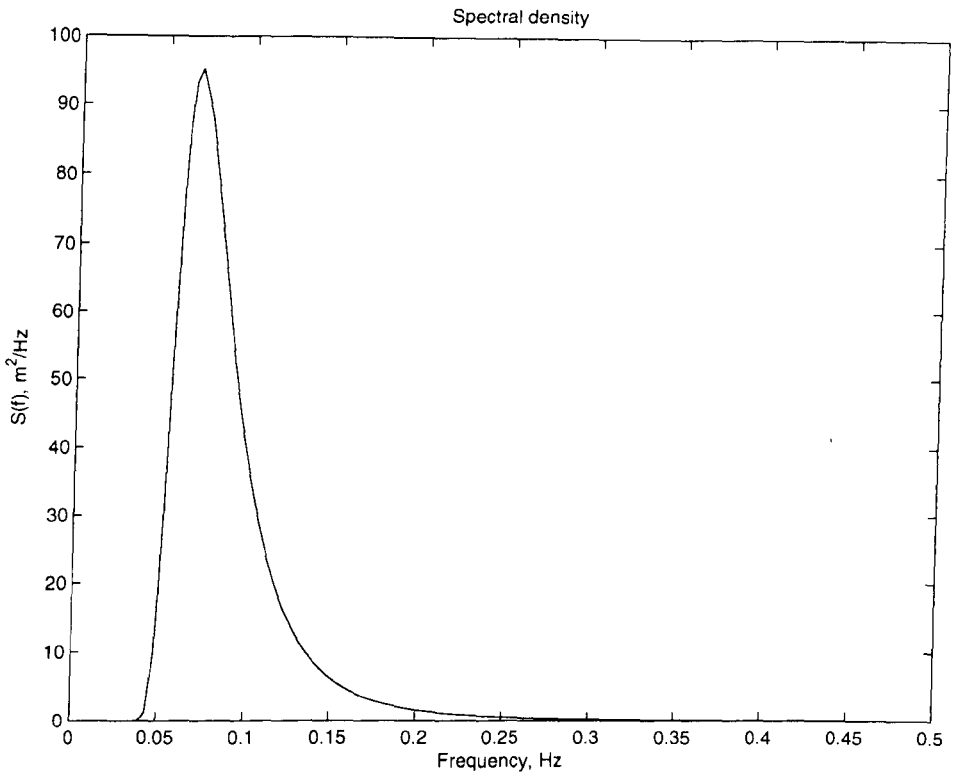


Figure 3.14: Non Harmonic spectral density

numbers are generated in the range 0 to 0.5 Hz; 0.5 is added to these numbers to ensure an upper limit and they are placed in ascending numerical order. The distance between each frequency is then calculated to give a series of 100 randomly-spaced $\Delta f_n$ values. The centre of each of these new frequency bins (a frequency band $\Delta f_n$) is found, giving the two desired series: a random normally-distributed series of frequencies and the width of the frequency bin corresponding to each frequency.

The amplitude of each frequency bin must be proportionate to the energy contained in the range of the wave spectra which it is to represent. The basic equation $a_n = \sqrt{S(f_n)2\Delta f_n}$ gives this relationship. Fig. 3.13 shows the randomly spaced nature of the frequencies. Previously, as shown in Figs. 3.9 and 3.10, the amplitude spectra can be seen to exactly match the shape of $S(f)$. This was due to the harmonic nature of the chosen frequencies. The new representation shows that there is more variation in amplitude from $S(f)$ whilst still retaining the overall shape. In places where the wave vectors are more densely packed in frequency the amplitudes are correspondingly reduced to maintain the energy in that part of the spectrum.

Fig. 3.15 shows the time series produced by using this non-harmonic method. It can be seen that the series is no longer periodic but the spectrum derived from this time series is of

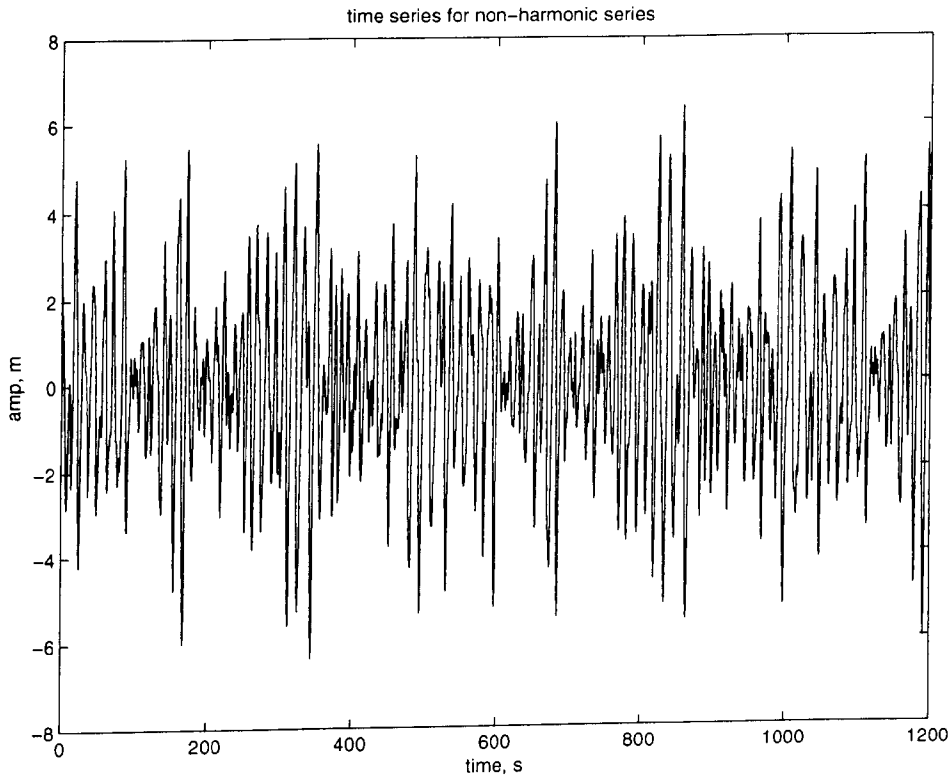


Figure 3.15: Time series for non harmonic simulation

the same order of magnitude and shape as the original, the comparison between the original and simulated spectra are shown in Fig. 3.16.

### Directional input

The next level of sophistication in the model is to generate simulations for a full directional sea implementing the equations from Section 3.2.3. This is achieved by a two-stage process. First of all the omni-directional spectrum is calculated; this is a P-M spectrum. The directional spreading function $D(\theta, f)$ is calculated separately. In this instance, the Mitsuyasu [37] equations are used to calculate the spreading function and the cosine power model, proposed by Cartwright [39] is utilised. The spectrum is multiplied by the directional spreading function and all of the wave vectors are calculated using Eqs. 3.51. An example of the directional spectrum as an animation was shown in Fig. 3.7. To prove this has no effect on the original spectrum, the time series at a chosen point was again analysed, Fig. 3.17 shows a comparison between the original omni-directional spectrum and one recovered from a directional sea simulation. There is a discrepancy, with the large spike at 0.8 Hz, but if the area under both graphs is considered, the total energies would appear to be similar.

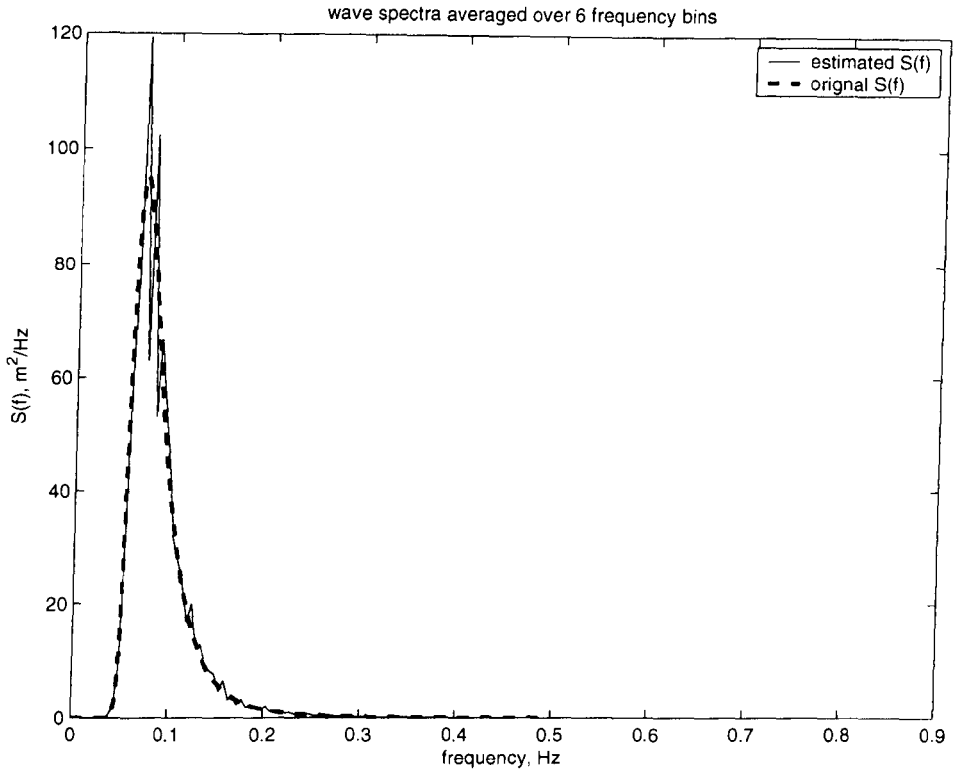


Figure 3.16: Comparison of spectra for the non harmonic P-M spectra

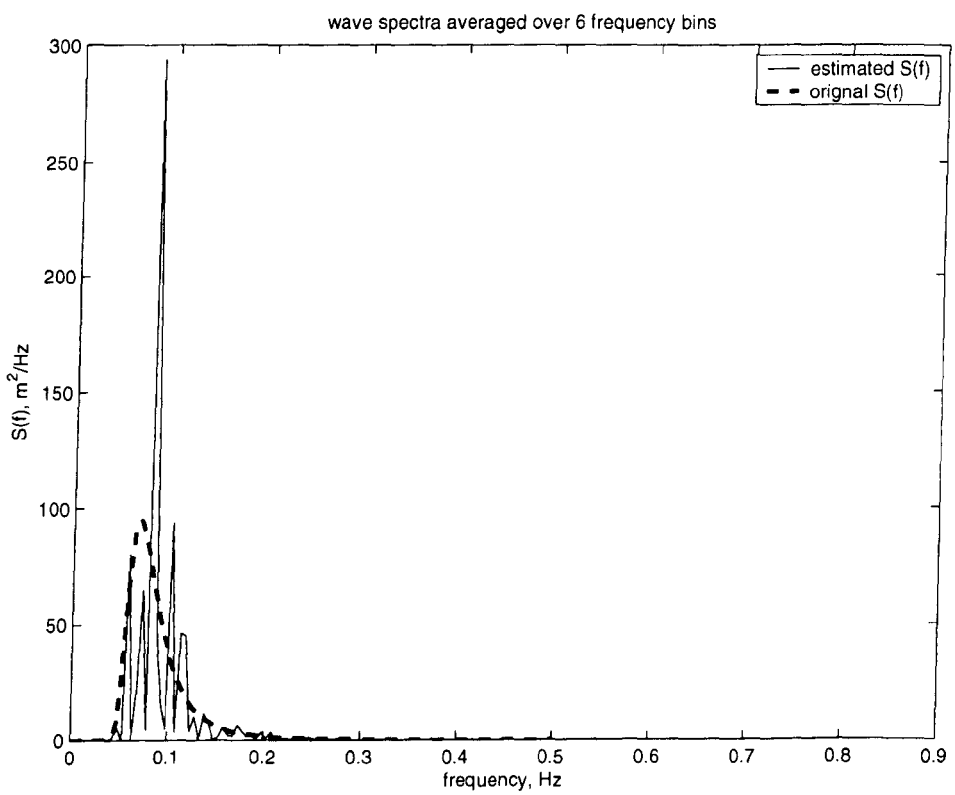


Figure 3.17: Comparison of spectra for the harmonic directional case.

The non-harmonic version of this input file is also available. This follows the same procedure as for the onmi-directional input file.

### Superposed inputs

For creating real directional seas, the superposition of several local and swell sea states could be used. It is proposed that this may be possible, however there may be an issue here. In adding multiple seas together, it is highly likely that some frequency/direction bins will hold more energy than can be supported and it will have to be dissipated to other areas of the spectrum. In the real sea this would occur through white capping and wave breaking. Further research is required to model this.

# Chapter 4

# Measurement Technology

The usefulness of a prediction of wave behaviour in the short-term will ultimately stand or fall on the available wave data. In real operational circumstances this data is obtained from wave measurement devices. This chapter aims to present the available measurement equipment and briefly describe the methods used for conditioning and presenting wave data. Devices used for omni-directional measurements will be presented first. The directional equipment will then be detailed and a discussion of specific problems associated with the prediction problem will conclude the chapter.

## 4.1 Omnidirectional wave measurement

The ultimate aim of all of these devices is to make a recording of surface elevation or some derived parameter for a fixed point. From this time series recording a wave spectrum and the spectral characteristics can be calculated (see Chapter 5). The parameters can then be used to fit one of the general spectra (as given in Chapter 3).

### 4.1.1 Fixed measurement

These devices are generally known as wave staffs. They are commonly mounted on an available structure such as an oil platform or where the resultant data merits the building of a special structure. One issue with these devices is that they must be mounted at least 10 m away from any sizeable structure, such as the solid base of an oil rig, since reflected wave energy can interfere with records.

#### Stepped-contact staffs

These are an early form of device. A series of electrodes is mounted on the staff at vertical intervals. As the sea surface rises it successively shorts out the electrodes, as it falls they become open-circuit. Errors are common due to sea-water making a film over the electrodes.

#### Resistance-wire staffs

With these devices two parallel wires are stretched vertically a fixed distance apart. The sea shorts across the bottom of the wires, so that the resistance across the top terminals changes linearly with the wave elevation. Another variation is to coil a wire around an insulating rod. The problem of film forming also occurs in this case. They can be effectively used in model tanks as they can be cleaned prior to use.

#### Capacitance-wire gauges

In this method a single wire is stretched vertically through the water looped under a structure then returned to the surface. The capacitance between the two ends of the wire is then measured. Again a film will form over the wires and they can become fowled with sea weed and other bio-organic material.

#### The Baylor wave gauge

This consists of two vertical parallel steel wire ropes stretched under tension through the sea-surface. They form an electrical transmission line terminated at its lower end by the sea. The impedance of this line is measured at a fixed frequency and transformed to an implied wave height. They are widely used on oil rigs but are often struck by supply boats as they need to be moored well away from the platform.

### 4.1.2 Sub-surface sensors

This family of sensor design can be mounted on the sea-bed but it is more usual for them to be mounted on platforms or surface-piercing piles for ease of maintenance. They can be self contained, with data stored and recovered from the device, or shore-connected via a cable. Shore connection is the preferred method to prevent loss of data due to malfunction or damage.

#### Pressure sensors

The pressure at a fixed point under a wave system fluctuates in phase with the waves, the relationship is given in Eq. 2.26. The pressure oscillation decreases with increasing depth (while the mean pressure increases). This attenuation leads to a loss of accuracy for higher frequencies and the data must be compensated for this. There is much disagreement as to the manner of compensation, Massel [22] gives a brief overview of the discussion.

#### Inverted echo-sounders

Installing an echo-sounder looking upwards would initially seem like a good idea. These devices have been suggested from time to time but suffer from a major flaw. A storm will cause the sea to aerate and distort the signal reflected back to the device rendering them of little use.

#### Particle velocity meters

In principle, a horizontal current meter can be used to measure the orbital wave particle velocities and then convert them to surface elevation. But the data cannot easily be converted to wave elevation if there is significant spread of wave direction (Tucker [12]). However if combined with a wave gauge it can be used as a viable method for directional wave measurement.

### 4.1.3 Sensors in buoys

The devices in this chapter have so far had the specific siting requirements of either requiring a structure, as in the case of staffs, or having a limitation to depth, as in the case of sub-surface devices. For offshore applications where there are no structures available or the depth of water is too great, buoy devices are almost universally chosen.

#### Accelerometer buoys

A small buoy (roughly 2 m in diameter), floating on the surface of the sea will tend to move with the same elevation as the waves. Commonly these have a flat response to 0.5 Hz. If the vertical acceleration of the buoy is recorded it can be integrated twice to give the elevation. The data can then be transferred to shore by radio telemetry or to a service vessel or oil platform.

The basic problem with this type of accelerometer is mounting it so that it stays vertical. There are only two practical options available: inertial stabilisation (usually by means of a gyroscope), or mounting the accelerometer on a short-period pendulum or its equivalent, which allows it to adjust to the apparent vertical.

Gyros are not practicable on a small battery-powered buoy because too much power is drawn. The alternative is to suspend the accelerometer on a heavy horizontal disc in a sphere of fluid. The compound pendulum formed by the water and the disc is adjusted to have a natural period of 40 or 120 sec which does not tilt significantly at wave frequencies and its axis stays effectively vertical. The acceleration is then integrated twice to give the surface elevation.

Double integration corresponds to multiplying the frequency spectrum by $1/\omega^4$ ($= -1/\omega^2$ in amplitude). Hence, any low frequency noise is amplified which leads to large drifts in the time-history unless it is filtered out.

The buoys must be moored securely but in a way that allows them to rise and fall with the highest waves to be measured (which may exceed 30 m crest-to-trough in exposed UK waters). An important part of the mooring is to use a 15 m length of rubber cord which can stretch, but this may not have enough give so the mooring must be arranged to be flexible also. This is commonly achieved by using a floater and sinker arrangement. Allender *et al* [41] found evidence that the Waverider, and other buoys with similar moorings, under-record the very highest waves, either by being dragged through the crests or by going around them. There was also evidence that they can overturn temporarily in one or two of the highest waves.

### Spar buoys

The general concept of this type of buoy is of a buoyant cylindrical spar riding vertically in the water with a heavy weight or damper plate at its lower end. Neglecting viscosity, the only vertical force that can act on the spar is the pressure on its bottom face. If this is deep enough to be below the action of the waves, the spar will not rise and fall. Such buoys have to be in the region of 100 m long, with a correspondingly large diameter to make them strong. Therefore these are major projects.

### 4.1.4 Shipborne systems

These were the first systems to produce reliable recordings. They were mounted inside weather ships and provided good data of wave elevation during storms. Many of the major spectral formulations originated from these recordings.

Two sensor boxes were mounted symmetrically on either side of a ship. Each contained a vertical accelerometer on a critically-damped short-period pendulum, and a pressure sensor connected to the sea through a hole in the side of the ship. The accelerometer outputs were each integrated twice and added to the corresponding pressure signals giving, in each case, the surface elevation relative to a fixed horizontal plane.

### 4.1.5 Omni-directional parameter extraction

A common characteristic of all the measurement devices so far described are the discrepancies between their recorded signals and the real sea-state they are attempting to measure. The time series from each device must be corrected to account for these apparent errors before meaningful use. As pressure sensors are most affected and commonly used, the correction methods for these devices are now described.

#### Pressure sensor correction

The pressure sensor response is adversely affected at high frequency depending on the depth at which they are sited. To a certain extent, this can be corrected by Fourier Transform Filtering. The point at which the correction to the frequency exceeds a multiplication factor of 5 is, generally, the limiting point since, above this factor, the noise from the sensor, rather than any data, will tend to be amplified.

Other sources of noise can also affect these sensors, namely:

**Digitisation noise** The lowest precision bit can represent a significant error at the higher frequencies due to the range that must be covered.

**Wave harmonics** In a local-wind sea, non-linearity causes much whitecapping. The harmonics associated with these waves are due to their fundamental having a longer wavelength than their free-wave equivalents. This leads to reinforcing of the recorded higher frequencies.

**Dynamic pressures** This depends on the design of the housing for the pressure sensor. The dynamic pressure fluctuation due to local orbital velocities can adversely affect

the wave record.

**Doppler effects** These are due to tidal and other currents. The frequency measurements due to these effects are related to the classic dispersion relationship.

Corrections methods exist for all of these problems and are discussed in Tucker [12].

### Available parameters

After correction to the recorded time series for instrumental problems, the most common method of analysis is to take the FFT of a time series to create the spectrum and spectral moments. This process is given in Chapter 5.

An early method of parameter extraction was introduced by Cartwright [42] and developed by Tucker [19] and Draper [43]. For a wave record, the mean level is drawn in by hand and the number of zero-crossing waves $N_z$ counted. The length of the record is then divided by $N_z$ to give the zero crossing period $T_z$.

The two highest peaks and two lowest troughs are identified and measured by hand and termed $A$,$B$,$C$ and $D$. Let

$$\begin{aligned} H_1 &= A - C \\ H_2 &= B - D \end{aligned}$$

Cartwright went on to show that

$$H_1 = 2(2m_0\alpha)^{\frac{1}{2}}(1 + 0.289\alpha_{-1} - 0.247\alpha_{-2}) \tag{4.1}$$

$$H_2 = 2(2m_0\alpha)^{\frac{1}{2}}(1 + -0.211\alpha_{-1} - 0.103\alpha_{-2}) \tag{4.2}$$

where $\alpha = N_z$ and $m_0$ is the mean-square surface displacement (zero spectral moment). From these $H_{m0}$ can be found as usual from

$$H_{m0} = 4\sqrt{m_0} \tag{4.3}$$

An additional method for calculating spectral moments from the time series rather than spectra is given in Massel [22]. Suppose the time series consisted of $N$ samples of a series $\zeta(n\Delta t)$. The $n^{\text{th}}$ spectral moment can be calculated from

$$m_n = \frac{1}{N}\sum_{k=1}^{N}(\zeta(k) - \bar{\zeta})^n \tag{4.4}$$

where $\bar{\zeta}$ is the mean of the record. From this definition the first central moment or the mean value is given by

$$\mu_1 = \bar{\zeta} = \frac{1}{N}\sum_{n=1}^{N}\zeta_n \tag{4.5}$$

The second central moment or standard deviation which gives the concentration of energy about the mean frequency is

$$\mu_2 = \sigma_\zeta = \left[\frac{1}{N-1}\sum_{n=1}^{N}\left(\zeta_n - \bar{\zeta}\right)^2\right]^{\frac{1}{2}} \tag{4.6}$$

The third and fourth central moments can also be given by

$$\mu_3 = \frac{N^2}{(N-1)(N-2)}m_3 \tag{4.7}$$

$$\mu_4 = \frac{N(N^2-2N+3)m_4 - 3N(2N-3)m_2^2}{(N-1)(N-2)(N-3)} \tag{4.8}$$

From these equations the general spectrum parameters given in Chapter 2 can be derived. An additional parameter not yet defined is the measure of bandwidth. The most commonly used definition is

$$\nu = \left(\frac{m_0 m_2}{m_1^2} - 1\right)^{\frac{1}{2}} \tag{4.9}$$

which is the normalised radius of gyration of the spectrum about its mean frequency $f_1$. In physical terms imagine forming the spectrum shape from a laminar sheet again. The moment of inertia about the axis $f = 0$ is $m_2$. The moment of inertia about the mean frequency $f_1$, i.e., the centre of gravity, is $m_2 - f_1^2 m_0$.

For very narrow bandwidths $\nu \leftarrow 0$; for the Pierson-Moskowitz spectrum $\nu = 0.425$ and for the JONSWAP spectrum, with the parameters given in Section 3.2.2, $\nu = 0.39$.

Another useful parameter is the wave steepness which is defined as the crest-to-trough height/wavelength and for a low amplitude sinusoid is given by

$$S = \frac{2\pi h}{gT^2} \tag{4.10}$$

For fully developed sea states, the formulation can be approximated to

$$S_s = \frac{2\pi H_{m_0}}{gT_z^2} \tag{4.11}$$

The time series recorded by a device can also be fitted to one of the general spectra through use of its derived spectral moments. Tucker [12] details these methods. This is usually done to allow a hypothesis of spectrum development to be verified. Or, in other cases, spectra can be fitted to a time series in order to determine if multiple sea states are

present. If the spectrum for a local wind sea can be found and fitted it can be used to filter this energy from a sea state to leave behind a possible swell sea.

In the case of wave prediction this method of spectrum fitting for local seas may prove beneficial because it can be filtered out leaving the more powerful swell data.

## 4.2 Directional measurement

Directional measurement devices do not produce results which are immediately useful. They instead produce time-series of wave elevations, accelerations, surface tilts, etc. These outputs are filtered into frequency bands and then the wave energy in each of these bands is distributed according to its direction of travel. Recalling that the full directional spectrum is

$$S(f,\theta) = S(f)G(f,\theta) \tag{4.12}$$

where $S(f)$ is the omni-directional spectrum and $G(f,\theta)$ expresses how the energy at frequency $f$ is distributed by direction of travel.

There are generally two ways in which time series for constructing the directional wave spectra are measured. In the first case, a number of variables are measured at a point, e.g., the pitch, the roll and heave of a surface following buoy, or the pressure and the two horizontal components of the particle velocity. The second procedure is to use an array of devices to measure surface elevations.

### 4.2.1 Triple point measurements

The term 'point measurement' includes buoys which are free to move with the wave particle displacements, and closely-spaced arrays which effectively measure gradients of pressure or the rate of change of the wave slope. Apart from the clover-leaf buoy (Section 4.2.2), these devices all measure variables along 3 axes in space $(x, y, z)$, although these may not necessarily be the same variable: for example, it is common practice to measure the elevation of the sea surface or pressure in the $z$-axis and the two components of the horizontal particle velocity. All these combinations use the same basic method of analysis. Hence, they all give the point spectrum $S(f)$ plus two of the components of the first two angular harmonics of $G(f,\theta)$.

The full theory on how the directional information is derived will be presented in Section 4.3.2, but a quick explanation using a pitch-roll-heave buoy will be useful before de-

scribing the devices themselves. Defining pitch as the north-south tilt of the buoy and roll as its east-west tilt, if an omnidirectional wave is coming from the west, the buoy will roll but not pitch. The roll angle will lag behind the heave displacement by a quarter of a cycle, or $\pi/2$ in phase. If it is coming from the east, the roll will lead the heave by $\pi/2$. Thus, the buoy can distinguish between positive and negative directions of travel.

An omnidirectional wave coming from slightly south of west will cause pitching and rolling in phase with one another. They will both lag the heave by $\pi/2$, but be 100 % coherent with it in this simple case, i.e., they will have the same waveform but be displaced in phase. A wave coming from slightly north of west will cause pitching in antiphase with the roll. The pitch will now lead the heave by $\pi/2$. If all three wave trains are coming at the same time there will be pitching, but it will not have a coherent phase relationship with the roll. The coherence between pitch and heave will also be zero, but that between roll and heave will still be high.

It can be seen that in broad terms, directional information is contained in the coherences and in the relative amplitudes and phases of the signals. These are measured by the auto and cross power spectra (defined in Chapter 5). In Section 4.3.2 it will be shown that the data recovered leads to an estimate of the amplitudes and phases of the first two angular harmonics of the spectrum, which in turn can be interpreted to give measures of mean direction and angular spread.

The same type of directional information can be obtained by other combinations of sensors. Allender et al [41] used a surface wave staff with current meters at its base. These measured the two horizontal components of water particle velocity as part of the WADIC project. The surface staff gives $S(f)$, and the attenuation of the short waves with depth does not affect the directional information that can be recovered from the current meters since noise will mask these. Another possible combination, that could be used for a coastal application, is to replace the wave staff with a pressure gauge and retain the two-component horizontal current meter.

### Spatial arrays

These devices are commonly used in shallow water or where a suitable structure is available. They can provide good approximations of directional spreading functions. The basic principle is to place the sensors in a line parallel to the shore with the maximum distance between the sensor equivalent to half the minimum wavelength of interest. By delaying and sum-

ming the records from the sensors the effective direction from which the waves (of a specific frequency) are arriving can be derived. The process is similar to that used in beam-forming radio astromony and a small section of Chapter 6 details some experiments.

Another method, more in common with the methods to be discussed later, is to place three or more sensors comparatively close together in a triangular pattern. For long waves, these can be thought of as giving the wave elevation and two components of wave slope. Hence, the outputs are similar in nature to those of the pitch-roll-heave buoys, and they are analysed in terms of the angular harmonics of a directional spectrum.

In principle, offshore multi-element arrays could be used in a manner similar to that described above for shoreline applications. A significant drawback to this method would be in mooring all the sensors required since sea bed mounted sensors would not be sufficiently accurate and the building of many structures for mounting wave staffs would be prohibitively expensive.

### 4.2.2 Surface following buoys

In general there are two principal approaches in common use for surface following buoys, i.e., buoys that follow the surface slope (pitch-roll-heave, or PRH buoys), and buoys that follow the orbit of the water particles in the sea surface. The later category divides into two classes: buoys that contain a triaxial accelerometer, and buoys that use signals from GPS satellites to measure velocity or displacement in three dimensions.

In the report on the WADIC project, Allender et al [41] found that particle-following buoys performed more satisfactorily in practice than PRH buoys. There are a number of reasons for this: they are cheaper, the mooring problems are more straightforward, and the buoys are more robust, smaller and easier to handle. Because they are smaller, they have a better high-frequency response; and because of their spherical shape, they are not so easily overturned by steep waves.

As discussed in Section 4.1.3, the main technical difficulty with all buoy measurement lies in providing a reference to the true vertical in a self-contained buoy with limited power availability (ruling out conventional gyroscopes). Until recently the metal-platform-in-fluid arrangement has been the only satisfactory device available. However, recently, angular-rate measuring devices have become cheap, accurate, robust and more compact with low power requirements, to the point where they have become a practical alternative. Also the advent of GPS technology has led to further developments in reducing the size and complexity of

on-board equipment.

### Pitch-Roll-Heave buoys

This class of buoy follows the surface slope, with their pitch, roll angles and the heave acceleration being measured. These were the first directional buoys to be developed [44]. In early deployments the buoys were attached to a ship by a cable and used a gyroscope for the vertical reference. It was a long time before a satisfactory sensor, which could be used in a self-contained buoy, was developed. This was the Wavec sensor which was described in an earlier section as a pendulum suspended in a sphere of fluid. The problems with the sensor are found in it's transportation, and if subjected to sudden shocks by large waves the pendulum will become resonant which will take some time to settle down again (Allender et al [41]).

PRH buoys must follow the water surface in heave as accurately as possible in order to give an accurate measure of $S(f)$. The heave response is affected by the shape of the buoy and the force of the mooring. Corrections of the response of the buoy are possible and can increase the accuracy of heave records for wavelengths which are similar to the diameter of the buoy (Steele et al [45]).

The tilt response of the buoy is not as critical as the heave response. As long as this is the same in all directions, the data processing system can be arranged so that the directional spectral parameters are independent of it (Section 4.3.2). However, if a buoy has an asymmetrical response it will degrade the directional spectrum. This can also occur due to the presence of drift forces caused by wind or currents. Various manufacturers have developed their own mooring designs to compensate for this.

### Triaxial accelerometer buoys

This buoy takes the form a sphere 900 mm in diameter moored in the same way as an ordinary omnidirectional device, and no attempt is made to keep its mean water level parallel to the water surface. At frequency wavelengths lower than its diameter it follows the motion of the water it displaces, but the mooring stops it following slow drift. A Hippy sensor, a common name for the floating pendulum arrangement, contains an inertial-stabilised platform carrying a vertical accelerometer. This accelerometer acts in the same way as an ordinary buoy and measures the true vertical acceleration. The pitch and roll of the buoy along two axes is also measured relative to the stable platform. A compass is fixed to the buoy hull and

is used to mathematically rotate the pitch and roll angles to give the magnetic components in the true horizontal, and hence the correct direction of magnetic north.

A two-axis "horizontal" accelerometer is fixed to the buoy and again, using the pitch and roll angles and the measured vertical acceleration, the accelerations in the true horizontal are calculated. These are then rotated about a vertical axis to give the N-S and E-W components of acceleration. These three acceleration signals can then be treated in the same way as described for the PRH buoys in Section 4.3.2.

The Hippy sensor, as mentioned earlier, is sensitive to sudden shocks and is expensive. Steele et al [46] experimented with replacing the hippy senor with angular velocity sensors arranged in three orthogonal axes. The signals from these three sensors can be integrated to give angular displacements which are used to rotate the 2-axis accelerometer axes into fixed axes. As before, the same process is followed with the compass outputs to calculate the north-south and east-west accelerations. This system has been developed by the Norwegian firm Seatex as their "Motion Reference Unit" (MRU-6), and more details of it are given by Krogstad *et al* [47].

### GPS buoys

A relatively recent improvement has been the development of the satellite-based Global Positioning System (GPS) to a sufficient accuracy such that, when used differentially to measure a 3-dimensional position, an accuracy of 10 cm or less can be achieved (Krogstad *et al* [47]). Very compact and low power consumption GPS location sets are now available. In practice, instead of trying to fix the absolute position, the Doppler shifts of the carrier signals are used to compute the buoy velocities and hence acceleration along three axes. The standard breakdown analysis for the directional spectrum can then be modified to use these signals. This new technology has reduced the size of the buoy to 800 mm and weight to 80 kg allowing for deployment from small research vessels.

### Clover-leaf buoys

The "clover-leaf buoy" is a long-established and successful system for research into recording and deriving directional information. It was developed by Cartwright and Smith [44]. In this device, three buoyant discs 1 m in diameter are mounted to a triangular framework with their centres forming an equilateral triangle of side 2 m. The joints to the frame are fitted with sensors measuring the two components of tilt relative to the frame, so that the

differences in these give the three components of curvature. If $\zeta_x(A)$ and $\zeta_y(A)$ are the tilts of buoy A relative to the frame (and so on with the other buoys), then the three curvatures are estimated (in radians/meter) using

$$\begin{aligned} \zeta_{xx} &= [2\zeta_x(A) - \zeta_x(B) - \zeta_x(C)]/2\sqrt{3} \\ \zeta_y &= [\zeta_y(C) - \zeta_y(B)]/2 \\ \zeta_{xy} &= [\zeta_x(C) - \zeta_x(B)]/2 \end{aligned} \tag{4.13}$$

where $\zeta_{xx} = d^2\zeta/dx^2$ and $\zeta_{xy} = d^2\zeta/dxdy$ etc.

At the centre of the buoy is a gyro-stabilised vertical accelerometer and a pair of tilt sensors giving the roll and pitch angles of the buoy as a whole. A compass gives the buoy's heading and this is suspended in a frame above it using gimbals. The slopes and curvatures are converted to north-south and east-west components using this compass as the first stage of processing. Due to the small size of the device the differences in slope are quite small and data can be easily lost.

## 4.3 Directional information extraction

The first attempts to derive directional information and spectra from data buoys were conducted by Cartwright et al. [39]. This classic method is described in this section along with the problems that can occur during its implementation.

### 4.3.1 Angular harmonics

The directional spreading function, introduced in Chapter 3, can be described by the angular harmonics of a Fourier series

$$G(\theta, f) = \frac{1}{\pi}\left\{\frac{1}{2} + \sum_{n=1}^{\infty}[A_n(f)\cos n\theta + B_n(f)\sin n\theta]\right\} \tag{4.14}$$

which has a period of $2\pi$ and the angular harmonics are given by

$$A_n(f) = \int_{-\pi}^{\pi} G(\theta, f)\cos n\theta d\theta \tag{4.15}$$

$$B_n(f) = \int_{-\pi}^{\pi} G(\theta, f)\sin n\theta d\theta \tag{4.16}$$

$$\tag{4.17}$$

Cartwright et al. [39] showed that by using the pitch, roll and heave parameters of a directional wave buoy the first five harmonics could be recovered.

### 4.3.2 Method

Suppose the recordings of heave, $\zeta$, and the two slopes of a wave buoy, $\frac{\delta\zeta}{\delta x}$ and $\frac{\delta\zeta}{\delta y}$ , are available as time series so that

$$\zeta = \int_{-\infty}^{\infty}\int_{-\pi}^{\pi} A(\omega,\theta)\exp\left[jk(x\cos\theta + y\sin\theta) - j\omega t\right] d\omega d\theta \tag{4.18}$$

$$\frac{\delta\zeta}{\delta x} = \int_{-\infty}^{\infty}\int_{-\pi}^{\pi} jk\cos\theta A(\omega,\theta)\exp\left[jk(x\cos\theta + y\sin\theta) - j\omega t\right] d\omega d\theta \tag{4.19}$$

$$\frac{\delta\zeta}{\delta y} = \int_{-\infty}^{\infty}\int_{-\pi}^{\pi} jk\sin\theta A(\omega,\theta)\exp\left[jk(x\cos\theta + y\sin\theta) - j\omega t\right] d\omega d\theta \tag{4.20}$$

where $A(\omega,\theta)$ is an amplitude spectrum. Now denoting these in sequence from $1 \rightarrow 3$ the cross spectra of each combination can be made by following the procedure in Chapter 5.

Six of these spectra are of interest and their formulations are

$$C_{11} = \int_{-\pi}^{\pi} S(f,\theta)d\theta \tag{4.21}$$

$$C_{22} = \int_{-\pi}^{\pi} k^2\cos^2\theta S(f,\theta)d\theta \tag{4.22}$$

$$C_{32} = \int_{-\pi}^{\pi} k^2\sin^2\theta S(f,\theta)d\theta \tag{4.23}$$

$$C_{23} = \int_{-\pi}^{\pi} k^2\cos\theta\sin\theta S(f,\theta)d\theta \tag{4.24}$$

$$Q_{12} = \int_{-\pi}^{\pi} k\cos\theta S(f,\theta)d\theta \tag{4.25}$$

$$Q_{13} = \int_{-\pi}^{\pi} k\sin\theta S(f,\theta)d\theta \tag{4.26}$$

Cartwright et al. [39] then related these co-spectra equations to the Fourier representation of the directional spectrum and gave the equations of the first five harmonics as:

$$a_0 = \frac{1}{\pi}C_{11} \tag{4.27}$$

$$a_1 = \frac{1}{\pi k}Q_{12} \tag{4.28}$$

$$a_2 = \frac{1}{\pi k}Q_{13} \tag{4.29}$$

$$b_1 = \frac{1}{\pi k^2}(C_{22} - C_{33}) \tag{4.30}$$

$$b_2 = \frac{2}{\pi k^2}C_{23} \tag{4.31}$$

They then went on to show that an approximation to the original directional spectrum can be given in terms of these harmonics so that

$$S(f,\theta) = \frac{1}{2}a_0 + \frac{2}{3}(a_1\cos\theta + b_1\sin\theta) + \frac{1}{6}(a_2\cos 2\theta + b_2\sin 2\theta) \tag{4.32}$$

where the harmonic reconstruction has been weighted to remove the possibility of $S(f,\theta)$ becoming negative. Tucker [12] also presents formulae for the extraction of the mean wave direction $\theta_M$ and the spreading parameter $s$ as functions of the harmonics.

The DIWASP [48] toolkit, as developed for the MATLAB environment (discussed in the next section) was used to check the formulations and for ease of implementation of the method presented above. The results were less than satisfactory and, in addition, direct implementation of these equations has proved virtually intractable.

### 4.3.3 DIWASP toolkit

The DIWASP [48] toolkit is a set of MATLAB functions developed by the Coastal Oceanography Group at the University of Western Australia for use by oceanographers. The toolkit calculates directional spectra from time series using one of five implemented routines. The input data can be from any derived wave parameter: surface elevation, slope, particle velocity, pressure, etc. The raw data, sample rate, sensor position and depth are passed in as a structure and the spectra are calculated.

The estimation methods were tested with the same spectra as used in the previous section. The results were as follows:

**Direct Fourier Transform Method** This is the method described in the previous section. It is implemented very quickly but returns poor results.

**Extended Maximum Likelihood Method** This has a much better directional resolution than the DFTM, and is accurate to within $\pm 10^0$.

**Iterated Maximum Likelihood Method** This is much slower than the previous methods and it returns negative power at some frequencies which are much removed from those simulated.

**Extended Maximum Entropy Method** This works to the same accuracy as the EMLM but it is a little slower.

**Bayesian Direct Method** This returns very accurate results but it is very slow when attempting to run real time simulations

The manual for the software [48] and Massel [22] give further references to these methodologies. In later sections of this thesis, information about the directional spectra may be

required but only to the extent of obtaining a mean propagation direction for one to possibly three mixed wave fields. This information can be obtained quickly and to reasonable accuracy using the Extended Maximum Likelihood Method.

## 4.4 Measurement for prediction

The problem of choosing which type of device to use for the short term prediction of wave behaviour is governed by cost and accuracy. For a measurement to record an entirely accurate representation of the sea surface it should ideally be taken at a fixed location. A wave staff mounted on a fixed structure would give this record but the additional cost would likely out-weight the benefit of any prediction made. Similarly a LIDAR device mounted on a fixed structure or an airborne altimiter would give accurate readings from a fixed point but are also prohibitively expensive.

A bottom-mounted sensor would also provide a good fixed reference point recording, but at the depths where wave farms are likely to be situated, the resolution of these device outputs would deteriorate and correcting the measurements in the post processing of the data will induce amplification of instrumentation noise.

A practical solution is to use wave buoys which are relatively inexpensive to moor and have a reasonably high data return. However, they also have drawbacks as described in the next section.

### 4.4.1 Wave buoy vs wave staff

From the earlier discussion it should be obvious that measurements made by a fixed position wave staff and those made by a floating wave buoy will be different. In terms of prediction, the information returned by a wave staff, plus a current meter, would be ideal but since fixed structures are likely to be expensive a floating wave buoy is the most economical option available.

A concise discussion of the two different techniques is given in James [49] and this section summarises that paper.

So far the concept of a mixed sea state has been represented by a superposition of many simple first-order sinusoids. This representation is adequate when the waves are not steep. For a more complete description, a higher-order wave-behaviour equation must be used in constructing models. In higher-order models the stokes drift term is introduced which is a

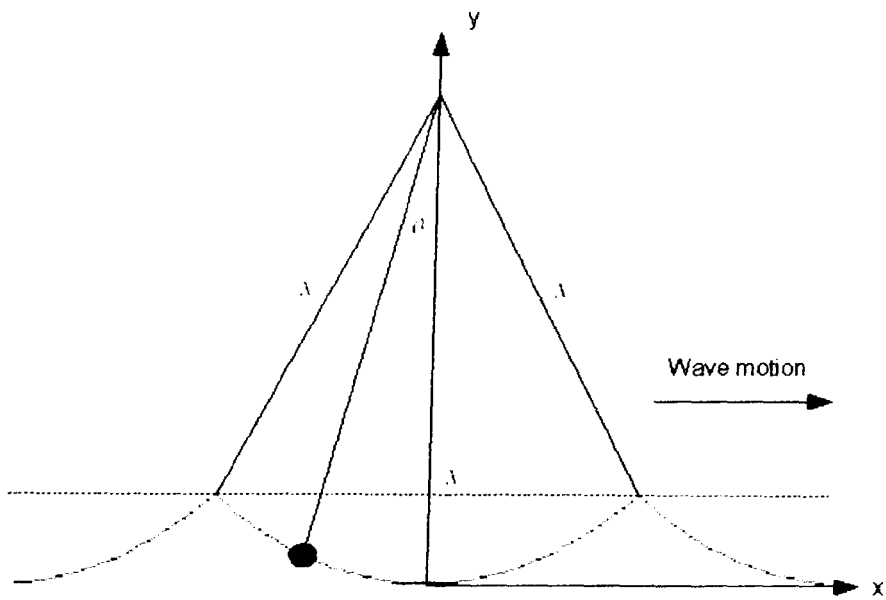


Figure 4.1: Pendulum approximation to the path of a surface particle

measure of the mean movement of water particles. In a linear model it is assumed that water particles remain about a fixed position and a buoy following the motion of these particles will also remain fixed. If a Stokes drift is introduced then the buoy will tend to follow this. In omni-directional waves the buoy will reach the end of its mooring tether and tend to be pulled through waves.

In a real mixed-state sea with waves arriving from many directions the buoy will tend to be pulled back to its mean position and not reach its extended point.

James explains this principle by introducing the clock model for the orbital motion of surface particles shown in Figure 4.1. Consider a wave buoy following the surface particles:

$$x = ct - \lambda \sin\theta \tag{4.33}$$

and

$$y = \lambda(1 - \cos\theta) \tag{4.34}$$

where $c$ is the phase speed.

Now consider the wave staff fixed at $x = 0$ and

$$\sin\theta = \frac{ct}{\lambda} + \text{constant} \tag{4.35}$$

where for maximum amplitude waves

$$c = 1.0923 \left( \frac{g\lambda}{2\pi} \right)^{1/2} \tag{4.36}$$

For the wave staff, choosing $t = 0$ for $y = 0$ then

$$y = \lambda \left( 1 - \sqrt{\frac{1 - c^2 t^2}{\lambda^2}} \right) \tag{4.37}$$

whereas for a free floating wave buoy

$$y = \lambda k^2 \left( 1 - \cos 2\sqrt{g/\lambda} t \right) \tag{4.38}$$

The free floating buoy will also be drifting with a velocity of $0.28c$ according to the clock model. In the real case of a tethered wave buoy, as mentioned previously, it will reach the end of its tether and move only in the vertical plane in a similar manner to the wave staff. James showed that if the FFT of the records from each instance are taken and compared then amplitude of the second harmonic is under recorded for the tethered wave buoy. The spectrum for the free floating buoy is shifted to the lower frequencies as it will tend to be measuring the Lagrangian rather than Eulerian values.

James goes on to state that in complex sea states the buoy will not remain at the end of its tether for long but will drift with the differing wave vectors, i.e., drifting freely for many periods while for other periods remaining taught.

### 4.4.2 A possible solution

This chapter has reviewed many of the advantages and disadvantages of wave measurement. It is still proposed that wave buoys are the most sensible solution. The recent introduction of GPS buoys gives the possibility of tracking the motion of the buoy very accurately. If the acceleration and position information are available there may exist techniques to resolve the surface elevation to a fixed Eulerian point rather than at the Lagrangian point (which the buoy is measuring).

# Chapter 5

# Spectral Analysis

The information that can be obtained about a wave spectrum via the output of a wave measurement device is dependant on the spectral analysis techniques used. In particular, the Fourier transform is exploited in the transformation of time domain wave histories to wave spectra in the frequency domain. This chapter aims to set out the background of the spectral analysis tools that are used in this thesis. The analysis will start from first principles for completeness.

## 5.1 Fourier series

### 5.1.1 The trigonometric Fourier series

Fourier series analysis theory states that a continuous periodic function $f(t)$ or, in this particular case, surface elevation $\zeta(t)$, can be represented over a finite interval of time ($t$ to $t+T$), as an infinite sum of harmonically related sinusoids, where $t$ is arbitrary and $f(t)$ is assumed to be periodic over the time period $T$. The basic Fourier series is written as

$$f(t) = \sum_{n=0}^{\infty} (a_n \cos n\omega_0 t + b_n \sin n\omega_0 t) \tag{5.1}$$

where $\omega_0 = 2\pi/T$, $n$ is the harmonic number, $b_0 = 0$, and $a_0$ is the mean of $f(t)$.

The time series of surface elevation $\zeta(t)$, in common with many instances where the Fourier series is used, is not strictly periodic. The series is generally used to extract information about the density of energy in certain parts of the spectrum. When taken over several records, this energy will tend to remain the same. This energy, as illustrated later in Chapter 6, can be used as the basis for modelling wave behaviour.

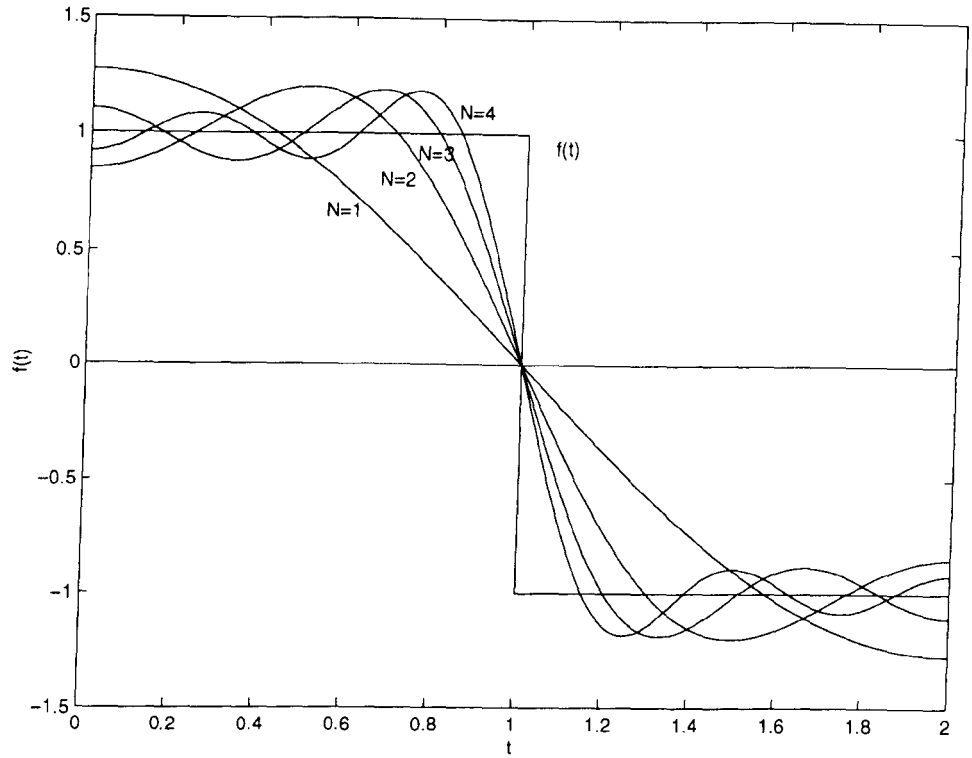


Figure 5.1: Fourier series representation of a square wave

The coefficients of the series $a_n$ and $b_n$ are given by

$$a_0 = \frac{1}{T}\int_t^{t+T} f(t)\, dt \tag{5.2}$$

$$a_n = \frac{2}{T}\int_t^{t+T} f(t)\cos n\omega_0 t\, dt \tag{5.3}$$

$$b_n = \frac{2}{T}\int_t^{t+T} f(t)\sin n\omega_0 t\, dt \tag{5.4}$$

### A square wave example

As an example of this process, Fig. 5.1 illustrates how a square wave can be built up from many individual sinusoids. It should be possible to see the converse of this theory, i.e., a complex function such as a square wave can be broken down into many individual sinusoids.

The representation of a function $f(t)$ by many individual sinusoids relates back to Chapter 2, where the principle of superposition was introduced. Hence the surface elevation $\zeta(t)$ can be thought of as the summation of many individual harmonic wave vectors. However, as discussed in other parts of this thesis, a harmonic representation of $\zeta(t)$ is very much a pseudo representation since a real sea state is not periodic, but can exhibit periodic characteristics.

### Parseval's theorem

In representing a complex function by a number of individual sinusoids the question arises as to how many sinusoids ($N$) are needed to accurately recreate the complex function. $N$ can be found by taking the mean square value of the time and frequency domain representations of the function where

$$\frac{1}{T}\int_{t}^{t+T} f^2(t)dt = a_0^2 + \frac{1}{2}\sum_{n=1}^{N}(a_n^2 + b_n^2) \tag{5.5}$$

This is Parseval's theorem. The theorem states that the energy present in the time domain representation of a signal must equal the energy present in the frequency domain representation.

In making calculations of this value it is usual to subtract the mean of $f(t)$, i.e., $a_0$ from both sides of the equation as it will possibly dominate the result. Calculating Eq. 5.5 with increasing values of $N$ leads to a reduction in error between the time and frequency domain.

### Theoretical extraction of wave spectra

As discussed in Chapter 2, one use for the Fourier theorem is in constructing an estimate of the wave spectrum $S(f)$ from a time history $\zeta(t)$. The estimate $\hat{S}(f)$ of the power spectral density (Section 5.2) can be obtained by summing the energies of all the Fourier components within a chosen spectral resolution $\Delta f$ so that

$$\hat{S}(f)\Delta f = 1/2\sum_{\Delta f}(a_n^2 + b_n^2) \tag{5.6}$$

It will be explained later that the summation of several frequencies is necessary to remove randomness in the estimated spectrum.

The concept of a wave spectrum is more fully expanded upon in later sections after the power spectral density function has been introduced. At present the above equation is included to illustrate the relevance of Fourier series to the wave prediction problem.

## 5.1.2 The complex Fourier series

The exponential form of the Fourier series, which is widely used, is obtained from the Euler identities

$$\begin{aligned} e^{jn\omega_0 t} &= \cos n\omega_0 t + j\sin n\omega_0 t \\ e^{-jn\omega_0 t} &= \cos n\omega_0 t - j\sin n\omega_0 t \end{aligned} \tag{5.7}$$

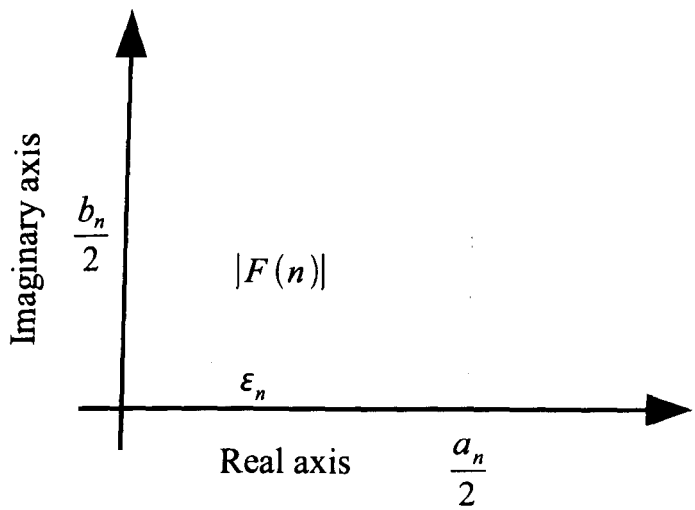


Figure 5.2: Argand diagram for a Fourier coefficient

where $j$ is a vector rotation through 90 degrees and, in the usual complex notation $j^2 = -1$. By combining these identities with Eq. 5.1 the exponential form is reached so that

$$f(t) = \sum_{n=-\infty}^{\infty} F_n e^{jn\omega_0 t} \tag{5.8}$$

where

$$F_n = \left\{ \begin{array}{ll} \dfrac{a_n - jb_n}{2} & \text{for } n \geq 0 \\ \\ \dfrac{a_n + jb_n}{2} & \text{for } n < 0 \end{array} \right\} \tag{5.9}$$

The Fourier coefficient terms $F_n$ may also be obtained from the time series $f(t)$ using

$$F_n = \frac{1}{T} \int_t^{t+T} f(t) e^{-jn\omega_0 t} dt \tag{5.10}$$

Eqs. 5.8 and 5.10 form a Fourier Transform pair.

### Representation of complex Fourier coefficient

Figure 5.2 shows a representation of the complex Fourier coefficient $F_n$. The real number is the abscissa and the imaginary number is the ordinate.

$$F_n = |F_n| e^{-j\varepsilon_n} \tag{5.11}$$

where

$$|F_n| = \frac{1}{2}\sqrt{a_n^2 + b_n^2} \tag{5.12}$$

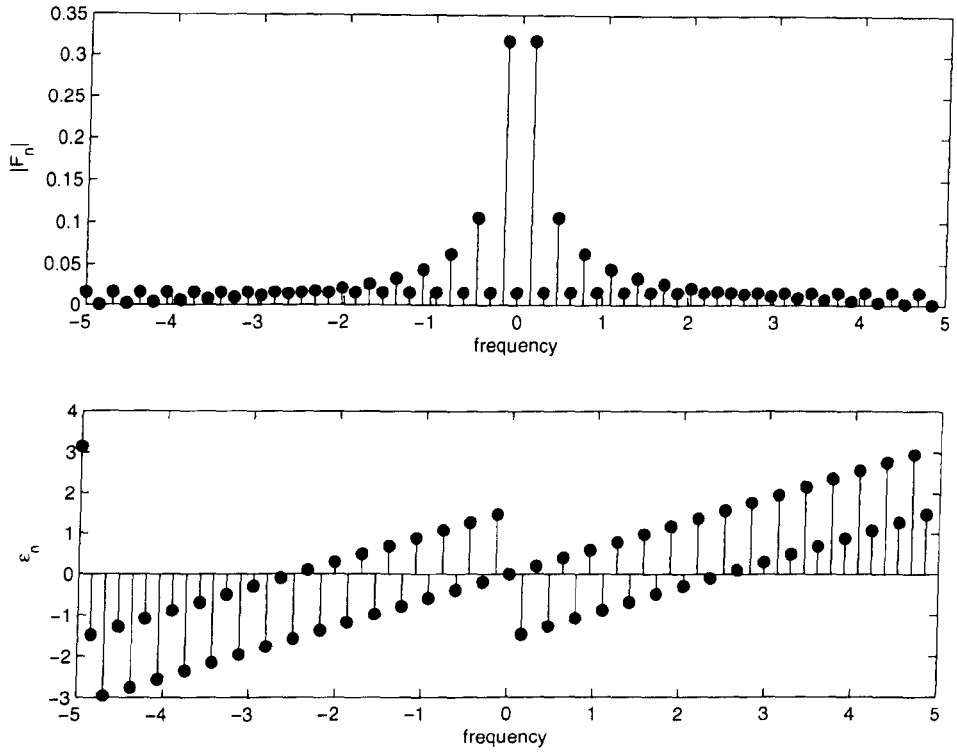


Figure 5.3: Complex frequency spectra

and

$$\varepsilon_n = \tan^{-1} \frac{b_n}{a_n} \tag{5.13}$$

The set of numbers $F_n$ for all $n$ uniquely describes the function $f(t)$. In many instances the magnitudes of each Fourier coefficient $|F_n|$ will be sufficient to describe the spectral characteristics of $f(t)$ and in the case of signal processing this is generally the information that is preserved. However, in trying to accurately recreate a dispersive water wave, the phase information must also be preserved. Neglecting the phase information can lead to large errors. For example, if the phase of each Fourier coefficient were assumed to be 0, then all of the component waves would reinforce one another to create a physically unstable waveform. This situation can occur (the 100 year wave) but since there are infinitely many wave vectors to be considered the possibility of this occurring naturally is extremely low.

### Amplitude and power spectra

The Fourier series is used to express a periodic function $f(t)$ by its sum of harmonic components spaced at multiples of $\omega_0$, where

$$\omega_n = \frac{n2\pi}{T} = n\omega_0 \tag{5.14}$$

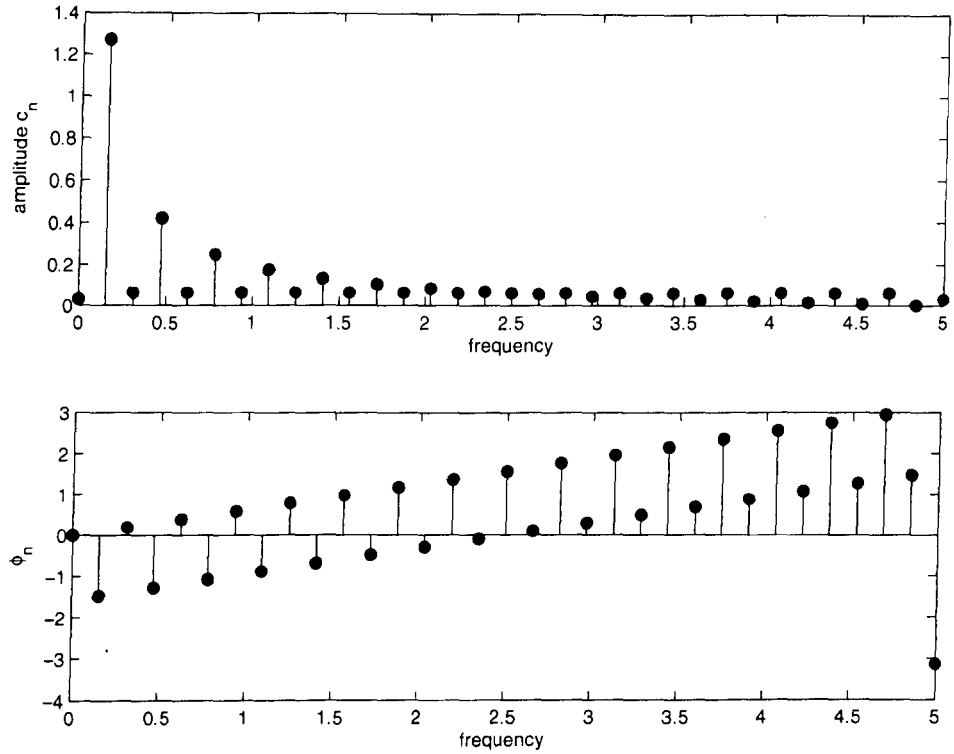


Figure 5.4: Real frequency spectra

A Fourier series may then be represented by a frequency spectrum of the periodic function $f(t)$. The complex form in Eq. 5.8 is obtained by plotting the complex coefficients $|F_n|$ against frequency and also the phase $\epsilon_n$ against frequency. Fig. 5.3 shows an example of this for the square wave in Section 5.1.1.

The coefficients returned by the complex form contain negative frequencies, which although useful in mathematical manipulation have no physical meaning. In order for the spectrum to become real, i.e., one that can be simulated in the real world, the energy associated with each negative-harmonic frequency must be redistributed to the corresponding positive-harmonic frequency so that

$$|F_n|e^{jn\omega_0 t} + |F_n|e^{-jn\omega_0 t} = c_n \cos(n\omega_0 t) \tag{5.15}$$

This is a rearrangement of Euler's identity in Eq. 5.7. Complex exponential signals cannot be readily simulated in the real world but a cosine signal can. The real amplitude components are therefore $c_n = 2|F_n|$ for $n > 0$ The phase component $\epsilon_n$ of each negative harmonic must also be translated into the positive domain. The resultant real spectrum is shown in Fig. 5.4. This representation of the complex coefficients as a summation of real signals leads to the

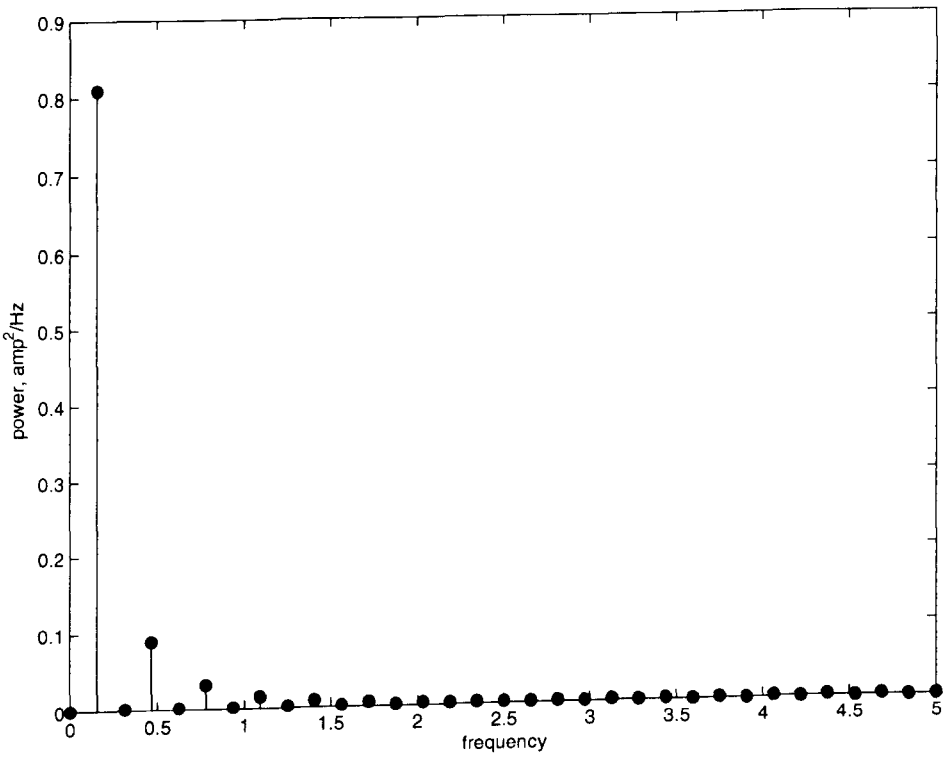


Figure 5.5: Power spectrum for a square wave

compact form of the trigonometric and exponential Fourier series

$$f(t) = \sum_{n=0}^{\infty} c_n \cos\left(n\omega_0 t + \phi_n\right) \tag{5.16}$$

where

$$c_n = \sqrt{a_n^2 + b_n^2} = 2|F_n| \tag{5.17}$$

$$\phi_n = \tan^{-1}(-b_n/a_n) = \tan^{-1}\frac{Im\{F_n\}}{Re\{F_n\}} \tag{5.18}$$

It should be readily verifiable that Eq. 5.16 bears a resemblance to Eq. 2.30 which is the basic directional wave modelling definition. The equation for the estimated wave spectrum can be restated in this form as

$$\hat{S}(f)\Delta f = \frac{1}{2}\sum_{\Delta f} c_n^2 \tag{5.19}$$

### Power spectra

An additional spectrum that is of use is the power spectrum, which is formed from the complex coefficients where

$$P_n = |F_n|^2 \tag{5.20}$$

which again has negative elements. Using the real coefficients it becomes

$$P_n = \frac{c_n^2}{2} \tag{5.21}$$

The real power spectrum for the square wave used in the previous example is shown in Fig. 5.5. Section 5.2 looks more closely at power spectral density functions.

### 5.1.3 The Fourier transform

The Fourier transform is essentially a mathematical device to allow for the representation of an aperiodic function, such as surface elevation $\zeta(t)$, as a periodic one. To achieve this the aperiodic function $f(t)$ is forced to repeat itself every $T$ seconds giving the periodic function $f_T(t)$. As $T \rightarrow \infty$ the aperiodic function is isolated and it's spectrum can be recovered. The definition given here is primarily for use with continuous time functions, but following this definition leads to a discrete time form that is widely used for signal processing.

Recalling Eqs. 5.8 and 5.10 the exponential Fourier series for a continuous periodic time function $f_T(t)$ was defined as

$$f_T(t) = \sum_{n=-\infty}^{\infty} F_n e^{jn\omega_0 t} \tag{5.22}$$

where

$$F_n = \frac{1}{T}\int_{-T/2}^{T/2} f_T(t) e^{-jn\omega_0 t} dt \tag{5.23}$$

and

$$\omega_0 = 2\pi/T. \tag{5.24}$$

Before taking $T \rightarrow \infty$ a few changes must be made so that the $F_n$ do not tend to zero as the period is increased, therefore, assume:

$$\omega_n = n\omega_o, \tag{5.25}$$

$$F(\omega_n) = TF_n \tag{5.26}$$

Using these definitions Eqs. 5.22 and 5.23 become

$$f_T(t) = \sum_{n=-\infty}^{\infty} \frac{1}{T} F(\omega_0) e^{j\omega_n t}, \tag{5.27}$$

$$F(\omega_n) = \int_{-T/2}^{T/2} f_T(t) e^{-j\omega_n t} dt \tag{5.28}$$

The spacing between adjacent lines for the spectrum of $f_T(t)$ is

$$\Delta\omega = 2\pi/T \tag{5.29}$$

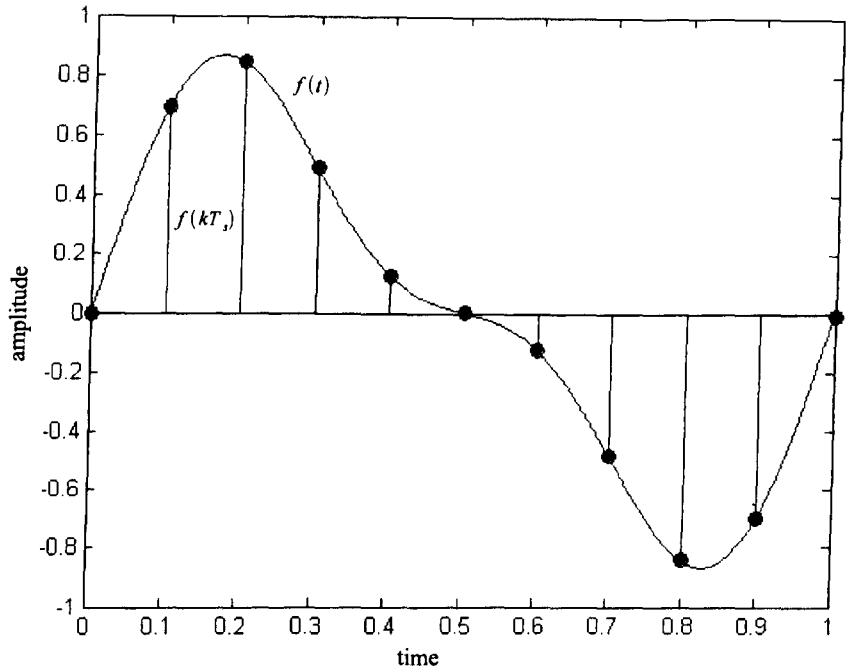


Figure 5.6: Waveform sampled at $t_s = 0.1s$

Substituting this into Eq. 5.27 gives

$$f_T(t) = \sum_{n=-\infty}^{\infty} F(\omega_n) e^{j\omega_n t} \frac{\Delta\omega}{2\pi} \tag{5.30}$$

When $T$ tends to infinity the spacing between frequency components, $\Delta\omega$ becomes very small and the discrete spectrum will tend towards a continuous one. In addition, the summation of Eq. 5.30 will become an integral, resulting in the Fourier transform pair where

$$\begin{aligned} f(t) &= \frac{1}{2\pi} \int_{-\infty}^{\infty} F(\omega) e^{j\omega t} d\omega \\ F(\omega) &= \int_{-\infty}^{\infty} f(t) e^{-j\omega t} dt. \end{aligned} \tag{5.31}$$

### 5.1.4 Sampling

Up to this point it has been assumed that the variable of interest $f(t)$ is a continuous one. In the ideal case, working with a continuous time variable does match with the theorems already presented. Unfortunately, the data available will usually be sampled in a discrete time form where

$$f(kt_s) = f(0), f(t_s), f(2t_s), \cdots, f([N-1]t_s) \tag{5.32}$$

Sampling involves taking regular measurements of $f(t)$ and storing these in the order in which they were taken. The theory of sampling a continuous waveform can take many pages

of convoluted explanation so it will be dealt with here in a simple manner using a few rules that must be followed.

Fig. 5.6 shows the basic process involved. A measurement of $f(t)$ is taken at intervals of $t_s$ seconds (the sampling interval). The reciprocal of this is the sampling rate or frequency $f_s = 1/t_s$. In order for all the frequency information of the continuous signal to exist in discrete time it must not contain any frequencies above half the sampling rate $f_s$.

This is achieved in practise by low pass filtering $f(t)$ and sampling with $f_s$ much greater than the above limit. For example we are rarely interested in frequencies greater than 0.5 Hz so a theoretical sampling frequency may be 1 Hz but, to avoid aliasing problems the sampling rate would generally be twice this and 2 Hz should be used.

### Aliasing error

If the rules in the previous section are not followed and frequencies greater than half the sampling frequency are present in $f(t)$ then aliasing of the spectrum will occur. Generally speaking, if this occurs, then the energy contained in the frequencies above the half sampling rate frequency will be folded over into the lower half of the spectrum. Correcting for these errors is complicated and far from ideal, so the best method is to prevent the errors from occurring in the first place by using the correct sampling frequency for $f(t)$.

## 5.1.5 Discrete Fourier transform

The implementation of the Fourier transform that is most widely used is the discrete Fourier transform (DFT). Much of the data available to engineers is in the form of sampled time series, for example surface elevation, pressure or acceleration. The Fourier transform pair introduced in Section 5.1.3 still needs a little adjustment to make it suitable for use on sampled data and for implementation on a personal computer.

Consider a time series, $f(kt_s)$, of length $Nt_s$ sampled at $N$ equally spaced samples with a sampling interval of $t_s$ so that

$$f(kt_s) = f(0), f(t_s), f(2t_s), \cdots, f[(N-1)t_s]. \tag{5.33}$$

The DFT is defined as the sequence of $N$ complex-valued samples in the frequency domain given by

$$F_D(n\Omega) = \sum_{k=0}^{N-1} f(kt_s)e^{-j\Omega t_s nk}, \quad n = 0, 1, \cdots, N-1, \tag{5.34}$$

where $\Omega = 2\pi/(Nt_s)$ and $\Omega t_s = 2\pi/N$. Note that $\Omega$ and $t_s$ do not explicitly enter into the DFT and are used as scaling factors for the interpretation of results.

In using a numerical approximation to the Fourier transform, it is necessary to restrict the observation interval to a finite length. Therefore the truncated function $\tilde{f}(t)$ in terms of $f(t)$ is

$$\tilde{f}(t) = \begin{cases} f(t) & 0 \leq t \leq Nt_s \\ 0 & \text{elsewhere} \end{cases} \tag{5.35}$$

The Fourier transform $\tilde{F}(\omega)$ of this truncated function is

$$\tilde{F}(\omega) = \int_0^{Nt_s} f(t)e^{-j\omega t}dt. \tag{5.36}$$

Making the variable changes $\omega \rightarrow n\Omega$, $t \rightarrow kt_s$ and $dt \rightarrow T$, Eq. 5.36 can be approximated to

$$\tilde{F}(n\Omega) \cong \sum_{k=0}^{N-1} f(kt_s)e^{-jn\Omega kt_s}t_s. \tag{5.37}$$

Comparing the two previous forms shows that

$$\tilde{F}(\omega)|_{\omega=n\Omega} \cong t_s F_D(n\Omega). \tag{5.38}$$

Additionally the DFT is analogous to the Fourier transform if:

1. the signal $f(t)$ is restricted to the interval $(0, Nt_s)$
2. within this interval the signal $f(t)$ is available as a sequence of $N$ equally spaced values
3. the interval is extended periodically yielding the discrete harmonic frequencies $n\Omega = 2\pi n/(Nt_s)$

In an analogy to the continuous case, the inverse discrete Fourier transform (IDFT) is

$$f(kT_s) = \frac{1}{T}\sum_{n=0}^{N-1} F_D(n\Omega)e^{j\Omega t_s kn} \tag{5.39}$$

and forms an exact transform pair with the DFT.

### DFT to complex Fourier series

The coefficients of the complex Fourier series may be computed using the DFT and then multiplying by $1/N$. The highest frequency component that can be determined corresponds to $n = N/2$ or $(N/2)\Omega = 1/(2t_s)$ Hz. This agrees with the sampling theorem.

### Standard form of complex variable transform

The DFT is often given in more general terms as the transform of one set of complex numbers to another. The common form of this is

$$C(k) = R \sum_{i=0}^{N-1} D(i) \exp \pm 2\pi jik/N \tag{5.40}$$

where

the $-$ sign in the exponent is used for the forward transform

the $+$ sign in the exponent is used for the backward transform

$C(k)$ and $D(i)$ are both complex numbers

$R$ is a scale factor The representations used in [12] takes the form of a forward and backward transform. The forward transform is

$$F(k) = \frac{1}{N} \sum_{i=0}^{N-1} \zeta(i) \exp \frac{-j2\pi ik}{N} \tag{5.41}$$

where $0 < k < N - 1$ is a frequency index, $i$ is a temporal index and $N$ is the number of samples in the record. The frequency of the $k^{th}$ harmonic is $k/D$, where $D$ is the length of the record in seconds.

The reverse transform is given by

$$\zeta(k) = \sum_{i=0}^{N-1} F(i) \exp \frac{j2\pi ik}{N} \tag{5.42}$$

where $0 < k < N - 1$ is a temporal index, $k$ is a frequency index and $N$ is the number of samples in the record.

### MATLAB FFT

When the DFT is implemented, the solving of the the equations, if followed as written, is too slow for real time applications. Therefore a computer algorithm called the Fast Fourier Transform (FFT) was developed during the 1960s. This considerably speeded up the process.

The software environment used in this thesis is MATLAB, which contains its own implementation of the FFT. Unfortunately it is slightly different to the formula used in Tucker [12] and this led to a great deal of confusion in the earlier stages of this research. The MATLAB implementation of the forward transform in terms of Equation 5.40 is

$$A(k) = \sum_{i=1}^{N} \zeta(i) \exp -j \frac{2\pi(i-1)}{D}(k-1) \tag{5.43}$$

where $1 < k < N$

It can be seen the scaling factor $R = 1/N$ is missing and the indexing values $i$ and $k$ are from $1 \rightarrow N$. This issue can be dealt with simply, by scaling the output $A(k)$ and by the careful use of MATLAB's indexing system.

## 5.2 Spectral density function

As already indicated in earlier sections of this chapter, the representation of a time series in various forms of spectra is instructive in visualising what is happening in a given waveform. The spectrum gives a measure of how energy and power are distributed with frequency. This section sets out in more detail the theory behind the spectra and their calculation.

### 5.2.1 Energy spectral density

The conservation of energy between the time domain, $f(t)$, and the frequency domain, $F(\omega)$, was stated earlier as Parseval's theorem (Eq. 5.5) where

$$\int_{-\infty}^{\infty} |f(t)|^2 \, dt = \frac{1}{2\pi} \int_{-\infty}^{\infty} |F(\omega)|^2 \, d\omega \tag{5.44}$$

The integral on the left hand side is the energy in $f(t)$ so that the quantity $|F(\omega)|^2$ is the energy per unit frequency. For this reason $|F(\omega)|^2$ is called the *energy spectral density* of the signal $f(t)$.

$|F(\omega)|^2$ describes only the relative amount of energy at various frequencies. For continuous $|F(\omega)|^2$, the energy at any given frequency is zero. It is the area under $|F(\omega)|^2$ that contributes the energy. To find the energy present, a range of frequencies must be given over which to integrate. It should be readily verifiable that, in the cases studied here, when dealing with real-valued time series, the energy spectral density function will also be real-valued, and the symmetry of the spectrum should hold true.

By examining Eq. 5.44, it should be noted that the spectral density function neglects the phase information and this is lost. In signal processing the spectral density functions are used in determining the transfer functions of linear systems, where the absence of phase information does not critically affect the solution. In the situation here, phase information is vitally important and spectral density functions are of more use in a checks and balances situation for confirming stochastic information.

In summary, the energy spectral density function of a signal represents its energy per unit of frequency and displays the relative energy contributions of the various frequency

components. The area under the energy spectral density gives the energy within a given band of frequencies.

### 5.2.2 Power spectral density

The time averaged power of a signal is given by

$$P = \lim_{T\to\infty} \frac{1}{T} \int_{-T/2}^{T/2} |f(t)|^2 \, dt. \tag{5.45}$$

For a periodic signal, each period contains a replica of the function, and the limiting operation can be omitted as long as $T$ is taken as the period.

Following similar reasoning to the energy spectral density function, it would be useful if a function could be defined that would represent the relative power contributions at various frequencies. This function is the power spectral density function $S(\omega)$, which has the units of watts per radian and its integral yields the power in $f(t)$. Writing this mathematically

$$P \equiv \frac{1}{2\pi} \int_{-\infty}^{\infty} S(\omega) d\omega. \tag{5.46}$$

Suppose we examine a section of a wave record of length $T$ and then take the Fourier transform of it to give $F_T(\omega)$. Parseval's theorem would then state that

$$\int_{-T/2}^{T/2} |f(t)|^2 \, dt = \frac{1}{2\pi} \int_{-\infty}^{\infty} |F_T(\omega)|^2 \, d\omega. \tag{5.47}$$

Hence, the average power is

$$P = \lim_{T\to\infty} \frac{1}{T} \int_{-\infty}^{\infty} |f(t)|^2 \, dt = \lim_{T\to\infty} \frac{1}{T} \frac{1}{2\pi} \int_{-\infty}^{\infty} |F_T(\omega)|^2 \, d\omega. \tag{5.48}$$

Combining equations 5.46 and 5.47 gives

$$\frac{1}{2\pi} \int_{-\infty}^{\infty} S(\omega) d\omega = \lim_{T\to\infty} \frac{1}{T} \frac{1}{2\pi} \int_{-\infty}^{\infty} |F(\omega)|^2 \, d\omega. \tag{5.49}$$

In addition, the cumulative power spectrum $G(\omega)$ can be defined as

$$G(\omega) = \frac{1}{2\pi} \int_{-\infty}^{\omega} S(u) du = \lim_{T\to\infty} \frac{1}{T} \frac{1}{2\pi} \int_{-\infty}^{u} |F(u)|^2 \, du. \tag{5.50}$$

This represents the cumulative amount of power in all frequency components below a given frequency $\omega$.

Interchanging the limiting and integrating operations in Eq. 5.50 gives

$$2\pi G(\omega) = \int_{-\infty}^{\omega} S(u) du = \int_{-\infty}^{\omega} \lim_{T\to\infty} \frac{|F_T(u)|^2}{T} du \tag{5.51}$$

| $m_{-2}$ | $m_{-1}$ | $m_0$ | $m_1$ | $m_2$ | $m_3$ | $m_4$ |
|---|---|---|---|---|---|---|
| 1188.7 | 81.864 | 6.0799 | 0.5005 | 0.0478 | 0.0057 | 0.0009 |
| $H_{m_0}$ | $T_z$ | $T_1$ | $T_E$ | $T_I$ | $T_c$ | $\nu$ |
| 9.86 | 0.0078 | 12.147 | 13.464 | 195.51 | 51.447 | n/a |

Table 5.1: Statistical spectral characteristics of the original spectra

The average power contained in any frequency interval $(\omega_1, \omega_2)$ is $[G(\omega_2) - G(\omega_1)]$ and in most cases $G(\omega)$ is differentiable, leading to the definition for the power spectral density function of $f(t)$ where

$$S(\omega) = \lim_{T \to \infty} \frac{|F_T(\omega)|^2}{T} \tag{5.52}$$

As with the energy spectral density, only the magnitude information is retained and the phase is discarded. This leads to the possibility of $S(\omega)$ representing many different time series and will not uniquely describe the time series $f(t)$.

Eq. 5.52 presents the possibility of obtaining a power spectral density of a wave record taken over a period $T$. The Fourier Transform of the record is taken and $|F_n|^2 / T$ is formed. The limit $T \to \infty$ in reality cannot be taken since the wave records are of finite length. This is because errors of the order of $1/T$ will appear in the resulting spectral resolution. This can be corrected by taking several time series of length $T$ and averaging the spectral densities, if the spectrum is known to be stable.

## 5.3 Example of spectral techniques

A wave record for a unidirectional sea state is generated, using the methods given in Chapter 3 and subjected to the various spectral manipulations detailed so far in this chapter. These illustrate each section and show how the methods are applied to a real world problem.

### 5.3.1 The original wave record

Using a linear model (Chapter 3) a unidirectional spectrum was generated for a Pierson-Moskowitz formulation using a wind speed of 20 m/s. The highest frequency in the spectrum was chosen to be 0.5 Hz and there were 100 wave vectors generated at a frequency spacing $\Delta f$ of 0.005 Hz. The statistical spectral characteristics are given in Table 5.1.

This spectrum is shown in Fig. 5.7 with the amplitudes of the simulated wave vectors

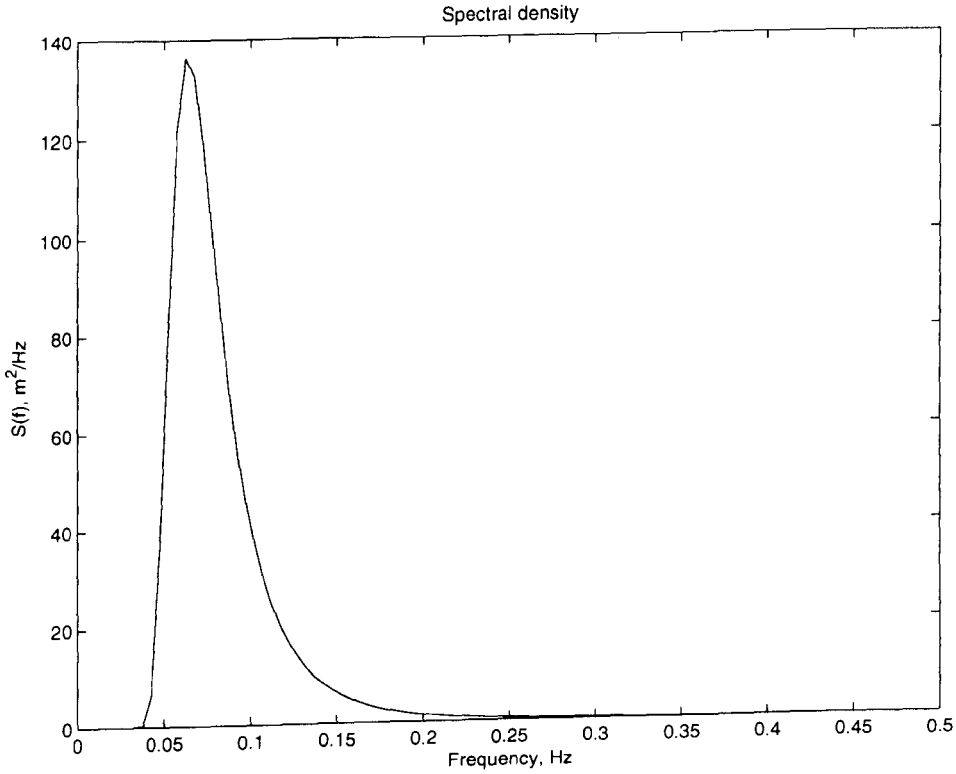


Figure 5.7: Original spectral density

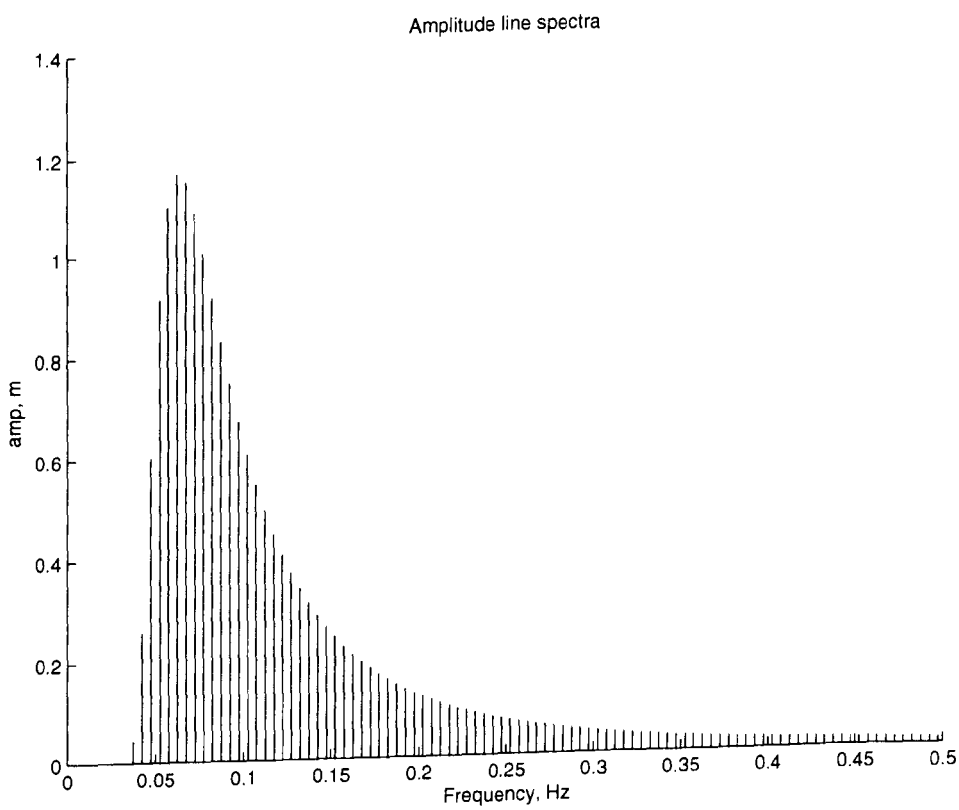


Figure 5.8: Amplitude line spectra of simulated wave vectors

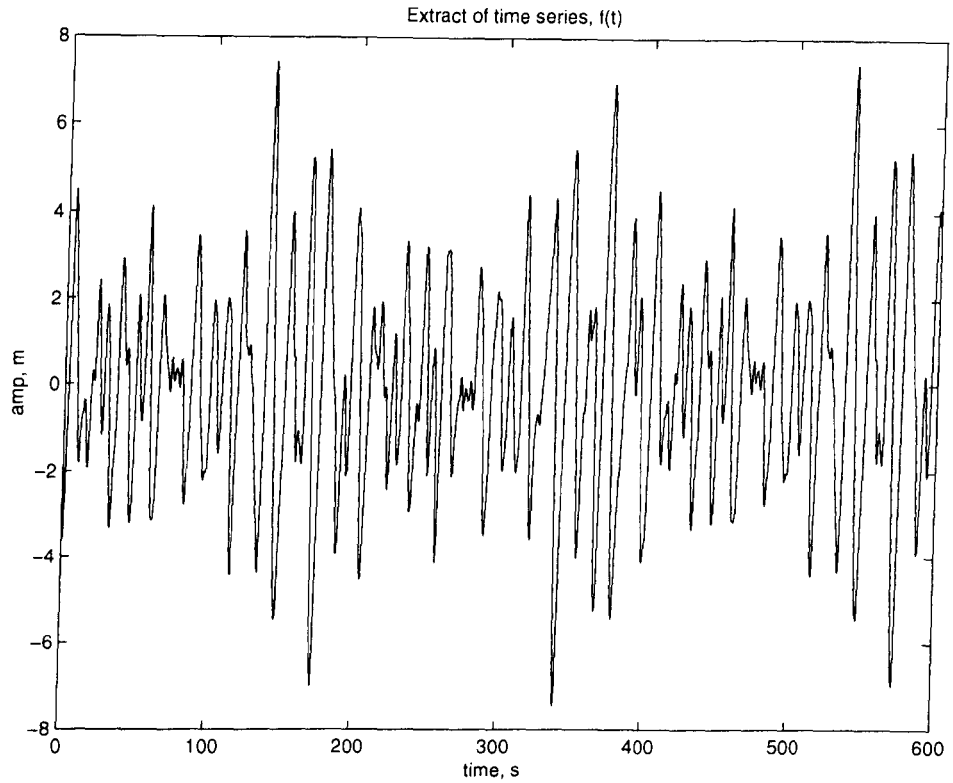


Figure 5.9: Extract of the time series, $f(t)$

given in Fig. 5.8 and an extract of the time series is shown in Fig. 5.9.

The length of the time series to be used is given by Tucker [12] where $T = 1200$ sec. This length of time series is chosen to avoid the need to use windowing functions. With shorter time series of length 100-400 sec the FFT process will induce frequency leakage between harmonics which will distort the results. To cure this, the data should ideally be windowed using any of the available types: Hanning, Bartlett, raised cosine, etc. The windowing of a time series involves multiplying the time series by a function that is commonly tapered to zero at either end rising to a value of one in the centre.

The problem with windowing the time series is the shifting of the phase values returned. As mentioned previously, the prediction methods are dependent on phase information. Tucker shows that, by using a longer record, the leakage between harmonics is reduced or the effects are passed up to higher frequencies which are not of interest. This eliminates the need for phase-shifting windowing to be used.

In order to determine the correct number of samples $N$ to be generated for this time series, the minimum and maximum frequency resolutions were calculated. This data is shown in Table 5.2. The length of the time series $T$ effectively decides the lowest frequency/longest

| $N$ | $f_{lower}$ | $f_{upper}$ | deepwater $\lambda$ range |
|---|---|---|---|
| 128 | $8.333 \times 10^{-4}$ Hz | 0.0533 Hz | $2.25 \times 10^{6}$–549.58 m |
| 256 | $8.333 \times 10^{-4}$ Hz | 0.1066 Hz | $2.25 \times 10^{6}$–137.39 m |
| 512 | $8.333 \times 10^{-4}$ Hz | 0.2133 Hz | $2.25 \times 10^{6}$–34.316 m |
| 1024 | $8.333 \times 10^{-4}$ Hz | 0.4266 Hz | $2.25 \times 10^{6}$–8.5792 m |
| 2048 | $8.333 \times 10^{-4}$ Hz | 0.8533 Hz | $2.25 \times 10^{6}$–2.1443 m |
| 4096 | $8.333 \times 10^{-4}$ Hz | 1.7066 Hz | $2.25 \times 10^{6}$–0.536 m |
| 8192 | $8.333 \times 10^{-4}$ Hz | 3.4133 Hz | $2.25 \times 10^{6}$–0.134 m |
| 16384 | $8.333 \times 10^{-4}$ Hz | 6.8266 Hz | $2.25 \times 10^{6}$–0.0355 m |

Table 5.2: Realisable bandwidth of experimental time series

wavelength that can be determined. The number of samples $N$ taken during this time determines the upper frequency/shortest wavelength resolution. Since we know that the highest frequency being simulated is 0.5 Hz, taking $N$ to be 4096 is the most economical choice in terms of processing power whilst having an upper frequency limit of 1.7066 Hz (which is more than twice the highest frequency being simulated).

### 5.3.2 Fourier representations

The results of the first process implemented are shown in Fig. 5.10 where the FFT of the time series has been taken. The series of complex Fourier coefficients $F_n$ have been shifted so that $F_0$ is at the centre of the record. The magnitude $|F_n|$ and the phase are plotted. It can be seen there are no components present above 0.5 Hz. It can be observed that the symmetry of the spectrum is close in shape to that of the original wave spectrum.

### 5.3.3 Tucker's method

This method exploits the symmetry to create the real discrete amplitude spectrum shown in Fig. 5.11. The equations given in Appendix 1 of Tucker [12] are mistaken in their formulation of the $b_n$ components which leads to some serious errors in prediction. The corrected formulae

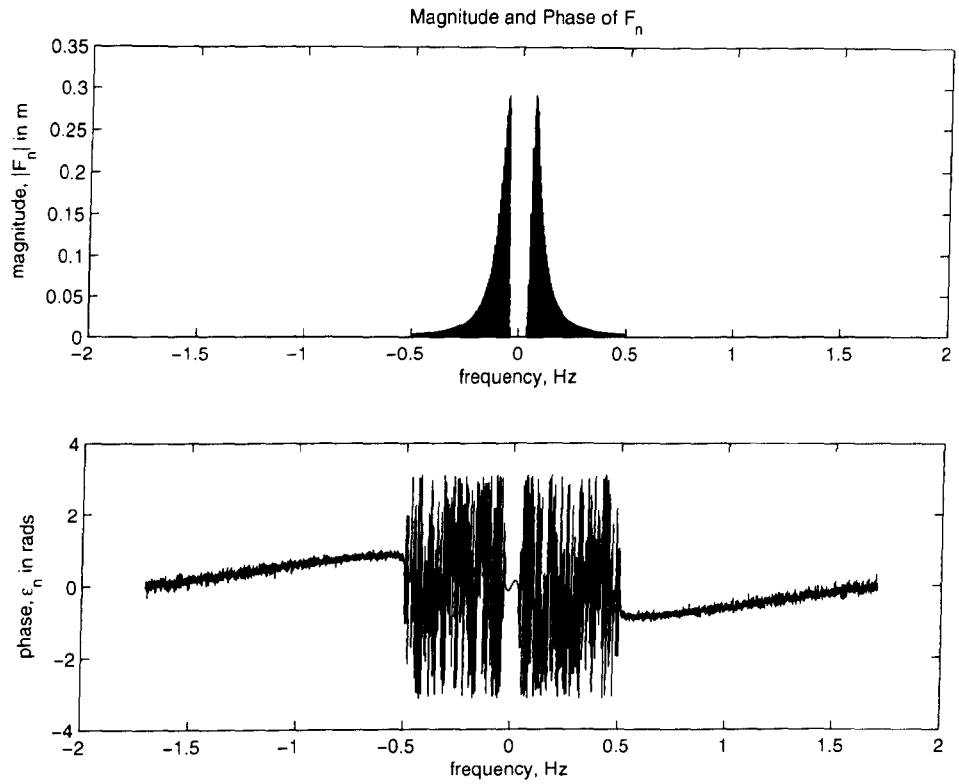


Figure 5.10: Plot of the Magnitude and Phase of $f(t)$

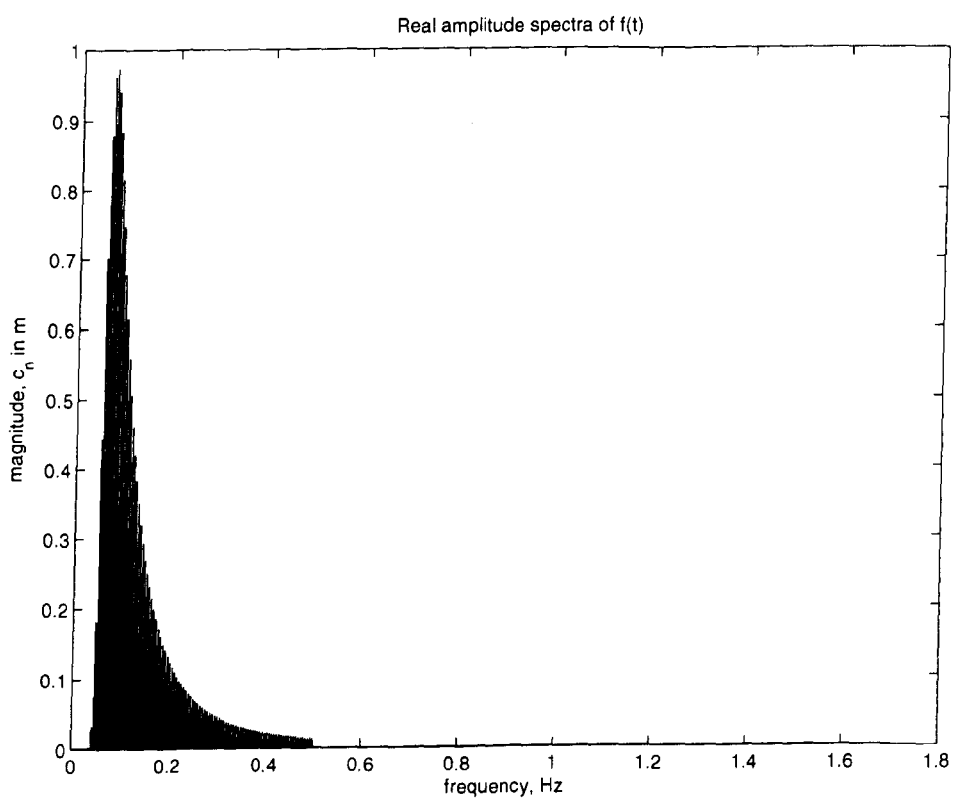


Figure 5.11: Plot of the real amplitude spectra of $f(t)$

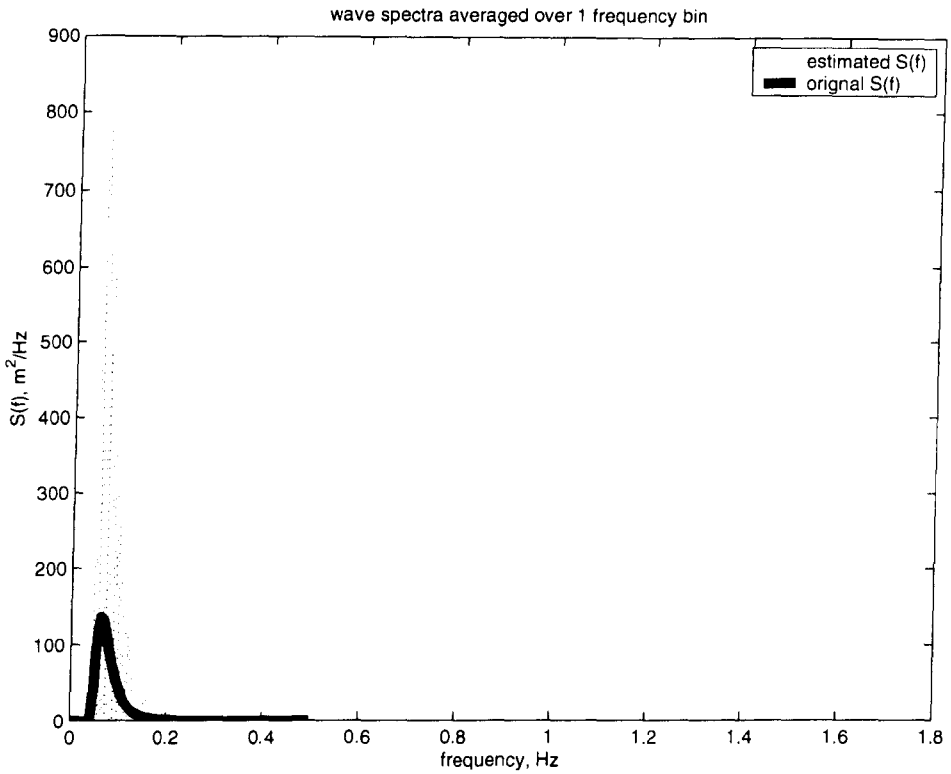


Figure 5.12: Estimated $S(f)$ taken over one frequency

are as follows

$$
\begin{aligned}
a(0) &= Re\{F(0)\} \\
a(1 \rightarrow (N/2-1)) &= 2Re\{F(1 \rightarrow (N/2-1))\} \\
a(N/2) &= Re\{F(N/2)\} \\
b(0) &= 0 \\
b(1 \rightarrow (N/2-1)) &= -2Im\{F(1 \rightarrow (N/2-1))\} \\
b(N/2) &= 0 \\
c(n) &= \sqrt{a_n^2 + b_n^2} \qquad (5.53) \\
\phi(n) &= \texttt{atan2}(-b_n/a_n) \qquad (5.54)
\end{aligned}
$$

The MATLAB `atan2` function is given explicitly here since the software used has two implementations of the $\tan^{-1}(\theta)$ function and the version given above must be used. Verification of the above formulations can be obtained by reconstructing the original record from either the full (Eq. 5.1) or compact (Eq. 5.16) form of the Fourier series using the coefficients as defined above.

Eq. 5.19 can now be used to recover the original spectrum. Fig. 5.12 shows the spectrum

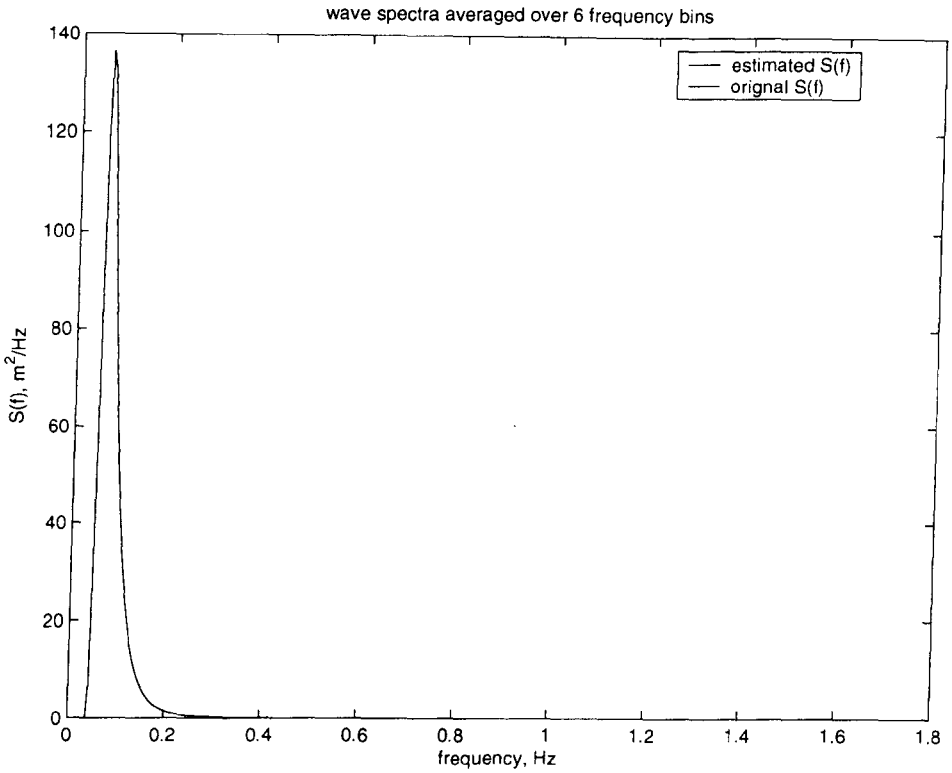


Figure 5.13: Estimated $S(f)$ taken over 6 frequencies

returned when $\Delta f$ is taken to be the width of one Fourier component $\Delta f = 8.333 \times 10^{-4}$. It can be seen the spectrum is very spiky but its shape is comparable to the original.

To obtain a smoother spectrum it must averaged over several frequency bins. The estimates returned for the harmonic amplitudes are very erratic and will change rapidly from one record to another. For the example above, if the record had been taken a few seconds earlier or later the amplitudes of the Fourier coefficients would have changed. The energy is likely to remain around the frequency of interest but not with the precise harmonic of interest. Averaging the energy over several harmonics gives a more stable result as some of the random nature will be spread over a range of frequencies.

It is useful to average over six frequency bins in this case since it will lead to $\Delta f = 0.005$ Hz, which is the exact width of the original record. The new frequency axis can be centred on frequencies 0.0025, 0.0075, 0.0125,..., 0.0475 Hz. The scheme used is

$$S(f) = \frac{1}{2\Delta f}\left(0.5(c_{p-3}^2 + c_{p+3}^2 + \sum_{n=p-2}^{n=p+2} c_n^2)\right) \tag{5.55}$$

where $p$ is the index of the centre of the original spectrum and $\Delta f$ is taken to be the new spectral width. Fig. 5.13 shows that this smoothed spectrum is a closer match to the original spectrum than in Fig. 5.12.

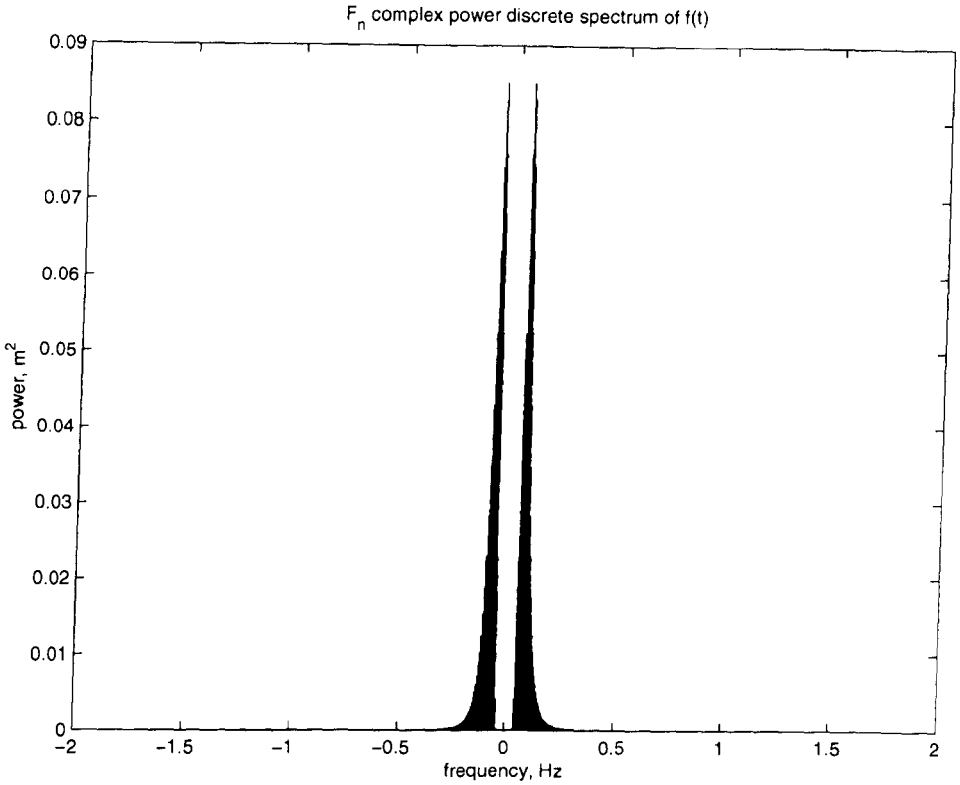


Figure 5.14: Complex magnitude $|F_n|$ squared

### 5.3.4 Power spectral density representations

A second method for calculating the power spectral density of a time series was given earlier in Section 5.2.2 and here the experiments above were repeated in order to compare the spectra returned by this method (found in Stremler [50]) to that found in Tucker [12].

The first stage (as above) is to calculate the complex FFT. Following this the magnitude of each component is squared as shown in Fig. 5.14. To create the real spectrum the magnitudes of the positive frequency values are doubled then squared (Fig. 5.15). If the process of squaring is carried out before the magnitudes are doubled a discrepancy of 0.5 occurs between this method and that of Tucker.

To complete the process the real discrete spectrum is divided throughout by $\Delta f$. The continuous spectrum is shown in Fig. 5.16 with the original spectrum. The equation for this process is

$$S(f) = \frac{(2|F_n|)^2}{\Delta f} \tag{5.56}$$

where $n > 0$. Again, the spectrum taken over one frequency bin is very spiked, and the averaging process must be performed.

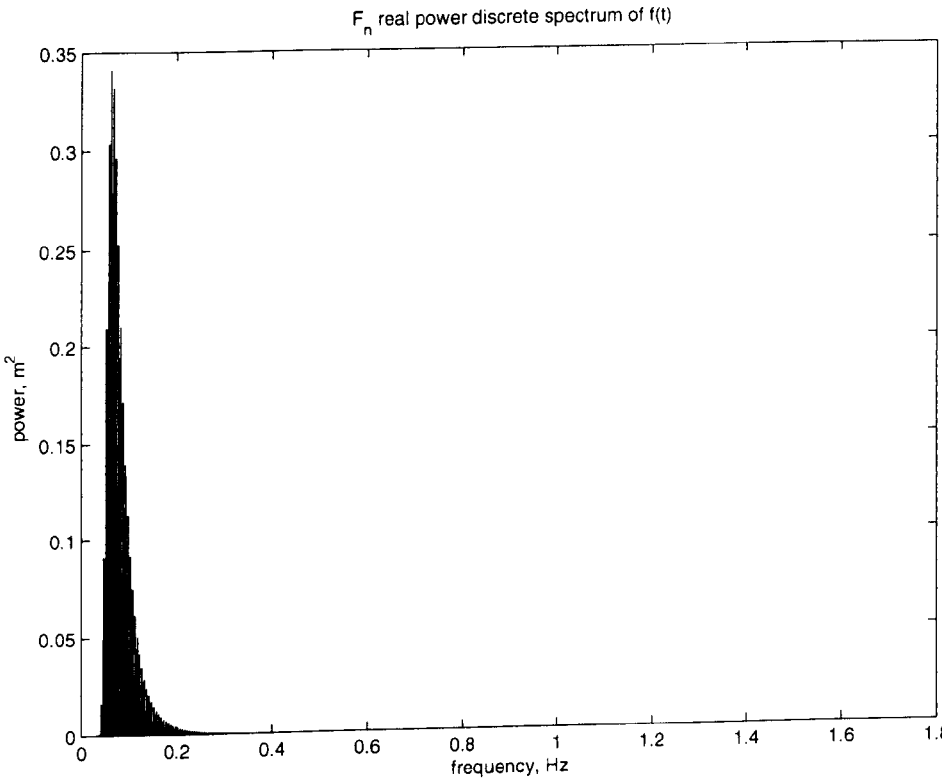


Figure 5.15: Real power or $(2|F_n|)^2$

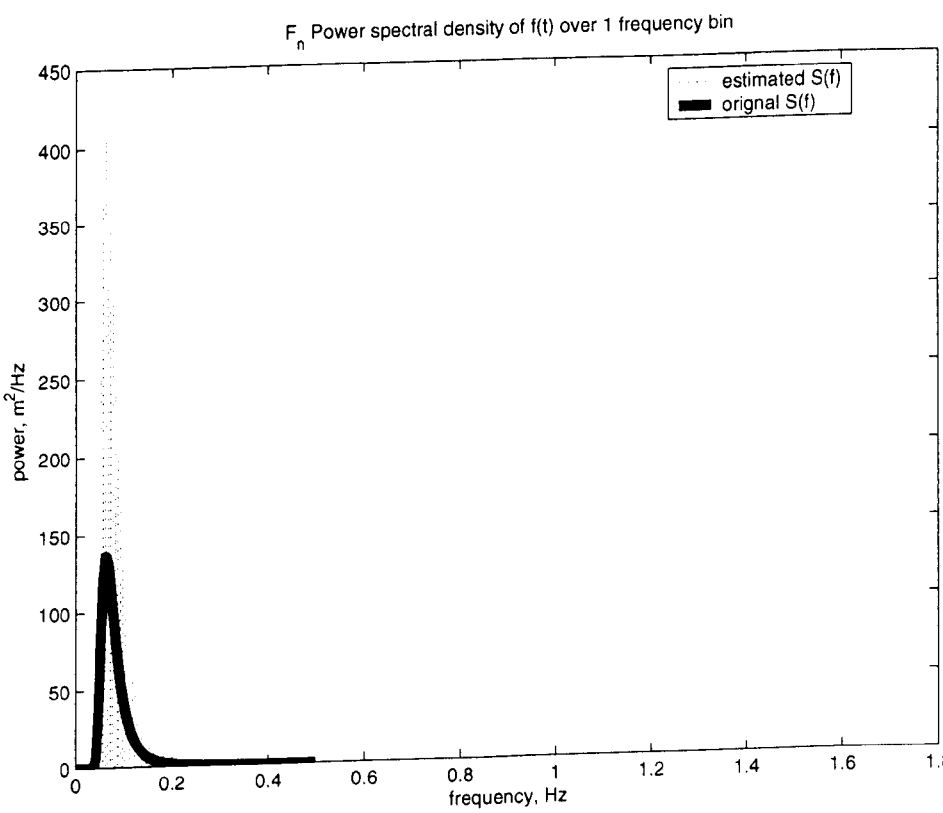


Figure 5.16: Comparison of calculated to original spectra

## 5.4 Correlation function

The correlation function is an important tool in recognising the similarities between two or more time series. It is useful when determining the parameters for estimating directional spectra from wave buoy records (see Chapter 4) and as an alternative method for extracting wave spectra from time series.

### 5.4.1 Definition

The correlation function of two time-varying quantities $f_i(t)$ and $f_j(t)$ can be defined as

$$C_{ij}(\tau) = \frac{1}{T}\int_t^{t+T} f_i(t) f_j(t+\tau) dt \tag{5.57}$$

where $\tau$ is a time delay. If $i = j$, then $C_{ij}$ is the autocorrelation function, while if $i \neq j$ then this quantity is the cross-correlation or cross-covariance function.

If we now substitute the Fourier series representation of $f_j(t+\tau)$ into the equation for the correlation, we obtain

$$\begin{aligned} C_{ij}(\tau) &= \frac{1}{T}\int_t^{t+T} f_i(t) \sum_{n=-N/2}^{N/2} F_j(n) e^{jn\omega_o(t+\tau)} dt & (5.58)\\ &= \frac{1}{T}\int_t^{t+T} f_i(t) e^{jn\omega_0 t} dt F_j(n) e^{jn\omega_o\tau} & (5.59)\\ &= \sum_{n=-N/2}^{N/2} F_j(n) F_i^*(n) e^{jn\omega_0\tau} & (5.60)\\ &= \sum_{n=-N/2}^{N/2} |F_j(n)||F_i(n)| e^{j(\varepsilon_j-\varepsilon_i)} e^{jn\omega_0\tau} & (5.61) \end{aligned}$$

where $F_i^*(n)$ is the complex conjugate of the Fourier coefficients of $f_i(t)$.

For the autocorrelation:

$$\begin{aligned} C_{11}(\tau) &= \sum_{n=-N/2}^{N/2} |F_1(n)|^2 e^{jn\omega_0\tau} & (5.62)\\ &= \sum_{n=-N/2}^{N/2} |F_1(n)|^2 \cos n\omega_0\tau & (5.63) \end{aligned}$$

since $C_{11}(\tau)$ is symmetric. For the case where the time lag $\tau$ is zero:

$$C_{11}(0) = \sum_{n=-N/2}^{N/2} |F_1(n)|^2 = \frac{1}{T}\int_t^{t+T} f_1^2(t) dt \tag{5.64}$$

which recovers Parseval's theorem and shows that $C_{11}(0)$ represents the energy contained within $f_1(t)$.

### 5.4.2 Power spectrum

The Fourier transform of the correlation function is defined as the power spectrum (for $i = j$) or the cross spectrum (for $i \neq j$). The Fourier transform of the autocorrelation function can be shown to recover the power spectral density function defined in Section 5.2.2. Taking the Fourier transform of $C_{11}(\tau)$:

$$\Phi_{11}(n) = \frac{1}{T}\int_{t}^{t+T} C_{11}(\tau)e^{-jn\omega_0\tau}d\tau = |F_1(n)|^2 \tag{5.65}$$

for $-N/2 < n \leq N/2$, which is the two-sided power spectral density. As with previous cases, this spectrum is real and even and the energy associated with the negative frequencies can be reassigned to the positive frequencies where

$$\Phi'_{11}(n) = 2|F_1(n)|^2, \; n > 0 \tag{5.66}$$

$$\Phi'_{11}(0) = |F_1(0)|^2, \; n = 0 \tag{5.67}$$

for $0 \leq n \leq N/2$ only.

A similar process is followed to obtain the cross spectrum $\Phi_{ij}(n)$ (for $i \neq j$) by taking the Fourier transform of the cross correlation so that

$$\Phi_{ij}(n) = \frac{1}{T}\int_{t}^{t+T} C_{ij}(\tau)e^{-jn\omega_0\tau}d\tau = F_i^*(n)F_j(n) \tag{5.68}$$

This is the product of the Fourier coefficients of the time series $j$ and the complex conjugate of the coefficients for series $i$. The method of using direct Fourier transforms will be discussed in the next section. The cross spectrum $\Phi_{ij}$, as opposed to the auto spectrum $\Phi_{ii}$, is in general complex. The real part denotes the co-spectrum (Co), and the imaginary denotes the quadrature (Quad) spectrum, i.e., $\Phi_{ij}(n) = \mathrm{Co}_{ij}(n) + j\mathrm{Quad}_{ij}(n)$.

### 5.4.3 Direct Fourier approach

Instead of using the correlation Fourier transform of two time series to obtain the cross spectrum, a direct method (based on the Fourier transform of the time series) can be used. An alternative definition of the co-spectrum is to consider it in terms of the time average of the multiple of two time series where

$$c_{xy}(f)\Delta f = \overline{x(t)y(t)} \tag{5.69}$$

Expressing $x(t)$ and $y(t)$ as their complex fourier series so that

$$x(t) = \sum_{n=-\infty}^{\infty} X_n e^{j\omega_n t} \tag{5.70}$$

and

$$y(t) = \sum_{m=-\infty}^{\infty} Y_m e^{j\omega_m t} \tag{5.71}$$

then the product term can be expressed as

$$x(t)y(t) = \left(\sum_{n=-\infty}^{\infty} X_n e^{j\omega_n t}\right)\left(\sum_{m=-\infty}^{\infty} Y_m e^{j\omega_m t}\right) \tag{5.72}$$

$$\tag{5.73}$$

$$= \sum_n \sum_m X_n Y_m e^{j(\omega_n+\omega_m t)} \tag{5.74}$$

The time varying term has a zero mean when time averaged except when $\omega_n + \omega_m = 0$. This occurs when $m = -n$ where it is equal to 1. Since $Y_{-n} = Y_n^*$ the time average can be shown to be

$$\overline{x(t)y(t)} = \sum_n X_n Y_n^* \tag{5.75}$$

And since $X_n = \frac{1}{2}(a_n - jb_n)$ and $Y_n = \frac{1}{2}(c_n - jd_n)$, where the $a_n, b_n, c_n, d_n$ are the real Fourier coefficients derived from the Fourier transform by Eqs. 5.53. The cross spectrum can be given by

$$\overline{x(t)y(t)} = \frac{1}{2}\sum_{n=1}^{N/2}(a_n c_n + b_n d_n) \tag{5.76}$$

As with all the spectra in this chapter, the results will be approximate due to the random nature of the process and the resulting spectrum should be averaged over several harmonics where

$$c_{xy} = \frac{1}{2\Delta f}\sum_{\Delta f}(a_n c_n + b_n d_n) \tag{5.77}$$

The previous section indicated that the power spectrum consists of the Co and the Quad spectra. By advancing the $y(t)$ series by $90^0$ and using the same theory as shown for the co-spectra, the resulting equation is

$$q_{xy} = \frac{1}{2\Delta f}\sum_{\Delta f}(a_n d_n - b_n c_n) \tag{5.78}$$

Recombining Eqs. 5.77 and 5.78 will give the full power spectra of the two time series as $c_{xy} + jq_{xy}$.

### 5.4.4 Correlation examples

The two methods of constructing the power spectrum from cross-correlated time series will now be implemented to check their usability. The same time series that was created for the

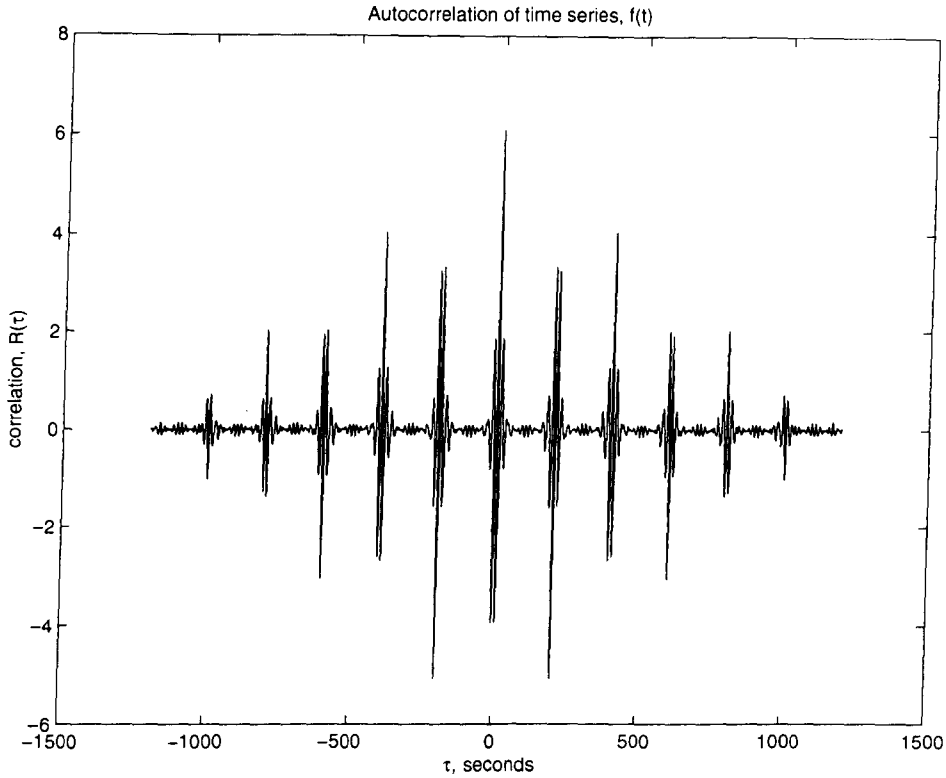


Figure 5.17: The autocorrelation of $f(t)$

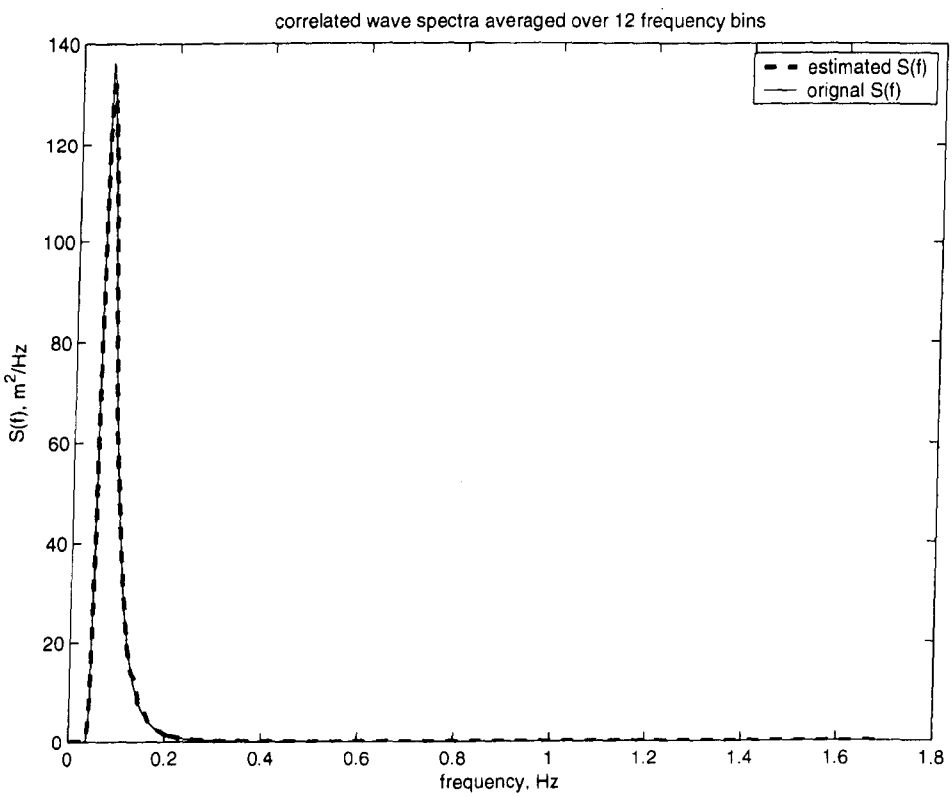


Figure 5.18: Power spectral density from autocorrelated $f(t)$

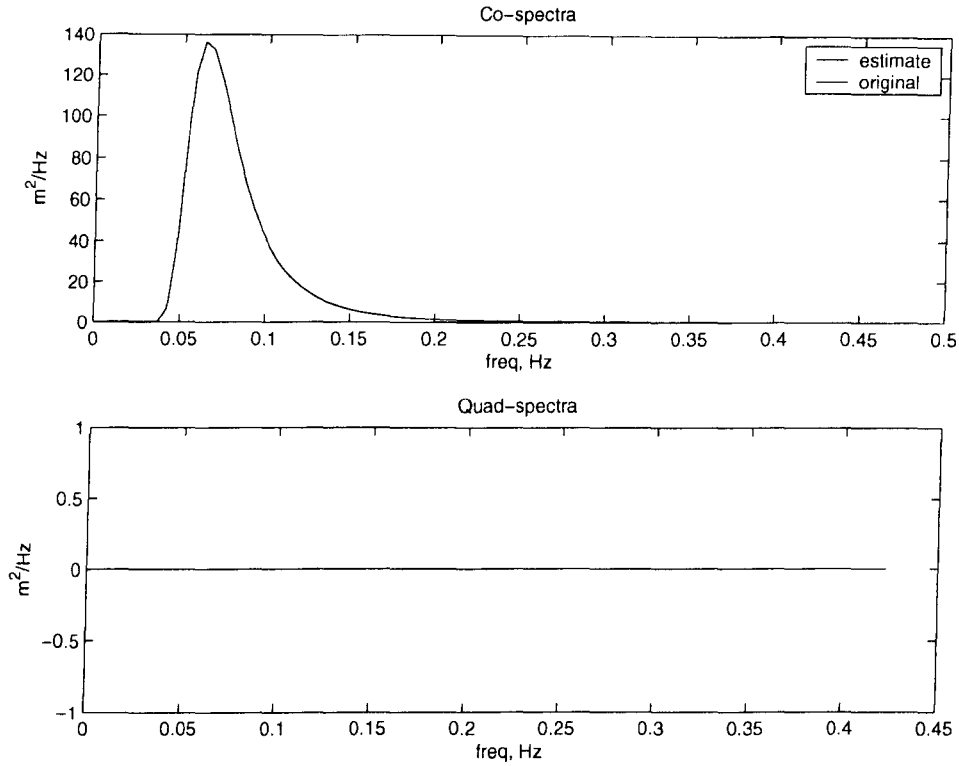


Figure 5.19: Co and Quad spectra calculated from direct fourier transforms

previous Fourier tests is used again here. This is a Pierson Moskowitz spectrum using linear frequency spacing and simulated for 1200 sec, sampled at 3.14 Hz to create an $N = 4096$ record.

Starting with the autocorrelation method the time series is processed as follows using MATLAB command `xcorr`:

$$\frac{1}{N}\texttt{xcorr(tSeries(1:N),tSeries(1:N));} \tag{5.79}$$

The autocorrelation is shown in Fig. 5.17. This shows a strong correlation of the time series intervals to a period of approximately 220 sec. The equation above shows the scaling of the autocorrelation required to obtain the correct results.

The next step is to take the Fourier Transform of the autocorrelation which is now of length $N = 8192$. The positive values of the spectrum are then doubled reducing the length to $N = 4096$ and the spectrum averaged over 12 harmonics to give the resultant spectrum shown in Fig 5.18.

The results of the second method, using the direct Fourier transform of the two time series, is presented in Fig 5.19. Using Eqs. 5.77 and 5.78 the Co and Quad spectra are calculated from the real Fourier coefficients given by Eq. 5.53. The results are then averaged

over six harmonics at a resolution of 0.005 Hz using Eq. 5.55. As expected, the co-spectrum is a good match to the Pierson-Moskowitz spectrum used in the generation of the time series and since this was the autocorrelation, the quadrature spectrum remains flat indicating exact agreement between the input signals.

### Discussion

The two methods of obtaining the complex power spectra presented above have returned good approximations. The second method of direct Fourier calculation will be used in the remainder of this thesis because it is quicker and it does not result in the doubling of the number of data points to be stored and manipulated.

# Chapter 6

# Experiments

The experiments in this chapter are laid out in approximately chronological order of implementation. This is done to show how the concept of wave prediction has developed through the course of this project. The first few sets of simulation experiments are simple in their implementation and in the thought behind them; the concepts described in the previous chapters were still in an early stage of development when these simulations were carried out. However, they give an insight into how the analysis techniques were implemented in the software environment.

The general flow of the chapter steps through the introductory modelling attempts: an implementation of spatial FFTs on a circular grid; correlation of time series and a brief discussion on beam steering. The chapter is concluded with an in-depth analysis of a simple one dimensional prediction over time and distance. Experimental verification, which was conducted in a small-scale wave tank, is also put forward at the end of the chapter.

## 6.1 Basic models and the spatial FFT

Mathworks' MATLAB is the main software environment used in the development of the experimental models. The first few groups of MATLAB files written dealt primarily with the setting up and use of simple models of surface elevation (Eq. 2.7). The first model simulated a two-dimensional (distance and time) travelling wave where:

$$\zeta(x,t) = a\sin(kx - \omega t) \tag{6.1}$$

Fig. 6.1 shows results from this simulation at a fixed point in time. This is the basic travelling wave equation in one spatial direction.

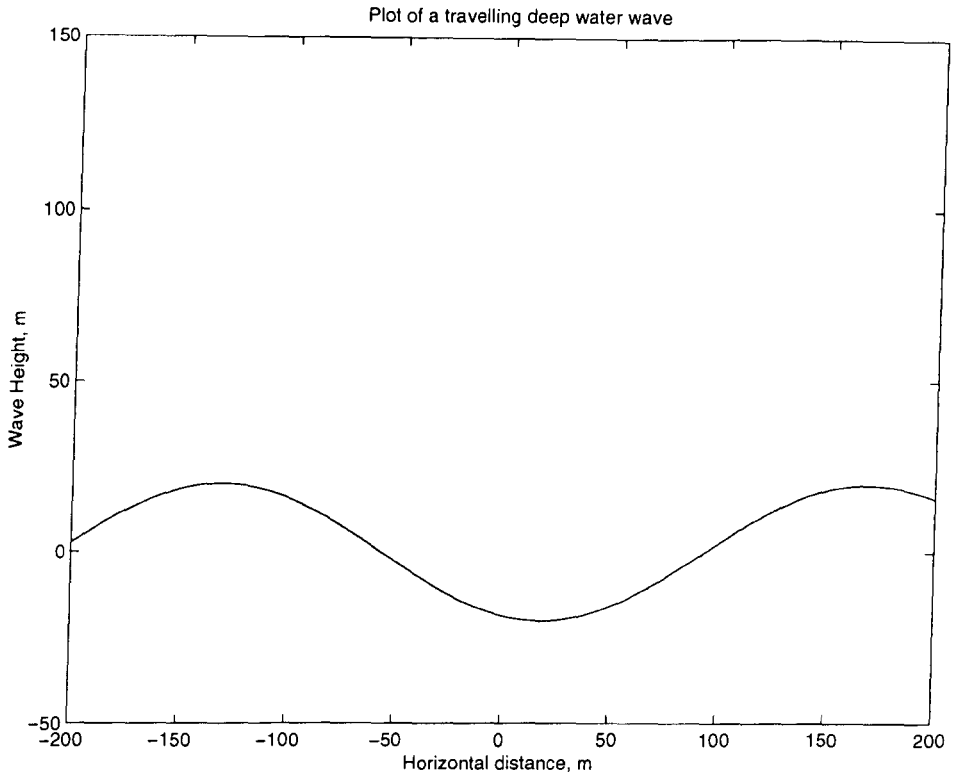


Figure 6.1: Simple test of a 2D travelling wave

Extending this test, the 2D output was extruded across the $y$ dimension to give a 3D display as shown in Fig. 6.2. The method by which this was achieved is very crude but gave an indication that MATLAB is capable of a 3D representation of surface elevation.

An extension to the code was added at this time to allow waves to travel in four directions: North, South, East and West. This was achieved by calculating a separate grid of values for each of the four directions (using the `circshift()` function to propagate the values) and summing the four grids to create the final output as shown in Fig. 6.3. This was a direct implementation of the superposition principle introduced in Chapter 2.

While this is not an ideal model, and it lacks in the ability to adequately define the input wave train directions of travel, it was sufficient to begin implementing the FFT over several spatial samples.

### 6.1.1 The Spatial FFT

Taking Eq. 2.7 at $z = 0$ and keeping $t$ constant (i.e., at a point in time), it becomes dependent only on distance $x$ with the $\omega t - \phi$ element becoming a static phase shift. Neglecting the direction of travel $\theta$ the resulting equation is

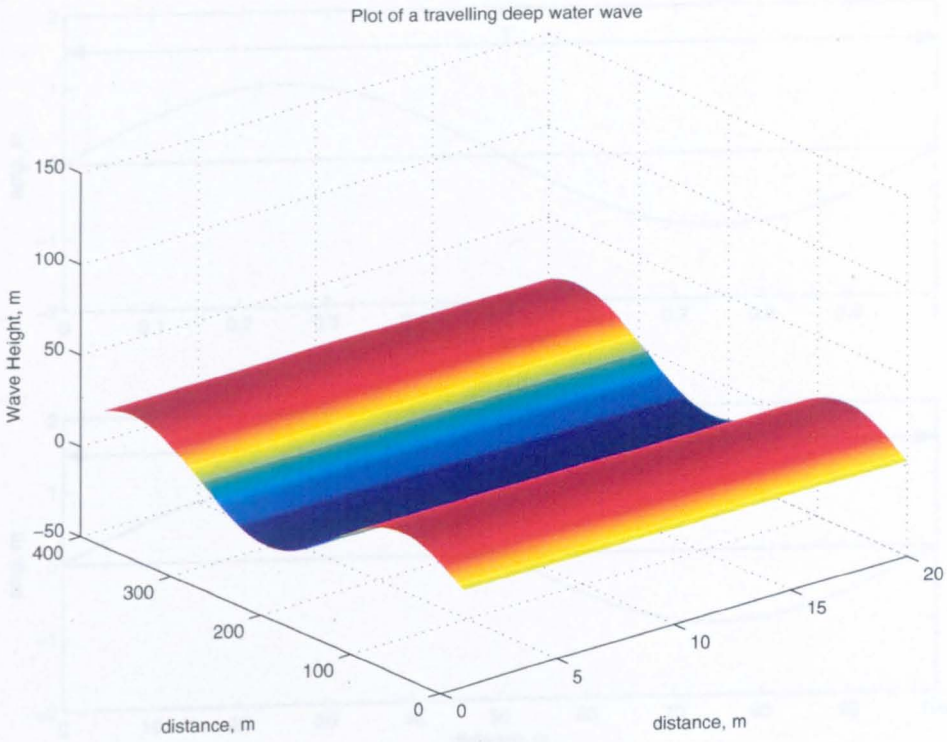


Figure 6.2: Simple test of a 3D travelling wave

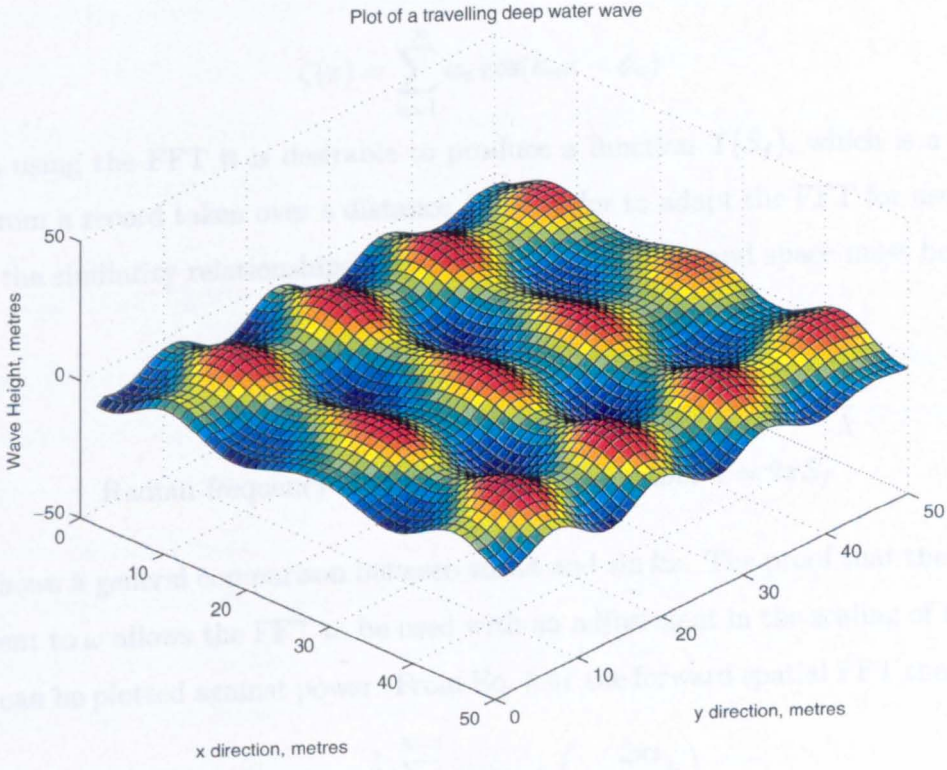


Figure 6.3: Simple test of a 3D set of travelling waves

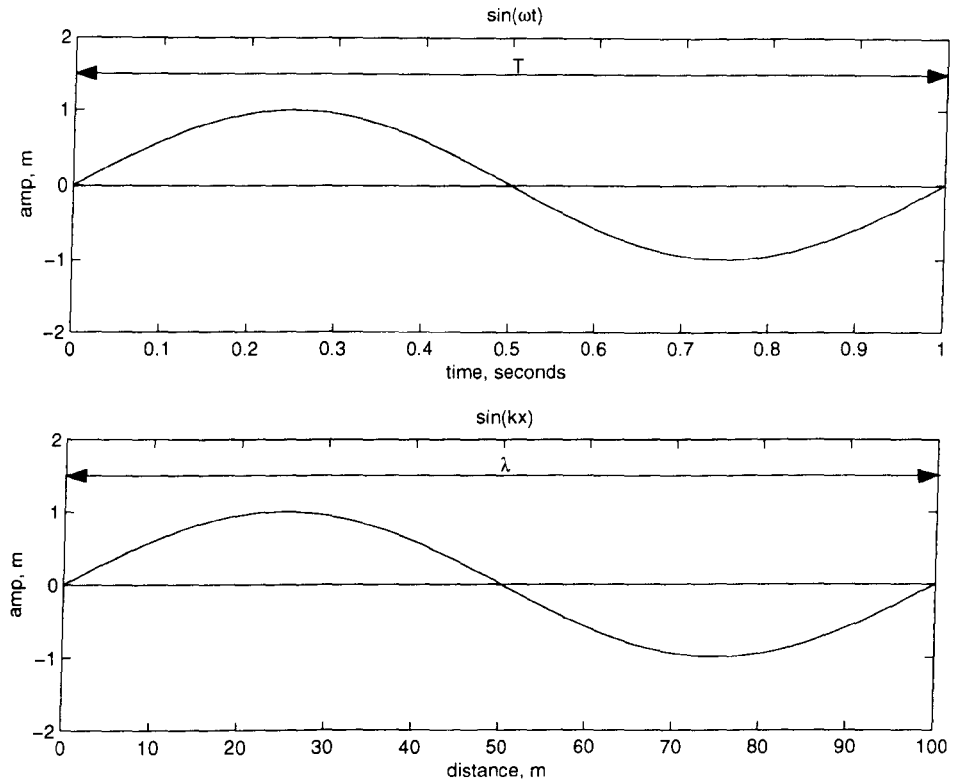


Figure 6.4: Showing the similarities between temporal and spatial sine functions

$$\zeta(x) = \sum_{n=1}^{\infty} a_n \cos(k_n x - \phi_n) \tag{6.2}$$

When using the FFT it is desirable to produce a function $\Upsilon(S_f)$, which is a transform of $\zeta(x)$, from a record taken over a distance $D$. In order to adapt the FFT for use with this equation the similarity relationships between variables in time and space must be stated.

$$\begin{aligned} \text{Time period } T &\equiv \text{wavelength } \lambda \\ \text{Frequency } f = \frac{1}{T} &\equiv \text{spatial frequency } S_f = \frac{1}{\lambda} \\ \text{Radian frequency } \omega = 2\pi f &\equiv \text{wave number } k = 2\pi S_f \end{aligned}$$

Fig. 6.4 shows a general comparison between $\sin \omega t$ and $\sin kx$. The proof that the $k$ number is equivalent to $\omega$ allows the FFT to be used with an adjustment in the scaling of the output so that $k$ can be plotted against power. From Eq. 5.41 the forward spatial FFT then becomes

$$\Upsilon(k) = \frac{1}{N} \sum_{i=0}^{N-1} \zeta(i) \exp\left(-j \frac{2\pi i}{N} k\right) \tag{6.3}$$

where $N$ is the length of the FFT and $0 < k < N - 1$.

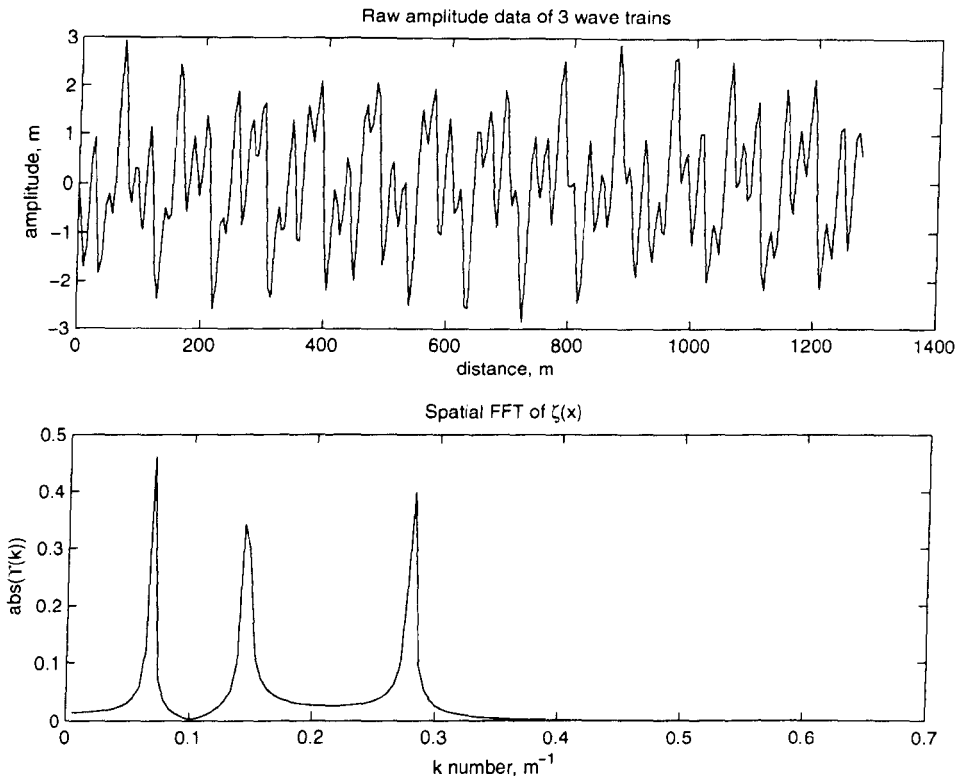


Figure 6.5: An example of a spatial FFT of 3 wave trains with $\lambda = 100$ m, 45 m and 23 m

The spatial frequency of the $k^{th}$ harmonic is $k/D$. Fig. 6.5 shows a test output for the superposition of three wave trains with $\lambda = 100$ m, 45 m and 23 m. The FFT of this was taken and the lower plot shows three peaks situated at the relevant $k$ numbers, thus proving that the FFT can be used with spatial data.

### 6.1.2 Experiments

The initial experiments extracted samples along the $x$ and $y$ axis of the generated grid then took the spatial FFT of these series. These simple results showed the same number of distinct spectral peaks as the number of wave trains used in generating the grid. It was felt that this method could be advanced upon.

Further development of the sea elevation modelling code took place in order to allow the user to specify a wave-field as a list of wave vectors allowing for easier manipulation of the test patterns (this is detailed in Chapter 3). Further development also took place in the modularisation of the code using the code profiler, taking advantage of MATLAB's matrix handling ability to allow for the simulation of increasingly complex wave-fields. In particular, the use of `meshgrid()` considerably reduced the processor load, releasing capacity for more

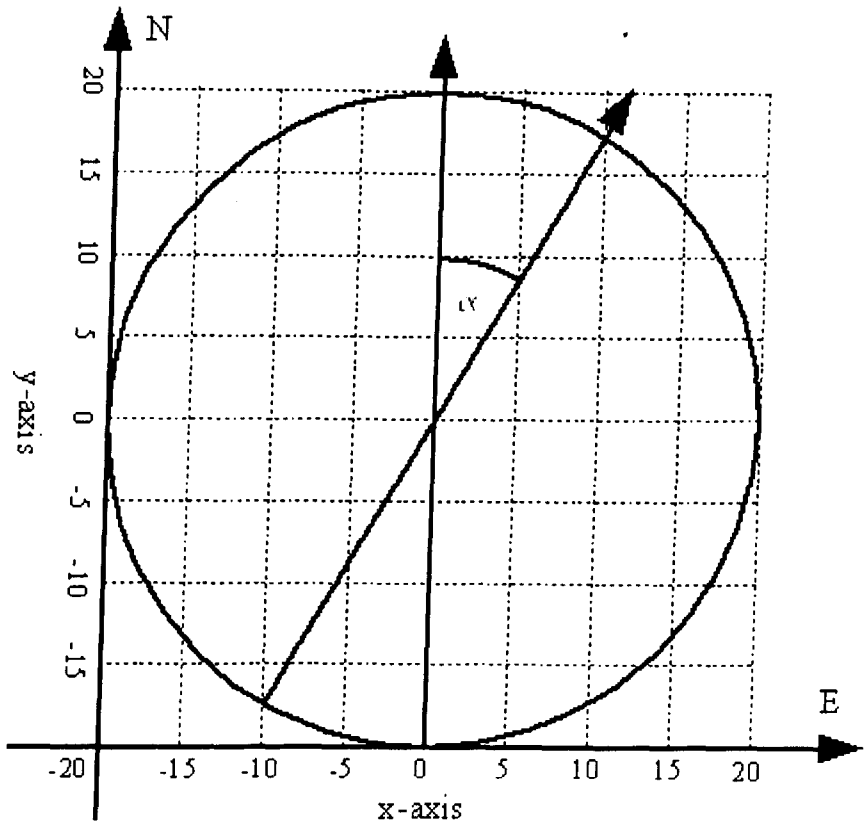


Figure 6.6: Showing extraction angle $\alpha$ with regards to the x and y axes

accurate FFT use.

In early instances, extraction took place perpendicular to the $x$ and $y$ axes along extraction angles $\alpha$ of 0° and 90°. This has an orthogonal relationship if the wave train is moving at an angle of 0°, then there will be a strong spectral peak at $\alpha = 0°$ but no power present at $\alpha = 90°$ (a similar argument was used in Chapter 4 when describing the correlation between pitch and roll with a buoy). This result showed promise in the detection of the direction of wave travel.

The next step was to allow the user to extract spatial information along any angle they may wish to choose as illustrated in Fig. 6.6. This gives the user the ability to compare the spectral frequency power density at many frequencies and angles. A suitable method for displaying this information was required.

Manufacturers of microphones display their sensitivity characteristics as plots of response against direction of the source of sound. An adaption of this approach is given in Fig. 6.7. This shows that at 90° intervals the spectral frequency alternately peaks or drops to zero.

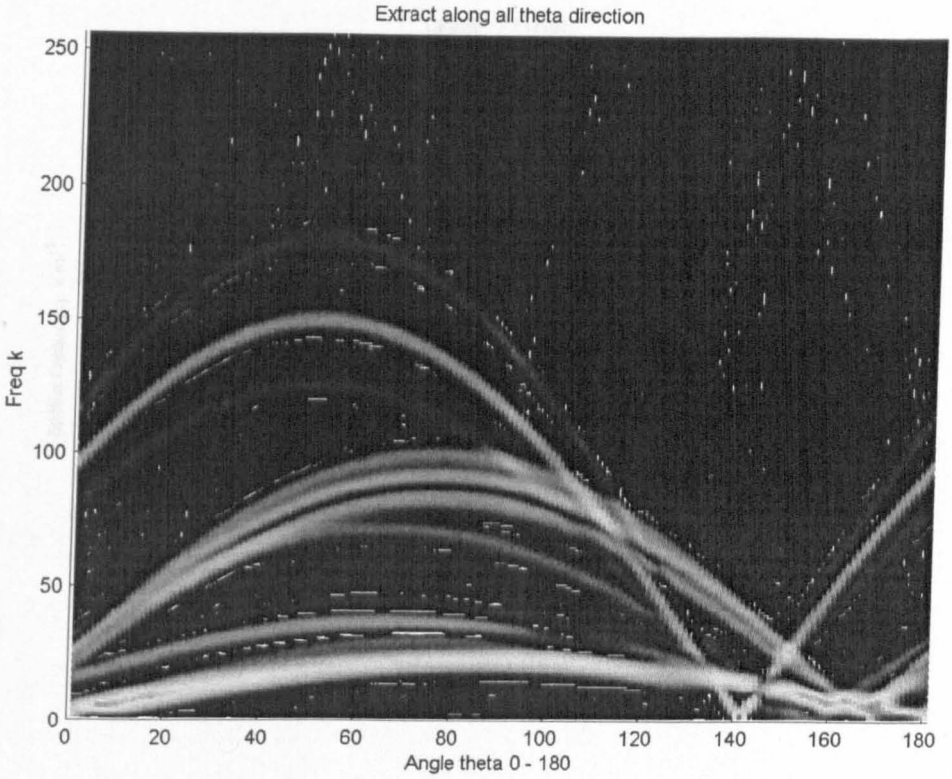


Figure 6.7: Raw circle FFT file with blurring

The angle of extraction, where the spatial frequency peaks, indicates that a wave vector may be present heading in that particular direction.

The image produced by plotting the output of the spatial FFT contains both the main peak and several spectral lobes. When many wave vectors are present this leads to a blurring of the image. In addition, while it is relatively easy for the human eye to pick out the parabolic arcs in Fig. 6.7, a computer cannot do this. By thresholding the image and using monochromatic colouring Fig. 6.8 is produced. From this image, a routine can be written to detect the parabolic curves by comparing them to stored images created for individual wave vectors.

### Discussion

Overall this method works reasonably well in detecting the direction of propagation of wave trains and in determining their wavelength. But, it comes at a cost. In order to produce a sharp image many data points are required. For a realistic application the number of data points available will be limited. The cost of deploying a 50 by 50 grid of data buoys or pressure sensors would be prohibitively uneconomic. In utilising the spatial FFT in software

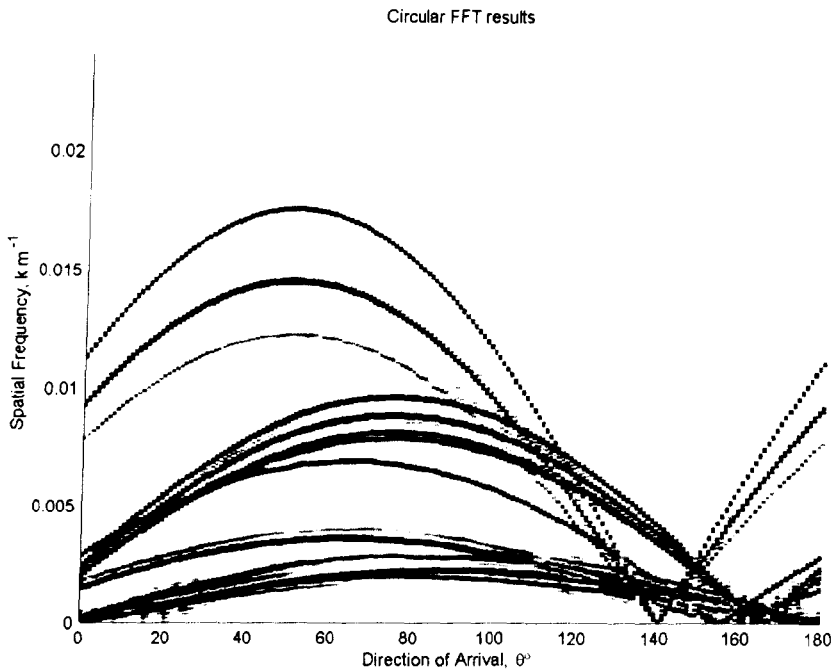


Figure 6.8: Processed circle FFT results

a grid of 1024 by 1024 was required before acceptable results could be obtained. A possible way of using this method in the field would be through satellite altimeter scans of the wave farm. For real-time results this would require a stationary satellite over the farm returning data in real time. But, again, the cost of this is prohibitive.

## 6.2 Correlation and linear arrays

Spatial FFT tests are reliant on too many data points therefore it was decided to focus on a method that uses as few data points (i.e., wave buoys) as possible. Early discussions with Dr Wood in Christchurch led to the suggestion that the correlation between two buoy records may prove fruitful in determining the mean direction of propagation for a wave-field. The correlation between two data point records is commonly used in astronomy for fixing the position of stars and galaxies.

### 6.2.1 Correlation experiments

The basic correlation equation [51] is:

$$\widehat{R}_{xyr} = \frac{1}{N-r} \sum_{i=1}^{N-r} x_i y_{i+r} \tag{6.4}$$

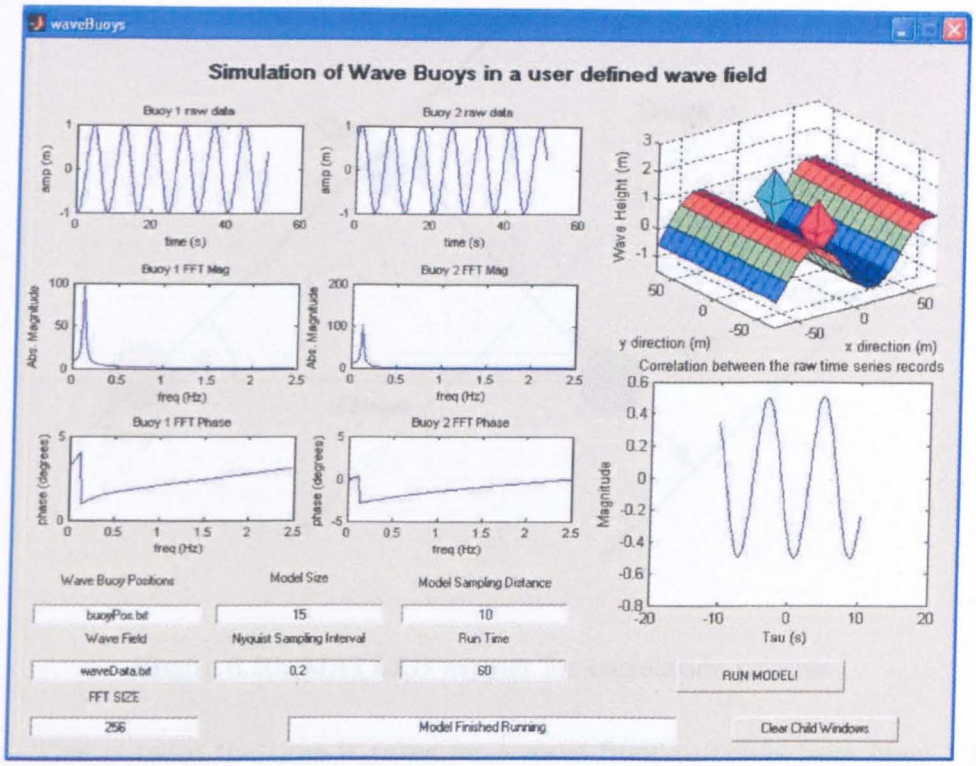


Figure 6.9: MATLAB extract for correlation process

where $r = -m, \ldots, -1, 0, 1, \ldots, m$, $x$ is the surface elevation time series taken from one buoy and $y$ is the series taken from the other. In addition, $N$ is the number of samples in each data set and $r$ is the number of samples by which $y$ is delayed; $m$ is generally taken to be 20 % of $N$. The basic concept in this method is to delay $y$ by $r$ samples, multiply this with $x$ for each sample and then sum the resultant series to give $\widehat{R}_{xyr}$. If the two signals are identical then, at $r = 0$, $\widehat{R}_{xyr}$ will have a peak value. For $r \neq 0$ the resultant value will be less than at the peak indicating that the two series are not fully correlated for the delay value $r$.

Fig 6.9 shows a MATLAB dialog used in testing the correlation principle. In this example a wave train of $\lambda = 100$ m, amplitude of 1 m and direction of travel $\theta = 90°$ was used. In the upper right corner the simulation of the wave-field is shown with two wave buoys. The position of the wave buoys can be given in a text file, as can the wave-field information. The wave records that are traced by the two wave buoys are shown in the top two windows on the upper left. Below these two windows the temporal FFT data is displayed showing that a frequency of 0.125 Hz is present in both of the wave records, which corresponds to $\lambda = 100$ m in deep water (see Table 2.1). The lower right window shows the result of the correlation of the two wave records and is sinusoidal in nature, repeating with a period of

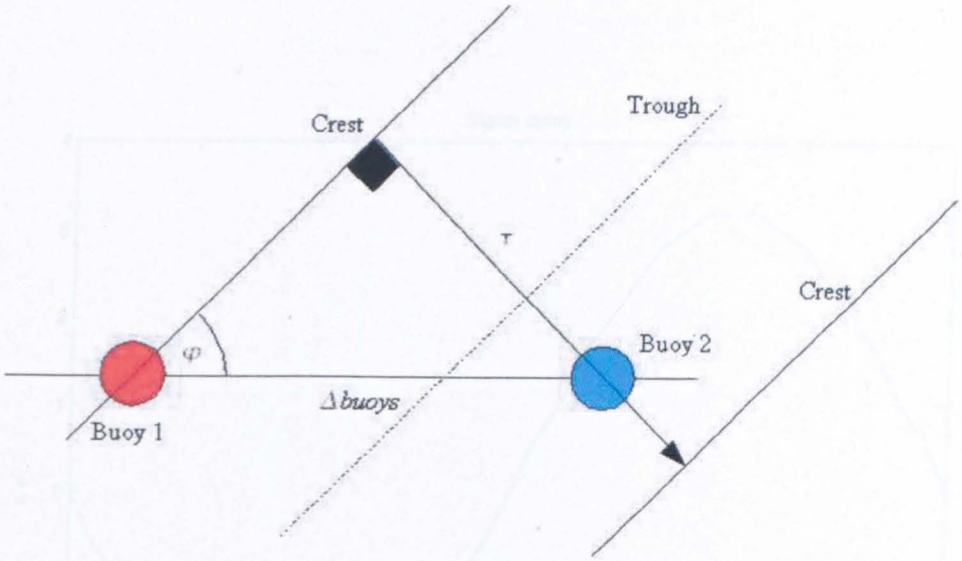


Figure 6.10: MATLAB extract for correlation process

6.402 sec. This is twice the time it takes for a wave front to travel from buoy 1 to buoy 2. The value of $\tau$, the delay between the two signals, is taken at the value of $r$ where $\widehat{R}_{xyr}$ peaks, in this case -3.201 sec.

### Interpreting $\tau$, the delay between signals

Fig. 6.10 illustrates how the delay between the two wave records can be used to determine the direction of wave propagation (the location of the wave source). The values of $\tau$, the delay between the two wave records, and $\Delta$buoys, the distance between the two wave buoys, are known. From the FFT performed prior to this operation, we know the frequency of the wave $\omega$, the wavelength $\lambda$ and hence the celerity (speed) of the wave $c_{100}$. The celerity of the wave and the distance between the two buoys can be used to calculate the length of the hypotenuse of the triangle shown in Fig. 6.10. From this:

$$\cos(\varphi) = \frac{c_{100}\tau}{\Delta\text{buoys}} \tag{6.5}$$

The result from this equation allows the direction of wave propagation $\varphi$ to be determined.

A series of model runs were performed with the direction of $\varphi$ varied from 0 to 360°. The results are shown in Fig. 6.11 with $\varphi$ plotted against $\tau$.

The direction of propagation of a wave can be inferred from the value of $\tau$. As $\tau$ approaches the time taken for the wave to propagate over the distance $\Delta$buoys the angle $\varphi$ tends to 90° and therefore the waves are arriving at 90° to the wave buoys. This is shown in Fig. 6.12 with the angle $\varphi$ approaching 80°.

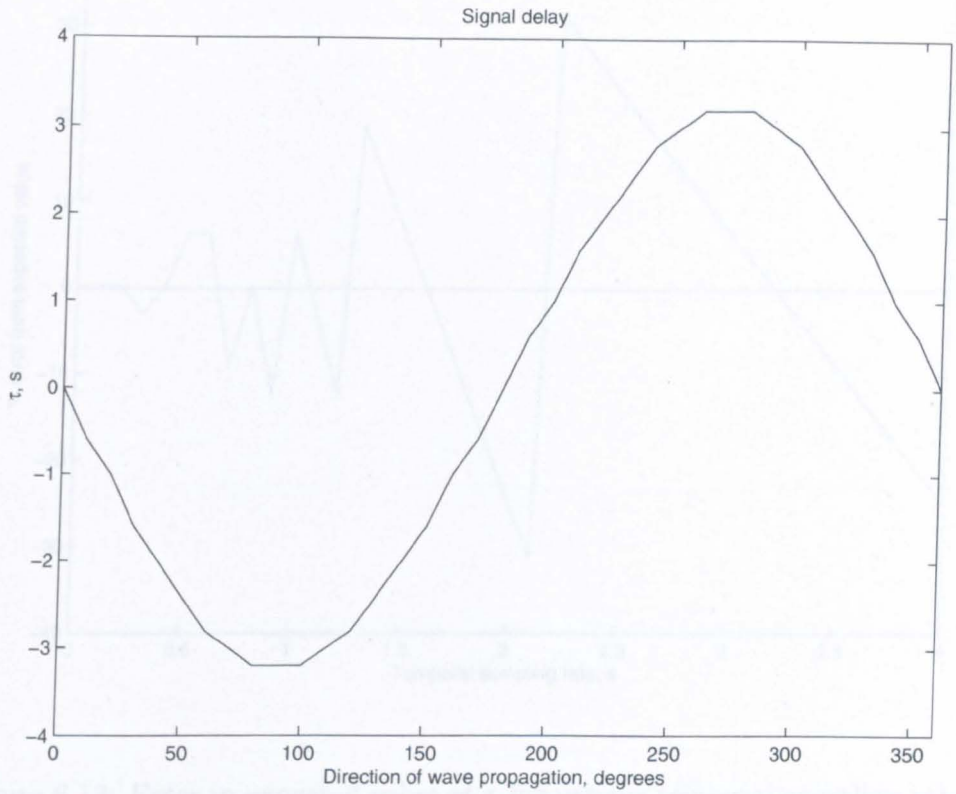


Figure 6.11: expected value of $\tau$ for various $\varphi$

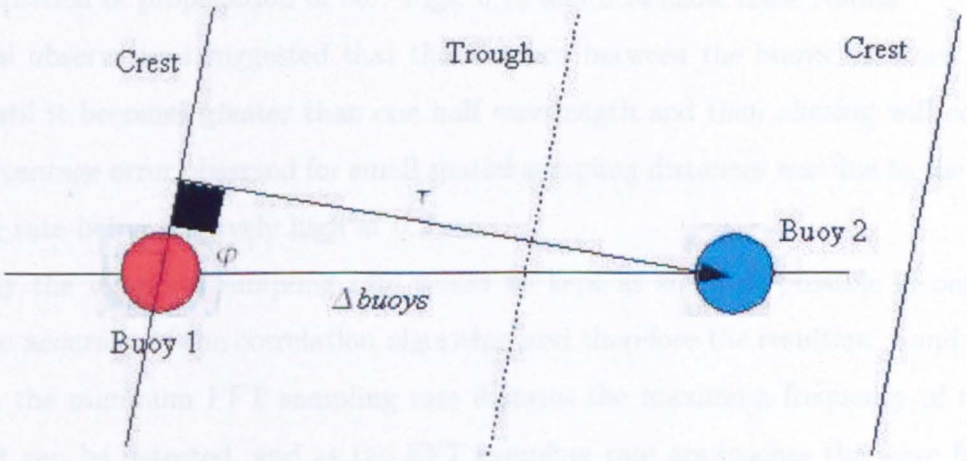


Figure 6.12: Wavefront approaching at $\varphi = 80°$

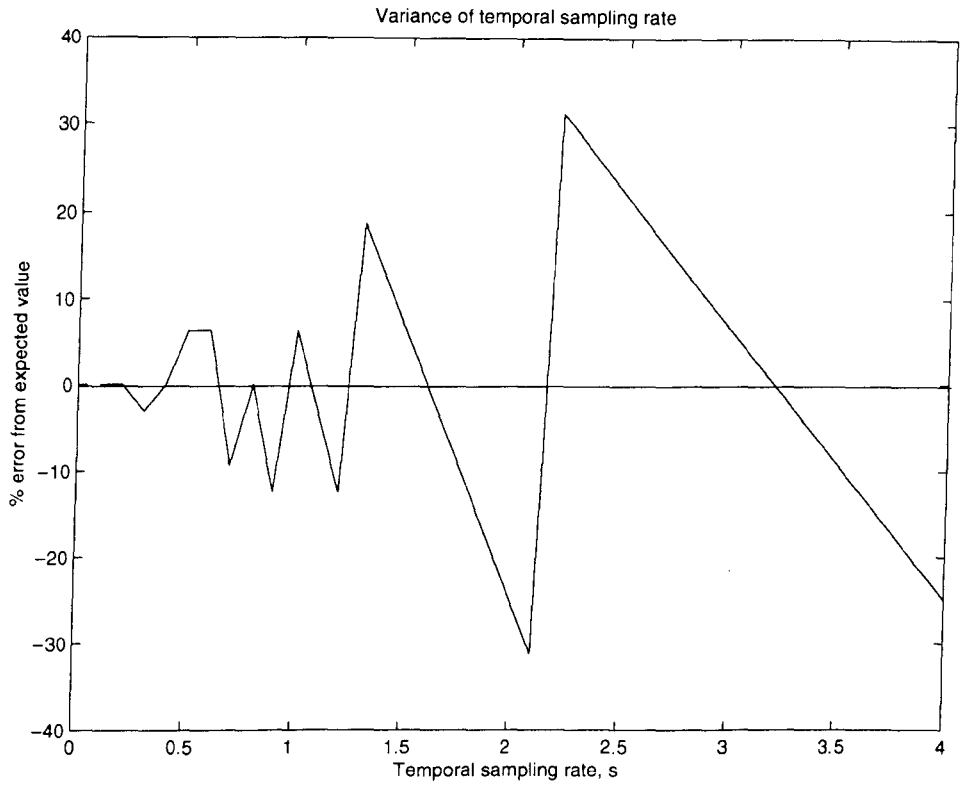


Figure 6.13: Error in expected value of $\tau$ for various temporal sampling rates

At present, with two wave buoys, the field of view is from 0 to 180°, i.e., the buoys cannot tell if a wave is coming from in front or from behind.

The effect of the spatial sampling rate (distance between the wave buoys) and the temporal sampling rate were also tested using an input wave train with a wavelength of 100 m and a direction of propagation of 90°. Figs. 6.13 and 6.14 show these results.

Initial observations suggested that the distance between the buoys does not affect the result until it becomes greater than one half wavelength and then aliasing will occur. The large percentage error observed for small spatial sampling distances was due to the temporal sampling rate being relatively high at 0.2 sec.

Ideally the temporal sampling rate would be kept as small as possible in order to increase the accuracy of the correlation algorithm and therefore the resultant $\tau$ and $\varphi$ values. However, the minimum FFT sampling rate dictates the maximum frequency of the wave-train that can be detected, and as the FFT sampling rate approaches the wave frequency, the FFT becomes less accurate. The best solution may be to sample every 0.01 sec, but only use every tenth sample in calculating the FFT, giving about 100 samples for a 10 sec fundamental wave period.

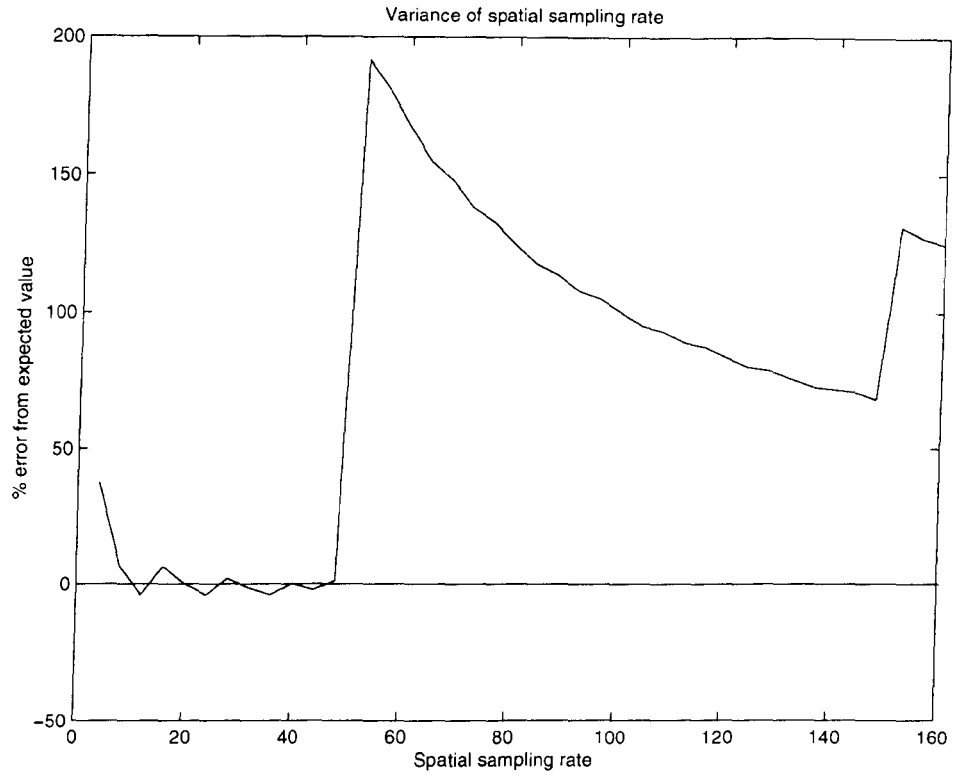


Figure 6.14: Error in expected value of $\tau$ for various spatial sampling rates

### 6.2.2 Linear array experiments

The correlation routines proved to be reasonably useful in determining the direction of the wave travel. A logical extension to this is to look at the correlation between more than two buoys. This approach leads to the more sophisticated uniform linear array method of processing which is commonly used in communications theory.

#### Uniform linear array theory

The experimental and theoretical work on this principle is not extensive, therefore the following section closely follows that presented in Naidu [52] in order to give an introduction to the methodology.

Consider a plane wavefront, having a temporal waveform $f(t)$ incident to a uniform linear array (ULA) of sensors (see Fig. 6.15) at an angle $\theta$. In signal processing literature, the angle of incidence is also known as the direction of arrival (DOA). Note that the DOA is always measured with respect to the normal of the array aperture. It is assumed that a source, in our case the origin of a storm, emits a stationary stochastic signal $f(t)$. Let $f_m(t)$, where $m$ = 0, 1, 2, ... ,$M$-1, be the outputs of the sensors. The signal arrives at successive sensors

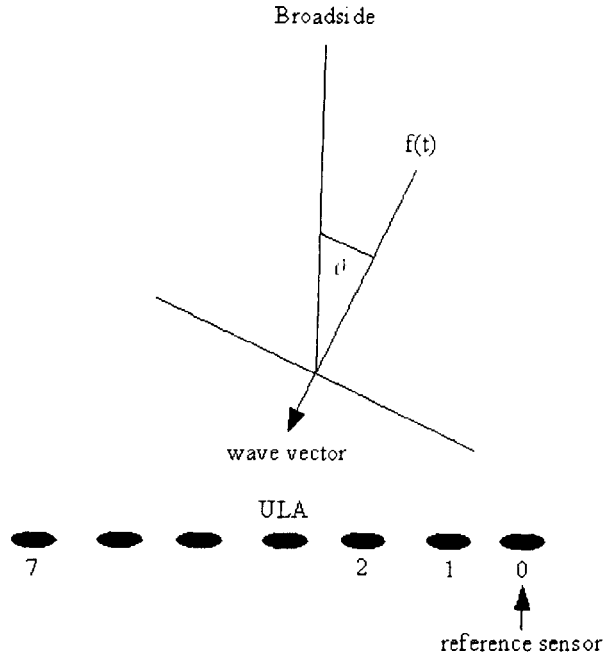


Figure 6.15: A Uniform Linear Array

with an incremental delay (similar to the correlation principle above). The output of the first sensor is $f_0(t) = f(t)$, the output of the second sensor is $f_1(t) = f(t - \Delta t)$ and so on. Thus, the output of the $m^{th}$ sensor is $f_m(t) = f(t - m\Delta t)$.

The output of the $m^{th}$ sensor can equally be represented by its Fourier transform where

$$f_m(t) = \frac{1}{2\pi} \int_{-\infty}^{\infty} F(\omega) e^{j\omega\left(t - \frac{md}{c}\sin\theta\right)} d\omega \tag{6.6}$$

The simplest form of array signal processing is to sum all of the sensor outputs without any delay so that

$$\begin{aligned} g(t) &= \frac{1}{M} \sum_{m=0}^{M-1} f_m(t) \\ &= \frac{1}{2\pi} \int_{-\infty}^{\infty} F(\omega) e^{j\omega t} \frac{1}{M} \sum_{m=0}^{M-1} e^{-j\omega \frac{md}{c} sin\theta} d\omega \\ &= \frac{1}{2\pi} \int_{-\infty}^{\infty} F(\omega) H(\omega\tau) e^{j\omega t} d\omega \end{aligned} \tag{6.7}$$

where $H(\omega\tau)$ is the array response function and $\tau = \frac{d}{c}\sin\theta$ with wave velocity $c$ and sensor spacing $d$. The array response function for a ULA is given by

$$H(\omega\tau) = \frac{1}{M} \sum_{m=0}^{M-1} e^{j\omega \frac{md}{c}\sin\theta} = \frac{\sin\left(\frac{M}{2}\omega\tau\right)}{M \sin\left(\frac{\omega\tau}{2}\right)} e^{j\frac{M-1}{2}\omega\tau} \tag{6.8}$$

A few samples of the frequency response function (magnitude only) are shown in Figs. 6.16, 6.17 and 6.18 for different values of array size $M$. The response function is periodic with a

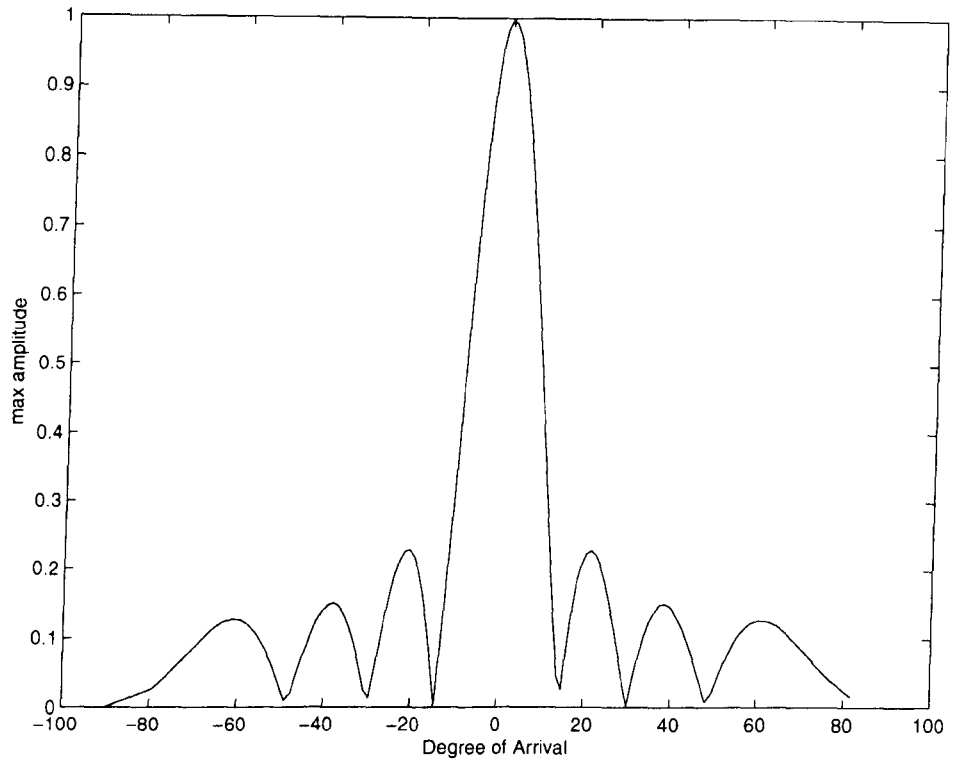


Figure 6.16: ULA response with 8 sensors

period of $2\pi$. The maximum occurs at $\omega\tau = 2n\pi$. The peak at $n = 0$ is known as the main lobe and other peaks at $n = \pm 1 \pm 2, \ldots$ are known as grating lobes. If the range of $\theta$ is reduced it is possible to increase the sensor spacing, for example, for $-\frac{\pi}{4} \leq \theta + \frac{\pi}{4}$ the sensor spacing needs to satisfy the constraint $\frac{d}{\lambda} \leq \frac{2}{\sqrt{2}}$. The phase of the frequency response is a linear function of $\omega\tau$. This useful property of a ULA is lost when the sensors are non-uniformly spaced.

The array response is a function of the product of frequency $\omega$ and delay $\tau$ or, more explicitly, $\omega\frac{d}{\lambda}\sin\theta$. The implication of this dependence is that two wavefronts whose waveform is a simple sinusoid but with different frequencies $(\omega_1, \omega_2)$ arriving at different angles $(\theta_1, \theta_2)$ will produce an identical array response if $\omega_1 \sin\theta_1 = \omega_2 \sin\theta_2$. The response function has a main-lobe which is surrounded by many side-lobes of decreasing magnitude just as we find in spectral windows. The first zero is at

$$\theta_{zero} = \sin^{-1}\frac{\lambda}{Md} \tag{6.9}$$

which, for large $M$, becomes inversely proportional to the array length expressed in terms of wavelength.

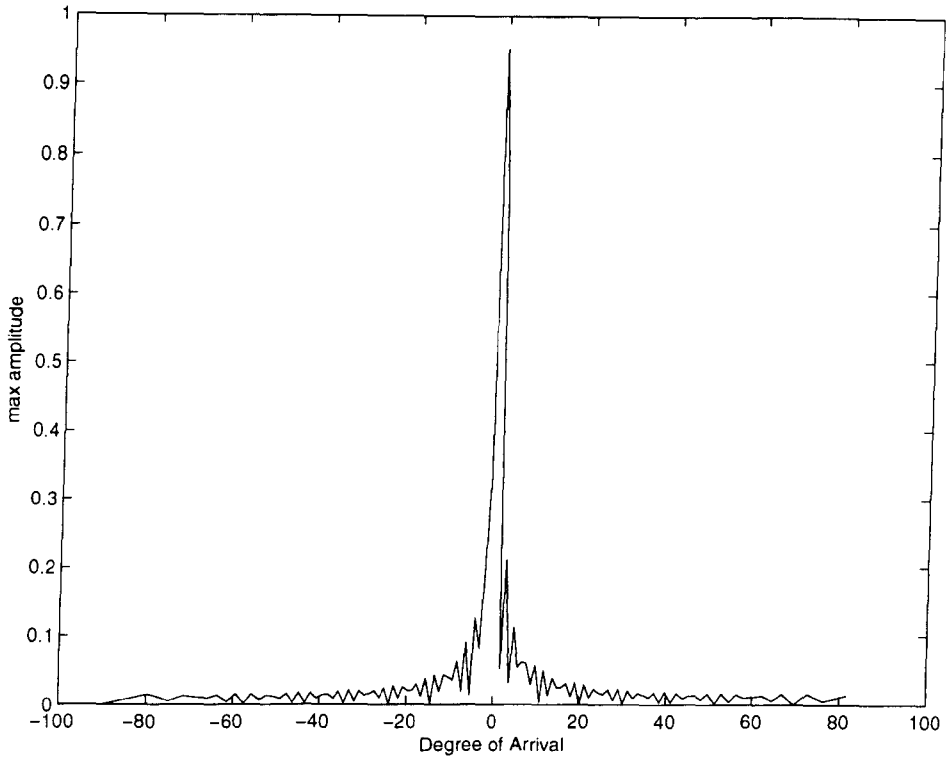


Figure 6.17: ULA response with 64 sensors

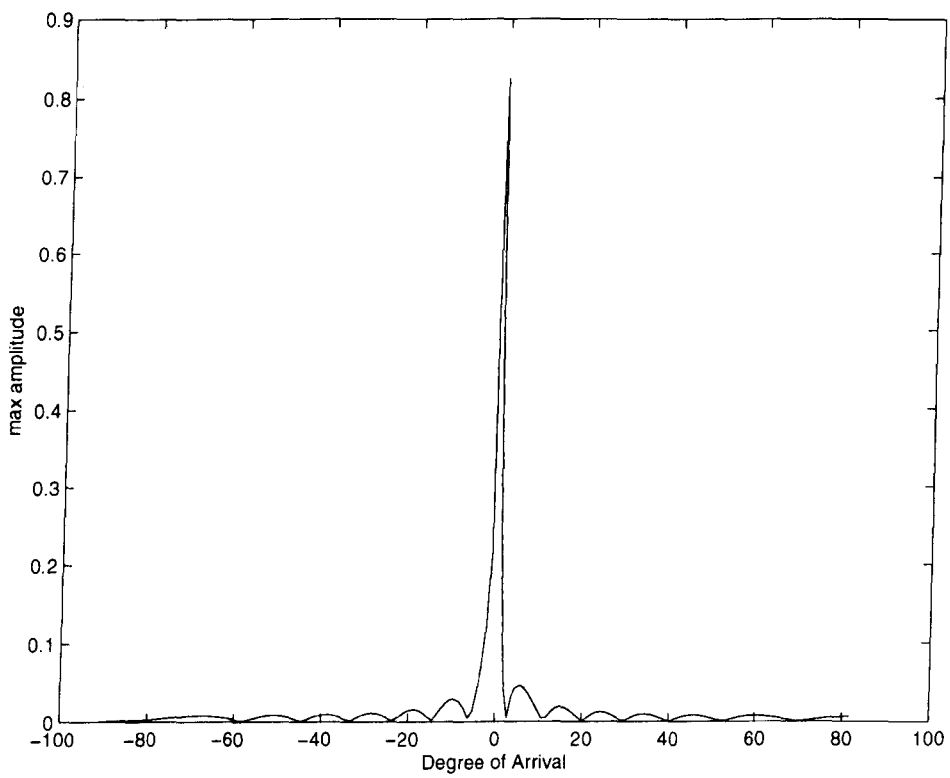


Figure 6.18: ULA response with 128 sensors

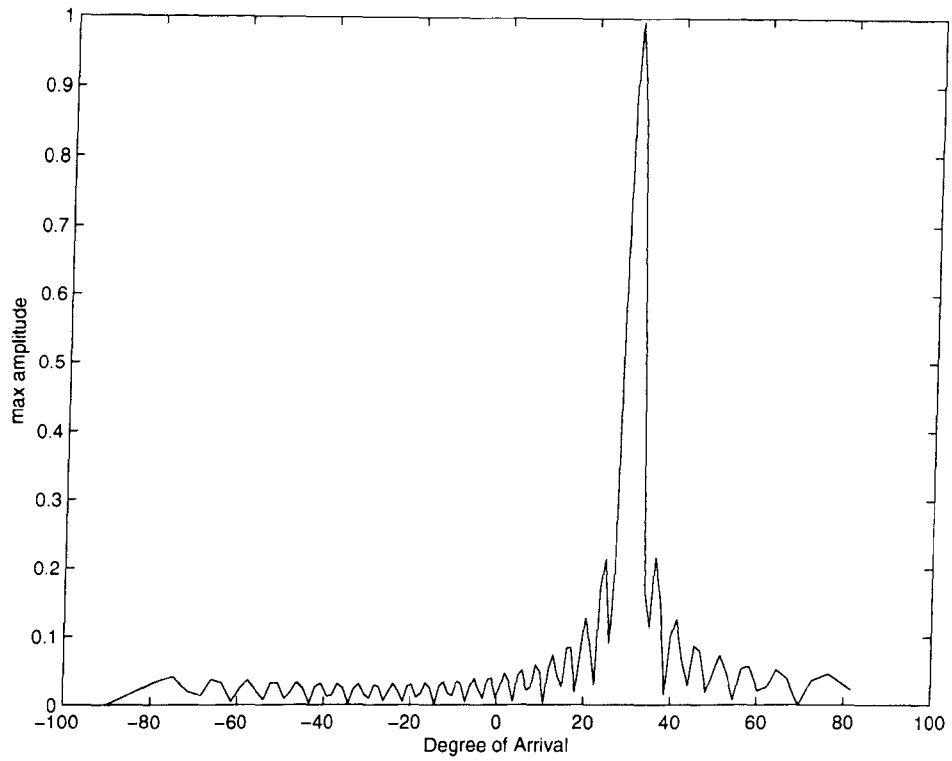


Figure 6.19: ULA response for a DOA of 30°

### Array Steering

In the previous section it was seen that the array response is a maximum when the direction of arrival (DOA) is perpendicular on ($\theta = 0$). The maximum, however, can be changed to any direction by introducing a time delay to each sensor output before summation. This is known as array steering. Let an incremental delay of $\tau$ per channel be introduced. The sum output of the array is now given by

$$\begin{aligned} g(t) &= \frac{1}{M}\sum_{m=0}^{M-1} f_m(t+m\tau) \\ &= \frac{1}{2\pi}\int_{-\infty}^{\infty} F(\omega)e^{j\omega t}\frac{1}{M}\sum_{m=0}^{M-1} e^{j\left(\tau-\frac{d}{c}\sin\theta_0\right)\omega m}d\omega \\ &= \frac{1}{2\pi}\int_{-\infty}^{\infty} F(\omega)H\left(\left(\tau-\frac{d}{c}\sin\theta_0\right)\omega\right)e^{j\omega t}d\omega \end{aligned} \tag{6.10}$$

where it is assumed that the DOA is $\theta_0$. Let $\tau = \frac{d}{c}\sin\theta$. The array response is maximum whenever $\theta = \theta_0$. The array is steered in the direction $\theta_0$, i.e., in the direction of arrival of the incident wavefront. The array response is now a function of the DOA. This is demonstrated in Figs. 6.19, 6.20 and 6.21. It is interesting to note that the width of the main-lobe increases

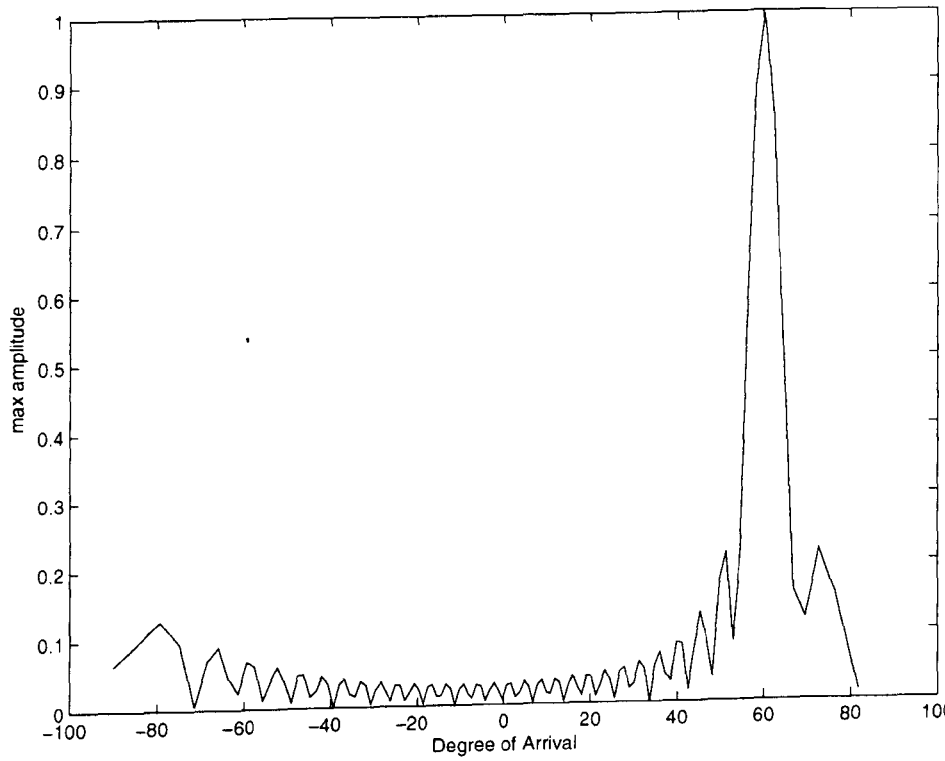


Figure 6.20: ULA response for a DOA of 60°

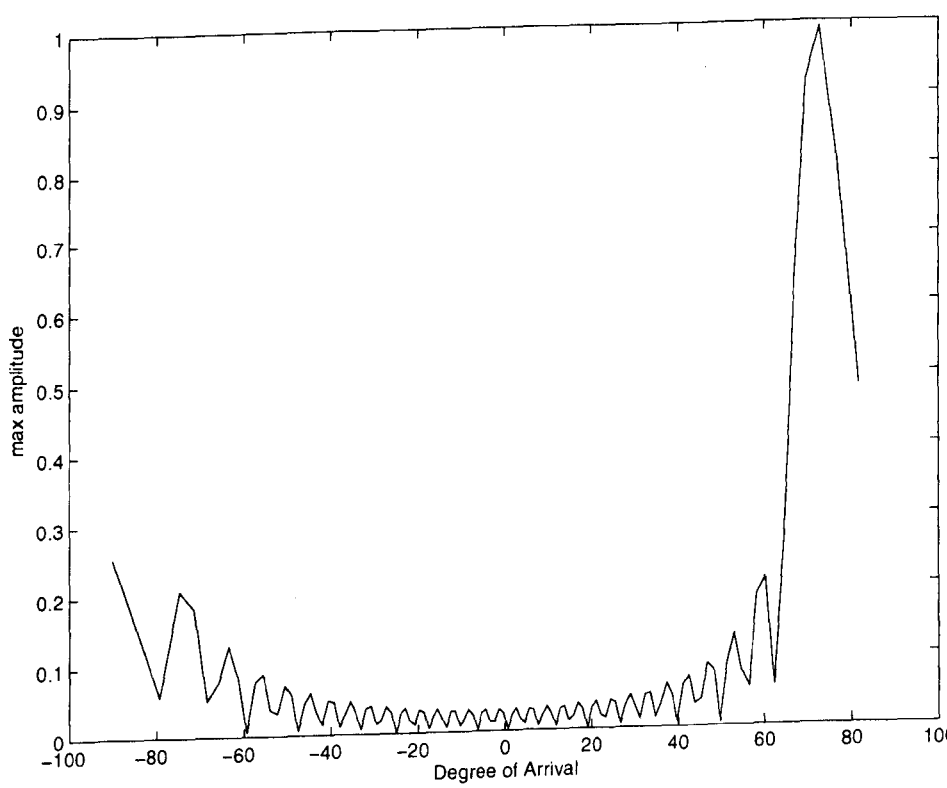


Figure 6.21: ULA response for a DOA of 72°

with increasing DOA.

### Discussion

On initial investigation it would appear the ULA technique would prove to be very useful in determining wave direction information; but, it suffers from several drawbacks. The most important is that it will (like the spatial FFT) depend on a large number of data points in order to give accurate results. A large number of data points means using many data buoys. A second problem is that the response of the array is dependent on the distance between each sensor. The array is most accurate at wavelengths which are twice the distance between the sensors and it loses accuracy outside this range. A fix is provided by using a sparse array arrangement and selectively choosing which sensors to accept information from. Unfortunately this would again require many sensors close together. If data sensors, such as the Waverider, are mounted too close together then there is a real risk of their moorings becoming entangled in storm sea conditions (see Chapter 4). There is also the problem that the Waverider buoys will tend to wander from their mean position distorting the final results.

However putting these issues aside, there is scope to use selective spatial filtering to narrow down the range of $\theta$ over which the array is applied. There is much literature on the subject of ULAs and how to improve their output, Barber [53] and Borgman [54] documented these improvements. The subject of ULAs will be discussed further in Chapter 7 since they can provide a means of analysis when used in conjunction with device displacement compensation in a full scale farm situation.

## 6.3 Fourier extension of time series

Previous simulations in this chapter have usually assumed multiple measurement devices. Taking into consideration the results of Chapter 4, a time-series recorded from a single device is what will be realistically available. This device will most likely be a Waverider buoy as it is the most widely available and cost effective. Although it will not accurately make a fixed point recording of the surface elevation, signal processing methods combined with positional information could foreseeably be used to recreate a fixed point measurement. In order to progress this assumption is made.

The question now arises as to how far ahead can a prediction be made, from a single directional wave buoy, in time and over distance.

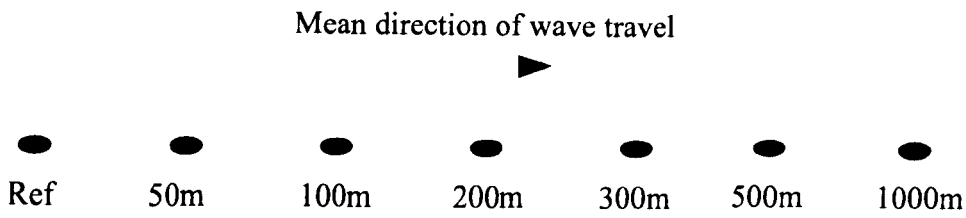


Figure 6.22: Layout of theoretical surface displacement measurements

### 6.3.1 Basic setup

In order to ascertain if a prediction is correct, and the extent to which it will hold true, a reference point must be selected. This is were the initial data gathering occurs. Then a series of comparison points are chosen to assess the validity of the prediction. To supply this data the wave model in Chapter 3 was implemented to create seven surface elevation time series. Fig. 6.22 shows the orientation of these records. These records assume deep water and a distance sufficiently removed from land as to preclude reflection of wave energy.

To begin simply, an omnidirectional non-harmonic input file was generated for a wind-driven fully-developed sea state, typical of that off of the west coast of Scotland. This corresponds to gale force $5-6$ or in the region of 12 $ms^{-1}$. To improve the calculation speed, 256 wave vectors were generated at randomly spaced frequencies with an upper limit of 1 Hz; a higher frequency limit is used here because at lower wind speeds a significant portion of energy is still contained within the upper frequency range. The simulated records had a sampling period of 3600 sec sampled at a rate of 3.4133 Hz, this gave 12288 samples per record. For the purposes of spectral analysis the recommendation of Chapter 5 was to use records of 1200 sec and 4096 samples. Hence the records generated were three times this length to allow the spectral evolution of the simulations to be studied.

Figs. 6.23 and 6.24 show the spectral density of the omnidirectional wavefield and the simulated amplitude spectrum. Fig. 6.25 shows an extract from the beginning of the reference time series. Fig. 6.26 shows the output of the first three sensors (i.e., the reference, 50 m and 100 m sensors). It should be noted that the 50 m and 100 m records are not simply copies of the reference time series delayed by the distance to the next sensor but evolutions of the series over distance and time.

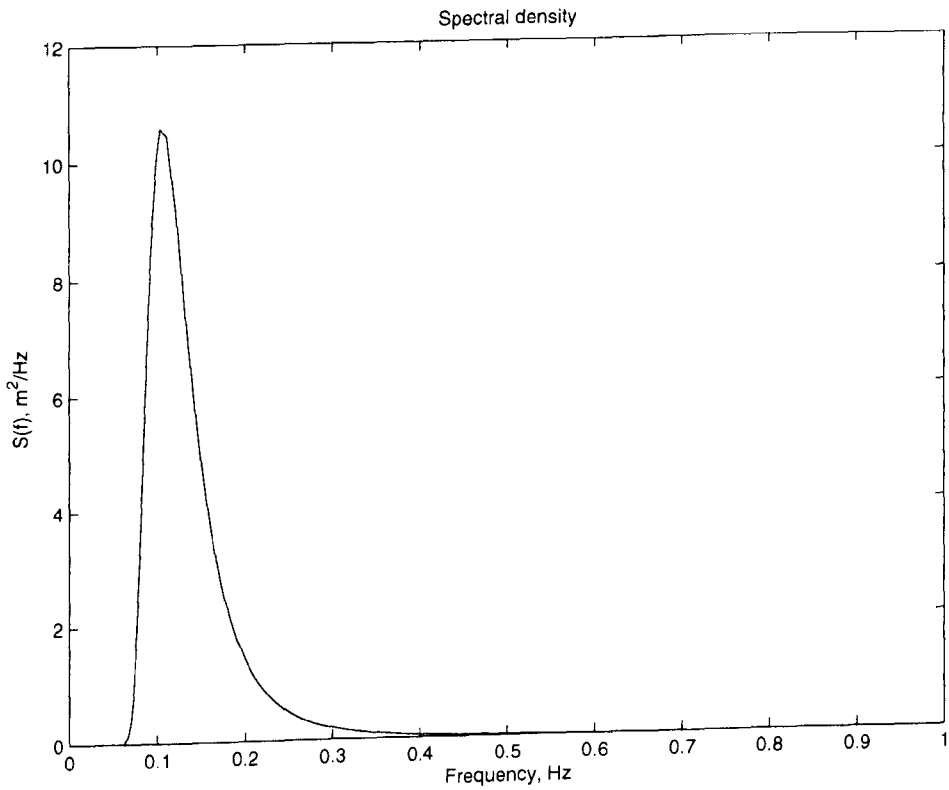


Figure 6.23: Spectra for the simulated omnidirectional wave field

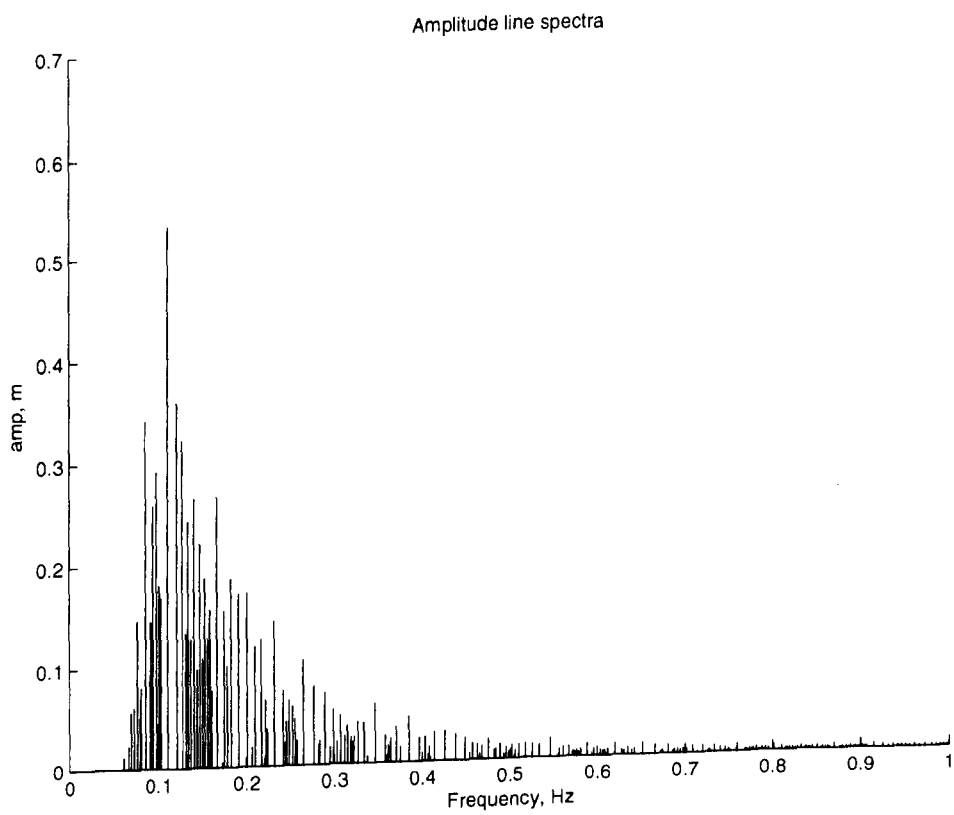


Figure 6.24: Amplitude spectrum for the simulated omnidirectional wave field

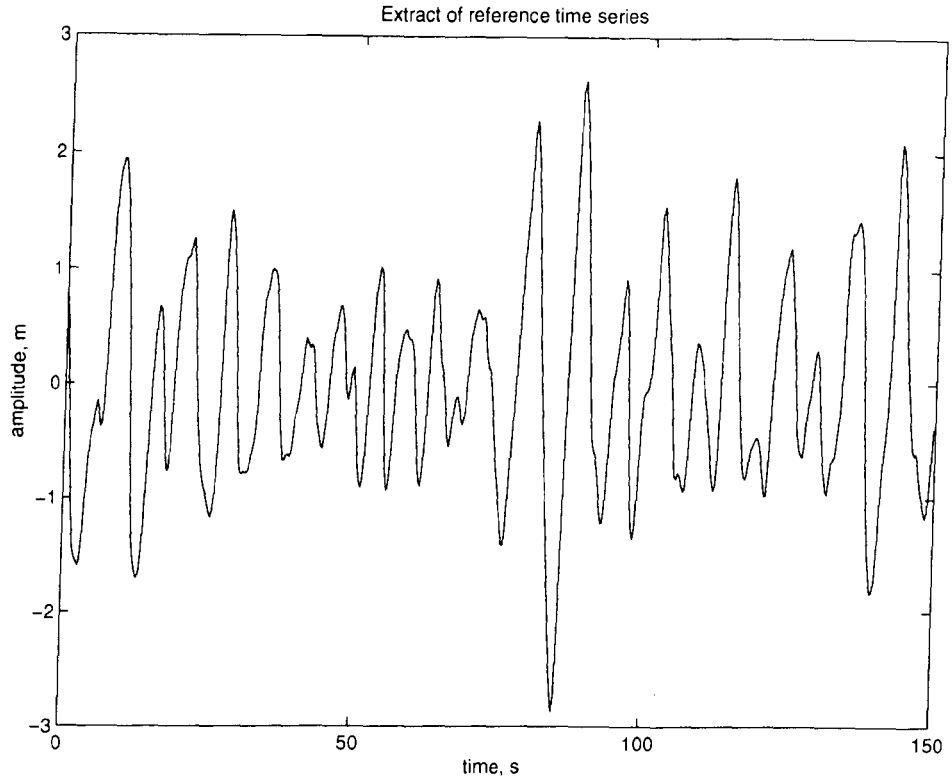


Figure 6.25: Extract of the reference time series

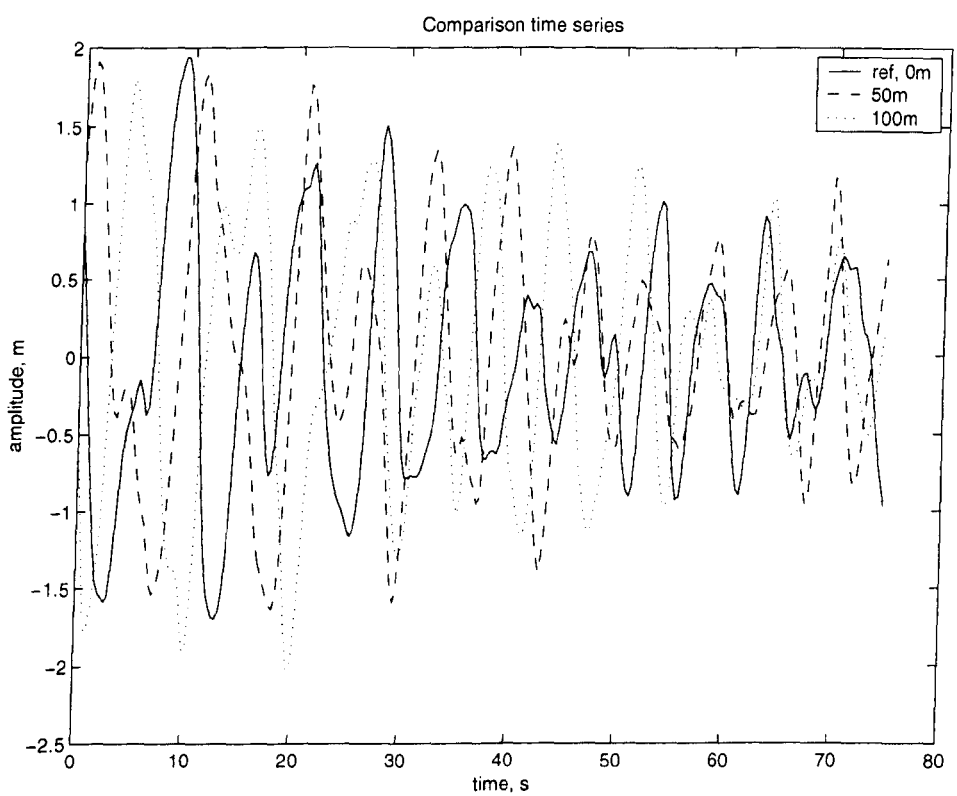


Figure 6.26: Time series from first three sensors

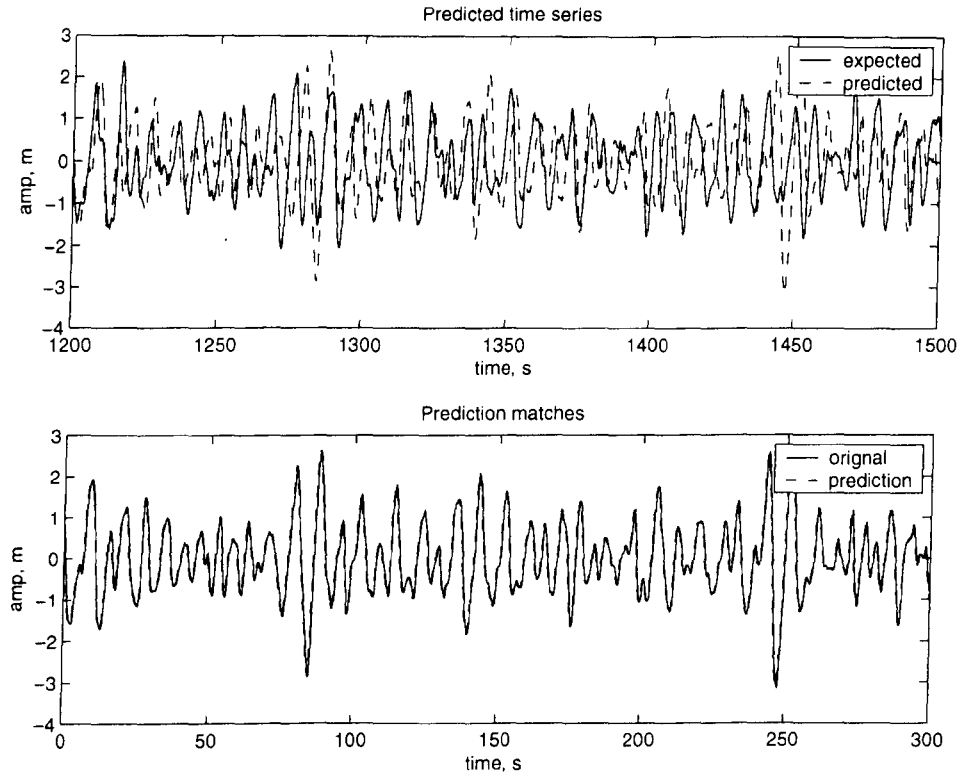


Figure 6.27: Predicted time series at reference sensor

### 6.3.2 Initial time analysis

The first step in analysing a time series is to take the FFT. Therefore it would seem reasonable to resolve a section of wave record into its real fourier components. If a time series of length $T$ is taken and decomposed into its real Fourier components of $a_n$ and $b_n$ it should be possible to recreate the time series by using a superposition of sinusoids. Extending this series in time would seem to be as elementary as using the same Fourier coefficients but calculating the reconstructed time series for $f(\Delta t \rightarrow T + \Delta t)$. To illustrate this Fig. 6.27 presents the results of the following test. Take the time series for the omnidirectional case from $t = 0 \rightarrow 1200$ sec and $N = 4096$, where $N$ is the number of samples. Take the Fourier transform of this using the method given in Chapter 5. From these Fourier coefficients use the equation

$$\zeta(x,t) = \sum_{n=1}^{2048} a_n \cos(k_n x - \omega_n t) - b_n \sin(k_n x - \omega_n t) \tag{6.11}$$

with $t = 1200 \rightarrow 2400$ sec to create a time-series prediction. Alternate configurations of Eq. 6.11 can be used but this is the most suitable since $k_n x$ is positive. Considering this equation at the reference sensor reduces the wave number term $k_n x$ to zero for all sinusoids. It can be seen in the upper figure that there is a poor match between the predicted and

actual (expected) time series. Instead the predicted time series exactly matches the original time series for $t = 0 \rightarrow 1200$ sec (i.e., the lower figure).

**Discussion**

The errors that appear in the time prediction are not due to the FFT, but rather they are due to the application method. The FFT assumes that whatever time series is used, it will be periodic. For example

$$f(-T \rightarrow 0) = f(0 \rightarrow T) = f(T \rightarrow 2T) \tag{6.12}$$

So in recreating the spectra at $t = 1200 \rightarrow 2400$ sec the original time series for $t = 0 \rightarrow 1200$ sec is being recreated. This inherent periodicity of the FFT does not fit well with the aperiodic nature of real sea waves. This was a test with a stable, unchanging, spectrum. In a real sea there will be a continuous blurring of frequencies that will be affected by energy transfer from one frequency to another as well as attenuation by wind, current, pressure and shallow water effects. To this end the Fourier methods are a good means of creating spectra and deriving statistical properties but can be limited when predicting, in time, a continuously varying aperiodic quantity such as a sea wave surface elevation.

### 6.3.3 Prediction over distance

Fourier components which extended the time series in the time dimension were not found to be very successful. However, an attempt to use the components to extend a prediction over distance was investigated to test the validity of the FFT method in the spatial domain.

The same time series data as used in the last section is again used here with records made at points 50, 100, 200, 300, 500 and 1000 m from the reference sensor. Eq. 6.11 is used, but in this instance the $x$ parameter is varied to reflect the point at which the record was projected to. The time period over which the predictions are made, match that of the reference series. The results of these predictions are shown in Figs. 6.28 – 6.33. For clarity, only the first 150 sec are shown.

The most obvious result of these simulations is that up to 300 m the predictions over distance show good correlation. This agrees with other studies ([4], [5], and [6]). The initial period of these simulations show some transient behaviour, with the predictions taking some time to settle down. This transient behaviour deteriorates with distance and it has in the past been attributed to the time series end points not tending to zero.

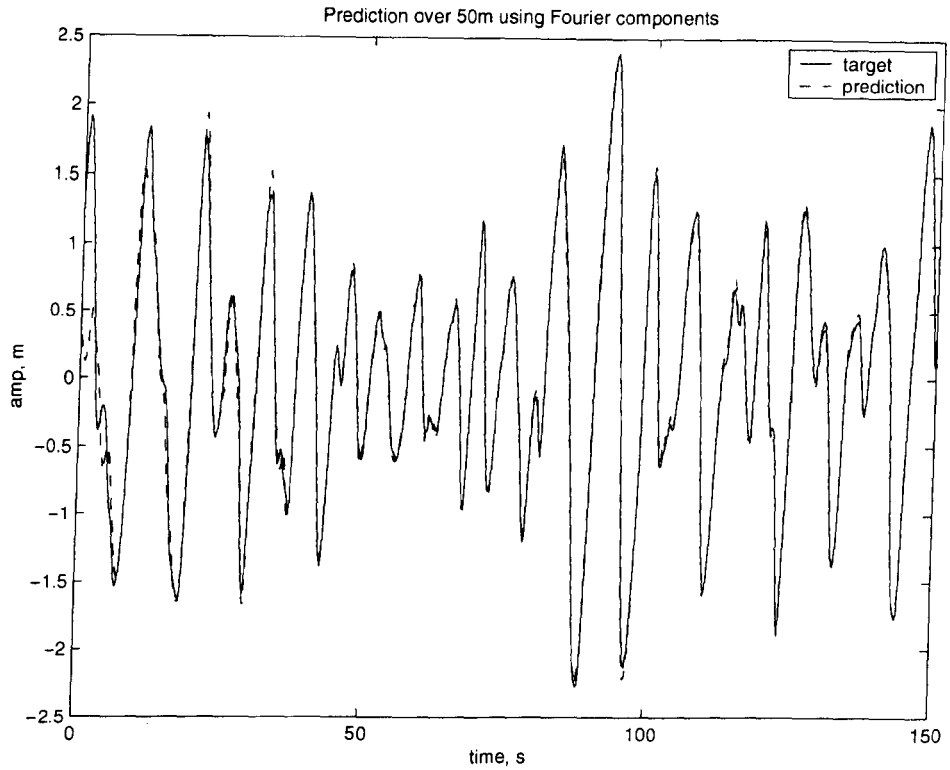


Figure 6.28: Prediction made over 50 m using Fourier coefficients

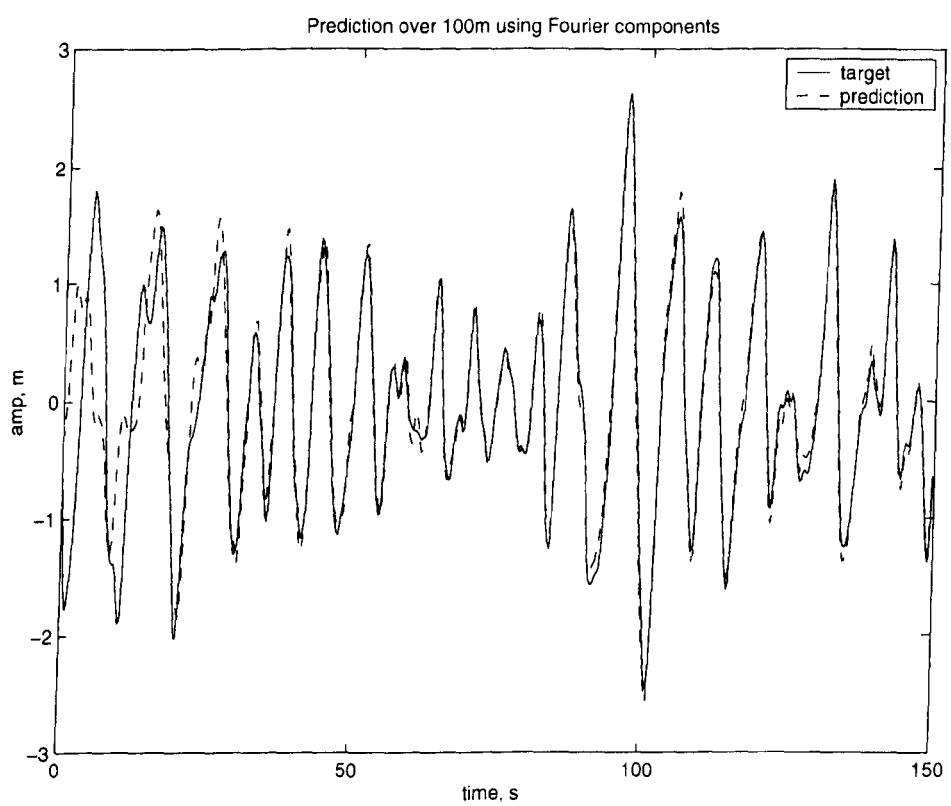


Figure 6.29: Prediction made over 100 m using Fourier coefficients

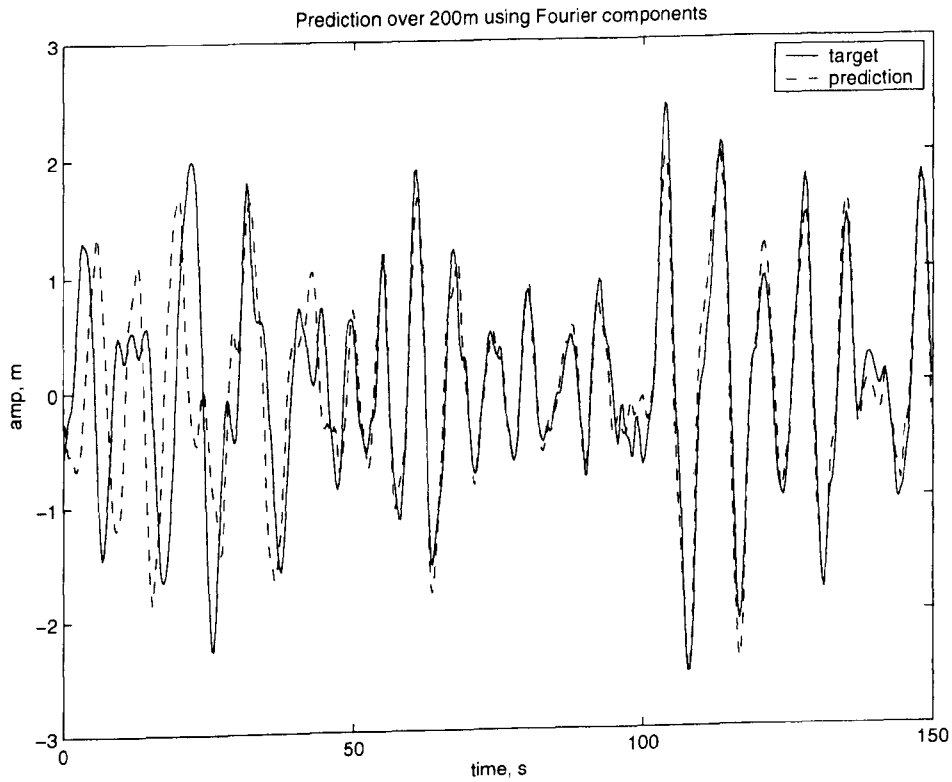


Figure 6.30: Prediction made over 200 m using Fourier coefficients

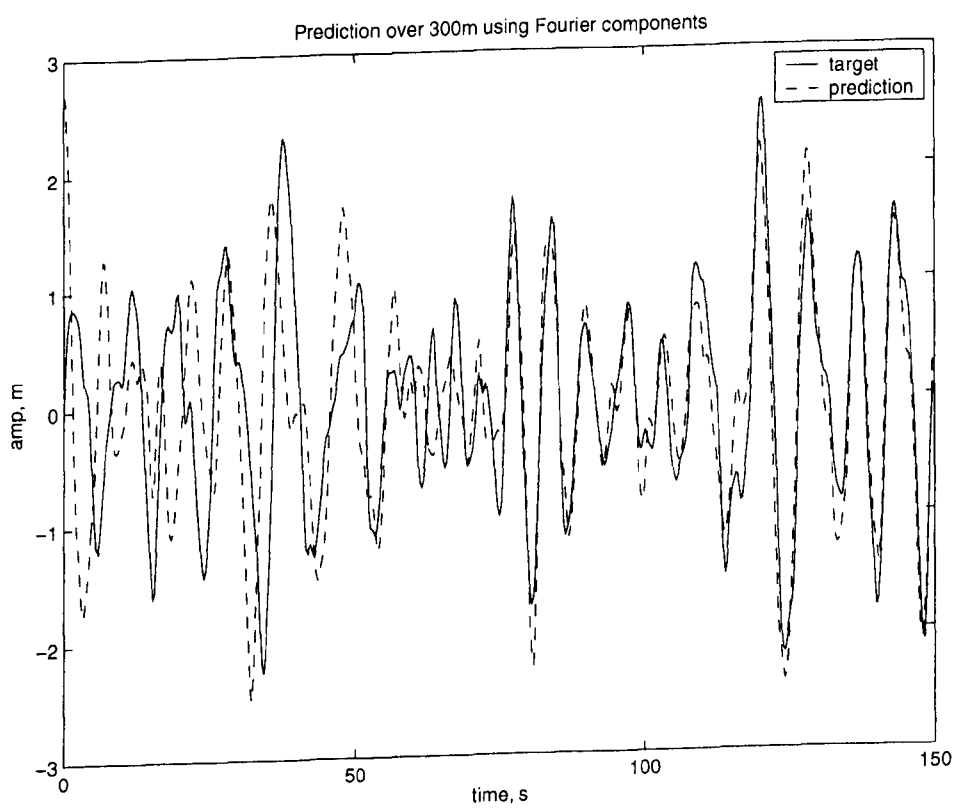


Figure 6.31: Prediction made over 300 m using Fourier coefficients

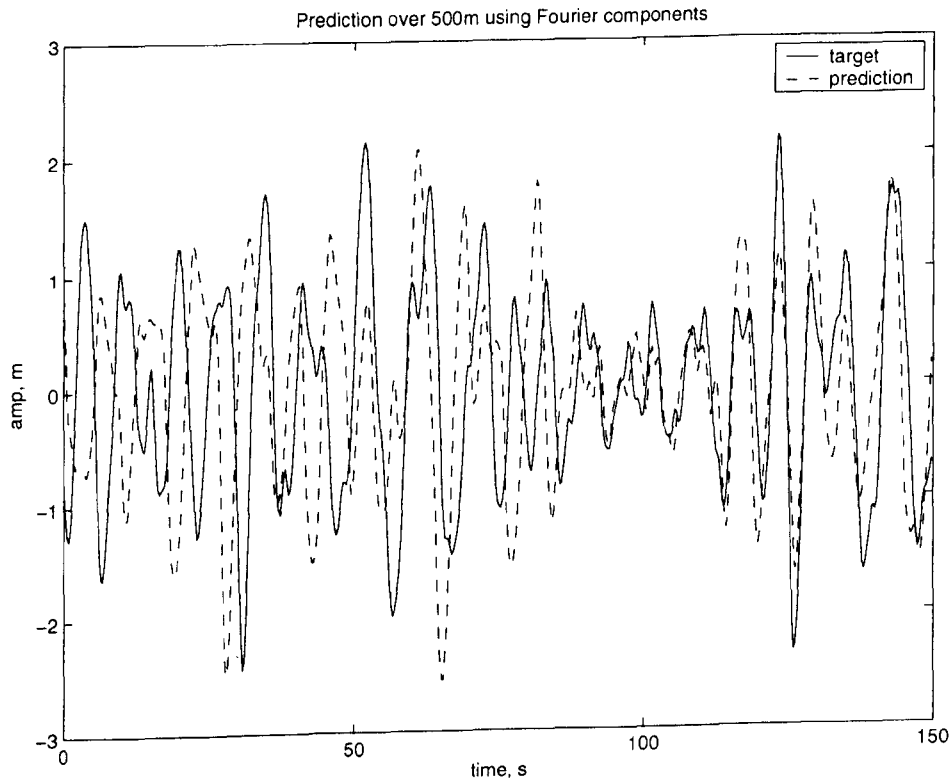


Figure 6.32: Prediction made over 500 m using Fourier coefficients

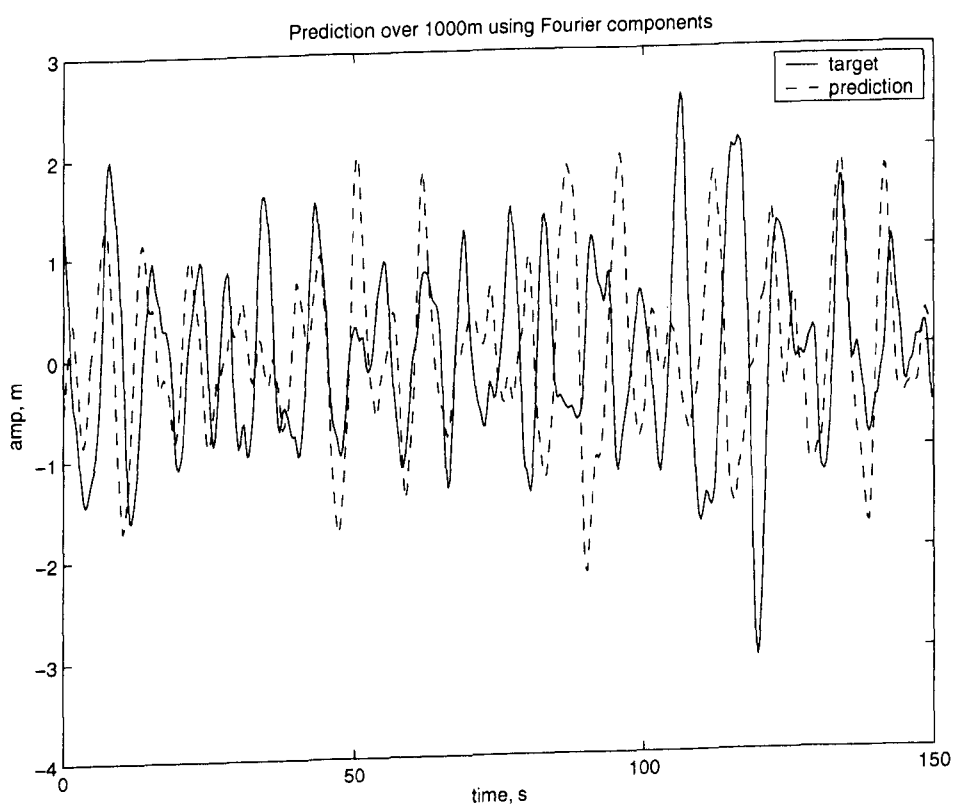


Figure 6.33: Prediction made over 1000 m using Fourier coefficients


Figure 6.34: Zero crossing method of transient elimination

### End fitting the record

The most common method of eliminating transient behaviour at the beginning of a series is to use a data window. Unfortunately the use of a data window will tend to corrupt the phase information associated with the time series. Belmont [3] suggests a method of end fitting the data to eliminate the sharp transients at the ends of records similar to the windowing method. Essentially, this means searching from the beginning of the time series to find a zero crossing point. The gradient of the line at this point is calculated. The time series is then searched from the end of the record to find a zero crossing point with a similar gradient match. The data to either side of these points is discarded and the FFT zero packed to make it up to a power of 2 in length, this process is shown in Fig. 6.34 where the shading indicates the discarded portion of the record. On reconstructing the predicted series it must be advanced in time by the number of samples cropped from the beginning of the original series. The results of the process were inconclusive with the new end fitted prediction being neither better or worse than the original method. The transient behaviour is more likely to be concerned with the shift from one spatial position to another and will be explored further in Chapter 7.

### Error calculation

A qualitative measure of the accuracy of the prediction is needed to show numerically how well the FFT reconstruction works. Sinusoidal time series are not immediately amenable to straight forward comparisons so a method of calculating the percentage errors between the two series was formulated. The percentage error between the prediction and target is calculated for each sample and averaged over the length of the series. The results from this

| Distance | % error |
|---|---|
| 50m | 1.34 |
| 100m | 2.26 |
| 200m | 4.49 |
| 300m | 6.75 |
| 500m | 11.11 |
| 1000m | 16.32 |

Table 6.1: Percentage errors in predicting over distance

procedure are presented in Table 6.1 for a 12 $ms^{-1}$ wind speed. Using these percentage values and addressing the results in Figs. 6.28- 6.33 it may be concluded that a percentage error greater than 10 % would be too great for the prediction to be of use. The manner in which the results are averaged over the length of a record will tend to mask large individual errors, such as a peak instead of trough.

The results of taking the percentage error between the prediction and the target series were also carried out for wind speeds from 10 $ms^{-1}$ to 30 $ms^{-1}$, covering a wide operating range, using the standard parameter values of $N = 4096$ and $T = 1200$ sec. Fig. 6.35 shows these results plotted with a $9^{th}$ order polynomial fitted to each data set for ease of reading. Interestingly the prediction deteriorates with increasing wind speed. It was thought that the accuracy would increase as the spectrum being simulated became more narrow. This point will be discussed in Chapter 7.

The reasons for the breakdown of the predictions with increasing distance are discussed in full in Chapter 7. However, it can be highlighted that it is due to the manner in which continuous energy is represented as discrete wave vectors and the way in which the dispersion equations translate energy from one point to another.

Further tests were carried out with the omni-directional prediction to ascertain the effects of the $N$ and $T$ parameters on the accuracy of the prediction. As in previous tests, a wind speed of 12 $ms^{-1}$ was chosen and an upper frequency limit for the input wavefield of 0.5 Hz. The time series for the seven prediction points were generated at a fixed length of $T = 1200$ sec and the value of $N$ increased from $2^3 = 8$ to $2^{16} = 65536$. Fig. 6.36 shows these results with $9^{th}$ order polynomials fitted, the $x$-axis here is on a log scale. As expected, the accuracy of the prediction increases as more terms are utilized before stabilising at around $N = 2048$, no further accuracy is gained by including more terms. Referring back to Table 5.2 in

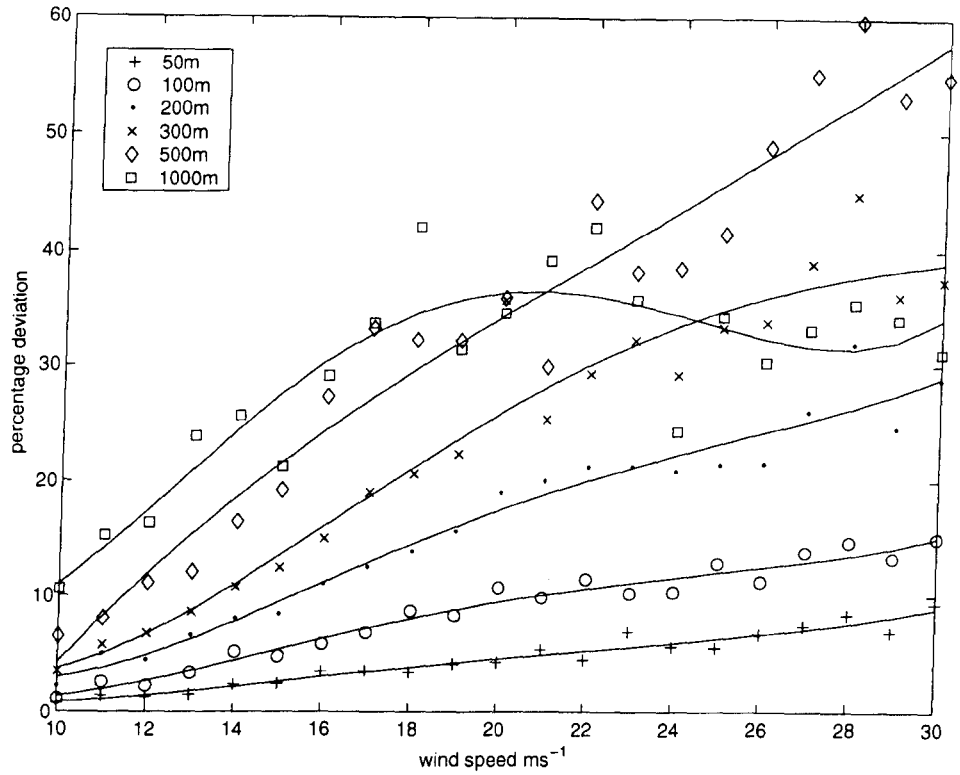


Figure 6.35: Accuracy of omni-directional predictions

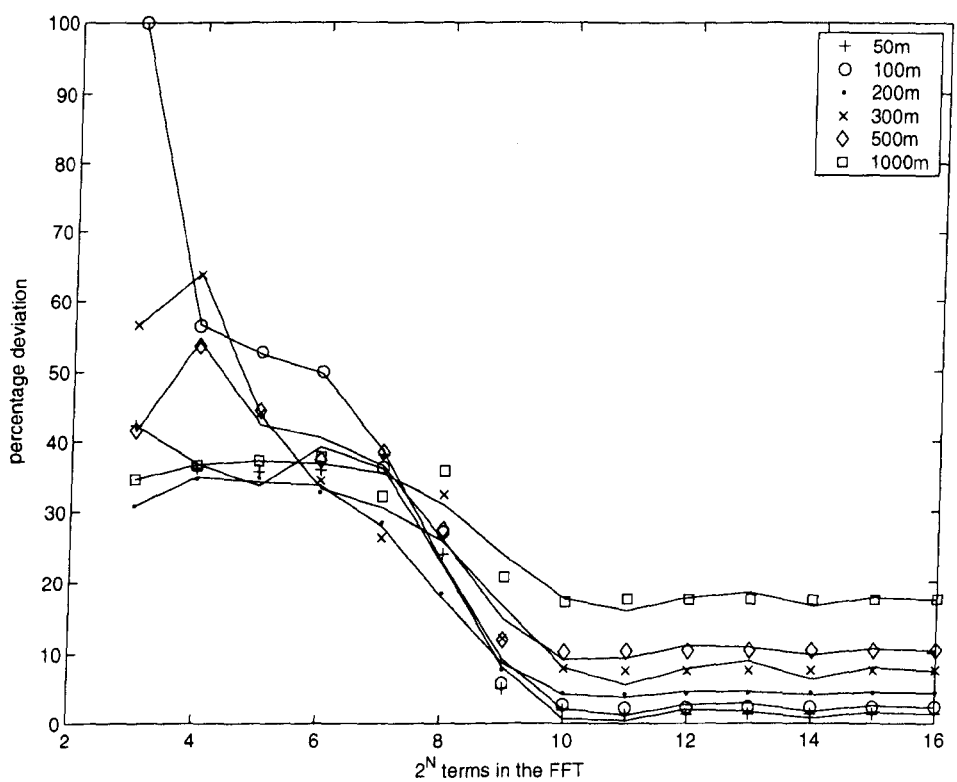


Figure 6.36: Errors from varying $N$

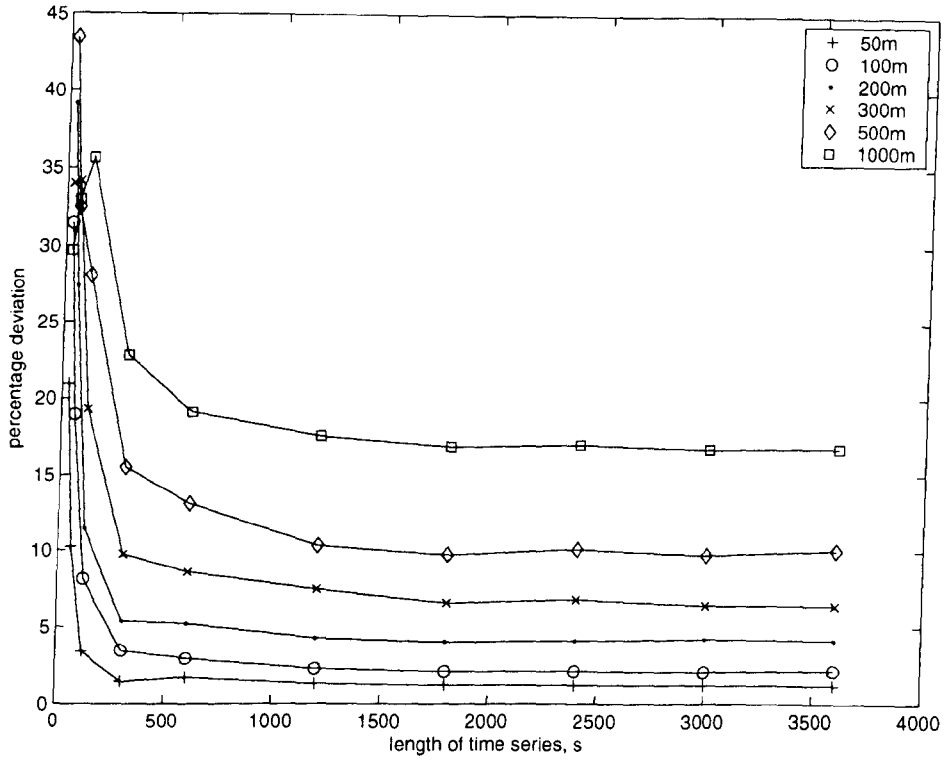


Figure 6.37: Errors from varying $T$

Chapter 5, the upper and lower frequency limits are given for a variety of $N$ and a fixed $T = 1200$ sec. Up to and including $N = 1024$, the upper frequency is below that simulated (0.5 Hz). At $N = 2048$ the upper frequency is passed, and extending the value of $N$ beyond this point is only adding to the ability of the algorithm to represent higher frequencies which are not represented and not required. Therefore extending $N$ past 2048 will not increase the accuracy of the prediction.

What may increase the accuracy of the predictions is to increase the frequency resolution by taking a longer time series. Referring back to Chapter 5 the frequency resolution is the inverse of the length of the time series $T$. By taking a longer interval for $T$, the resolution will become more focused. Again a 12 $ms^{-1}$ wind speed was used for generating an omni-directional spectrum, the value of $N$ was fixed at 4096 allowing the upper frequency simulated at 0.5 Hz to be reached at the longest $T$ in use. The value of $T$ was increased from 30 sec to 3600 sec covering a record length of half a minute to one hour. These results are again presented as a scatter plot with a $9^{th}$ order polynomial fitted for clarity in Fig. 6.37. Again an increase in accuracy is seen with an increase in frequency resolution. The errors fall much faster at shorter prediction distances stabilising to the general error levels seen in other experiments using this spectrum.

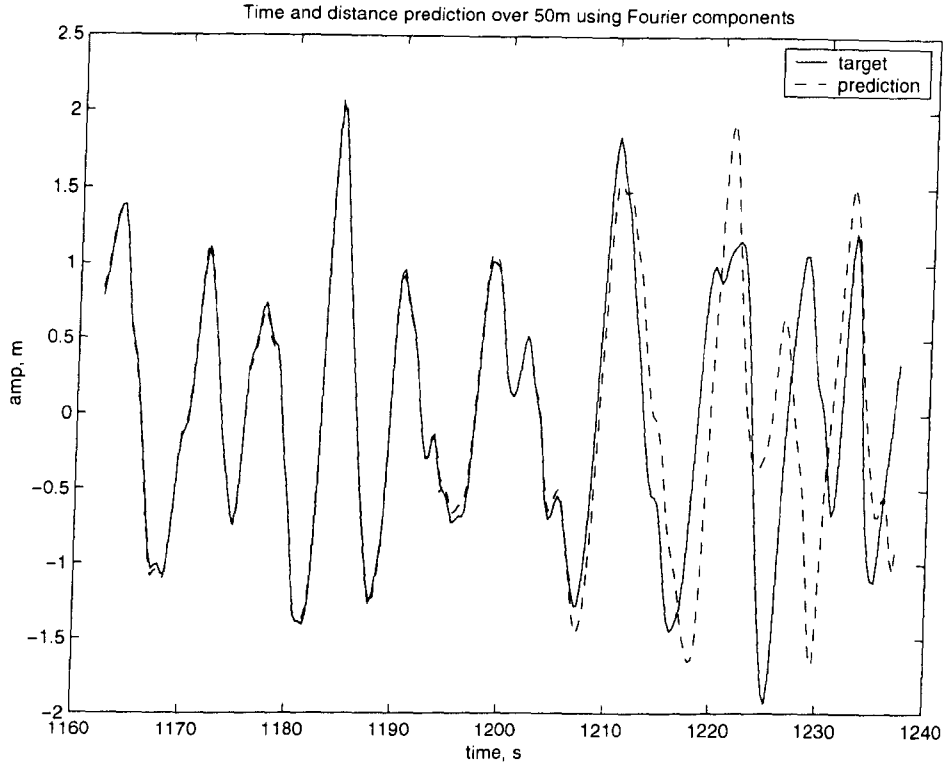


Figure 6.38: Prediction made over 50 m and ahead in time using Fourier coefficients

### 6.3.4 Time and distance

It was found that prediction over distance is possible for short distances. Therefore it was decided to combine the prediction over distance with that over time. The same omni-directional wave-field used in previous sections was utilized to calculate data for a reference sensor at 50 m. Eq. 6.11 was used but this time setting $x = 50$ m and extending the time series by 128 samples. The results are shown in Fig. 6.38 focused at the point where the prediction begins at 1200 sec. As expected, from the time prediction section, the prediction matches the target record up to 1200 sec but is incorrect after this point.

### 6.3.5 Omni-directional prediction for a directional field

Real sea states do not consist of omni-directional wave-fields so testing the prediction-over-distance method with a directional wave-field is the next step to take. The same basic spectrum as used in the omni-directional cases was used with a Mitsuyasu directional distribution (see Chapter 3) fitted. The number of frequencies was reduced to 128 to speed up the simulation of the wave record since 60 degrees of freedom in the directional spectrum was utilised. The records were again simulated at 3.1433 Hz.

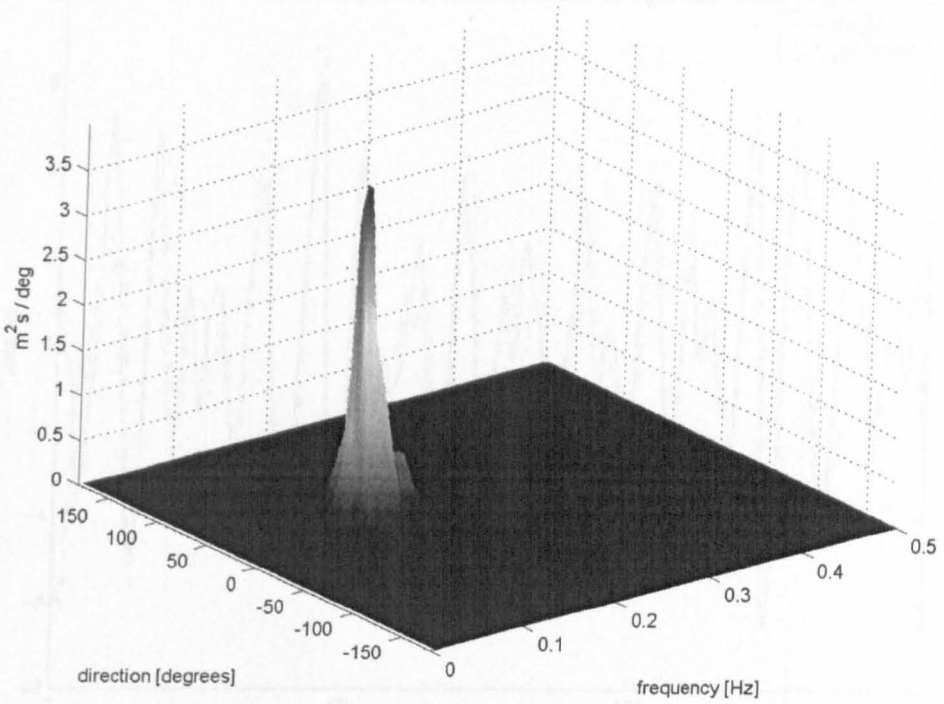


Figure 6.39: Spectrum calculated by DIWASP

Using the DIWASP toolkit and the Extended Maximum Likelihood Method (Chapter 4) the wave records were examined in order to determine the mean wave direction. The output spectrum from the DIWASP is shown in Fig. 6.39.

With the directional information, Eq. 6.11 is used to obtain predictions at the desired output points. Figs. 6.40 and 6.41 show the results of fitting an omnidirectional prediction to directional information; as can be expected the results are not particularly accurate but there is some correlation with the target series. The percentage error at each prediction point is given in Table 6.2.

At a low wind speed of, say, 12 $ms^{-1}$ the spectrum is still relatively widely spread in many directions. Increasing the wind speed should improve the spectral spread and hopefully decrease the prediction error. To test this theory, directional data files were generated for wind speeds of 10 to 30 $ms^{-1}$ and omni-directional predictions were fitted to these results. The percentage errors returned in each case for each data point are plotted in Fig. 6.42, again with $9^{th}$ order polynomials fitted. The errors in fitting the omni-directional prediction here are greater than when using simpler wavefields. The theory of an increasing wind speed leading to reduced errors is again proved incorrect and will be discussed in Chapter 7.

However it can be concluded that the predictions for 50 m and 100 m may be usable but

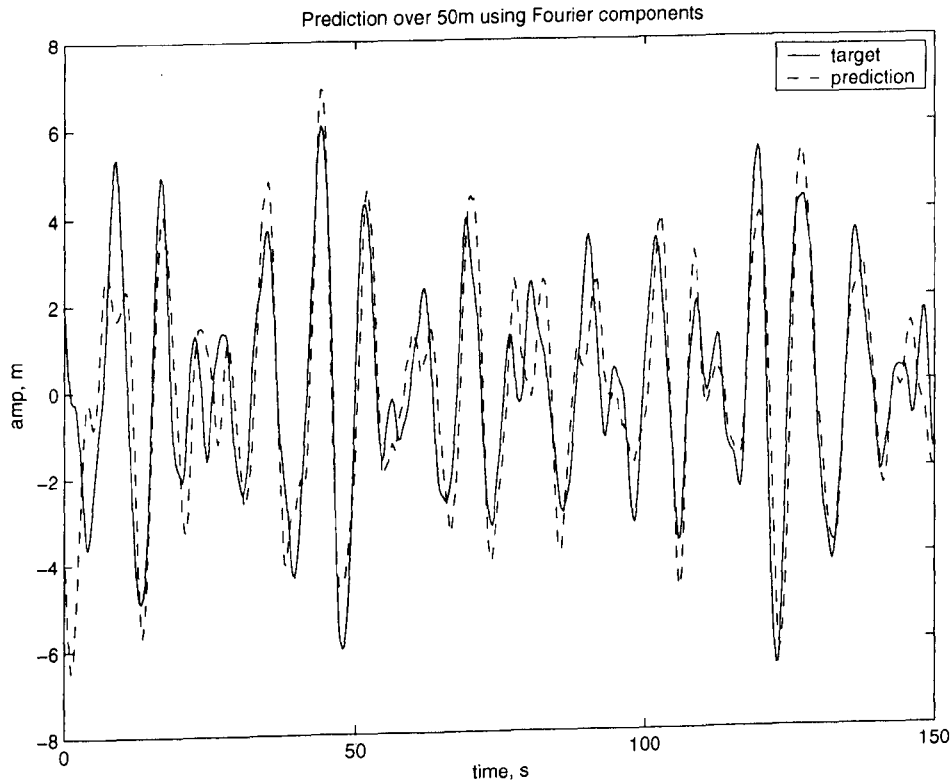


Figure 6.40: omni fitted prediction to 50 m

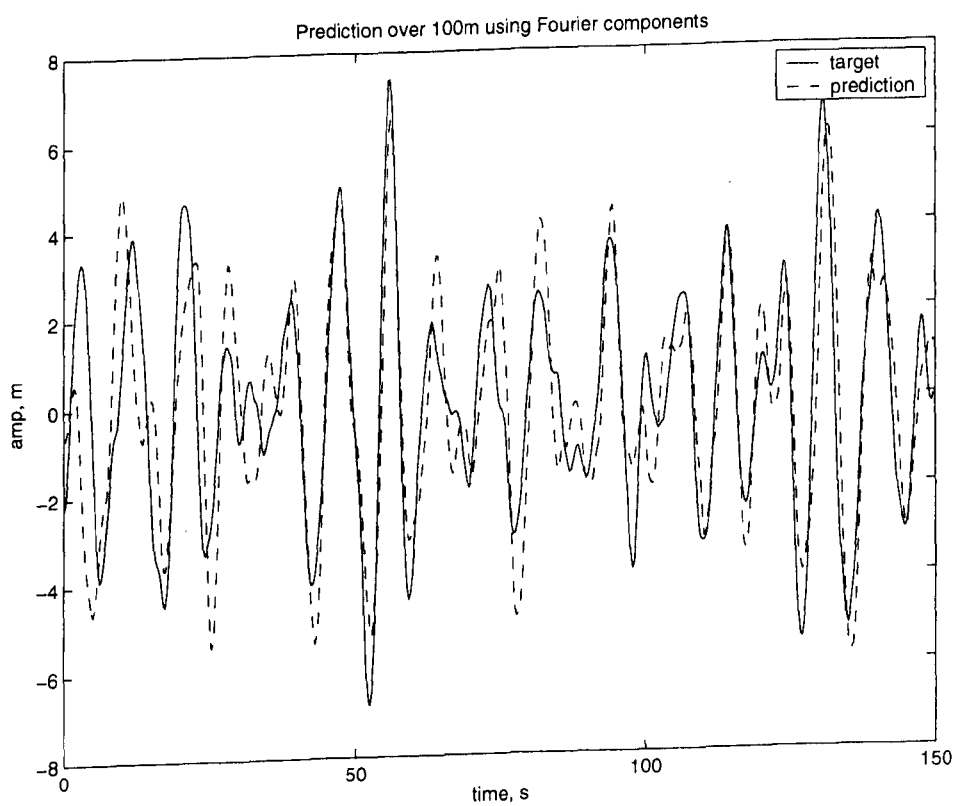


Figure 6.41: omni fitted prediction to 100 m

| Distance | % error |
|---|---|
| 50m | 13.54 |
| 100m | 14.08 |
| 200m | 21.16 |
| 300m | 23.82 |
| 500m | 26.34 |
| 1000m | 28.91 |

Table 6.2: Percentage errors in predicting omni-fitted spectra over distance

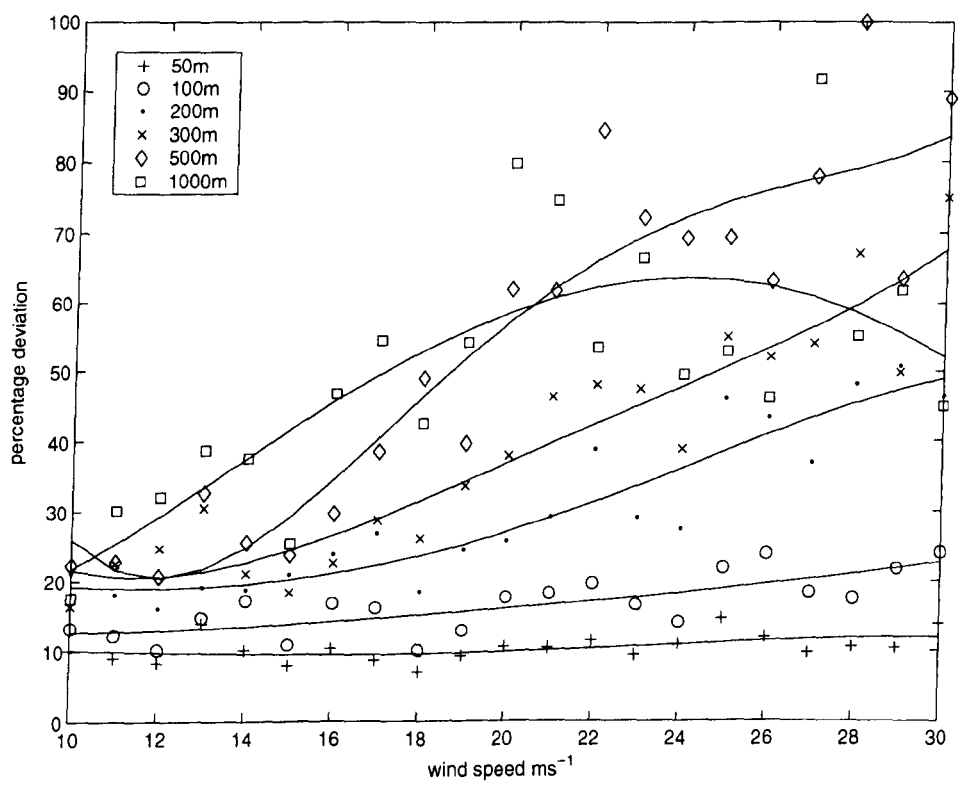


Figure 6.42: Errors in omni-fitted directional predictions

at distances greater than this the effect of wave-trains present in other directions overcome the omni-directional approximation.

## 6.4 Wave tank experiments

After setting out a methodology for the short term prediction of wave behaviour by Fourier means in the previous sections of this chapter, a real-world experiment was deemed appropriated to demonstrate the theorem. A simple experiment was implemented in a modified wave flume.

### 6.4.1 Experimental equipment

#### Wave maker

The wave tank used in the following experiment was a modified flume. Figure 6.43 shows the dimensions of the tank. The wave maker used a rectangular paddle hinged at its lower edge. A crank driven by an overhead motor/gearbox was connected to the paddle via an adjustable connecting rod which moved the paddle to and fro inducing wave oscillations. Lengthening or shortening the crank connection rod varied the wave-height of the generated waves while the motor speed (and hence wave frequency) could be varied via the motor inverter.

#### Shape

The shape of the flume affects the shape of the waves generated. The slight incline kicks up the amplitude of the wave as it enters the shallower main channel. Additionally the narrowing of the tank into the main channel focuses the wave. The wave maker had previously been sited at this narrow section but, not being the full width of the tank various diffraction and reflection effects caused a complex wave pattern. By moving the wave maker to the rear of the tank, the shape focusses a slightly messy wavefront into a clean straight one.

#### Beach and flow

To avoid reflections from the end of the tank an artificial beach was installed and is made from shaped polystyrene foam and rough plastic matting which absorbed wave energy to prevent reflections. The tank is filled by means of the pump below the main structure. As the tank is situated 1 m above ground level the pump must run continuously to prevent the water level in the tank from dropping. If the mean water level is kept below the upper lip

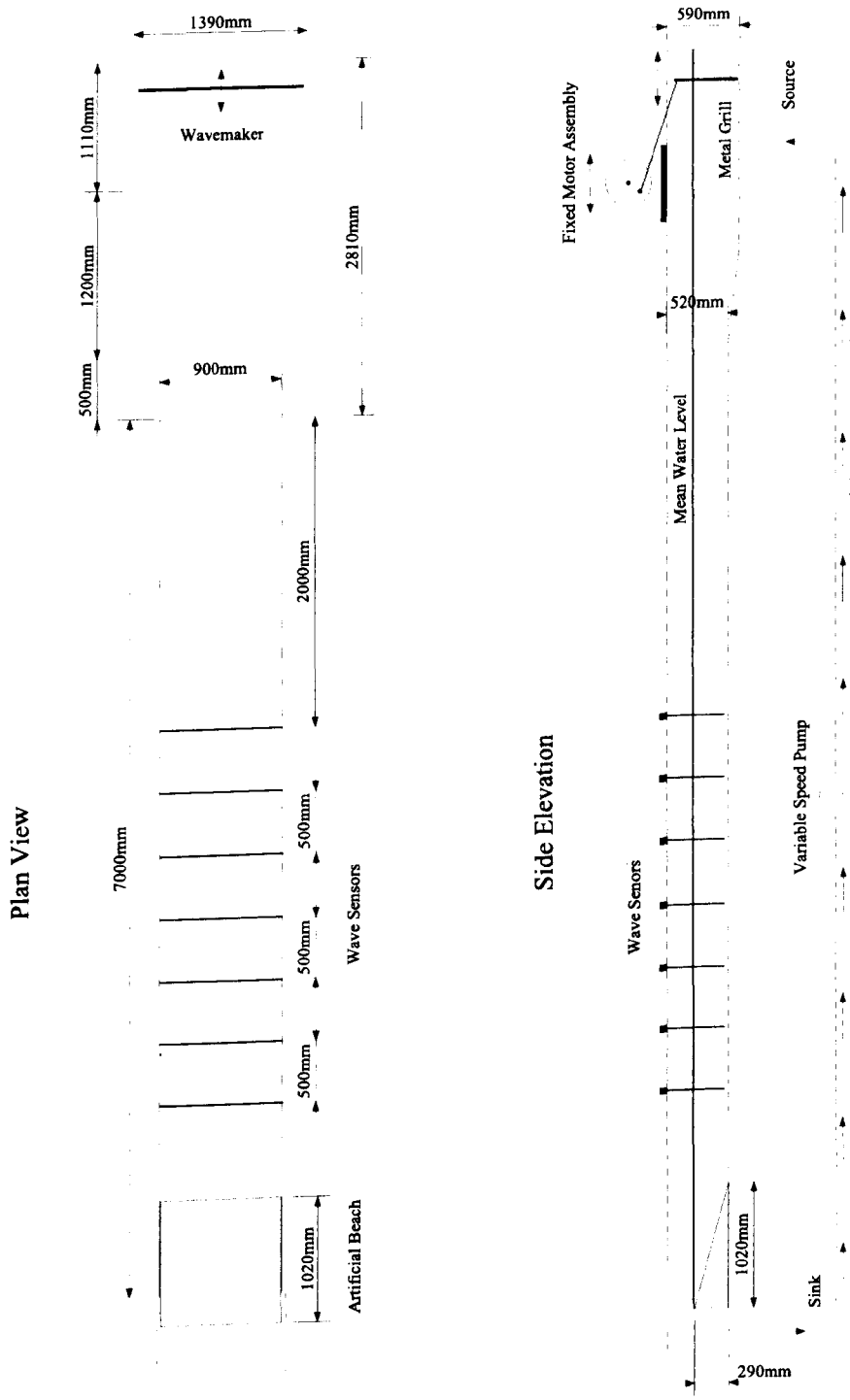


Figure 6.43: Wave tank and sensor placement

of the beach very little current flows in the tank. As the water level rises and begins to spill over the lip and into the sink a current will flow. Using a mean water depth of 0.288 m a current of 0.0166 m/s was found to be flowing. In normal operation the beach is overtopped by the waves.

#### Sensors

The wave sensors used in this experiment were of the capacitance type. Lengths of wire measure the capacitance in the water and in the air above the mean surface level. From these measurements a reading of the water depth is created. 8 sensors were made as part of a MSc project, seven of these were operational on the day of the experiments. The sensors were mounted on wooden support beams and are placed across the flume with the sensor hung midway. The first sensor was placed 2 m from the beginning of the main channel to allow the generated wave to settle down. Further sensors were placed at 0.5 m intervals. The sensors were calibrated by setting an extreme minimum level, 130 mm, in the tank and then an extreme maximum, 330 mm. A final level is then set for the tank, 288 mm, and the motor for the wave maker was then set in motion.

#### Software

The software used to collate the wave data was developed in the Labview environment. The outputs from the sensors were fed through an A/D converter card and displayed on the PC monitor. The on-screen data was then exported as an Excel spreadsheet. After the experiments had been concluded it found to be missing a time index to the time series. This is corrected in the next section as unfortunately the flume then became unavailable for further testing.

### 6.4.2 Data preparation

#### Error removal

The data presented in the Excel files was 6000 samples in length, these were first of all truncated to 4096 samples to speed the FFT process. The data discarded should not affect the final results as they showed signs of corruption when being saved in the Excel file format. The act of saving the data produced data spikes as the OS subroutines were implemented. The data from all 8 sensors were saved in each Excel file so the data from sensor 7, which was not operational, was also removed. The mean was subtracted from each record and

the data converted from centimetres to metres. The remaining data was then transferred to plain-text tab-delimited files for ease of use in MATLAB.

### Time index

As noted previously, a time index was not stored with the time series and the sampling rate indicated by the Labview software was deemed too high to correctly relate to the returned data. However, information on the wave-train of interest was recorded and this can be used to fit a time index. The motor driving the paddle was known to be running at 25 Hz. The step down ratio was 1/25 giving a nominal wave frequency of 1 Hz. The slip of the paddle motor when driving large volumes of water is likely to be in the region of 3 %, this is the maximum error in wave frequency.

With the frequency of the underlying wave-train and thus its time period known, the data sets were searched to find a record showing a peak as near as possible to the first sampling instance. From here the number of peaks in the record were calculated and multiplied by the time period to give an overall length for the series. A small fraction of a wave was found beyond the last peak which was also included in the estimate. With the length of the time series now know, $T = 18.2$ sec, and the number of samples $N = 4096$ the sampling period and sampling rate could be calculated and a time index fitted. The returned values were checked by taking the FFT of each time series and observing with which frequency the majority of energy lay.

### Sensor motion

As the wave in the tank propagated, each sensor responded to it by oscillating back and forth in a pendulum like motion with a period roughly one sixth that of the incident wave. This motion is caused by the forces exerted by the wave particles on the wire. Fig. 6.44 shows a typical response for the majority of sensors. The period of oscillation in each case is similar, with the amplitude dependant on the flexibility of the wire used for each sensor. The response of sensor 6, Fig. 6.45, was not found to be consistent in the sets of data and so was discarded. This motion would be something akin to that experienced in measurements taken in the real ocean, where the response of the wave buoy must be taken into consideration and suitable processing of the data implemented to restore the original signal.

The motion of the sensor has two effects on the time series. The first is amplitude modulation. The second is a phase shift in the recording of the data points.

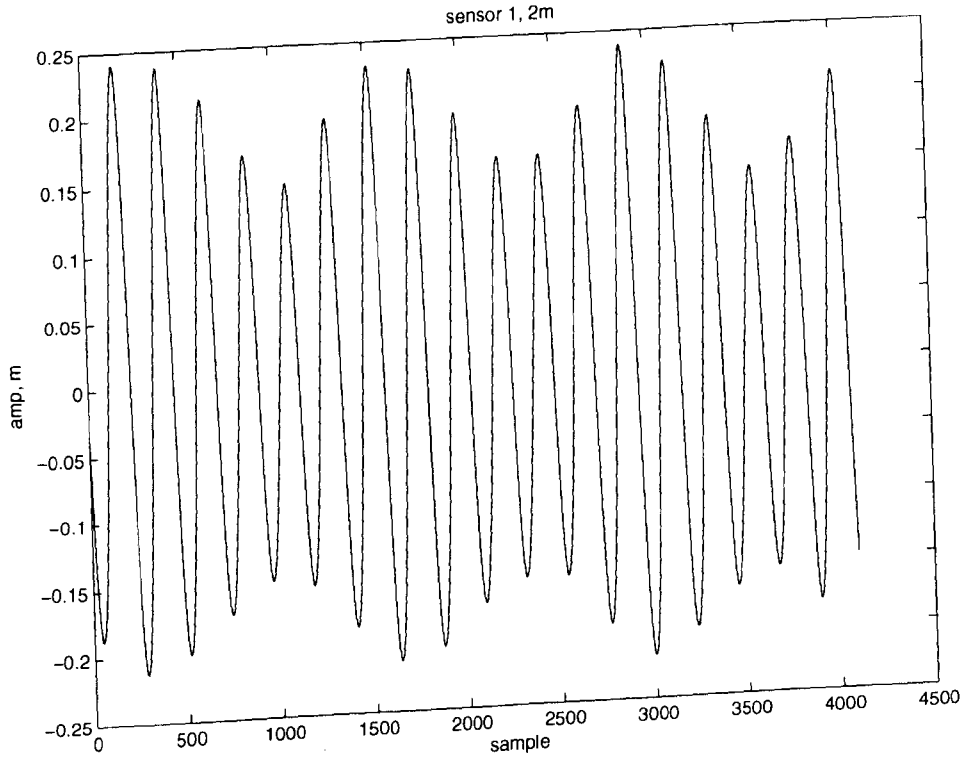


Figure 6.44: Time series from sensor 1 showing oscillation

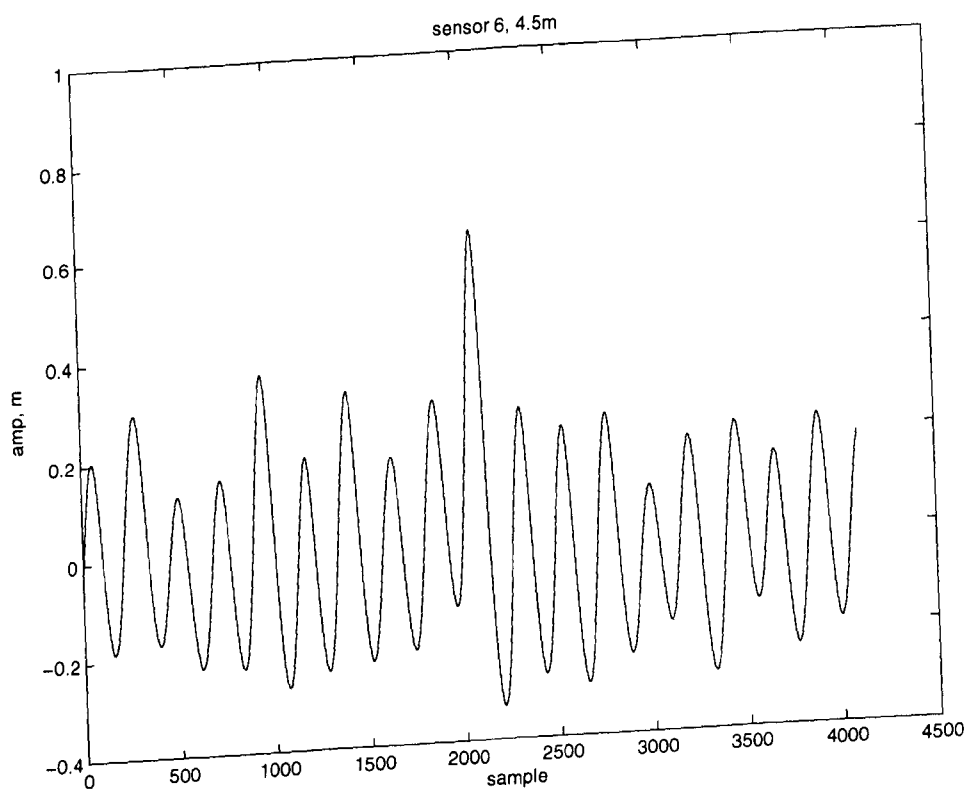


Figure 6.45: Time series from sensor 6 showing deviation

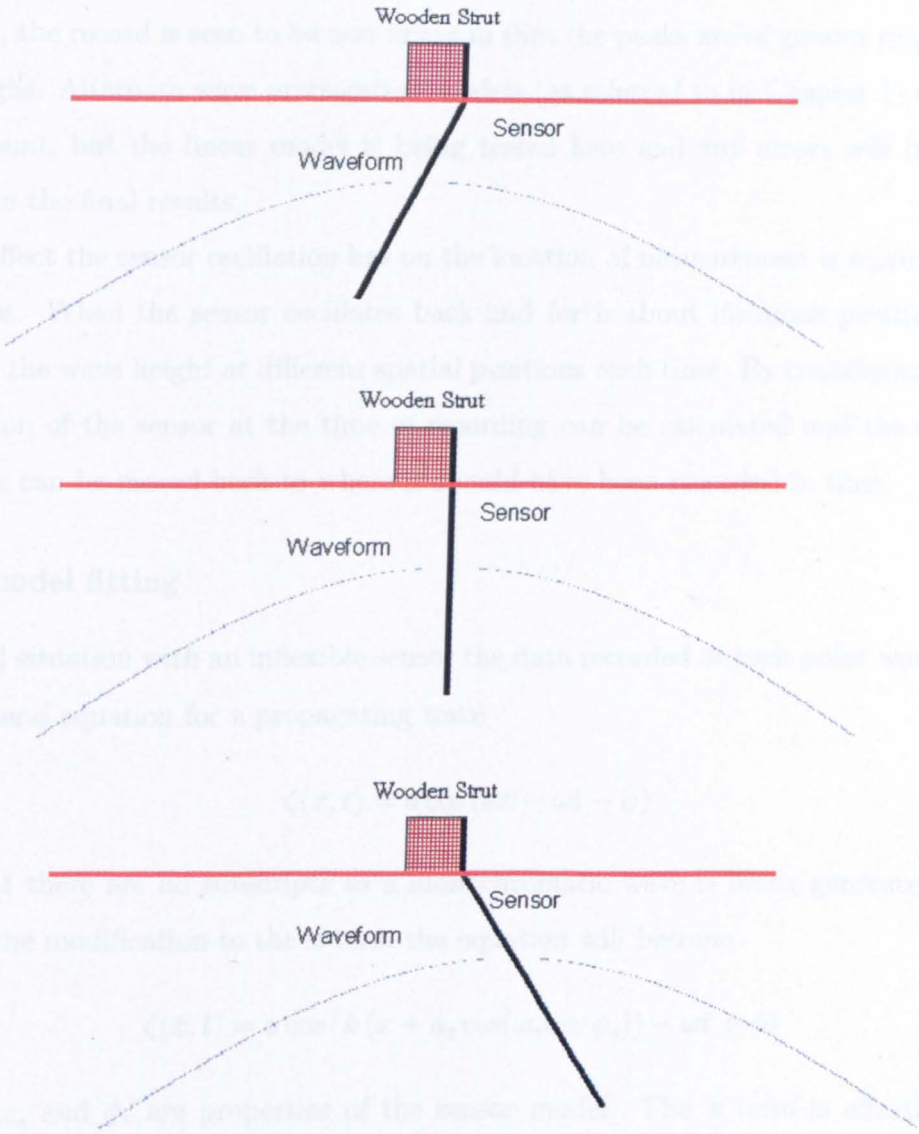


Figure 6.46: Motion of sensors relative to wave peaks

Dealing first with the amplitude problem. As the sensor passes through the vertical, hence being perpendicular to the wave surface, the least length of wire will be exposed to the air and an accurate reading of the wave height will be recorded. At either end of its motion more of the wire will be exposed as it is at an angle to the wave surface, Fig. 6.46 shows this reasoning graphically. The points where the sensor is near vertical can be identified by the maximum amplitude in each record and the peaks raised to this value. Reviewing Fig. 6.44, the record is seen to be non-linear in that the peaks are of greater magnitude than the troughs. Alternate wave propagation models (as referred to in Chapter 1) can take this into account, but the linear model is being tested here and any errors will be taken into account in the final results.

The effect the sensor oscillation has on the location of measurement is more complicated to address. When the sensor oscillates back and forth about its mean position it will be recording the wave height at different spatial positions each time. By considering this effect, the position of the sensor at the time of recording can be calculated and the offset of the wave peak can be moved back to where it should have been recorded in time.

### Sensor model fitting

In an ideal situation with an inflexible sensor the data recorded at each point would conform to the general equation for a propagating wave

$$\zeta(x,t) = a\cos(kx - \omega t - \phi) \tag{6.13}$$

Notice that there are no subscripts as a monochromatic wave is being generated. Dealing first with the modification to the $x$ term the equation will become

$$\zeta(x,t) = a\cos(k(x + a_s\cos(\omega_s t + \phi_s)) - \omega t + \phi) \tag{6.14}$$

where $a_s$, $\omega_s$ and $\phi_s$ are properties of the sensor model. The $x$ term is effectively being modulated. Estimates for the $a_s$ and $\omega_s$ terms can be visually judged. The sensors horizontal movement was not greater than 0.1 m and the frequency of the motion as seen in Fig. 6.44 has already been estimated to be one sixth that of the propagating wave train.

Using this data, a fitting process can be implemented to ascertain the correct values for the sensor model. The three terms were swept about the estimated values and the resultant waveform, from Eq. 6.14, was compared to the actual recorded data. The results were examined and the best fit chosen. This fitted model is shown in Fig. 6.47. The fit to the periods is reasonably accurate but the peaks are still slightly displaced to the right of the

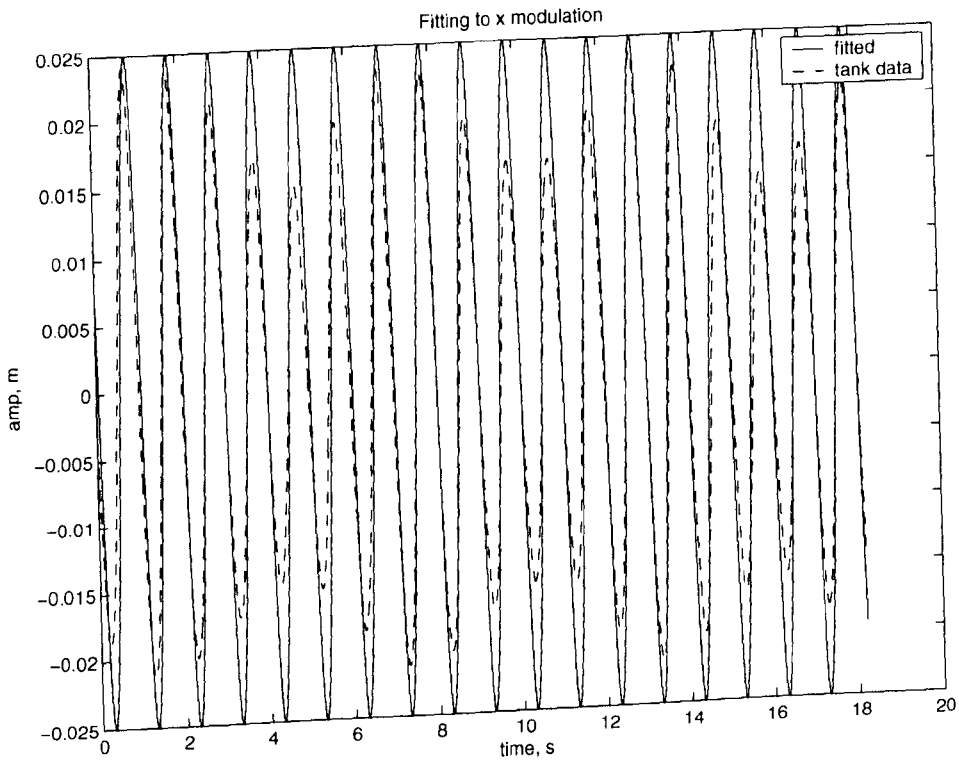


Figure 6.47: Sensor model fitted to $x$ modulation

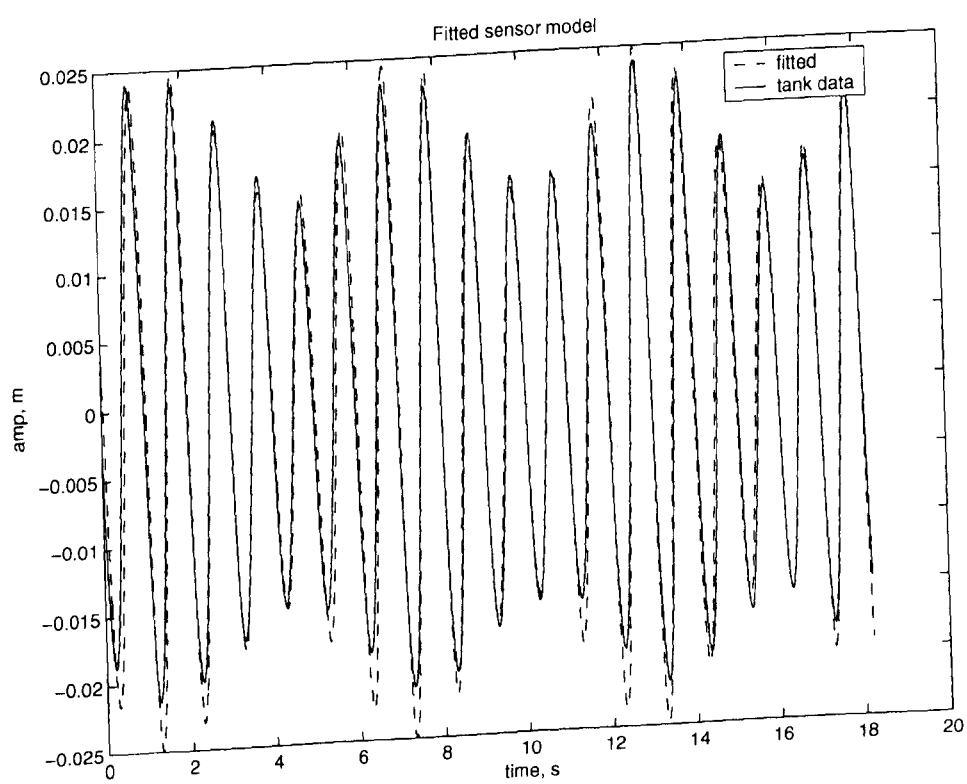


Figure 6.48: Sensor model fitted for full modulation

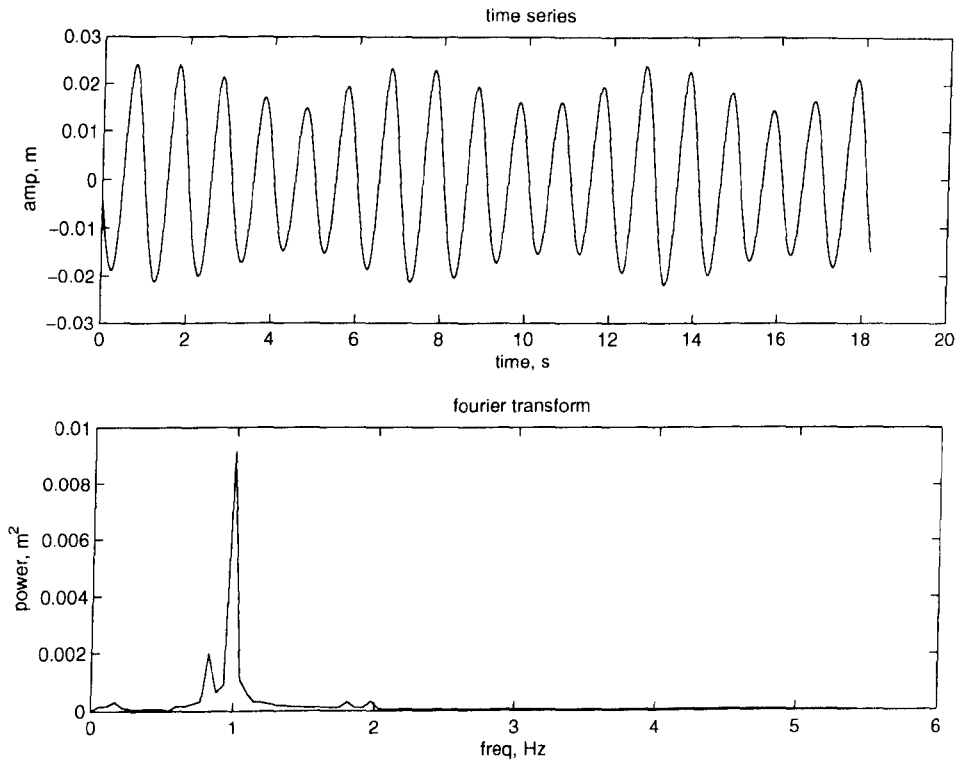


Figure 6.49: Time series and FFT using $T = 18.2s$

amplitude trough. This is due to the acceleration effect on the sensor (due to the wave motion). When swinging back into the wave-train the sensor will be affected differently than when it is accelerating with the wave-train.

Now, addressing the amplitude modulation, the terms calculated for the horizontal displacement can be reused where

$$\zeta(x,t) = \left(a - \frac{a_s}{2}\left(1 + \cos(\omega_s t + \phi_s)\right)\right)\cos\left(k\left(x + a_s\cos(\omega_s t + \phi_s)\right) - \omega t + \phi\right) \qquad (6.15)$$

This simulates the amplitude modulation due to the effective sensor length shortening. The results of this process for sensor 1 are shown in Fig. 6.48. The result shows good agreement for the peaks of the waveform but are not so well fitted to the troughs. This again may be a higher order effect of the wave propagation and the sensor motion.

A similar process was implemented for the other 5 operational sensors in order to derive bespoke sensor models.

### 6.4.3 Trial prediction

Recognising that the prediction is based on a monochromatic, progressive wave, parameters can be derived from examining the time series of the first sensor. After having fitted and

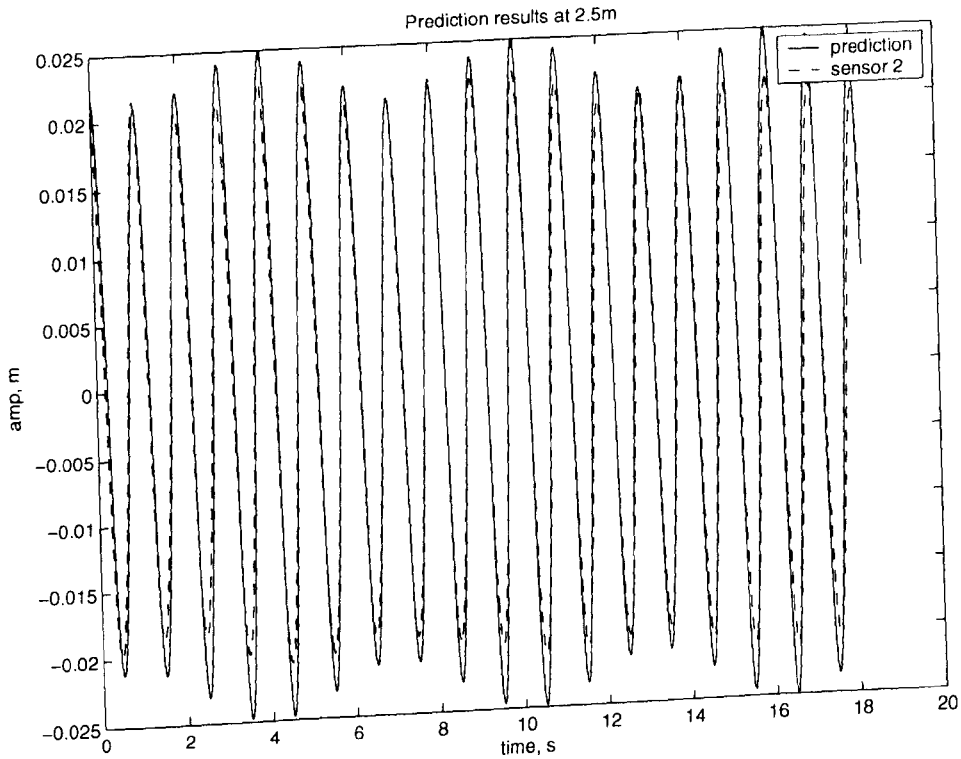


Figure 6.50: Prediction made at $x = 2.5$ m

checked the time series of the FFT (Fig. 6.49), it was found that a single frequency at 1 Hz dominated the record. The subsidiary peak below this corresponds to the sensor motion.

The other known data about the wave can be used to calculated the wave-train properties. The FFT data for the 1 Hz bin will give a phase for the wave. The amplitude can be obtained by taking averages of the maximum wave height experienced in each record. This is done because small calibration errors for each probe can indicate slightly higher or lower values for individual records.

The frequency can be used to derive the angular frequency, but as the depth of water ($h = 0.288$ m) in the tank is relatively shallow for the wavelength the full dispersion equation (Eq. 7.1) must be used in deriving wave number, wavelength and phase speed.

With this information the idealised wave record for the prediction points can be calculated and the sensor model fitted. The resultant predictions are given in Figs. 6.50 to 6.54. The results from taking the average percentage deviation showed each prediction to be within a few percent of the true values.

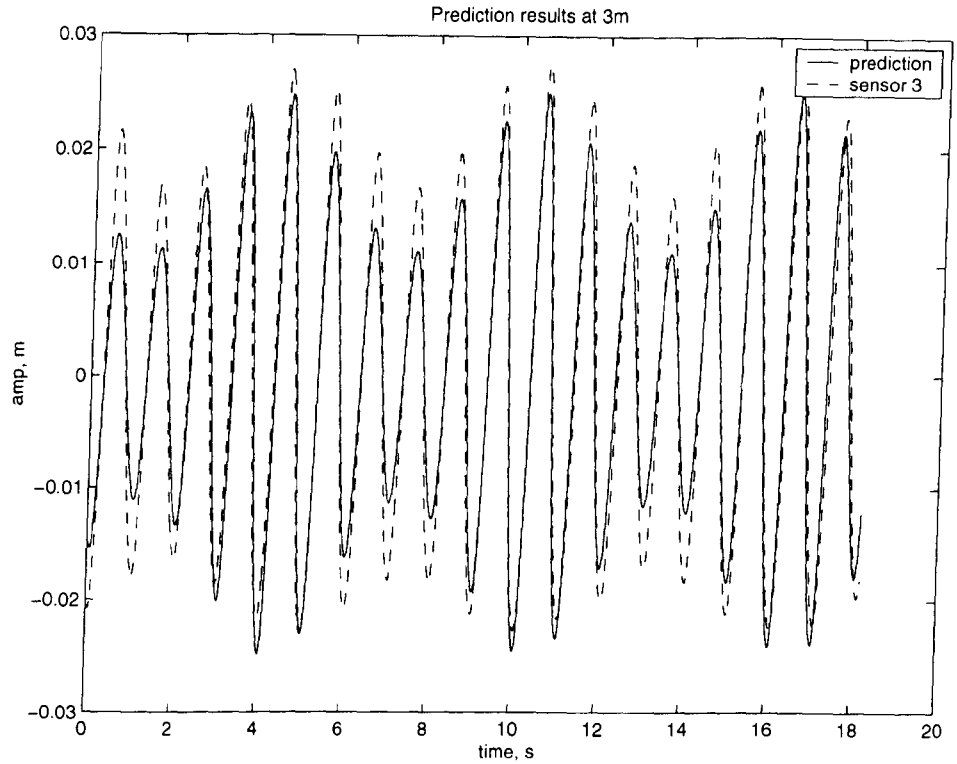


Figure 6.51: Prediction made at $x = 3.0$ m

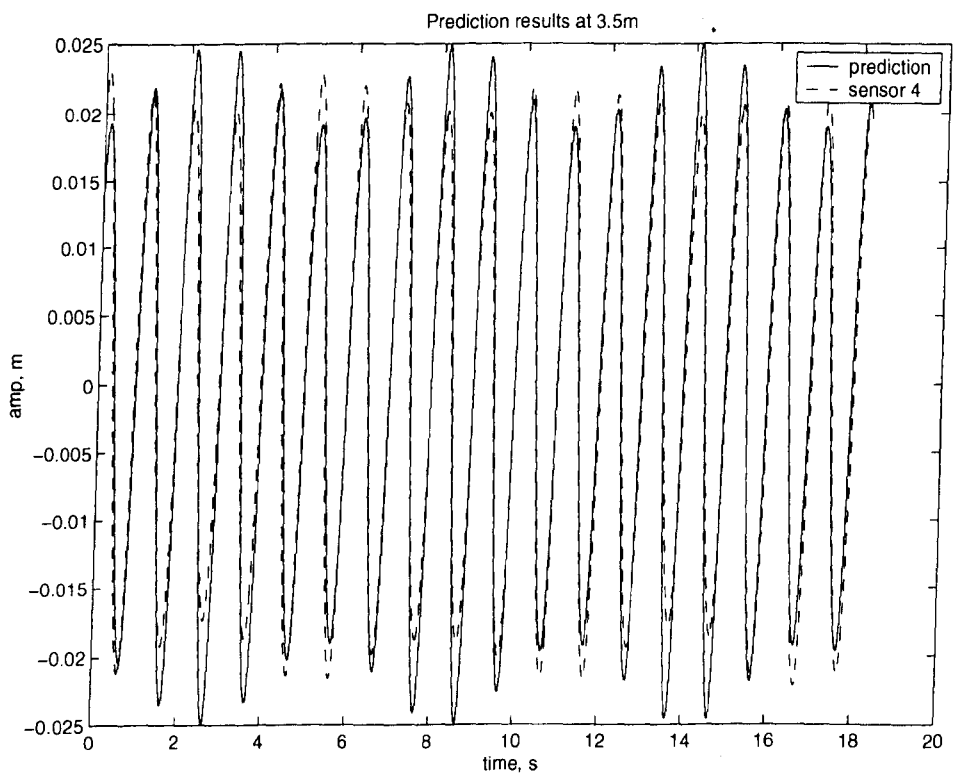


Figure 6.52: Prediction made at $x = 3.5$ m

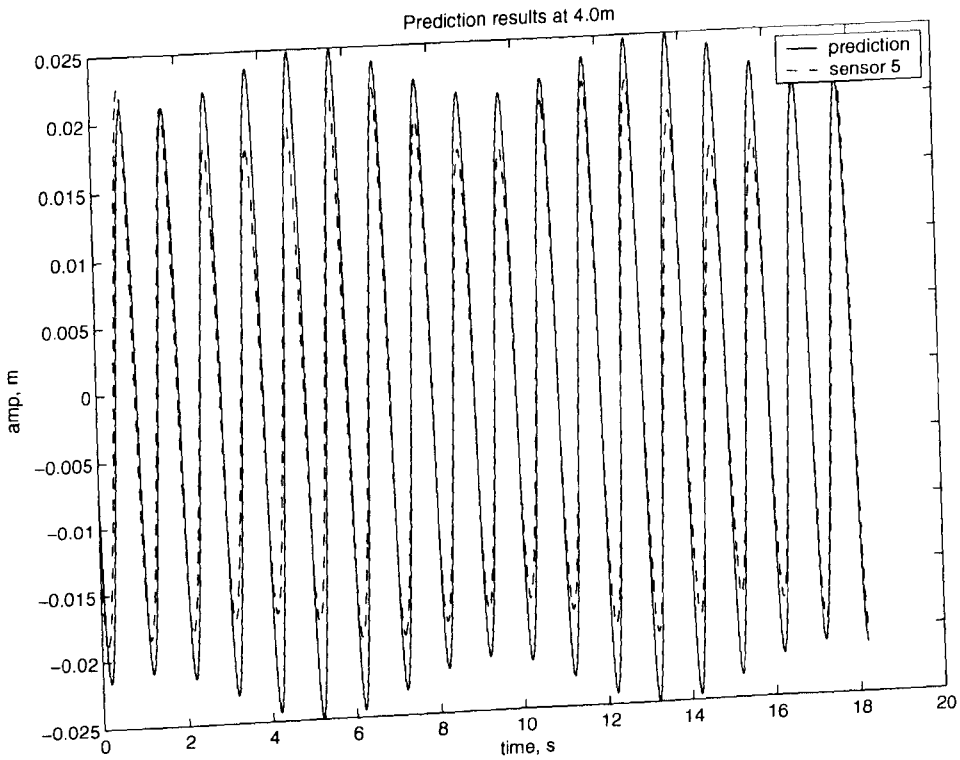


Figure 6.53: Prediction made at $x = 4.0$ m

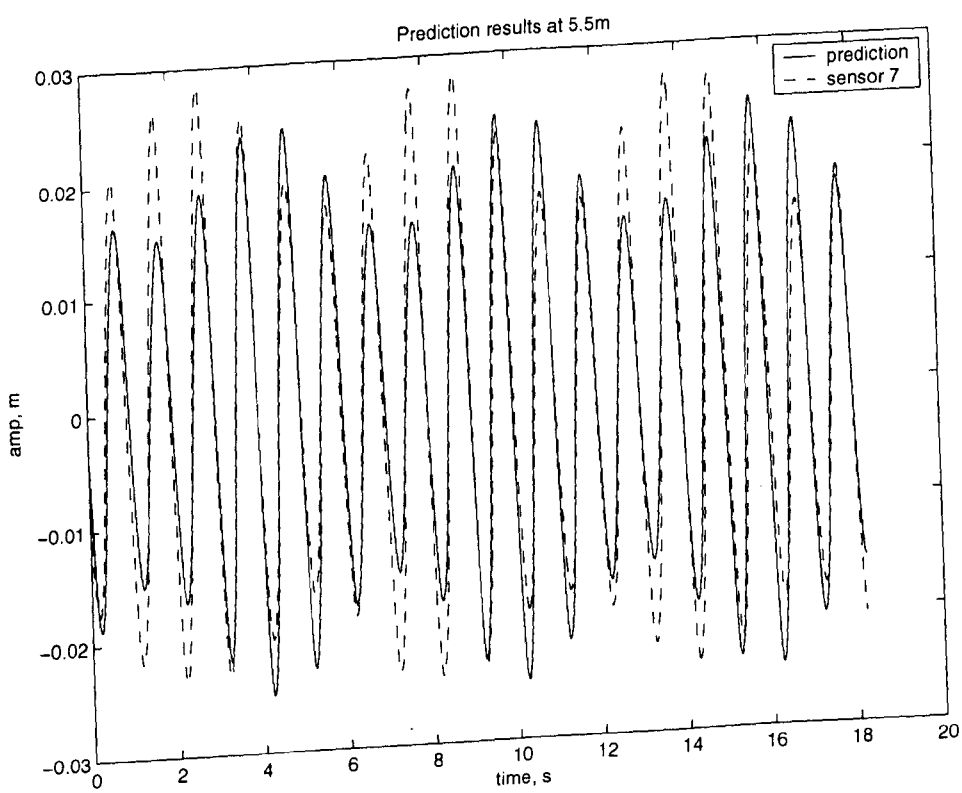


Figure 6.54: Prediction made at $x = 5.5$ m

### 6.4.4 Discussion

Making a prediction with a monochromatic wave over distance has been proved in this and in previous sections to be straightforward. The challenge in making real-world predictions is dealing with the instrumentation and the non-linearities that cannot be easily controlled.

Eliminating and modelling the response of the sensors to the passing waves is an interesting problem and one that needs to be addressed in measurements made in real conditions. With wave buoys, the response will be more complex with three degrees of movement. A more complex system of tracking the buoys motion will need to be developed. From each buoy position the surface elevation can be calculated and from previous sampling instances a three dimensional representation of the ocean surface can be created. The position of the buoy superposed on to this surface may show that it has slid down the side of a peak and is under-recording the wave height, similar to the manner in which the sensor oscillated away from its centre point and under recorded.

Non-linearities are present in the tank results. These are primarily caused by compromises made in setting up the equipment. The most noticeable effect being the non-symmetrical profile with the peaks exceeding the troughs. In a small-scale facility, such as that used here, the range of wavelengths available are constrained by the dimensions of the tank. Outside a specific range the shape of the tank will cause unwanted reflections.

In constraining the available wavelengths the ratio of the amplitude of the wave to the depth of the water becomes a factor. In order to be working with "deep water" waves either the wave amplitude must be decreased (reducing accuracy in the sensors) or the water depth must be raised. Increasing the water depth leads to a greater current flowing, which may be counteracted with a higher beach but at a cost in the reduction of the amplitude range. As mentioned above, reducing the wave amplitude affects the accuracy of the sensors so in the above experiment the values chosen allowed for the best compromise between these conflicting factors.

# Chapter 7

# Discussion

The previous chapter detailing the experiments conducted throughout this study contained several possible methods for the prediction of wave behaviour. The discussion here will examine the results of those experiments and try to bring together reasons as to why the predictions may be suitable in certain instances. The first two sections will examine the primary experimental results from the latter half of the last chapter, whilst the final section will discuss the earlier experiments and the other chapters of this thesis in the context of a wave device farm.

## 7.1 Transients

The transient at the beginning of each predicted record in Section 6.3 of Chapter 6 proves rather troublesome as it raises the value of the average percentage deviation, leading to a somewhat skewed result. Looking beyond this transient behaviour, the prediction shows a reasonably accurate match to the desired time series. Removing the transient in the record should lead to a more accurate measure of the error in the prediction.

### Transient errors

The errors between the targets and predictions for the case of a wind speed of 12 $ms^{-1}$ are plotted at each prediction point in Figs. 7.1 to 7.6. Examining the figures the first point to be noted is that the errors increase with distance, a hypotheses on this will be discussed later in this chapter. Looking at the beginning of each record the transient can be seen both in the amplitude and in having a different structure to the rest of the error series. By visual examination the transient lengths appear to grow from approximately 30 sec in the 50 m

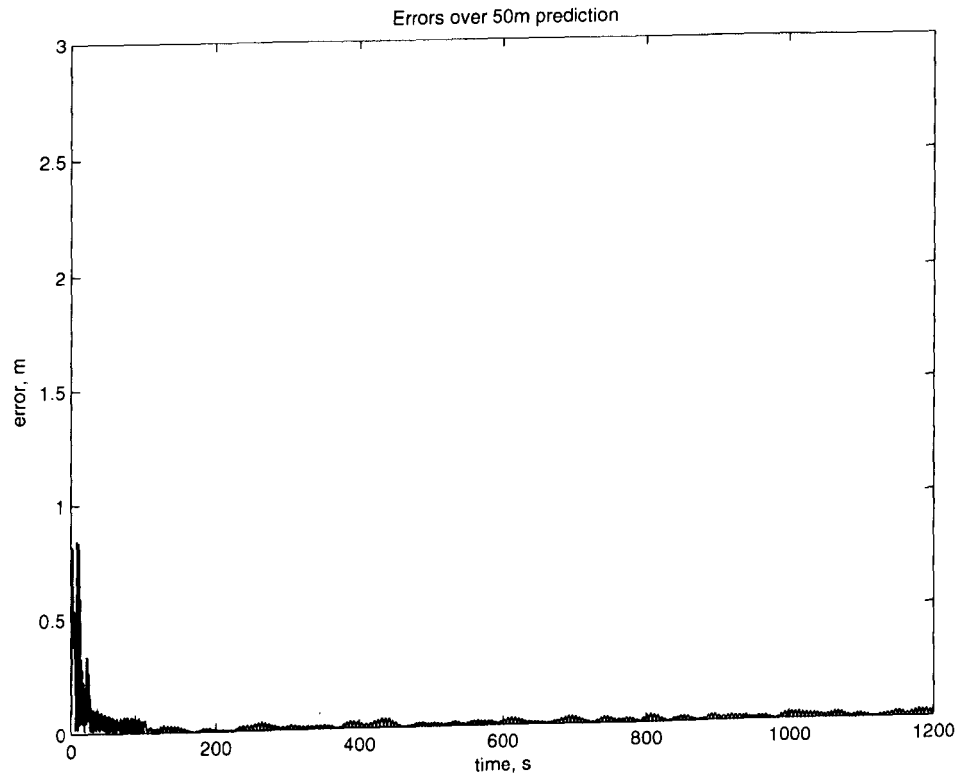


Figure 7.1: Errors between prediction and target at 50 m

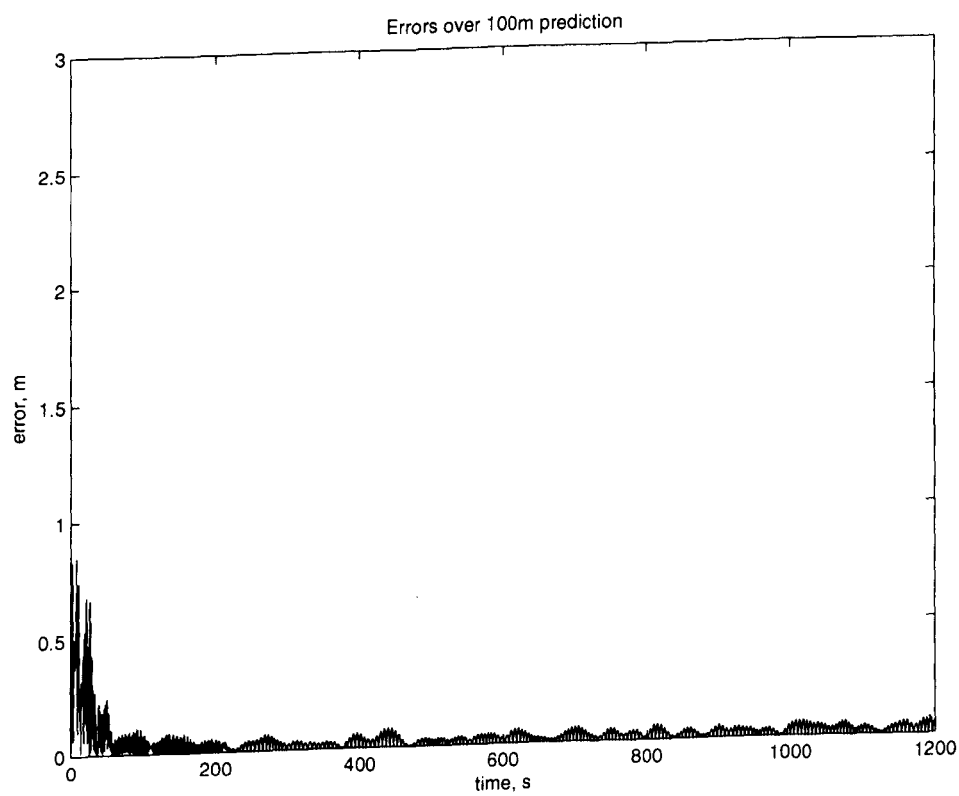


Figure 7.2: Errors between prediction and target at 100 m

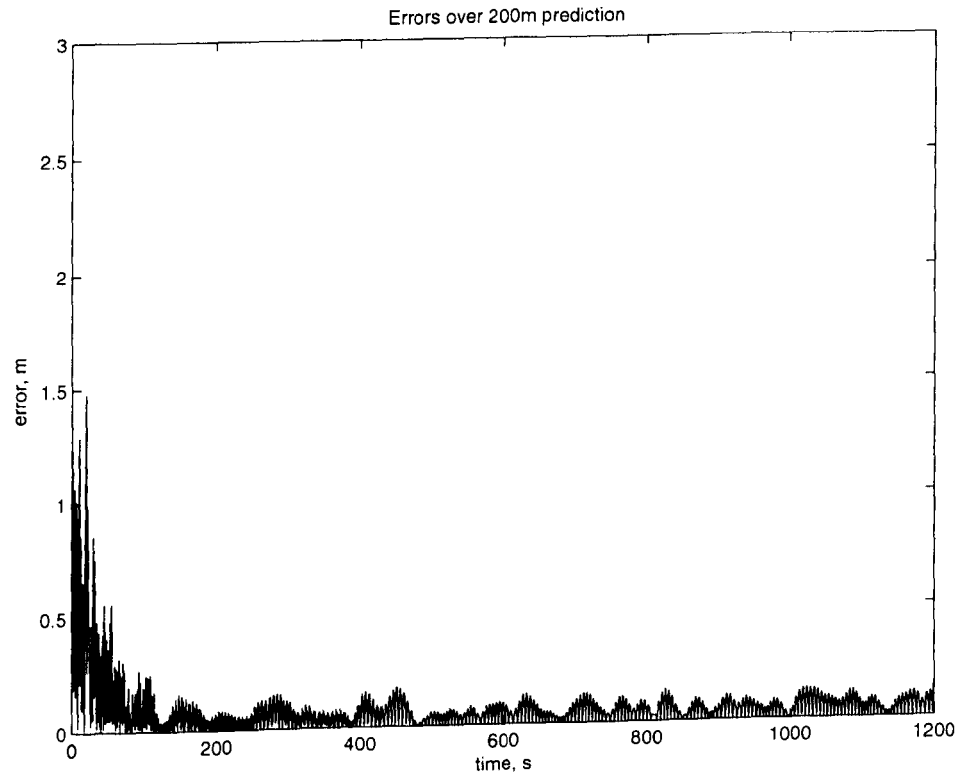


Figure 7.3: Errors between prediction and target at 200 m

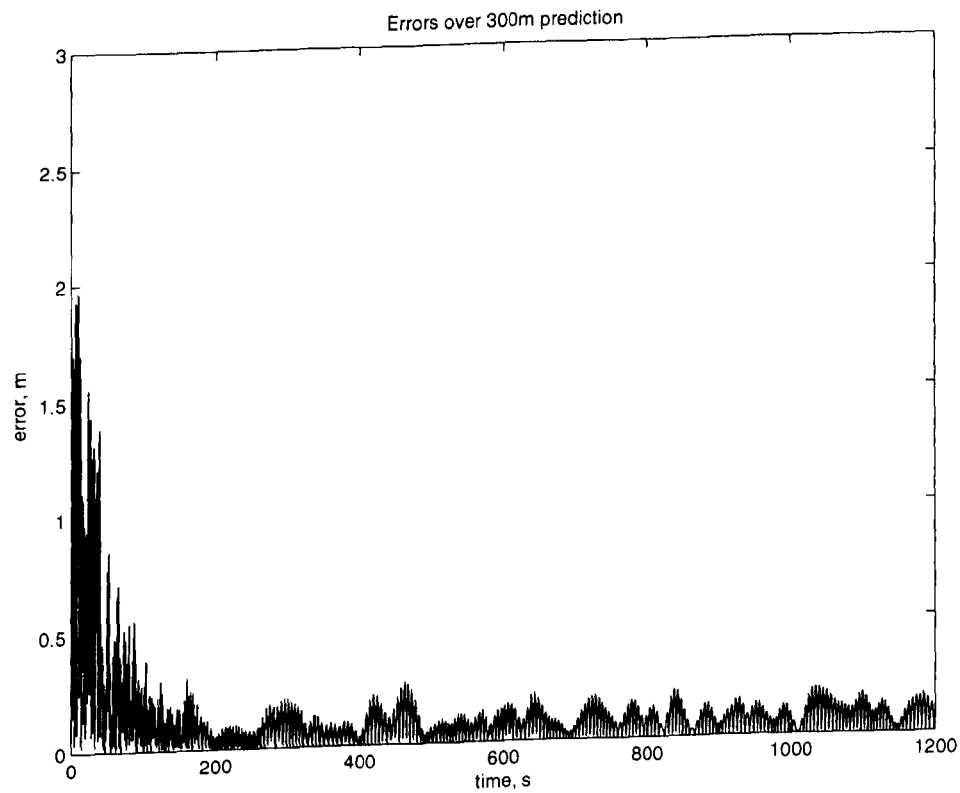


Figure 7.4: Errors between prediction and target at 300 m

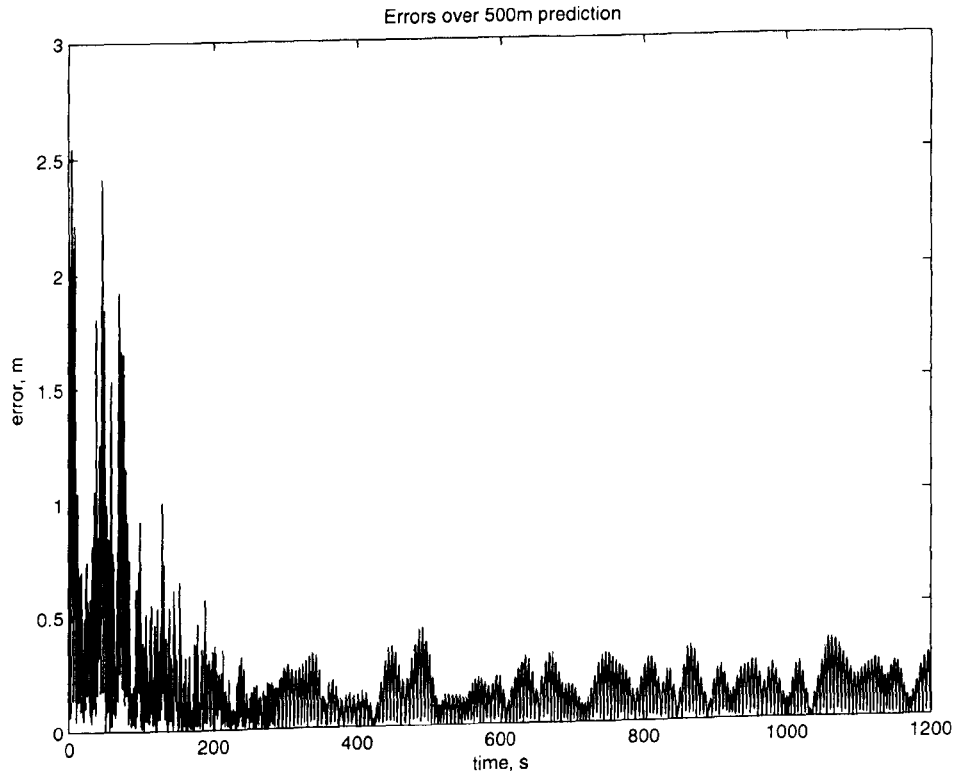


Figure 7.5: Errors between prediction and target at 500 m

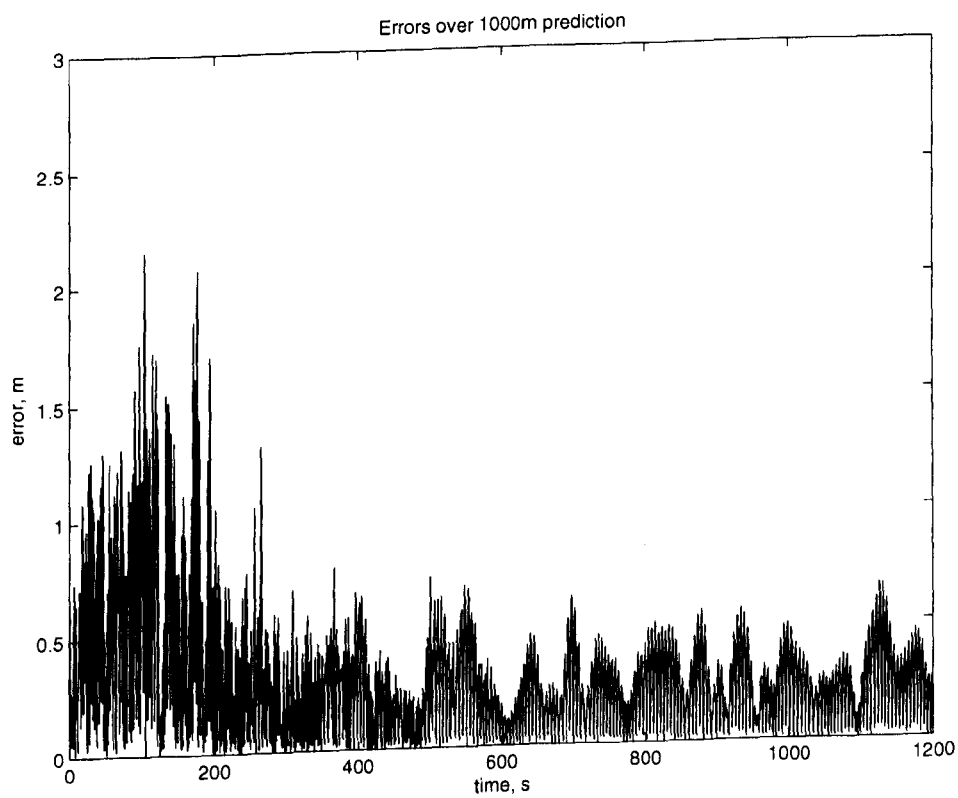


Figure 7.6: Errors between prediction and target at 1000 m

| Distance | time |
|---|---|
| 50 m | 32 s |
| 100 m | 64 s |
| 200 m | 128 s |
| 300 m | 192 s |
| 500 m | 320 s |
| 1000 m | 641 s |

Table 7.1: Time taken for 0.5 Hz energy to propagate

case to approximately 500 sec in the 1000 m case.

This transient may be caused by making predictions at a point removed from the reference sensor based on waves which have not yet reached that point. Essentially a prediction is being made for which no information is yet available. As the predictions are all made with the same time frame, i.e. 0 to 1200 sec, the wave that is present at the beginning of the record taken at 0 m, the reference point, will not reach the record predicted to be at 500 m for some time. Therefore the prediction made at the 500 m point can be considered inaccurate until this wave has propagated to that point.

### Transient velocity

Every frequency component in the spectrum will be travelling at a different velocity, with the lower frequency waves travelling faster than the higher frequency waves. The highest frequency simulated in these tests is at 0.5 Hz which will have a phase velocity of 3.12 $ms^{-1}$. In the context of this problem, where a number of waves are considered to have a group velocity, i.e., the velocity at which the energy associated with a wave travels, the group velocity is a more appropriated measure. For a 0.5 Hz wave this will be 1.56 $ms^{-1}$ and the energy will take 32 s to travel 50 m. Table 7.1 indicates the time taken for the energy to travel to the six prediction points. Looking back at Figs. 7.1 to 7.6, these times correspond to the length of the transients. In the case of the predictions at greater distances, other errors may mask the extent of the transient.

The transient has an exponentially decreasing form. This can be explained by the wave energy reaching the prediction point progressively. The lower frequency energy arriving before the higher frequency, and as each band of energy catches up to the prediction point the errors reduce to the point where the missing energy is small enough not to affect the

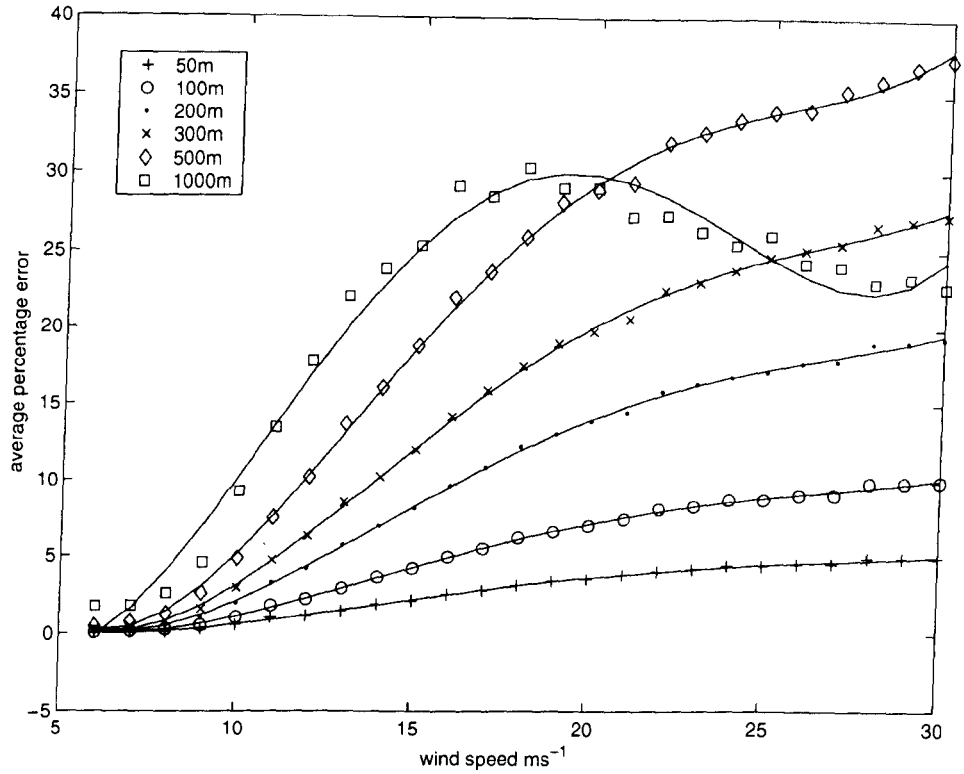


Figure 7.7: Errors with wind speed minus the transient

prediction.

### 7.1.1 True errors

In order to compare like for like predictions without the presence of the transient the time from which a stable prediction can be expected must be found. By examining the FFT of the original record, the highest frequency at which 1 % of the maximum power of the spectrum still remains can be found. Using this frequency its group velocity can be calculated, and at each prediction distance, the length of the transient to be eliminated can be found.

Also, in order to give a more accurate representation of the error at each wind speed, the average error for the remaining length of record is taken as a percentage of the mean significant wave height $H_{m0}$ for the specific wind speed. In this way the error value returned is scaled to its relevant wind speed. Using the combined method of removing the transient and comparing the average error to $H_{m0}$ the revised errors for wind speeds $6-30$ ms$^{-1}$ were calculated and the new results for an omni-directional spectrum are shown in Fig. 7.7. Again the record was of length $T = 1200$ sec with $N = 4096$ samples; the records are this time extended to lower wind speeds to cover a wider range, where wave devices are more likely

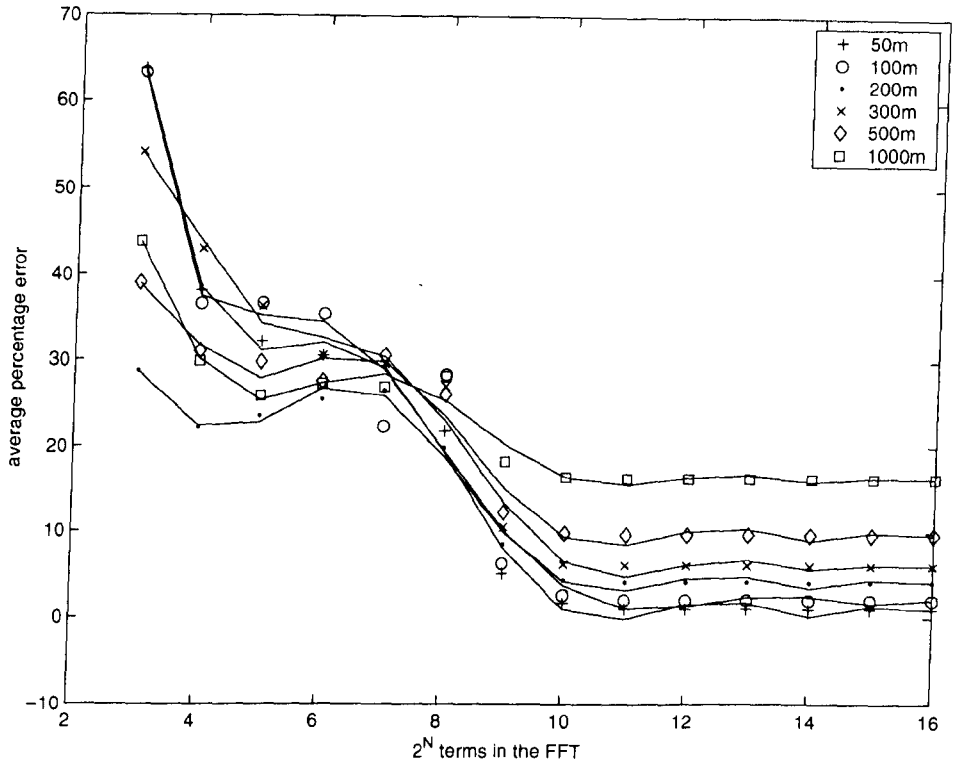


Figure 7.8: Errors with $N$ minus transient

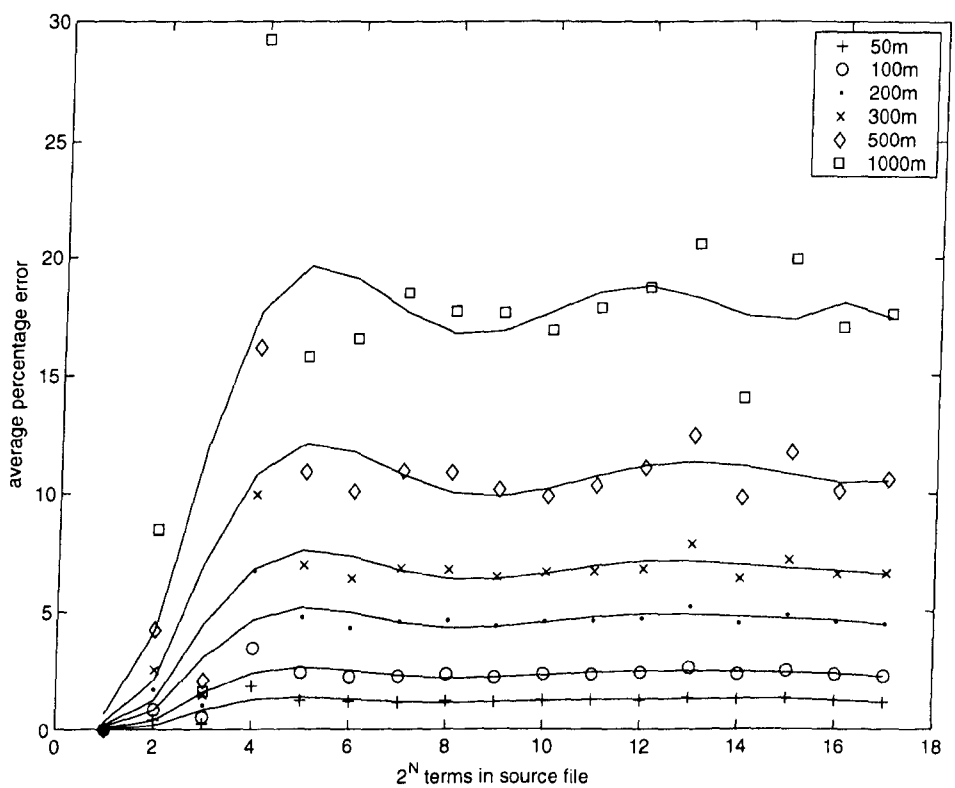


Figure 7.9: Errors from source file $N$ terms

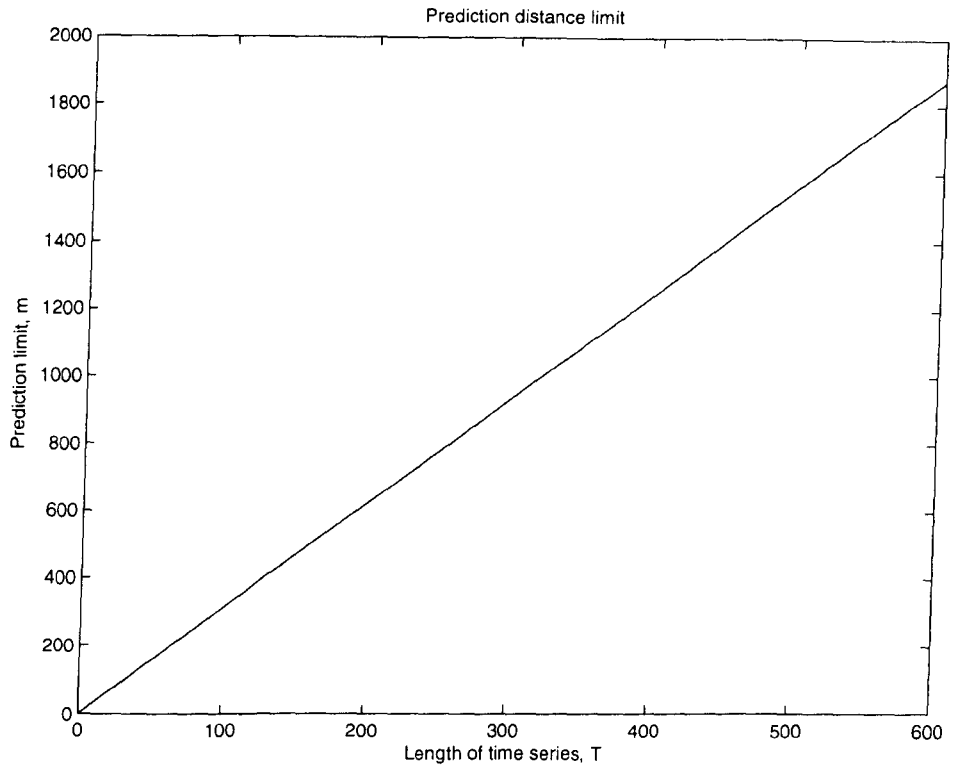


Figure 7.10: Prediction distance limited by $T$

to operate for much of the time. At wind speeds lower than 6 $ms^{-1}$ the highest frequency present in the FFT, at 1 % of the maximum power, is too high for its energy to cover the 1000 m to the final prediction point so this is discounted in the figures.

Fig. 6.36 of Chapter 6 can be recalculated using the new error measurement, this is plotted in Fig. 7.8. Again extending the $N$ term to ever increasing values has no effect after the highest frequency in the record has been passed. Only those results for a time series greater than 600 sec can be accepted as being valid for all prediction distances. As discussed earlier, making a prediction at a distance requires, as a reference, a time series long enough to allow the highest frequency present to travel to the prediction point. For shorter lengths of time series there is a restriction on the distance to which a prediction can be made. Fig 7.10 shows this limit taking an upper frequency of 0.5 Hz and plotting the possible prediction distance against the length of the time series. In [3] a time series of length 64 sec is quoted which would restrict the prediction limit to 180 – 190 m. At such a short distance between wave devices mooring problems would occur as discussed for correlation arrays in Chapter 6.

## 7.2 Other possible errors

Returning to Fig 7.7, errors increase with the distance from the reference sensor and with wind speed. There are two possible reasons for this: the increasing nonlinearity of the sea states, or the focusing of the energy of the spectrum into the lower frequency range where the spectral resolution of the FFT becomes weaker.

### 7.2.1 Non-linearity

The nonlinearity of the wave field would be a factor if the models used were accurate for real wave behaviour. As the wind speed and wave height increase in real situations non-linear effects become more important and the simple linear model breaks down. The profile of the waves becomes more trochoidal with narrow sharp peaks and wider troughs. The orbit of the water particles opens up and they start to be transported with the wave rather than remaining static. As particles reach the peak of the wave they will be travelling faster than the wave itself and will become detached and whitecapping will occur. As mentioned in Chapter 3, this is a major factor in limiting the wave height in high wind speeds. Other models have gone on to deal with the situation with more advanced techniques, which are reported in [7], [4] and [55]. In these papers, the authors have specifically modelled non-linear wave fields by using Gertsner or higher order Airy waves. These studies do not model whitecapping effects which have, in general, been considered in spectral models such as [28]. They have then gone on to use higher-order prediction theories; in some cases using real waves in flumes or test basins. The results of these papers were introduced in Chapter 1.

These non-linear errors can be discarded from the discussion of the errors here as linearity was specifically specified in designing the model structure. This would leave the shift of energy to the lower frequencies as a focus for finding the cause of the errors.

### 7.2.2 Dispersion errors

Using the evidence from the previous sections it has been shown that the errors in predicting over distance increase with wind speed and distance (Fig. 7.7). An increase in wind speed leads to a shift in the peak frequency to lower frequencies and an increase in wave amplitude. A concept that relates the frequency of the wave to its wavelength, and hence distance, is the dispersion relationship. This may be the key to why prediction errors increase.

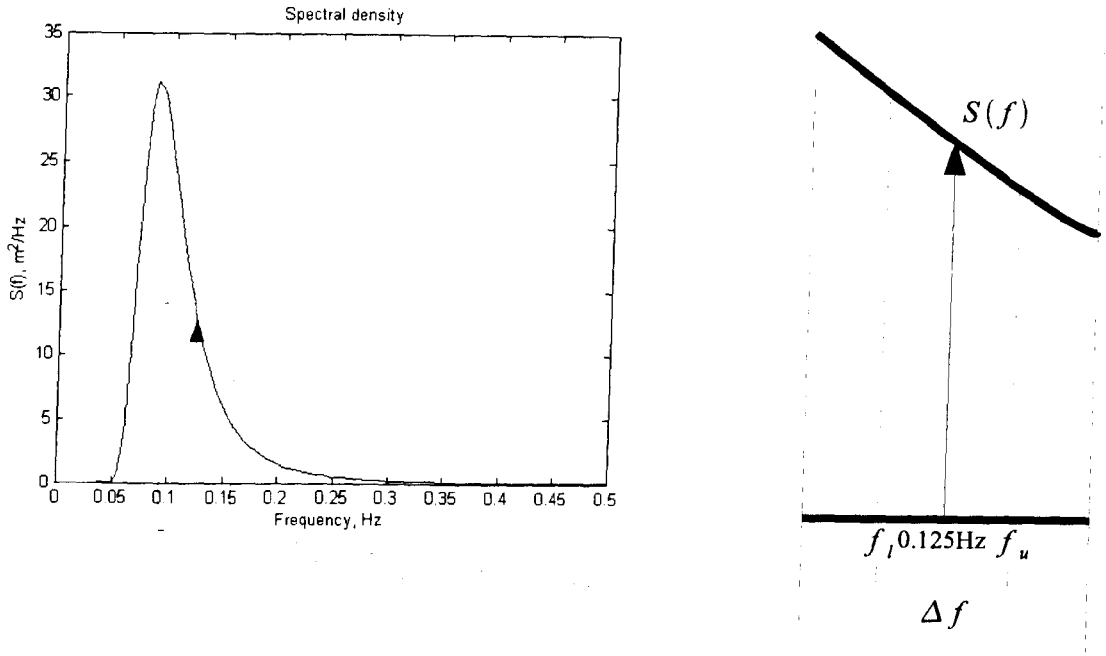


Figure 7.11: The energy band represented by a Delta function

### Energy representation

The basic theory behind making a prediction, and one fundamental to the FFT, is that a continuous function has to be broken down into a set of sinusoidal functions spaced at harmonic intervals. These sinusoids are then propagated according to a dispersion relationship and reconstructed into a final waveform. It may be that this discretisation of a continuous spectrum, in conjunction with the dispersion relationship, is the cause of the prediction errors.

Suppose a wave field derived from a continuous omni-directional Pierson-Moskowitz spectrum for a 16 $ms^{-1}$ wind speed is created. This is a continuous spectrum which is to be modelled as a set of idealised wave vectors located at discrete frequencies.

For the purposes of this discussion the simulated wave field can be considered as continuous, or nearly so, and the process of sampling this continuous function and taking the FFT as being the discretisation.

The amplitudes of these wave vectors are then proportional to the energy represented by the area below the curve bounded by $S(f)$ and $\Delta f$. Fig. 7.11 shows this with a Dirac delta function at $f = 0.125$ Hz. The amplitude $a$ of this function is derived from $a = \sqrt{S(f)2\Delta f}$. With $\Delta f = 0.005$ Hz, this function represents the continuous energy over the range 0.1225 Hz to 0.1275 Hz. In the predictions used so far, with $N = 4096$ and $T = 1200$ sec, the value

of $\Delta f = 0.000833$ Hz. The value of $\Delta f = 0.005$ Hz is used in the following discussion to make the reading more straightforward.

As illustrated previously, an idealised wave vector can be easily propagated using Eq. 6.11 if and only if all the energy in the original spectrum can be exactly represented as a single wave vector. For real waves this will never be the case. The energy is spread continuously over the spectrum and not concentrated at specific frequencies. Considering the modelling assumption made in the previous paragraph, the delta function at 0.125 Hz represents the range from 0.1225 Hz to 0.1275 Hz. Restating this in terms of wavelength, a 99.8 m wave represents the range from 95.9 m to 103.9 m. The difference here is 8 m, which, when accurately trying to predict wave behaviour, can mean the difference between a trough and a peak.

A further problem arises with water waves in the form of the dispersion relationship where

$$\omega^2 = gk \tanh(kh) \tag{7.1}$$

This equation in simple terms states that a wave of longer wavelength will travel faster than a wave with a shorter wavelength. Considering the range of $\Delta f$ here, the energy at the lower end of this range will tend to travel faster and overtake the energy at the higher end. In a different context this has already been shown to affect the point in time at which a stable prediction can begin to be made.

An experiment to show this effect is required. To model the situation, the energy in the band $\Delta f$ can be subdivided and modelled by an infinite number of idealised wave vectors. This is valid if the sum of the energy of these wave vectors is equal to the energy in the band $\Delta f$. To show this consider the energy in $\Delta f$ as being split into two and each of the new energy bands modelled by an idealised wave vector located at either 0.12375 Hz or 0.12625 Hz. The amplitudes of these vectors are proportional to the new energy bands. Squaring and summing these amplitudes gives the same energy as in the original $\Delta f$. This process can be continued *ad. infinum.* In this example, 128 subdivisions were carried out. Table 7.2 shows the energy assigned to each subdivision and the summation of these values.

Simulating each of these representations for 1200 sec and taking the FFT of each result gives the same general spectral shape and magnitude but, if the time series are compared, the differences between each become apparent. Fig. 7.12 shows the time series when the single frequency representation is shown with the 2, 4 and 8 frequency instances. The differences between the representations can be easily observed. This example is given for only one

| $\Delta f$ [Hz] | f [Hz] | lambda [m] | amp [m] | Energy = $\sum$ amp$^2$ [m$^2$] |
|---|---|---|---|---|
| 0.005 | 0.125 | 99.9238 | 0.3528 | 0.1246 |
| 0.0025 | 0.12375 | 101.9526 | 0.1118 | |
| | 0.12625 | 97.9549 | 0.0821 | 0.1246 |
| 0.00125 | 0.123125 | 102.9903 | 0.0629 | |
| | 0.124375 | 100.9306 | 0.0497 | |
| | 0.125625 | 98.9320 | 0.0402 | |
| | 0.126875 | 96.9922 | 0.0333 | 0.1246 |
| 0.000625 | 0.122812 | 103.5151 | 0.0629 | |
| | 0.123437 | 102.4695 | 0.0497 | |
| | 0.124062 | 101.4397 | 0.0402 | |
| | 0.124687 | 100.4253 | 0.0333 | |
| | 0.125312 | 99.4260 | 0.0629 | |
| | 0.125937 | 98.4416 | 0.0497 | |
| | 0.126562 | 97.4718 | 0.0402 | |
| | 0.127187 | 96.5162 | 0.0333 | 0.1246 |

Table 7.2: The summation of energies when assigned to multiple frequencies

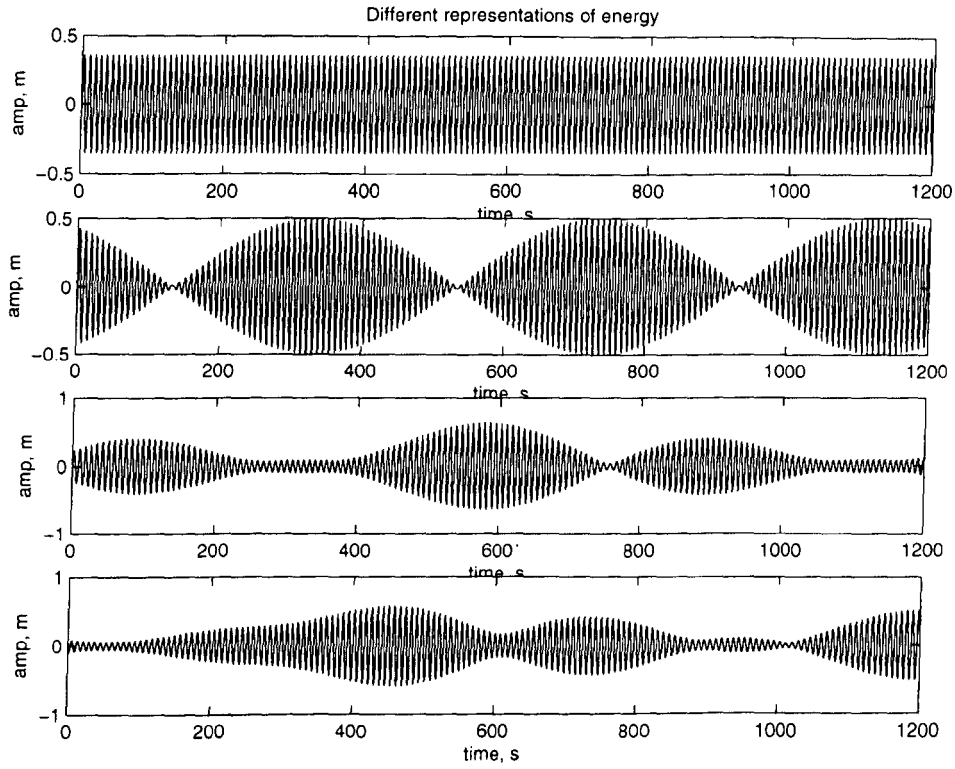


Figure 7.12: Different representations in time of the same energy, top 1 freq, 2 freqs, etc

frequency interval $\Delta f$. Over the entire spectrum, frequencies relatively far removed from those of interest would be affected.

### Application to FFT prediction

The above theory for the transfer of energy can be applied to the prediction of wave behaviour by means of the Fast Fourier Transform (FFT). By using the FFT to deconstruct the simulated wave-field, idealised harmonically-spaced wave vectors can be fitted to a nominally continuous spectrum. Now suppose that the length of the time series was taken to be $T$ sec. The frequency spacing between the wave vectors would therefore be $\Delta f = 1/T$ Hz. The idealised energy associated with each harmonic can be propagated with its own singular group velocity. hence the energy at either extreme of this range would have travelled either too far or not far enough.

For greater-distance predictions, this effect will grow as the energy becomes further out of synchronism from where it should be. With an increase in wind speed, the energy of the spectrum grows and moves to a lower frequency range. Initially the energy would have been spread over many harmonics but will now be concentrated into fewer since the range $\Delta f$ will not have changed. Concentrating more energy into an unchanged frequency range will

result in an amplification of errors as seen in Fig. 7.7.

As a corollary to this theory, Fig. 6.37 shows how an increase in time series length $T$, and hence a decrease in $\Delta f$, results in a decrease in error. It can be implied that the idealised wave vector represents a smaller range of frequencies, and hence smaller propagation error. An obvious solution to this problem would be to infinitely increase the length of the time series, however the stationarity of the spectrum will not be guaranteed to hold for ever increasing time-series lengths.

## 7.3 Applications to wave device farms

So far this discussion has narrowly focused on the prediction of surface elevation from one point to another, which has been shown to be valid to a certain degree of accuracy depending on the wave conditions and distance. If the scope of this discussion is broadened to look at a farm-size model with approximately 50 devices then the early experiments in Chapter 6 can find an application.

### 7.3.1 Device farm layout and instrumentation

When farms of devices are deployed their layout will probably be in a grid pattern, aligned to the mean wave direction of the site. For Scottish sites, the highest concentration of waves are located on the north and west coasts. In these areas, the mean wave direction tends from the South-West to the North-East. The farm arrangement of the directional wave devices: Pelamis, Wavedragon, etc., which can move to face the mean wave direction, are predicted to be in a format with 3 to 4 layers and 10 to 15 devices in each layer. For point absorber devices, a square grid is thought to be the favoured design.

Whist the experiments to date have concentrated on the omni-directional prediction, with good results to 500 m in operational wave conditions; the fitting of an omni-directional spectrum to a directional sea-state was understandably less accurate. However, the results in [55] show good promise so that extending the analysis to include directional information, and fitting multi-directional wave vectors, would result in accurate predictions, if not to the 500 m point then at least to several hundreds of metres. This work will be further discussed in Chapter 8.

Assuming that these predictions are possible, wave rider buoys could be situated around the device farm to provide predictions of wave behaviour to the devices. In multiple layered

farms, a prediction of wave behaviour should be possible from one layer to another. For example, the first layer of devices would be able to record vertical displacement which can then be propagated to the next layer and extended in time by means of neural network prediction (Chapter 8) to give the surface elevation at the next device layer interface.

The separation of the wave riders from the devices and indeed from each other, is dependent on the operating range of the farm and the extent to which a prediction at that level would remain accurate. In low wind conditions, where the prediction is more accurate, and devices outputs are also low, a prediction will help to increase power output. Whereas at higher wind speeds, where the prediction is less accurate, the wave amplitudes and power outputs are greater and a performance-improving prediction is not necessary. In this state the wave rider buoys can be used to provide warning of extreme wave events rather than the precise time series prediction.

### Earlier prediction methods

Recapping the earlier methods in Chapter 6, if very large scale device farms, such as those proposed by the SEADOG device team [56], became a reality large static-mounted devices in a grid structure will begin to appear and the circular FFT may find an application for enhancing the directional resolution of time-series predictions. The circular FFT can be considered as an additional check to the existing directional resolving methods implemented in software such as DIWASP (Chapter 4). The method for displaying the data itself (taking its shading from the magnitude of the power present at each frequency/direction) may help in identifying bands of swell.

The correlation method, also introduced at the beginning of Chapter 6, is more difficult to place as a method until the resolution of the buoy motion problem is solved and a static wave record from a fixed point can be produced. But, for directional devices like the Pelamis, where three or four long rows of devices are moored as a farm, a method is available of increasing the correlation resolution without requiring the buoys or devices to be less than one wavelength apart.

Referring to Fig. 7.13, if the time series from each buoy/device is predicted forward to a line behind the device farm, but not parallel to the devices themselves, then a base line of time series data points can be produced. This base line time series can then be treated as a linear array where the data points are placed closer to one another compared to a farm with a single row of the devices. Again this would be useful as a verification of wave directionality.

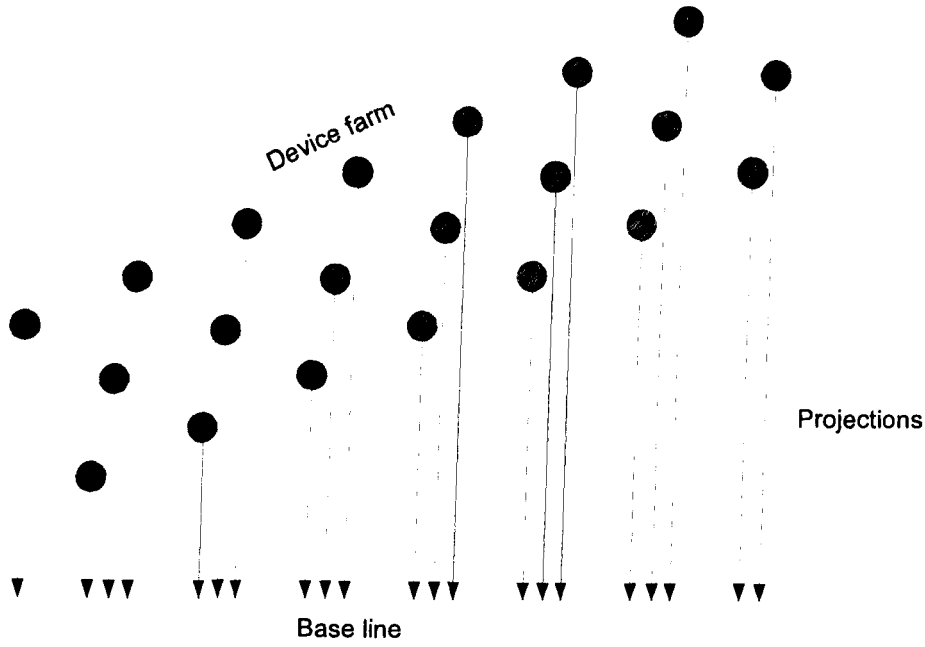


Figure 7.13: Increased resolution through forward projection

Although these two methods in themselves do not specifically assist in the time series prediction, they do provide an additional analysis for wave directionality, which, when a device farm is in place, will be available for little additional cost.

### SWAN model

As an alternative method of prediction (using existing theory and models) the SWAN model [28] may be employed to cover the device farm area. The SWAN model tracks the transformation of wave energy from point to point over an area of ocean in the near shore environment. Essentially the wind speed is input to the model. This is obtained from a global weather model, often supplied by the MET office in the UK. This wind speed is used in combination with the equations in Chapter 3 to create a wave spectrum and therefore stochastic wave parameters over a grid of data points. The model is adapted to adjust the wave spectrum as it passes over shallow water (including shoaling, diffraction and focussing effects). It can also be interfaced to a tidal model to simulate the currents that will flow.

The model can be adapted so that at each point (where a device is situated) a filter can be placed to model to the power extraction from each device. Using the data from wave riders and information from the devices themselves, this model can be used to estimate power production from the device farm on a stochastic basis. While this is not the second by second prediction this work was aimed at, the SWAN model may be of more benefit to

power production managers for informing the grid operators of expected power outputs.

## 7.4 Conclusion

This discussion has analyzed and put into context the results of Chapter 6. Firstly, by examining the errors presented in the prediction results (and hence providing explanation for their occurrence and therefore a better understanding of the limitations of the Fast Fourier Transform); and secondly, the early experiments of this study have been incorporated in a device farm scenario, as supplementary methods for directional wave measurement.

# Chapter 8

# Further Work

The limits of the Fourier transform have been explored in the main body of this thesis which has exposed several areas where continued research would be valuable. This brief chapter introduces a few ideas for future work. The first area of research is in the application and derivation of the limits for alternative signal processing algorithms. The second is the implementation of the full methods as given in the six papers referenced in the introduction. The final suggestion is the exploration of the neural network as a technique for time series prediction.

## 8.1 Alternate time series transforms

The research in this thesis has highlighted an interesting paradox with regards to the Fast Fourier Transform. While, in itself, the FFT can be used to made predictions over distance, it becomes less accurate as sea states become more energetic and this energy becomes concentrated in the lower frequency range. The frequency resolution of the transform is fixed by the maximum length of the record over which it can be considered as stationary. If the frequency resolution could be increased, whilst not extending the length of the time series, an improved prediction may be possible.

### 8.1.1 Wavelet transform

The FFT is ultimately based upon the summation of the source time series multiplied by a set of orthogonal basis functions. For the FFT, this is a set of sinusoids placed at multiples of a fundamental frequency $\Delta f = 1/T$, where $T$ is the length of the time series. This effectively sets a bank of harmonically spaced band pass filters of fixed width $\Delta f$. The energy of the

signal is separated out into each of these frequency bins.

The wavelet transform allows for a different set of basis functions, one which is equivalent to a bank of constant Q bandpass filters [57]. Consider this in other terms, for a 128 sample time series, using an FFT, the lowest frequency wave that can be analysed is one which is exactly 128 samples in length. The next frequency to exactly match is one half of this length or twice the frequency, i.e., 64 samples. This pattern continues in the series 32, 16, 8, 4, 2 and 1. Any energy that does not fit into this pattern is spread amongst the other harmonics.

In using a wavelet transform the pattern is different. The lowest frequency will remain tied to 128 samples but the next available frequency term can be 127 samples rather than 64. The sequence continues for the interval series 126, 125, 124, ... ,1. This gives a greater frequency resolution in the lower frequency range, where the energy propagation is most affected for dispersive waves.

This increased resolution is at a cost in that the basis function now becomes more complicated and must be scaled and stretched to fit the appropriate analysis conditions. Additionally, the Wavelet transform is still based on linear superposition.

### 8.1.2 Hilbert Huang transform

Throughout this thesis the concept of linearity and superposition has been put forward as a basic property of the prediction problem. The real-world situation is inherently different. Non-linearity and non-stationarity are the defacto properties for natural wave progression and development. Sea states do not generally add together as a simple superposition. The energy in the wave can usually remain in a fixed band, but with some being transported to other areas of the spectrum; Hasslemann's third-order interactions is a good example of this [27].

An interesting and informative example is the case of a short wave riding on a longer wave. The linearity principle would simply add the two waves together and a spectral plot would show the two wave frequencies as well separated delta functions. The reality is that the two waves will modulate each other, the higher frequency to a greater extent than the lower. An FFT will attempt to resolve this in terms of harmonically related sinusoids and the energy will be spread over many frequencies at times far removed from the two original frequencies.

The Hilbert-Huang transform aims to address the problem of non-linearity by looking for this modulating behaviour during the transform process. Instead of using a fixed orthogonal

basis function as in the case of the FFT and the wavelet transform, the Hilbert-Huang method applies a time-varying function as a basis, i.e., with frequency and amplitude varying in time.

The method has been developed relatively recently [58] and has not been applied to wave studies to any great depth, although Soares has investigated its application to deriving wave spectra [59]. The basic premise of decomposing a time series into time varying functions may prove to be difficult, but it would be worthwhile investigating this.

## 8.2 Second order theories

The introduction of this thesis included a description of six existing studies into wave prediction. The further implementation of these methods and the calculation of error tolerances with distance and with increasing wind speed, would be an interesting avenue to explore. Each of these methods, as has been mentioned, is based to some extent on the FFT of a wave record. The methods proposed may reduce the errors as found by using the FFT on its own. However, the concept of stationarity and higher-order effects, which the Hilbert-Huang transform aims to address, may still be superior to the prediction methods.

## 8.3 Time series prediction

The latter half of Chapter 6 attempts to use the FFT for prediction in time, this failed through the inherent periodic nature of the transform. Predicting ahead in distance would still be a desirable achievement in terms of control, and other possible solutions are possible as discussed below.

### 8.3.1 Recursive neural networks

Over the past four decades the theory of neural networks has progressed from an abstract mathematical theory to the point where there are many specialist research groups in this area. However, the underlying concept is a very simple process [60]. For brevity, in this chapter, only the network used in this preliminary test will be described in detail.

The prediction method is based on the training of the weights shown in Fig. 8.1. In this network a delay line of ten samples is multiplied by a set of weights and summed with a bias value to give a predicted value of the next sample in the time series. To train the network weights an example of the process to be predicted is required. In this case the time series for which a prediction is desired.

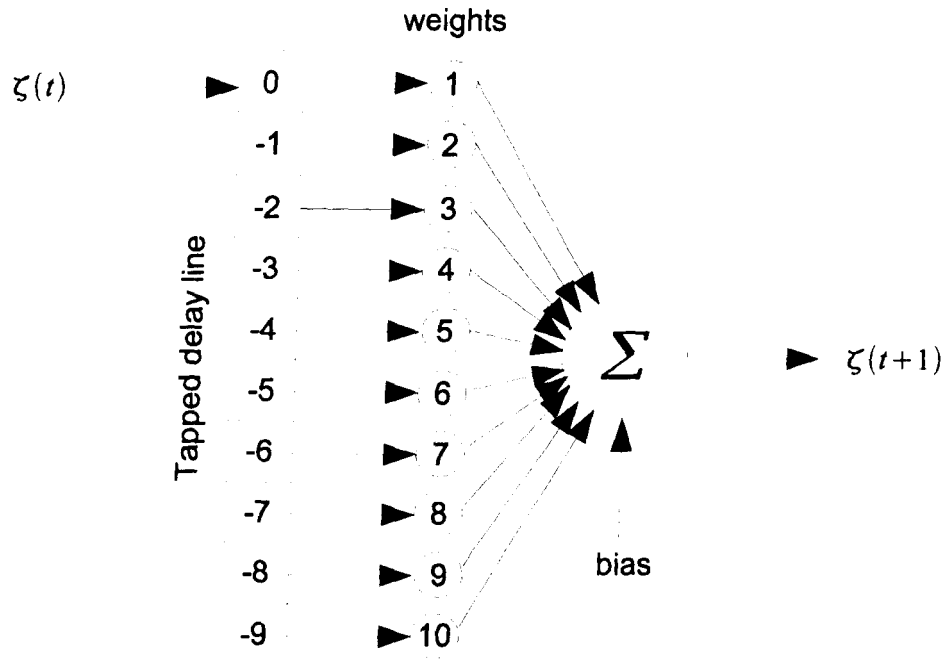


Figure 8.1: Layout of neural network

Initially the weights are set to random values between 0 and 1. At the start of the time series the first 10 samples are placed into the delay line, they are then multiplied by the initial weights and summed to give a predicted answer. This prediction is compared to the target answer (sample 11) and the error calculated. This process continues for the length of the time series until a completed error function has been generated. This error function is then used to correct the weights by a process called backpropagation. There are many different training methods and error functions that can be used [60].

This training process is iterated until a desired error level is reached. In order to predict

| | | | | | | | | |
|---|---|---|---|---|---|---|---|---|
| 4096 | p1 | p2 | p3 | p4 | p5 | p6 | • | p10 |
| 4095 | 4096 | p1 | p2 | p3 | p4 | p5 | • | p9 |
| 4094 | 4095 | 4096 | p1 | p2 | p3 | p4 | • | p8 |
| 4093 | 4094 | 4095 | 4096 | p1 | p2 | p3 | • | p7 |
| 4092 | 4093 | 4094 | 4095 | 4096 | p1 | p2 | • | p6 |
| 4091 | 4092 | 4093 | 4094 | 4095 | 4096 | p1 | • | p5 |
| 4090 | 4091 | 4092 | 4093 | 4094 | 4095 | 4096 | • | p4 |
| 4089 | 4090 | 4091 | 4092 | 4093 | 4094 | 4095 | • | p3 |
| 4088 | 4089 | 4090 | 4091 | 4092 | 4093 | 4094 | • | p2 |
| 4087 | 4088 | 4089 | 4090 | 4091 | 4092 | 4093 | • | p1 |

Figure 8.2: Contents of delay line for recursive prediction

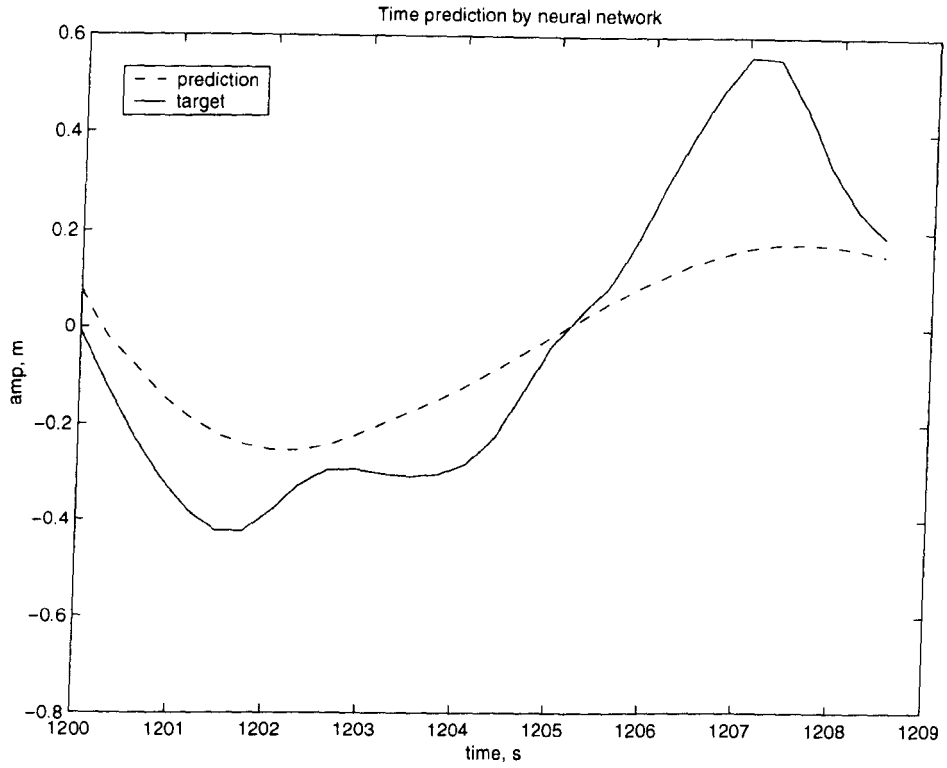


Figure 8.3: Time series prediction by neural network

ahead in time a scheme such as that shown in Fig. 8.2 needs to be followed. Starting from the left the last 10 samples of a 4096 sample series are placed in the delay line and the prediction p1 made. This predicted sample is then placed back into the delay line and the last nine samples of the time series used to fill the remaining space. Again a prediction is made and p2 is now placed into the delay line and the process continued.

The use of this recursive process very rapidly leads to a build up of errors as they are amplified in a similar manner to the feedback effect in a sound system. Nevertheless over a short time scale the method can pick up on the general gradient of the time series, this is illustrated in Fig. 8.3. While this is not an exact match to the target series, the gradient, minimum turning point and zero crossing point are correct.

Further work is required on this promising method. This is a simple method and there are already many different neural network techniques that have been developed that refine the learning process and reduce the error. Those implemented by financial organizations are of most interest since they deal almost exclusively in the prediction of time series. Also of interest is the competition run by the Santa Fe Institute [61].

### 8.3.2 Faster methodologies

While the neural network methodology does show great promise in providing a time prediction it is very computationally demanding. The training of the network takes of the order of 1 to 2 minutes (although it is written in MATLAB code and rewriting it in a compiled language environment would significantly improve the speed). The network needs to be retrained every 10 predictions. If two processors were available then one could be used to make the predictions whilst the other is preparing and training the next network.

In situations where only the next sample ahead is required a simpler method of averaging the past 5 samples or curve fitting could be used and implemented using a programmable micro-controller.

## 8.4 Conclusion

This brief chapter has introduced some of the possibilities for future work based on this thesis. The exploration of the Hilbert-Huang transform and the extension of time series through neural network principles offers the widest and most promising scope for future research.

# Chapter 9

# Conclusion

This study has been undertaken to fully explore the usage of the Fast Fourier Transform (FFT) for the prediction of surface wave elevation. The earlier chapters set out the problem from the principle equations and theories in order to provide a foundation to the subject. To address this issue, the basic wave equations (Chapter 2) and the theory of wave generation and propagation (Chapter 3) were given in detail in order to highlight and discuss the simplifications that are made in the analysis of a process which is inherently complex.

A full description of Fourier Theory (Chapter 5) was also given because, although the concept of the theory is generally used and understood by many, the details are often lost in its use as a frequency analysis tool. This casual familiarity with the process of decomposing a complex series into component harmonics (using the same guidelines and simplifications as used in spectral analysis) has led to the assumption by some that these components can be used for prediction in time by extension.

Having provided this background, the thesis then goes further to focus on the experimental work which was conducted in order to validate the FFT representation of real sea waves and to explore the limits of the validity (Chapters 4 & 6). While targeting a specific problem from the outset would have been the ideal path, this is a developing subject area, so that a certain degree of experimental and abstract thinking is required in order to eliminate early concepts, explore the correct route for the analysis to take and then to allow time for the core subject knowledge to develop. This is very much the rational behind the development of this work and the order of this thesis

With the key conceptual problem formulated (i.e, the constraints under which the FFT can be use to predict wave behaviour), a simple experiment was developed. This experiment took the form of a prediction of a complex sea state from one point to another in time and

over distance (Section 6.3).

The results from the experimental work showed that the prediction in time is constrained by the inherent periodicity assumed by the FFT, i.e. a further continuance of the time series $f(\Delta t \rightarrow T)$, as given by the FFT, will produce another series which is a repetition of this, so that the method of harmonically decomposing the time series ensures that the series is periodic with a period length $T$. Attempting to predict in time results in a repetition of the initial time series (Section 6.3.2).

The prediction over distance proved to be more promising, because within certain bounds, the prediction appeared valid. Before the prediction can be examined, the transient has to be removed and a valid section after a time period found for each distance prediction point (Section 7.1). The time taken to transport energy was shown to be the cause of this transient error. Once this transient is removed, predictions to 200 m could be considered valid to the end of the time series length. Obviously at greater distances the valid period decreases because the transient period is longer. Increased wind speed will also decrease the valid period.

The problem of increasing error levels with greater distance and wind speed was found to be due to the resolution of the FFT and the discretisation process (Section 7.2.2). In representing a continuous process as discrete wave vectors, a single harmonic effectively takes the place of a band of energy. Whilst the single harmonic can be adequately translated in time and distance by the FFT, the dispersive nature of gravity waves leads to the band effectively evolving and changing shape and structure. The extent to which this evolution takes place is governed by the width of the energy band, which is in turn determined by the frequency resolution of the FFT. The resolution is set by the length of the time series $T$. The length of the time series is limited by the extent to which the wave surface can be considered stationary.

It was suggested that the increase in errors with wind speed is due to the movement of energy to the lower regions of the spectrum, where the FFT has limited resolution because of the length of time series that can be utilised. Possible further work (Chapter 8) was suggested in areas that can increase the resolution of the transform processes. It is proposed that a wavelet or Hilbert-Huang transform can be used for this.

The most interesting path of further research to build on this thesis would appear to lie with the neural network prediction briefly introduced in Section 8.3.

In conclusion, this thesis has brought together the various different background principles required to examine the use of the FFT in the prediction of wave behaviour. This background

information has included a review of possible measurement techniques and their inherent advantages and disadvantages. After presenting this background information the FFT was tested and the results of these experiments analysed. A theory to explain the errors returned from the experiments was then given and defended with supporting experiments. The thesis is concluded by a discussion of the possible future work in this area.

In summary this thesis has disproved the use of FFTs in sea wave prediction and a return to the use of probabilistic methods seems to be more appropriate to the wave energy industry and its needs.

# Bibliography


[1] Anon, "Results from the work of the European Thematic Network on Wave Energy," Tech. Rep. ERK5-CT-199-20001, European Wave Energy Network, March 2003.

[2] S. Naito and S. Nakamura, "Wave energy absorption in irregular waves by feedforward control systems," in *Hydrodyamics of Ocean Wave Energy Utilisation* (D. Evans, ed.), (Lisbon), pp. 269–280, IUTAM, 1985.

[3] M. Belmont, E. Morris, and H. Zienkiewicz, "Short term forecasting of the sea surface shape," *Journal of International Shipbuilding Progress*, vol. 45, no. 444, pp. 383–400, 1998.

[4] J. Skourup and M. Sterndorff, "Deterministic reproduction of non-linear waves," in *OMAE'02*, (Oslo), June 2002.

[5] J. Pizer, C. Retzler, R. Henderson, F. Cowieson, M. Shaw, B. Dickens, and R. Hart, "Pelamis WEC - recent advances in the numerical and experimental modelling programme," in *6th European Wave and Tidal Energy Conference* (C. Johnstone and A. Grant, eds.), (Glasgow), pp. 373–378, University of Strathclyde, August 2005.

[6] V. Voronovich, B. Holmes, and G. Thomas, "A preliminary numerical and experimental study of wave prediction," in *6th European Wave and Tidal Energy Conference* (C. Johnstone and A. Grant, eds.), (Glasgow), pp. 535–542, University of Strathclyde, August 2005.

[7] W. Sulisz and M. Paprota, "Modeling of the propagation of transient waves of moderate steepness," *Applied Ocean Research*, vol. 26, pp. 137–146, 2004.

[8] J. Zhang, L. Chen, M. Ye, and R. Randall, "Hybrid wave theory for unidirectional irregular waves-part I. Theory and numerical scheme," *Applied Ocean Research*, vol. 18, pp. 77–92, 1996.

[9] C. Spell, J. Zhang, and R. Randall, "Hybrid wave theory for unidirectional irregular waves-part II. Comparison with laboratory measurement," *Applied Ocean Research*, vol. 18, pp. 93–110, 1996.

[10] J. Zhang, J. Yang, J. Wen, I. Preslin, and K. Hong, "Deterministic wave model for short-crested ocean waves: Part I. Theory and numerical scheme," *Applied Ocean Research*, vol. 21, pp. 167–188, 1999.

[11] J. Zhang, I. Preslin, J. Yang, and J. Wen, "Deterministic wave model for short-crested ocean waves: Part II. Comparison with laboratory and field measurements," *Applied Ocean Research*, vol. 21, pp. 189–206, 1999.

[12] M. Tucker and E. Pitt, *Waves in Ocean Engineering*, vol. 5 of *Elsevier ocean engineering book series*. Elsevier Science ltd., Oxford, UK: Elsevier, first ed., 2001.

[13] J. Falnes, *Ocean waves and oscillating systems*. The Edinburgh Building, Cambridge: Cambridge University Press, 1st ed., 2002.

[14] J. Townson, *Free Surface Hydraulics*. London: Unwin Hyman Ltd., 1st ed., 1991.

[15] Anon, *Waves, tides and shallow water processes*. Open University Volumes in the Oceanography Series, Oxford: Butterworth Heinemann, 2nd ed., 1999.

[16] R. G. Dean and R. A. Dalrymple, *Water Wave Mechanics for Engineers and Scientists*, vol. 2 of *Advanced Series on Ocean Engineering*. Farrer Road, Singapore: World Scientific Publishing Co. Pte. Ltd., 1991.

[17] S. G. Airy, *Tides and Waves*. Encyclopaedia Metropolitana, 1845.

[18] S. H. Lamb, *Hydrodynamics*. Cambridge, UK: Cambridge University Press, sixth ed., 1932.

[19] M. Tucker, "Analysis of sea waves," *Proceedings of the Institute of Civil Engineers*, vol. 26, pp. 301–315, 1963.

[20] S. Rice, "The mathematical analysis of random noise," *Bell System Technical Journal*, vol. 23 and 24, pp. 82–232 and 46–156, 1944–45.

[21] G. Komen, L. Cavaleri, M. Donelan, K. Hasselmann, S. Hasselmann, and P. Janssen, *Dynamics and Modelling of Ocean Waves*". Cambridge, UK: Cambridge University Press, 1st. paperback ed., 1994.

[22] S. R. Massel, *Ocean Surface Waves: Their Physics and Prediction*, vol. 11 of *Advanced Series on Ocean Engineering*. Singapore: World Scientific, 1996.

[23] O. Phillips, "On the generation of waves by a turbulent wind," *Journal of Fluid Mechanics*, vol. 2, pp. 417–445, 1957.

[24] J. Miles, "On the generation of surface waves by shear flow," *Journal of Fluid Mechanics*, vol. 3, pp. 185–204, 1957.

[25] P. Janssen, "Quasi-linear theory of wind-wave generation applied to wave forecasting," *Journal of Physical Oceanography*, vol. 21, pp. 1631–1642, 1991.

[26] R. Snyder, F. Dobson, J. Elliot, and R. Long, "Array measurements of atmospheric pressure fluctuations above surface gravity waves," *Journal of Fluid Mechanics*, vol. 102, pp. 1–59, 1981.

[27] K. Hasselmann, "On the non-linear energy transfer in a gravity-wave spectrum. 1:General theory," *Journal of Fluid Mechanics*, vol. 12, pp. 481–500, 1962.

[28] R. Booij, R. Ris, and L. Holthuijsen, "A third-generation wave model for coastal regions: 1. Model description and validation," *Journal of Geophysical Research*, vol. 104, pp. 7649–7666, April 1999.

[29] K. Hasselmann, "On the spectral dissipation of ocean waves due to whitecapping," *Boundary Layer Meteorology*, vol. 6, pp. 107–127, 1974.

[30] G. Komen, S. Hasselmann, and K. Hasselmann, "On the existence of a fully developed wind-sea spectrum," *Journal of Physical Oceanography*, vol. 14, pp. 1271–1285, 1984.

[31] O. Phillips, "The equilibrium range in the spectrum of wind-generated waves," *Journal of Fluid Mechanics*, vol. 4, pp. 426–434, 1958.

[32] S. Kitaigorodskii, "Applications of the theory of similarity to the analysis of wind-generated wave motion as a stochastic process," *Izvestia Acad. Nauk., SSR, Geophysical Series*, no. 1, pp. 105–117, 1961. Original paper in Russian.

[33] W. J. Pierson and L. Moskowitz, "A proposed spectral form for fully developed wind seas based on the similarity theory of S.A. Kitaigorodskii," *Journal of Geophysical Research*, vol. 69, pp. 5181–5188, December 1964.

[34] K. Hasselmann, T. Barnett, E. Bouws, H. Carlson, D. Cartwright, K. Enke, J. Ewing, H. Gienapp, D. HAsselmann, P. Kruseman, A. Meerburgh, P. Muller, D. Olbers, K. Richter, W. Sell, and H. Walden, "Measurement of wind-wave growth and swell decay during the Joint North Sea Wave Project (JONSWAP)," *Deutschen Hydrogr. Zeitshcrift Reihe*, vol. A12, pp. 1–95, 1973.

[35] W. Pierson, G. Neumann, and R. James, "Practical methods for observing and forecasting ocean waves by means of wave spectra and statistics," Tech. Rep. 603, U.S. Hydrographic Office, 1955.

[36] M. Longuet-Higgins, D. Cartwright, and N. Smith, "Observations of the directional spectrum of sea waves using the motions of a floating buoy," in *Ocean Wave Spectra*, (Englewood Cliffs, N.J.), pp. 111–136, National Acedemy of Sciences, Prentice-Hall, Inc., 1963.

[37] H. Mitsuyasu, T. Suhaya, S. Mizuno, M. Ohkuso, and T. Honda, "Observations of the directional spectrum of ocean waves using a cloverleaf buoy," *Journal of Physical Oceanography*, no. 5, pp. 750–760, 1975.

[38] D. Hasselmann, M. Dunckel, and J. Ewing, "Directional wave spectra observed during JONSWAP 1973," *Journal of Physical Oceanography*, vol. 10, no. S, pp. 1264–1280, 1980.

[39] D. Cartwright, M. Longuet-Higgins, and N. Smith, "The use of directional spectra in studying the output of a wave recorder on a moving ship," in *Ocean Wave Spectra*, (Englewood Cliffs, N.J.), pp. 203–218, National Acedemy of Sciences, Prentice-Hall, Inc., 1963.

[40] M. Donelan, J. Hamilton, and W. Hui, "Directional spectra of wind-generated waves," *Philosophical Transactions of the Royal Society*, vol. A, no. 315, pp. 381–387, 1985.

[41] J. Allender, T. Audunson, S. Barstow, S. Bjerken, H. Krogstad, P. Steinbakke, L. Vartdal, L. Borgman, and C. Graham, "The WADIC project: a comprehensive field evaluation of directional wave instrumentation," *Journal of Ocean Engineering*, vol. 16, no. 5, pp. 505–536, 1989.

[42] D. Cartwright, "On estimating the mean energy of sea waves from the highest waves in a record," *Proceedings of the Royal Society*, vol. A, no. 247, pp. 22–48, 1958.

[43] L. Draper, "Deriation of a design wave from instrumental records of sea waves," *Proceedings of the Institute of Civil Engineers*, vol. 26, pp. 291–304, 1963.

[44] D. Cartwright and N. Smith, "Buoy techniques for obtaining directional wave spectra," in *Transactions of Buoy Technology Symposium*, (Washington), The Marine Technology Society, March 1964.

[45] K. Steele, C. Teng, and D. Wang, "Wave direction measurements using pitch-roll buoys," *Ocean Engineering*, vol. 19, no. 4, pp. 349–375, 1992.

[46] K. Steele, D. Wang, M. Earle, E. Michelena, and R. Dagnell, "Buoy pitch and roll computed using three angular rate sensors," *Coastal Engineering*, vol. 35, pp. 123–139, 1998.

[47] H. Krogstad, S. Barstow, S. Aasen, and I. Rodriguez, "Some recent developments in wave buoy technology," *Coastal Engineering*, vol. 37, pp. 309–329, 1999.

[48] D. Johnston, "DIWASP, a directional wave spectra toolbox for MATLAB: User Manual," Tech. Rep. WP-1601-DJ(V1.1), Center for Water Research, University of Western Australia, 2002.

[49] I. James, "A note on the theoretical comparison of wave staffs and wave rider buoys in steep gravity waves," *Ocean Engineering*, vol. 13, no. 2, pp. 209–214, 1986.

[50] F. G. Stremler, *Introduction to Communication Systems*. Addison-Wesley series in electrical engineering, Reading, Massachusetts: Addison-Wesley, third ed., 1990.

[51] R. Otnes and L. Enochson, *Digital Time Series Analysis*. John Wiley & Sons, 1972.

[52] P. S. Naidu, *Sensor Array Signal Processing*. Boca Raton, Florida: CRC Press LLC, 2001.

[53] N. Barber, "The directional resolving power of an array of wave detectors," in *Ocean Wave Spectra*, (Englewood Cliffs, N.J.), pp. 137–150, National Acedemy of Sciences, Prentice-Hall, Inc., 1963.

[54] L. Borgman, *Ocean Wave Climate*, vol. 8 of *Marine Science*, ch. Directional wave spectra from wave sensors, pp. 269–300. New York: Pelnum Press, 1st ed., 1979.

[55] J. Zhang and I. Preslin, "Deterministic decomposition of deep water short-crested irregular waves," *Journal of Geophysical Research*, vol. 102, no. C6, pp. 12677–12688, 1997.

[56] http://www.inri.us/pages/2/index.htm.

[57] O. Rioul and M. Vetterli, "Wavelets and signal processing," *IEEE Signal Processing Magazine*, vol. 8, pp. 14–38, October 1991.

[58] N. Huang, Z. Shen, S. Long, M. Wu, H. Shih, Q. Zheng, N. Yen, C. Tung, and H. Liu, "The empirical mode decomposition and the Hilbert spectrum for nonlinear and non-stationary time series analysis," *Proceedings of the Royal Society of London*, vol. A, no. 454, pp. 903–995, 1998.

[59] A. Veltcheva and C. Soares, "Identification of the components of wave spectra by the Hilbert Huang transform method," *Applied Ocean Research*, vol. 26, pp. 1–12, 2004.

[60] B. Widrow and M. Lehr, "30 years of adaptive neural networks: perceptron, madaline and backpropagation," *Proceedings of the IEEE*, vol. 78, pp. 1415–1442, September 1990.

[61] U. Hübner, *Time series prediction, Forecasting the future and understanding the past.* Reading, MA: Addison Wesley, first ed., 1994.

[62] D. Ross, *Power From The Waves.* Oxford University Press, 1995.

[63] J. Falnes and J. Lovseth, "Ocean wave energy," *Energy Policy*, vol. 8, pp. 768–775, 1991.

[64] R. Dettmer, "Wave energy gets seaworthy," *IEE Review*, pp. 14–19, September 2000.

[65] "Wave energy resources and economic assessment for the state of Hawaii." http://www.hawaii.gov/dbert/ert/wave92/wave92.pdf, 1992.

[66] M. Jafar, "Renewable energy in the South Pacific — options and constraints," *Renewable Energy*, vol. 19, pp. 305–309, 2000.

[67] M. Pontes, "The European wave energy resource," in *3rd European Wave Energy Conference*, (Patras, Greece), 1998.

[68] E. Broome, "Renewable energy to boost job creation," *Renewable Energy Journal*, p. 16, June 2001.

[69] T. Thorpe, "An overview of wave energy technologies: status, performance and costs," in *Wave Power: Moving Towards Commercial Viability*, (London), pp. 13–30, IMechE, November 1999.

[70] T. Thorpe, "The wave energy program in the UK and the European Wave Energy Network," in *4th European Wave Energy Conference*, (Denmark), Alaborg University, October 2000.

[71] T. Thorpe and et. al., "Wave energy in Europe: current status and perspectives," *Renewable and Sustainable Energy Reviews*, vol. 6, pp. 405–431, 1999.

[72] P. Davis, M. Cloke, K. Major, D. Page, and R. Taylor, "Wave energy," Tech. Rep. ETSU-R26, Department of Energy, Harwell, 1985.

[73] J. Leishman and G. Scobie, "The development of wave power," Tech. Rep. EAU M25, NEL, East Kilbride, Scotland, 1975.

[74] A. W. Bott, "Power plus proteins from the sea," *Journal of the Royal Society of Arts*, vol. CXXIII, pp. 486–503, 1975.

[75] K. Scott, "Electricity from waves," *Sea Frontiers*, vol. 11, no. 4, pp. 202–207, 1965.

[76] R. Shaw, *Wave Energy: A Design Challenge*. 1982.

[77] "Alternative energy sources, house of lords select committee on the european communities, session 1987–1988, pp 196," 1988.

[78] "Alternative energy sources, house of lords select committee on the european communities, 27th july 1988, pp 178 et seq.," 1988.

[79] T. Thorpe, "A review of wave energy," Tech. Rep. ETSU R-72, Department of Energy, Harwell, 1992.

[80] T. Thorpe, "A brief review of wave energy," Tech. Rep. ETSU R-120, Deparment of Energy, Harwell, May 1999.

[81] M. Mueller and R. Wallace, "Developing a research route map for marine renewable energy technology in the UK," Working Paper UKERC/WP/FSE/2006/02, UK Energy Research Centre, August 2005.

[82] J. Callaghan, "Future Marine Enegry," Tech. Rep. CTC601, The Carbon Trust, London, January 2006.

[83] http://www.epri.com/oceanenergy/default.asp.

[84] F. Gardner, "Learning experience of AWS pilotplant test offshore Portugal," in *6th European Wave and Tidal Energy Conference* (C. Johnstone and A. Grant, eds.), (Glasgow), pp. 149–154, University of Strathclyde, August 2005.

[85] http://www.waveswing.com.

[86] A. Mill, "Archimedes wave swing evaluation of test procedures and results from deployment in Portugal 2004," Tech. Rep. AM//EMEC//0100, European Marine Energy Centre, Stromness, Orkney, December 2004.

[87] M. Prado, F. Neuman, M. Damen, and F. Gardner, "AWS results of pilot plant testing 2004," in *6th European Wave and Tidal Energy Conference* (C. Johnstone and A. Grant, eds.), (Glasgow), pp. 401–408, University of Strathclyde, August 2005.

[88] A. Weinstein, G. Fredrikson, M. Parks, and K. Nielsen, "AquaBuOY - the offshore wave energy converter numerical modeling and optimization," in *OCEANS'04*, vol. 4, pp. 1854–1859, IEEE, 2004.

[89] http://www.aquaenergygroup.com.

[90] Y. Masuda, T. Kuboki, M. Ravindrum, A. Pathak, V. Jayashankar, and X. Liang, "Development of backward bent duct buoy (BBDB)," in *Proceedings of the Ninth International Offshore and Polar Engineering Conference*, vol. 1, pp. 142–149, ISOPE, May 1999.

[91] T. Ogilvie, "First and second-order forces on a cylinder submerged under a free surface," *Journal of Fluid Mechanics*, vol. 16, pp. 451–472, 1963.

[92] http://www.seapowerpacific.com.

[93] http://www.giec.ac.cn/english/index.htm.

[94] F. Lockett, "The CLAM wave energy convertor," in *Proceedings of the Seminar on Wave Energy*, (United Kingdom), pp. 19–25, Institution of Mechanical Engineers, 1991.

[95] M. Institute, "Options for the development of wave energy in Ireland," tech. rep., Sustainable Energy Ireland, 2002.

[96] T. Bjarte-Larsson, J. Falnes, and T. Moan, "Comparison of results from time-domain simulations and model tests of a water-pumping wave-power unit," in *Proceedings of the Sixteenth International Offshore and Polar Engineering Conference*, (Cupertino, CA), pp. 416–422, ISOPE, May 2006.

[97] http://www.energioplysningen.dk/English/WaPo.htm.

[98] http://www.ramboll.dk.

[99] http://www.yale.edu/horizon/prog1.htm.

[100] D. Hicks, C. Pleass, and G. Mitcheson, "DELBUOY: Wave-powered desalination system," in *Oceans' 88 Proceedings*, vol. 3, (Washington, DC), pp. 1049 1055, Marine Technology Society, 1988.

[101] http://www.energetech.com.au.

[102] A. Brito-Melo, T. Hoffmann, A. Saramento, A. Clement, and G. Delhommeau, "Numerical modelling of OWC-shoreline devices including the effects of surrounding coastline and non-flat bottom," *International Journal of Offshore and Polar Engineering*, vol. 11, no. 2, 2001.

[103] http://www.seapower.se.

[104] http://www.seewec.org/index.html.

[105] G. Lemonis, "Development of a shoreline operating wave energy conversion plant," in *6th European Wave and Tidal Energy Conference* (C. Johnstone and A. Grant, eds.), (Glasgow), pp. 267–272, University of Strathclyde, August 2005.

[106] http://www.iitm.ac.in/research/depts/ocean.html.

[107] http://www.ips-ab.com.

[108] L. Claeson, "Recent wave energy research in Sweeden," in *OCEANS'88*, vol. 4, p. 1638, IEEE, 1988.

[109] G. Payne, J. Taylor, P. Parkin, and S. Salter, "Numerical modelling of the sloped IPS buoy wave energy converter," in *Proceedings of the Sixteenth International Offshore and Polar Engineering Conference*, pp. 396–402, ISOPE, May 2006.

[110] http://www.wavegen.com.

[111] http://www.manchesterbobber.com/index.htm.

[112] http://www.wave-power.com.

[113] D. Kraemer, "Simulation of the motions of the McCabe wave pump system," in *6th European Wave and Tidal Energy Conference* (C. Johnstone and A. Grant, eds.), (Glasgow), pp. 251–258, University of Strathclyde, August 2005.

[114] http://www.jamstec.go.jp/jamstec/myt.html.

[115] M. Suzuki, T. Kuboki, C. Arakawa, and S. Nagata, "Numerical analysis on optimal profile of floating device with OWC type wave energy converter," in *Proceedings of the Sixteenth International Offshore and Polar Engineering Conference*, pp. 466–473, ISOPE, May 2006.

[116] http://www.oceanmotion.ws.

[117] http://www.owec.com.

[118] http://www.oceanwavemaster.com.

[119] http://owel.co.uk.

[120] J. Kemp, A. Derrick, J. O'Nians, and D. Upadhyay, "The OWEL wave energy converter as a platform for combined wind and wave power generation," in *6th European Wave and Tidal Energy Conference* (C. Johnstone and A. Grant, eds.), (Glasgow), pp. 231–236, University of Strathclyde, August 2005.

[121] http://www.oceanpowertechnologies.com.

[122] http://www.hawaii.gov/dbedt/ert/wavereport/wave.pdf.

[123] http://www.orecon.com.

[124] A. von Jouanne, "Wave energy developments at Oregon State University," in *Energy Ocean 2006*, (San Diego), Ocean Energy Council, June 2006.

[125] Anon, "New wave energy," *Renewable Energy Journal*, p. 16, November 2001.

[126] C. Mingham, L. Qian, D. Causon, and D. Ingram, "A numerical study of the OWSC wave power device using a two fluid free surface code," in *6th European Wave and Tidal Energy Conference* (C. Johnstone and A. Grant, eds.), (Glasgow), pp. 313–320, University of Strathclyde, August 2005.

[127] http://www.oceanpd.com.

[128] R. Henderson, "Design, simulation and testing of a novel hydraulic power take-off system for the Pelamis wave energy converter," *Journal of Renewable Energy*, vol. 31, pp. 271–283, 2006.

[129] "Wave and marine current technology." http://www.iea-oceans.org, 2002.

[130] http://engineering.lancs.ac.uk/REGROUPS/LUREG/activities/content.asp?ID=28.

[131] A. McCabe, A. Bradshaw, J. Meadowcroft, and G. Aggidis, "Developments in the design of the PS Frog Mk 5 wave energy converter," *Journal of Renewable Energy*, vol. 31, pp. 141–151, 2006.

[132] http://www.mech.ed.ac.uk/research/wavepower.

[133] S. Salter, "Wave power," *Nature*, vol. 249, pp. 720–724, June 1974.

[134] http://www.sara.com/energy/WEC.html.

[135] M. Thomas and K. Welch, "SEADOG: Pump technology wave energy converter," in *Proceedings of the Sixteenth International Offshore and Polar Engineering Conference*, pp. 485–487, ISOPE, May 2006.

[136] A. Clement, A. Babarit, G. Gilloteaux, C. Josset, and G. Duclos, "The SEAREV wave energy converter," in *6th European Wave and Tidal Energy Conference* (C. Johnstone and A. Grant, eds.), (Glasgow), pp. 81–90, University of Strathclyde, August 2005.

[137] J. Kofoed, D. Vincinanza, and E. Osaland, "Estimation of design wave loads on the SSG WEC pilot plant based on 3-D model tests," in *Proceedings of the Sixteenth International Offshore and Polar Engineering Conference*, pp. 452–459, ISOPE, May 2006.

[138] http://www.waveenergy.no/index.htm.

[139] B. Sjostrom, "The past, present and future of the hose pump wave energy convertor," in *European Wave Energy Symposium*, (Edinburgh), 1993.

[140] http://www.wavebob.com.

[141] http://www.wavebob.com.

[142] http://www.windwavesandsun.com/welcome.htm.

[143] http://www.wavedragon.net.

[144] J. Kofoed, P. Frigaard, E. Friis-Madsen, and H. Sørensen, "Prototype testing of the wave energy converter wave dragon," *Journal of Renewable Energy*, vol. 31, pp. 181 189, 2006.

[145] http://www.wavemill.com.

[146] http://www.waveplane.com.

[147] E. Skaarup, "Waveplane in a bigger spectrum and smaller exploitation area," in *6th European Wave and Tidal Energy Conference* (C. Johnstone and A. Grant, eds.), (Glasgow), pp. 475–480, University of Strathclyde, August 2005.

[148] http://www.seavolt.com/product.html.

[149] http://www.aw-energy.com/index.html.

[150] P. Scheijgrond, A. Schaap, and B. Sustronk, "Performance prediction of a combined wells-darius rotor with model tests and a computational vortex model," in *6th European Wave and Tidal Energy Conference* (C. Johnstone and A. Grant, eds.), (Glasgow), pp. 451–454, University of Strathclyde, August 2005.

# Appendix A

# A Brief History of the Wave Industry

This appendix is intended as a primer to set out elementary wave terminology and recount the progress of wave energy in the modern era. Much of the information is covered in greater detail in the rest of this thesis. The main driving force in the area of wave device development during the late 70s and 80s was the public sector. After this time, with the major worldwide economic reforms, development was taken up by private companies, albeit funded with public grants. The later device designs are covered in greater detail in Appendix B. The main information source for this appendix is Ross' "Power from the Waves" [62] and the sources referenced within this work. Additional citations are made to other sources in order to corroborate Ross' views.

## A.1 Introduction

Modern wave energy technology began in the UK in 1973 when Salter began to look for a reliable way to extract energy from ocean waves. Thirty years on and wave energy is on the brink of breaking into the main stream of electrical energy generation, with several test and demonstration installations either built or in the advanced stages of design. The opening of the EMEC test centre in Orkney (for the testing of commercial wave energy conversion devices) has been seen as a major milestone in the realisation of a marine energy industry. The resurrection of wave energy during the 1990s shows a return to the extraction of energy directly from water. This, in reality, is an old concept. Energy has been obtained for many centuries in the form of water wheels.

## A.2 Basic wave properties

Waves are, in actuality, a very concentrated form of solar energy. Heat from the sun warms the earth at different rates causing air to flow from area to area depending on temperature differentials. The winds interact with the uppermost layers of the oceans. As the wind blows tangentially to the oceans surface it causes the particles to rotate in a circular motion (see Chapter 3). Over a large area this rotation penetrates deeper into the the surface creating larger waves. The process can be seen on a windy day if you look along a stretch of water with the wind blowing towards you, the waves farthest away from you will have a small amplitude whereas the waves nearer to you will have a greater amplitude.

In a technical description, it is possible to say that the wind is an integral of solar energy, and in turn, wave energy is an integral of the wind.

### A.2.1 Terminology

The following sections give the basic qualitative parameters used in describing devices and their behaviour. More information on these properties are given in Chapter 2.

#### Height and power

The most basic information about a wave is the wave height, this being the vertical distance from the trough to the crest. The distance between successive crests is the wavelength and the time it takes between the crests is the wave period (this is roughly 8 seconds for the Scottish west coast). The term Significant Wave Height is used to describe the one-third highest waves; this is usually the measure sailors give when describing the height of waves. The fetch is used to describe the uninterrupted distance over which the wind, that is creating the waves, has blown. For most cases the longer the fetch the larger the waves will be. The power in a wave is roughly proportional to the square of the height, therefore larger waves give more power. The power is defined in terms of Watts per meter of wave front.

#### Pressure

Some devices work on the principle of pressure changes as a wave passes over them. If a device is resting on the sea bed and the sea is calm then a constant pressure will be experienced related to the depth of water in which the device is sitting. As a wave passes over the device, during the trough of the wave the pressure will decrease, and as the crest passes over the pressure will increase.

#### Primary motion

There are four motions that an object will make when moving freely in the ocean:

**Pitching** describes a rocking back and forth movement.

**Rolling** is the same rocking motion as pitching but from side to side

**Heaving** is the up and down bobbing motion that an object will make.

**Surging** is used to describe the lateral movement parallel to the ocean surface.

### A.2.2 Potential resources

The resources available around the globe, and in particular to the UK, are impressive in scale. Falnes [63] made an estimate of worldwide resources of 1 TW of onshore energy and 10 TW of offshore potential. Many possible sites exist in the world with the main criterion being that they have a shoreline facing a prevailing wind that has been blowing over a considerable stretch of ocean. Much of the western coast of Europe, South Africa, Australia, New Zealand, the USA and Chile all have high potential resources in excess of 40 kW/m [64]. However many other countries without resources of this magnitude have also been developing wave programs; the Norwegians, Japanese and Indians, in particular, are at the forefront of research. Interest is also high in Pacific Island communities where diesel fuel generators are the main energy source; in some areas, imports of fuel oil are running at 500 % of the islands total exports [65] [66].

#### European resource

Recent studies claim [67] to show that the Atlantic resources are in the region of 290 GW. This is the area from the Iberian peninsula to the northernmost reaches of Norway. The power in these areas range from 25 kW/m in the Canary Islands to a maximum of 75 kW/m off the Irish and Scottish coasts before decreasing to 30 kW/m when reaching the Arctic circle in Norwegian waters. Also included in this figure are the resources available in the North Sea which range from 21 kW/m in the best sites to 11.5 kW/m in more sheltered areas. Although a smaller resource, the Mediterranean sea could add another 30 GW of potential to this figure taking total European resources to 320 GW. This potential for generation will prove useful in the future since Europe's electrical needs are predicted to reach 13,000 TWh by 2020 [68].

### UK resource

This resource is potentially vast but it is spread over the entire coastline. Many areas will be unreachable and so realistic resources are smaller. The UK share of the EU resource is roughly 50 TWh per annum [69] but, after considerations of efficiency and transmission loses have been taken into consideration, Scotland's potential landable resource could be 14 GW [64]. This would be sufficient to supply Scotland at present demand, but more importantly there would an excess to supply some of the 80 GW used in the UK as a whole.

### Cost of recovery

In a recent estimate, the worldwide potential for recoverable energy was some 2000 TWh per annum, this would be equivalent to the current world installed capacity for hydro generation [70] and would represent 10% of world consumption at this time. The cost of building this infrastructure would be around £500 billion. The technology at this present moment is capable of delivering this energy at a cost of 5 p/kWh which is twice the European average, but, as has been discussed in many papers and reports, this figure is based on a developing technology and is estimated to be falling with every new generation of device.

### Energy density

In comparison with other alternative renewable energy resources wave energy has many factors in its favour. In terms of density, the energy of the ocean is roughly contained in the upper 10–20 m, whereas for wind it is dispersed over many kilometres, with the best resources located higher above the ground than a structure could physically survive. The average density for wind energy is rated as 1 kW/m$^2$; for the area off the western coast of the Hebrides the average wave power averages between 40 kW/m and 60 kW/m. Solar energy does not have a high energy density in northerly latitudes with an average value of 0.1 kW/m$^2$.

## A.3 The case for wave energy

Questions have been asked as to why we should undertake the technical challenge of recovering electricity from the oceans and indeed why this resource should form part of Scotland's future energy mix. As suggested by Ross [62] it is a case of using the most appropriate technology for a given situation.

### A.3.1 Alternate technologies

Large-scale use of solar and geothermal energy is not foreseeable in the United Kingdom. Geothermal energy was investigated as a possibility during the 1980s but was discontinued by 1992. The United Kingdom is not in a particularly active geological region, unlike Iceland or New Zealand. Solar energy can be utilized in the UK but it is mainly reserved for heating purposes. An additional issue with solar, is that the power density is rather low and the footprint of a viable solar station (say 2 GW) is, at the present time, of the order of 50 square miles. Solar is an option in more southerly latitudes and Mediterranean countries make use of it for heating or cooling of their homes.

Wind energy has, for the past ten years, been seen as the renewable energy source to meet the UK Renewable Obligation. The perennial problem with a wind farm is the visual intrusion and consequent legal difficulties in securing planning permissions. The UK has a population of approximately 56 million and finding agreeable locations for wind farms on land is becoming more contentious. Planners and authorities argue that if less than a certain number of people can see the farms then they should be built. Wind turbines have recently gone offshore; the resource is higher and technology has allowed it to be exploited. However, sites are again limited and tourist organisations and environmental campaigners will find reasons to block their progress. In addition, maintenance issues related to turbine access also exist.

### A.3.2 Environmental impact

On the surface, wave energy will cause the least environmental impact. Devices will be rarely seen from the shore, although the effects of energy extraction on coastal erosion and site selection on sea ecology cannot be ruled out. A brief examination of the environmental impacts was made in [69], it concluded that the environmental impacts were of lesser concern than with other renewable sources. The Scottish Executive is presently undertaking a large-scale Strategic Environmental Assessment of Scottish waters.

### A.3.3 Additional benefits

Some benefits of wave power schemes may be possible for the fishing industry, where the calm waters behind devices can be used for fish farming. Some of the largest devices researched in the past (which utilise an overtopping reservoir) have highlighted that the fish farms could be located within the device reservoirs themselves, where there is a constant flow of fluid

aerating the water. Other benefits may include a relatively cheap source of power for the production of hydrogen, an early description on the deployment of Salter's Ducks spoke of them being pushed back from their original mooring by the waves and storing this energy as hydrogen. The Ducks would then use this stored power to sail back to their starting point depositing the unused hydrogen on the shore.

## A.4 Basic device design

The wind energy industry has settled on a basic design of three-bladed horizontal-axis turbines. The wave industry however is still exploring the best possible design and at a recent count there were over 1000 patented ideas for wave energy conversion worldwide. The perfect wave device design may not exist and several technologies will evolve to fill roles according to differing wave climates and situations. The existing device designs can be broken down into five basic technology groups (Thorpe [71]):

- Oscillating Water Column (OWC)
- Overtopping Device
- Point Absorbers (floating or mounted on the sea bed)
- Surging Devices
- Mechanical Extraction

### A.4.1 The oscillating water column

One of the most studied devices is the Oscillating Water Column (OWC). This was described by Thorpe [69], as:

> "...a partially submerged, hollow structure, which is open to the sea below the water line. This structure encloses a column of air on top of a column of water. As waves impinge upon the device they cause the water column to rise and fall, which alternately compresses and depressurises the air column. If this trapped air is allowed to flow to and from the atmosphere via a turbine, energy can be extracted from the system and used to generate electricity. Because of the oscillation in air flow, OWCs normally use Wells turbines to power the electricity

generators. These turbines have the property of turning in the same direction regardless of which way the air is flowing."

There are a great many of these devices around the world: Scotland, Portugal, Japan, India and Australia. They are relatively simple to construct on land and as such whenever a government wants to begin wave power development their first step is usually to commission the construction of an OWC type device.

### A.4.2 The overtopping device

The first plant to develop electricity on a grid connection was a device of this type and it owes much of it's design to the hydro electric industry. In order to create electricity a reservoir is situated a certain height above the turbine. This height is called the head. The higher the head the more potential energy the water will have and will be able to turn the turbine faster. The concept of a raised reservoir is used in several device designs: Tapchan, Wave Dragon and the Floating Wave Power Vessel. Essentially the water in the waves are forced into this reservoir by a variety of techniques where it will then drain through a small outlet to turn a Kaplan turbine.

### A.4.3 The point absorber

The classical example of point absorber is a buoy. The definition is made as a device being smaller in dimension than the wavelength of the waves it wishes to capture. The majority of these devices are based on systems involving a buoy or a float that moves in a heave motion. This motion is used in reference to a fixed point, commonly the mooring point, on the seabed or to an inertial mass of water. This motion can be used to pump sea water or oil to drive a turbine or to directly engage with the power take-off.

### A.4.4 Surging devices

These are wave energy conversion devices that utilise the horizontal forces of the waves. Generally the surging motion of a device is twice that of the heaving motion. There are not many devices that attempt to capture this motion but some, in particular those of French, make use of this higher power level.

### A.4.5 Mechanical devices

This is a category that Thorpe did not list, but it is included in this Appendix as a catch-all situation for the various mechanical devices that cannot be comfortably placed into one of the above categories. In particular Salter's Duck, Cockerell's Raft and the Pelamis are three of the members of this category

## A.5 Problem areas

Wave Energy has many issues and problems. The following are a selection of the generic issues that are in need of attention.

### A.5.1 Cabling

A major problem is the cabling required to transport the energy to shore and in turn how to transmit this energy to the customers. The cables have to be long and able to withstand the forces at their termination points at the device farms. Ordinarily, in laying sub sea cabling, a location is chosen were extreme forces on the cable will be at a minimum. For the wave energy industry it is exactly these extreme locations where the cables are needed.

### A.5.2 Scaling

An issue faced by designers is scaling up models from tank testing at $\frac{1}{4}$, $\frac{1}{10}$, $\frac{1}{25}$ scale models to full size. In many cases a doubling of scale can mean a squaring of forces and with them new problems to solve. A further issue is that in wave energy you do not design to reach maximum energy conversion. A device that reaches 100 % conversion at a definite wave period and height will invariable have bad capture conversion at other levels. What is required is a design that will cover the largest catchment area, where the most power is available for the most time in the year. Hence allowing the device to generate for the majority of its life time.

### A.5.3 Grid strength

In deploying wave energy devices, the locations where the best resources are available are in some of the remotest locations. In these areas the grid infrastructure is very weak; principally consisting of distribution rather than transmission lines. Significant reinforcement would be

required if a large wave farm were to be constructed. Previous plans for a farm off the coast of South Uist [72] showed collection points along the length of the islands then a major undersea cable to run from Benbecula to Skye. The cables were then to run down to Craigroyston or Blairgowrie. The recent announcement of the Scottish and Southern Energy's planned upgrade to the A9 transmission lines have met with much opposition. As has a proposed wind farm on Lewis that would require an upgrading of its connection to the main national grid. If these two projects were to proceed the grid infrastructure to the Western Isles would be opened up and the likelihood of a large scale wave farm in the best location may be possible.

### A.5.4 Operations and maintenance

As with all power stations, the issue of availability has been raised. This is the time that the devices are available to generate electricity. If a device requires maintenance then it is unavailable to generate and hence costs money. Quite a few device teams in the past tried to design with modularity in mind, so that if one device module breaks down the rest of the device farm will be able to keep operating. When this issue was raised, distributed generation, such as that used in wind farms with multiple generator sets, was not the norm, so investors were fearful of breakages. At this time, with the generation onto distribution networks more widely accepted, this issue may not be so important. The maintenance associated with offshore structures will also be complex since teams will have to be based onshore and be ready to fly or sail out whenever a weather window occurs. This being said device developers are making their devices more suitable for ROV (Remotely Operated Vehicle) maintenance, which requires less stringent weather windows for operation.

### A.5.5 Design for survivability

Perhaps the single greatest problem faced by the designers of Wave Energy Converters (WEC) is how to balance capture efficiency, cost of construction and the survivability of the design. Many designs that look promising on paper and have high capture efficiency would, if constructed, be destroyed by the largest of the storm waves. Although the west coast has an average of 60–80 kW/m of wave front, under servere storm conditions this can rise to upwards of 10,000 kW/m. The parameter used by designers of offshore structures in the oil industry is to use what is termed as the 100 year design wave i.e. the largest expected wave in a 100 year period. For the west coast of Scotland this is thought to be a wave of the

order of 30–40 m (the size of a 5 storey building).

### A.5.6 Environmental concerns

In addition to these potential problems certain environmental concerns would have to be addressed before any large-scale development could take place. In the era of the large schemes (during the seventies and eighties) it was proposed that massive farms stretching many hundreds of kilometres would be built. With many of these devices sitting parallel to the wavefronts they would have extracted a damaging amount of energy. Damaging from the point of view that the power arriving at the shore would be reduced. The effects of this reduction would not be good. Reduced erosion would decrease the minerals and silt in the water and change the local ecosystem killing off some species. The problem is less relevant today because devices are becoming more oriented towards point absorbers or long thin devices such as the Pelamis. In these cases the devices will be separated in arrays and there will be no brick-wall-type effects.

Fishing and navigation are also issues of concern. Areas of most active waves are also the best fishing grounds as nutrients are brought to the surface by the wave action. Fishermen would be affected if required to refrain from fishing these areas. Navigation will also prove a problem, with exclusion areas needing to be set up around device farms.

## A.6 Early designs/patents

The following section is largely historical charting the progress of the early device designs up to the UK's wave energy programme of the 1970s. Further device designs are given in Appendix B, including those of the post 1974 period.

### A.6.1 Pre 1945 designs

The first recorded description of a wave powered device dates from a patent filed by a father and son team named Girard in Paris on the $12^{th}$ of July 1799. The device consisted of a lever attached at one end to a boat, floating in the sea, and at the other end to a pump sitting on the shore. The motion of the ship would cause the lever to work the pump. This was one of the first mechanical devices of the many to follow.

Some 340–350 patents had been filed by 1975 in the United Kingdom [73]. Many designs were wild and wonderful but all are based on the reality that the waves are ceaseless in their

activity. The bulk of these patents were filed prior to the First World War, the first British patent being filled in 1855.

One of the most successful of these early designs was an Oscillating Water Column device built by Mr. Bochaux-Praceique in 1910. The device was built into a cliff face at Royan, near to Bordeaux, and supplied his house with 1 kW of energy. A floating buoy device followed in 1911 built on Young's "Million Dollar" pier in Atlantic City, New Jersey. The company, the United States Wave Power Company, that constructed the device claimed a power output of 110 kW. The mechanism, built of levers and ratchet wheels, extracted power from the sideways, "slantways" and vertical motion of the sea.

The 1930s produced two interesting devices that were constructed. The first being the Savonius Rotor. Originally designed to operate as a wind turbine the rotor looked like a hollow cylinder sliced vertically then either end attached to a strut. It was able to turn in the same direction irrespective of the air flow. Trials in the Baltic sea found that the rotor worked well as a wave turbine down to depths four or five times the wave height. Documents have been found that show a Savonius rotor was installed at the Muse Oceanographique in Monaco to drive a pumping system to fill its aquariums. A floating device also found a home at the same museum which lasted for ten years until it was destroyed by a storm.

### A.6.2 Masuda

The next step forward came through the efforts of Commander Yoshio Masuda, a former Japanese naval commander, who designed the first wave power navigation buoy for use in the sea of Japan during the years preceding the end of the Second World War. The ingenious step in his design was to change a shifting, slow moving, force into something more controllable. This was achieved by transferring the energy of the waves into a column of air. The principle is best illustrating by thinking of an upturned can floating in the sea. As the waves move around the can the water level inside the can moves at the same time. If you put a hole in the top of the can the air inside will be alternately forced out then sucked back in. By the use of valves this stream can be rectified so that it is continuously moving in one direction and used to turn a turbine. This was in 1947 and was the first modern example of an Oscillating Water Column.

These early buoys generated 30 W in the relatively calm seas around Japan and were sufficient to power a navigational lamp. The OWC concept also became the power supply for a lighthouse in Tokyo Bay. Masuda was additionally responsible for several other designs

which were tested but unfortunately did not survive. One of these devices consisted of three rafts tied together and resembled early versions of a Cockerrel Raft or McCabe Wave Pump.

### A.6.3 Mauritius 1953–1966

A.N. Bott arrived in Mauritius in 1953 in order to set up the electricity board and as part of his work he came across the idea of utilising the wave energy arriving on the island's shores. The island of Mauritius is fringed by a broken ring of very tough coral. Bott proposed to use the coral as a base and build a basin into which waves would over-top, keeping it filled up. The water would then run out of the basin through low head turbines and generate electricity. The problem was, to what height should the wall be built. Too high, and there would be times when the waves were not big enough to keep the basin filled; too small, and there would not be enough of a head to run the turbines. The solution was to use a low wall to keep the basin constantly topped up and to use the energy of the incoming waves to pump the water from the lower reservoir up to a higher one. A higher reservoir gave a greater head and reduced the turbine costs. Unfortunately the scheme was never built as oil prices fell during the sixties and funding was withdrawn in 1966. The experience was however delivered in a paper to the Royal Society of Arts in March 1975 [74].

### A.6.4 American buoy 1960s

A few devices were put forward and tested during the sixties. One of these came from an American company, Avco Corporation [75], and predated some of the devices to follow during the late seventies. The device worked by exploiting the pressure difference which occurs when a wave passes over a certain fixed point. As the wave passed the submerged device the depth of water over it caused a pressure difference between the outside water and air stored in the device. This pressure was used to run a hydraulic motor. Initial tests conducted in Buzzard's Bay, Massachusetts, resulted in 0.25 W being produced. A level just about powerful to run a navigational buoy. The company was hopeful for further offshore testing but it was unlikely to have been carried any further forward as the initial test buoy was badly weathered in a storm.

## A.7 UK government involvement

UK Government interest in wave energy began in 1974, with a letter to Prof. Stephen Salter of the University of Edinburgh concerning his device, known universally as the Duck.

### A.7.1 1970s oil crisis

The war in 1973 between the Arabs and the Israelis had led to much tension between OPEC, the group of oil producing countries, and western governments. This tension led to the oil supply being reduced to countries that had supplied Israel with weapons. This tightening of oil exports led to a great leap in oil prices during the 1970s. In 1970 one barrel of crude oil cost \$1.80, by June of 1973 it had reached \$2.90, Dec 1973 \$11.65 and reached as high as \$45 by 1979. This conflict is reflected in the current high oil price (2006) due to the ongoing confict in Iraq, and consequently interest in wave energy is again at a peak.

In 1973 North Sea oil was only beginning to come on-line and the reserves of the Alaskan oil fields were, as yet, untapped. As with any industrialised country the UK ran on oil, burning many thousands of barrels a day. The energy usage can be broken down into 25 % for transport, 25 % for industrial use, 20 % for residential and commercial heating and 20 % for conversion into electrical energy [76]. With the search to supply an ever growing GNP, the looming energy gap was a problem for governments worldwide. Since oil supplies were limited then coal was the only viable substitute, but in taking this approach, coal miners were handed much pollical strength. In 1974 they brought down the Heath government. Hence alternative energy sources were sought and the UK put much funding into the development of nuclear power. Renewables were considered as a secondary option and the limited funding given to this area reflected that opinion.

### A.7.2 Initial investment

In 1976, with the announcement of £1 million [62] to fund research into wave energy, made by the Chief Scientist Dr Walter Marshall, government interest in the development of wave energy was officially confirmed. Setting an ambitious goal of a 2 GW power station, to be situated off of the Hebrides, design teams across the country were set to work.

The search for a wave power design began by falling back on research carried out into investigating the wave regime of the UK waters; a task compiled after the second world war by Draper. An important technique that grew from this era, courtesy of Darbyshire,

was that of hindcasting; the ability to predict the wave regime based on knowledge of wind speeds and the distance over which they have blown. Initial investigations of wave power involved sitting a Waverider buoy at Benbecula in the Hebrides to record data.

Several device groups working at that time were ready to test models but the funding available was not sufficient for viable experiments. Nuclear stations were being built and North Sea gas and oil were flowing from the ocean floor into homes.

Funding increased in the second year of the programme to £2.5 million, but the following year saw only a small increase to £2.9 million for 1978. The minister for energy at that time, Tony Benn, observed that

> "... the limitation to making progress is not the level of funding but the state of the technologies involved."

### A.7.3 The first devices

The first gathering of wave power professionals involved in the "Big Projects" phase was in November 1978 at Heathrow, London. At this conference the existing designs: the Duck, the Raft, the OWC and the HRS Rectifier, were discussed, progress was updated and some of scale testing was reviewed. The second generation of devices were introduced, these being: the Airbag, the Belfast Buoy, Vickers' OWC and the Bristol Cylinder.

### A.7.4 Economic realisation

The event that would eventually halt the UK wave energy programme and constrain development for the next decade was also announced at the Heathrow conference. The government had set the consultancy firm of Rendel, Palmer and Tritton (RPT) the task of evaluating the present state of the wave energy development programme and were to present their results at the conference. The bulk of their report contained information that was well received and acknowledged as problems that were in need of attention: feasibility of projects, efficiency of components, transmission of the output. The sticking point was the price of electricity generated by the devices under review. The electricity from the devices ranged from 2 to 30 times the cost of domestic electricity at the time of the report (1978).

This issue was enough to dampen investors interest. RPT had diligently completed their report and evaluated the devices using the methods recommended by the treasury for public financed schemes. Unfortunately the methods were not sympathetic to capital-intensive projects, where all the funding is required before a return on capital is achieved.

The wave power projects would have been similar to the hydro schemes of the 1920s and 1950s which had large capital expenditure to begin with but are now reduced to operations and maintenance costs.

### A.7.5 Winding down the programme

Despite promising designs and enthusiastic developers the economic realisation of the RPT report was key in the closure of the wave energy programme. The programme was wound up in a series of government reports siting the uneconomical costs of capital intensive projects. Up to that point in 1982 some £15 million had been invested in the programme, spending on the nuclear industry ran to orders of magnitude much greater than this.

The UK Wave Development Programme was closed in 1982 after a meeting of ACORD (the Advisory Council on Research and Development). The issues encountered with the UK programme led the International Energy Authority and the European Community to hold back on wave energy as it was following the UK lead. The results of the UK Wave Programme were published in 1985, and were to be the end of wave development in the UK [72].

### A.7.6 A lost decade

The following ten years were relatively quiet after the big push that the UK programme had given to research and device development. Investigation into the RPT report found some problems in the figures used in costing various devices schemes.

Some funding was made available in 1987 for the initial OWC project on Islay. This came after the Norwegians had built and operated two working plants in November 1985. The cost of the Norwegian plants were less than the consultancy work carried out by RPT [77] (approximately £1.1 million for two plants). The House of Lords published an inquiry in July 1988 [78] indicating that it was concerned over the ending of the wave programme. The government response was to conduct a study of wave energy that lasted over three years. The report published in 1992 [79] was supposed to end speculation over wave power.

As the European Commission announced funding for wave energy projects during December 1993 the UK government was in a compromised position. The OSPREY project was not receiving support from the then energy minister or from ETSU. In contrast to this position, ETSU's parent body (the AEA - Atomic Energy Authority) was providing data to the OSPREY team on the siting of the device. Additionally the Highlands and Islands En-

terprise, a government body, were providing assistance. A further confusing announcement was made on the 31$^{st}$ March 1994 when the funding for the Islay OWC project was ended.

### A.7.7 Growing support

By the mid-90s the feeling inside Westminster towards renewable energy was beginning to change. The views of the world population were eventually being educated as to the consequences of the use of fossil fuel resources and political pressure on world governments was moving them into reconsidering renewable fuels. After several reports, in particular Thorpe's 1999 review [80], and commissions had convened, wholeheartedly recommending the recommencement of funding for wave energy, the government announced that the wave program was to be reinvigorated as part of a £43 million packaged for renewable development over three years. These commissions consisted of the UK Marine Technology Foresight Panel, a Scottish commission to promote wave energy and a Royal commission on Environmental Pollution.

In the Scottish Renewables order of that year (1999) three successfully bidding projects were chosen for development: the FWPV from Sea Power International, the Limpet 500 from Wavegen and the Pelamis from Ocean Power Delivery (OPD). All of these devices were to be developed by private companies with the DTI allocating funding depending on success in generating market funding and technical progression. In addition to funding for the Wavegen and OPD devices, the DTI were to finance the development of a sloped IPS Buoy from The University of Edinburgh, a study of linear generators and hydraulic systems from The University of Durham and commission a report on the industry from Ove Arup.

### A.7.8 Post 2000 development

The Ove Arup report of 2000 set out the issues that could help drive the marine industry forward and these have been the focus of recent government funding. A major issue is in the co-ordination of research so that effort is not duplicated and major project ending problems are found quickly and tackled. Reports produced since 2000 have also highlighted that offshore oil and gas technology could be transferred to marine energy. Within academia the £2.6 million Supergen programme was established in October 2003 by the Engineering and Physical Sciences Research Council to co-ordinate university level research and provide funding for device testing. A further body, the UK Energy Research Centre Marine Energy Research Network, is also being established to coordinate industry requirements and

academic research [81].

### DTI

The DTI through the later years of 1990s had, on a small scale, been funding some marine projects. This funding has increased over the past five years to the point where several full-scale wave devices have been built and tested. Funds were made available for the construction of a full-scale testing facility in Orkney where near production ready devices can be tested in open water conditions. The New and Renewable Energy Centre (NaREC) has also been fitted with a $10^{th}$ scale dry dock and plans are underway for a test site for small device farms in Cornwall at the WAVEHUB project. They have also announced a fund of £50 million for technology developers.

### The Carbon Trust

The Carbon Trust Marine Energy Challenge (MEC) was run through the period 2002 2005 to identify and assist in the development of promising wave and tidal energy devices. The work of the MEC was to identify areas of device design, where cost reductions could be made through collaborative investment with consultancy firms. The device developers in question are all small to medium enterprises and as such do not have the necessary resources to tackle development issues on a rapid scale. An additional facet to the MEC's remit was to identify the potential cost of future marine energy [82]. The MEC has also resulted in several publications of use to developers and investors in guiding their decisions.

## A.8 European Union involvement

The European commission has been monitoring wave energy development since 1985 when it commissioned a report to be prepared by Lewis of University College Cork [62]. Five years later members of the parliament raised the issue of wave energy and the Lewis report was unfortunately misrepresented. Upon acknowledging this error the EU released €1.2 million for demonstration projects and announced a seminar to be held in Brussels on 25-26 April 1991. The seminar was held but no agreement was reached as to which designs to take forward. The EU member countries were most enthusiastic about plans for an OWC device since they had had the most development time behind them.

Several further conferences were unable to reach agreement over the way forward for the device development. A further €2 million from the Joule 2 programme was added to

the budget in 1992. At the first European Wave Energy Conference (EWEC), held at the National Engineering Laboratory in East Kilbride during October 1993, the EU funding plans were given: a near-shore station (the OSPREY) rated at 2MW was to be moored off Dounreay, a new gully OWC was to be built on Islay, and a proposed 500kW device was to be built on the island of Pico. These planned devices were to be part of the Fourth Framework programme.

The series of EU sponsored conferences has continued with meetings taking place in: Lisbon in 1995; Patras (Greece) in 1998; Aalborg (Denmark) in 2000, Cork (Ireland) in 2003 and Glasgow in 2005. Between 1995 and 1998 a computerised European Wave Energy Atlas was developed but this now seems to be the commercial property of Norwave.

The EU, as part of the Joule 5 programme in 1999, set up a WAVENET thematic network. The network was a collation of information on wave energy and was responsible for a concise and detailed report published during 2003 [1]. The report covered several areas deemed to be relevant to wave energy developers: cooperation with the power industry; social, planning and environmental impact; financing and economic issues; R&D on wave energy devices; generic technologies and promotion of wave energy. The Thematic network has also been responsible for various publications and the establishment of the annual All Energy conferences held in Aberdeen.

Funding for European wave energy projects has continued to be provided for by the sixth framework programme due for review in 2006. Further details on specific funding can be found in Appendix B, where the device designs are described.

Individual countries have also provided funding for device development. The Scandinavian countries in particular have invested large sums of money and time. Projects of note are the Norwegian program in the 1980s, where two full scale devices were constructed, and the Danish wave energy programme of the late 1990s, where many different scale device designs were tested.

## A.9 Rest of the World

The potential to extract energy from the ocean has been acknowledged in other countries around the world. Some have developed extensive wave energy programmes (e.g., Japan) while others have relied more on privately funded companies (e.g., the USA). The following is a brief review on progress.

### A.9.1 Oceania

In Australia and New Zealand progress on wave energy has not, so far, been given much importance as they have both enjoyed good oil and gas supplies. As these have ran out both countries are starting to put investment into marine renewables. New Zealand has begun a small research programme at IRL in Christchurch, working in collaboration with NIWA in Wellington. The Australians have two possible devices in the water at present and are looking to capitalise on the extensive resources of their Southern coast.

The islands of the Pacific are also taking an interest in their own wave resources as electricity supply is a major expense for their populations. Various projects have been reported over the past 10 years but few have progressed.

### A.9.2 Asia

Research in Asia began with Masuda's navigational buoys in the years proceeding the second world war and has continued ever since. There are few commercial devices or developers, with research limited to academic projects. The OWC technology is favoured by almost all countries with test devices (i.e., Japan, China, Sri Lanka and India). Thorpe [71] also reported a device being developed in Korea but no further information could be found.

### A.9.3 North America

#### Canada

Canada has shown some interest in wave energy, but possessing extensive hydro and oil resources, funding for development has not been forthcoming. Studies in the mid 1990s showed that the British Columbia coast of Canada has good wave potential and various developers discussed the possibilities of supplying device farms. Interest in these schemes appears to have dwindled but the Canadian National Laboratories continues device testing for private companies.

#### USA

The USA has not to date had heavy involvement, in marine energy investment relying more on private investors and companies. In 2004 this approach changed when the EPRI announced a $4 millon project to investigate the feasibility of wave and tidal energy projects [83]. Nineteen developers were asked to provide device information for consultation. From this

process, several proposals for wave energy test sites in six states were put forward: Maine, Massachusetts, California, Washington, Oregon and Hawaii. Each state/site has been matched to a specific device that will be best suited to the site conditions.

Several of these site/device matches have been in development for several years. The biggest obstacle being faced in the USA is the number of governmental agencies having an interest in the seabed. From the multiple layers of state and federal agencies the cost to a planned farm in Washington is some 25 % of total budget.

# Appendix B

# Device Designs

Over the past thirty years many different device designs have been put forward. Whilst only a few have reached the stage of full scale implementation, their genesis has relied on the ideas of past designs. This appendix is intended as a reference for designs, their history and present state of development. The information in this appendix and the web sites linked to are correct as of the summer of 2006. There do exist many more designs than are documented here. The majority of devices financed under the Danish Wave Energy Programme have been neglected to allow for those that have survived.

## B.1 A

### B.1.1 Archimedes Wave Swing (1993–present)

The Archimedes Wave Swing was developed to the prototype stage by a consortium of research teams under Teamwork Technology BV, Netherlands and is now being commercialised by a Scottish-based company, AWS Ocean Energy Ltd. The device has changed from the original but it has essentially remained a sub-surface point absorber [84]. The current design consists of an air filled chamber (the "floater") which can move vertically with respect to the cylindrical "basement", which is anchored to the sea bed. The "floater" is neutrally buoyant so will remain at rest unless a wave passes over the device. The wave causes a change in pressure and the floater to move. The relative movement is used to power a linear generator take-off system. In extreme wave conditions, a water braking system is used to damp the motion of the device and prevent structural damage. All the service and maintenance operations can be carried out by an ROV [85].

While early development of the device proceeded without major difficulty, the submer-

gence of a 2 MW prototype, funded partly by the EU, took many years. The first attempts were made in 2001 before the parent company entered financial difficulties. The deployment was stalled until May 2004 but the delays proved costly and many of the control and measurement electronics had been damaged, as had the water braking system [86]. Some measurement equipment was retro-fitted and the test results published [87]. The device was grid connected for 15 minutes.

The rights to the device were transferred in 2004 and work on a commercial prototype is now underway. A full scale test model is due to be built in 2007 for test deployment in early 2008.

### B.1.2 AquaBuOY (Late 90s–present)

This device grew from the amalgamation of the original IPS buoy and the Swedish Hose Pump design [88]. It consists of a slack-moored buoy, an acceleration tube and a hydraulic power take-off housed within the buoy. The motion of the buoy moves the piston in the acceleration tube which in turn expands or contracts a hose pump causing pressurised sea water to turn a Pelton wheel inside the buoy. AquaEnergy Group Ltd, the owner of the technology, is currently in the process of site measurement and completion of permits in order to install a 1 MW pilot farm at Makah Bay, Washington state, USA, [89] by the end of 2006.

Funding for this device is predominately now coming from private investors (Finavera in particular). Additional funding for research has come from the Carbon Trust and the Danish government through academic research.

## B.2 B

### B.2.1 Backward Bent Duct Buoy (late 80s-present)

The basic design for this device is a modification to a floating OWC [90]. The air duct in which the turbine is situated is bent away from the incoming wave field increasing the output capacity. The new design was tested at University College, Cork. Deployment took place in Japan and China during the 90s. Some development would appear to be focused in India at the National Institute of Technology and with additional research occurring in Ireland, Japan, the USA and the UK. The funding for this device has been mixed coming, from various governmental and private organisations.

An Ocean Energy Buoy based on this design has recently been built in Ireland as fourth scale model by Ocean Energy Ltd. The company appears to be aiming for a scale model test at the Galway test centre.

### B.2.2 Belfast Buoy (late 70s-1982)

Developed at Queen's University Belfast by Long this was one of the first OWC type devices to make use the Wells Turbine. It was originally a floating design but this was later changed in favour of a sea-bed-mounted device. It was to be situated in a near-shore environment and had dimensions of 51 m in height and roughly 30 m in diameter [72]. Funding ended in 1982.

### B.2.3 The Bristol Cylinder (late 70s-1982)

This device was based on a theoretical research paper produced in 1963 by Ogilvie [91]. He had conducted experiments by suspending a cylinder shaped object below a wave and observing it's movements. As the wave passed over the device it's motion replicated the circular motion that the wave particles themselves made. Evans of The University of Bristol used this research to create his design.

The Bristol Cylinder design consisted of a 100 m by 16 m cylinder floating on its side 3 m below the surface and held to the sea bed by moorings. At the base of the moorings were hydraulic pumps. As the cylinder moved it pulled on the moorings activating the pumps. These pumps were then used to drive sea water to a Pelton wheel turbo-generator mounted on a platform above sea level. The cost of a 2000 MW station as per the UK government programme would have been £5100 million [72], but the maintenance of undersea equipment would have been prohibitively expensive. Some research continues at The University of Bristol and the device receives attention in some masters theses when used as a breakwater.

## B.3 C

### B.3.1 CETO, Seapower Pacific (2003–present)

Owned by Renewable Energy Holdings plc, the CETO is essentially a large pump that uses the force of the waves to pump seawater to shore. It is situated on the sea bed, and as a wave passes over a large disc it alternately compresses and moves the arm to which the

disc is attached. This in turn drives two pumps transporting pressurised sea water to shore. The detailed development of the design began in 2003 with construction beginning in the December of that year. Following a 12 month construction and 3 month dry testing period the device was launched on 22nd March 2005. At the present time the on-shore electrical equipment is being installed and the provision of reverse osmosis is being investigated [92].

### B.3.2 Chinese OWC

In the South China Sea a small device was constructed in 1991 [93] with another device situated in the Guangdong Province rated at 100 kW.

### B.3.3 Cockerell's Raft (late 70s-1982)

Cockerell was the inventor of the hovercraft. The problems that he encountered with waves while trying to design the hovercraft led him to design a wave energy converter. The problem with the hovercraft and the waves was that as the craft was moving over them the force was trying to break the craft. If the craft was allowed to break and the two halves left to rest on the surface of the water then a pump of some sort fixed between the two could be used to drive a hydraulic motor. Tests were carried out as too how many pontoons would be required. The optimum number was found to be three. The forward pontoon absorbing most of the energy, the second a little bit more and the final being held more stable by being larger than the other two.

The pontoons essentially rode on top of the waves and achieved best efficiency in seas where the wave length matched the length of the device, approximately 100 m. A tenth scale model was built and tested on the Solent in April 1978, by Wavepower, and produced an average of 1 kW. At full size the Raft was expected to produce 2 MW. The scale model used oil as a hydraulic fluid but, a full size model would have utilised water as reduced efficiency would be beneficial in larger seas. The Raft was essentially discarded before the ACORD (Advisory Council on Research and Development) meeting of June 1980 with the cost of the device being sited as the reason for funding being withdrawn [62].

### B.3.4 Coventry Clams (1978 to early 90s)

The team at The University of Coventry, after demonstrating their concept of the Duck, investigated another device - The Lancaster Bag. In partnership with Sea Energy Associates Ltd, they recognised the weakness in the air bags and decided that if they were protected

by a steel flap then it would be less liable to damage. The Clam is a large box structure with one side having the flap attached to it, hinged at it's base. As the bag expands the flap is pushed outwards and as it contracts the flap is pulled in. The air that was in the bag is then passed through a Wells turbine.

The next step in the design process was to arrange the bags around a 60 m diameter steel ring. As a wave passed the device some of the bags would be inflated and some would be deflated; the air in the system passing between them and through turbines to generate power. The design was to have been tested at a two thirds scale in Loch Ness in 1982, after a 1/10th scale test had been successful, but the funding for the project fell through. A fifth scale test occurred on Loch Ness and theoretical work continued to appear until the early 90s [94].

### B.3.5 ConWEC (1994–present)

This is a device that is a development of Falnes' research into latching as a control method for oscillating point absorbers. Reports would indicate that it is a float type device which drives a pump. Since 1994 work has been carried out between Brodrene Langset AS and the Department of Physics of the University of Science and Technology in Trondheim. In 1998 a company ConWEC AS was formed [95]. The device was funded in the late 90's by the Norwegian government and some research is still continuing [96].

## B.4 D

### B.4.1 Danish Wave Power Float Pump (1989-1996)

This device is a combination of a point absorber and an OWC type device. The Danes tested a 45 kW model of this device in 1989. It consisted of a floating buoy on the surface and a hollow concrete structure on the sea bed. Inside the sea bed structure was a piston on a big spring that was in turn attached to the buoy on the surface. As the buoy rose the piston was pulled out of the concrete base and water rushed in past a generator. As the buoy fell the water was pushed out of the base. A second test rig was launched in the summer of 1994 but unfortunately suffered some technical difficulties. A final test was performed in May 1995 and run successfully until January 1996 [97][98].

### B.4.2 DelBuoy (1982–late 80s)

Work began on this device in 1982. It was was developed by Hicks and Pleass at The University of Delaware. This buoy system was designed to produce fresh water for areas around the Caribbean Sea and the arid coasts of Africa [99]. A 2.1 m buoy was tethered to the sea bed by way of a hydraulic cylinder with a bore of 40 mm. This arrangement was used to drive an osmosis system to deliver fresh water. The system was demonstrated off the coast of Puerto Rico where a single buoy produced 950 lites of water in a day [100]. The test device was lost when hurricane Hugo struck the island of St. Croix where the tests were taking place.

## B.5 E

### B.5.1 Ecovision Lilypad (late 70s–1990)

This British device was designed in the late seventies by Collier and Michaelis. It was essentially a variation of the Swedish Hose Pump design. It consisted of two mattress-like objects. One floating on the surface and the other submerged and anchored below it. The second mattress was deep enough for the internal motion of passing waves not to affect it and was held relatively stationary. The two mattresses were connected by pumps similar to the hose pump. A 200 m by 60 m device was expected to be rated at 3.1 MW [79]. It was last tested in 1990.

### B.5.2 Energetech OWC (late 90s-present)

The Energetech OWC has been developed by Energetech in Australia [101]. It incorporates a novel Dennis-Auld variable pitch turbine and a parabolic reflector wall to focus the height of the incoming waves. The device was originally designed to be built into harbour walls, but has recently taken on a floating form as it's use as a desalination plant has become the priority. A full-scale demonstrator was deployed in October 2005 at Port Kembela, 80 km south of Sydney. Connection to the grid is expected in 2006.

Increased funding has been made available to Energetech by three New England states for the development of a 500 kW demonstration device at Point Judith Harbour, Rhode Island.

### B.5.3 European OWC Pico Plant (early 90s-present)

The European Pilot Plant is sited on the island of Pico in the Azores at Porto Cachorro and is a 400 kW OWC-type plant designed by the Insituto Superior Technico of Lisbon, Portugal [102]. The wave regime on the island is around 20-40 kW/m at the entrance to the gully in which the device is situated. The plant was designed as a testing and development facility but is also used to provide a large part of the islands energy needs. University College Cork, Queen's University Belfast and The University of Edinburgh have all been involved in it's development. The device sits in 7 m of water and has a column area of 150 $m^2$. The plant experienced some initial problems when it was first set up that have taken several years to remedy. A high speed stop valve and a variable pitch turbine have been built to test at the facility.

## B.6 F

### B.6.1 Falnes Point Absorbers (early-late 70s)

Falnes and Budal created this device during the seventies. It was a point absorber that utilised the heaving motion of the waves. In essence it was a large 5 m diameter buoy with a vertical rod through the centre of it. The rod was anchored to the sea bed and the buoy travelled up and down the rod in synchronisation with the waves. The device implemented Falnes and Budal's control mechanism (known as latching). The buoy was clamped to the rod at certain times then released depending on the wave climate, this was found to increase power absorption by a factor of 5. The device was rated at 500 kW and was designed to be deployed as a grid like wave farm. It is assumed that this research has evolved into the CONWec device design.

### B.6.2 Floating Wave Power Vessel (early 80s–present)

The Floating Wave Power Vessel is an overtopping device for offshore operation developed by Sea Power International, Sweden. It consists of a floating basin into which water is channelled before being run out through a low-head Kaplan turbine. It was originally designed to dredge for uranium and rare metals. A pilot plant was tested near Stockholm in the 1980s and a 1.5 MW vessel was planned for operation off the coast of Shetland by the end of 2004 at a depth of 50-80 m and 500 m offshore, as part of the Scottish Renewables Order. The company

has announced further schemes in the Maldives, India, the Azores and Tonga [103]. Further information on these schemes and the Shetland devices could not be found.

### B.6.3 $FO^3$, Fred Olsen (2001–present)

Developed quietly and without much media attention Fred Olsen's device has been demonstrated as a one third scale model in 2005. A full scale deployment is due in 2007 and has been selected to become part of the Wavehub project in Cornwall. The device is essentially a small oil-rig type of structure built from fibre-glass technology rather than steel. Below the platform are a set of floats which drive a power take-off mechanism. Technical details are very limited. The acronyms SEEWEC and $FO^3$ are now in use with this device and a €2.3 million funded consortium has been setup [104].

## B.7 G

### B.7.1 Greek Pump System (2000–present)

This straightforward system returns to Girard's first patent. A float is held in the sea at the end of a long lever connected to a generator. The system has been tested at a larger scale in an open water situation [105].

## B.8 H

### B.8.1 HRS Rectifier (late 70s)

This was a huge device when compared to modern wave energy converters. It was the size of a large oil tanker and was to be built 5-10 km from shore in 15-20 m of water. The general concept was to build storage reservoirs in the sea. The device was box shaped with a hinged flap, that would only open inwards. As a wave came in the force of the water would cause the flap to swing open allowing the reservoir to fill. As the wave retreated the reservoir was left sitting higher than the outside sea level. The reservoir was open to the sea by means of a pipe and turbine. As the wave pulled away the combined weight of the water in the reservoir and the suction of the wave caused the water to be drawn through the turbine and out into the sea. It was later discontinued due to cost limitations [72].

## B.9 I

### B.9.1 Indian Oscillating Water Column Device (1982-present)

India began experimenting with OWC devices in 1982 at the Indian Institute of Technology in Madras. The device they have built is a 150kW test device situated 45 m offshore at Vizhinjam, near Trivandrum. It consists of a caisson 17 m by 23 m sitting on the sea bed with an opening in the front wall just under mean sea level. The first attempt to site the caisson failed but a second attempt in 1990 was successful and it began operating in the following year. The turbine for the device is situated in the roof, something that has since been discovered to be unwise during storm waves as they break over the caisson. In other devices the turbine is mounted in the rear wall and is protected by the body of the device. The device produces an average of 75 kW from April to November and 25 kW from December to March, showing the seasonal variability of the waves. Research is continuing on this device with an impulse turbine having been tested during 1997 [106].

### B.9.2 IPS buoy (1974–mid 90s)

The IPS (Interproject Service AB) project was begun by Fredrikson in 1974. The device was a point absorber of the slack moored buoy type for deployment in 50–100 m water depth [107]. Below the buoy was a 20 m tube open at both ends to the ocean. Within the tube was piston. As the buoy heaved with the wave motion the water column and piston would move relative to the buoy. The motion of the piston was used to drive a hydraulic setup within the buoy hull.

The device was developed through the 1970s and 80s eventually reaching a full scale deployment off the coast of Sweden [108]. The device was rated at 150–250 kW for Scottish sea waters.

An adapted version of this device with the piston tube sloped at an angle to the ocean surface has been studied by The University of Edinburgh [109].

### B.9.3 The Islay OWC Projects (1983-present)

The Islay device was developed by Whittaker of Queen's University Belfast (QUB). Whittaker had been a student of Wells and his PhD thesis reported on a study of Oscillating Water Columns. With the closure of large-scale offshore projects the research path available was onshore demonstration projects. In 1983 Cranston asked if wave energy was still being

studied and suggested a site on Islay since the natural shoreline gullies would provide ideal locations for an OWC device. QUB financed an initial studying that was followed up by a £62,000 feasibility study sponsored by the Department of Energy and the Cement and Concrete Association, of which Cranstoun was a member.

The wave regime of Islay was found to be very good with open sea all the way to Newfoundland giving 70 kW/m offshore reducing to 8 kW/m onshore. The proposed gully, near Portnahaven increased this to 20–30 kW/m as a result of the bathometry focussing effect. The device was to become an amalgamation of the OWC concept from Masuda of Japan and the TAPCHAN device developed in Norway. Construction began in April 1987 and lasted two years. Many problems were encountered in particular the weather and the transportation of the structure. Further funding was provided in the Spring of 1989 to equip the device with a turbine set and work was complete in December 1991.

Initial results were less than expected for the site characteristics; the average output was around 17 kW with peaks of 50 kW. The problems were found to stem from the height of the tides which reduced the energy of the waves. The solution was to build the devices further out to sea. The second problem was that the walls of the natural gully were too rough and absorbed too much of the incoming energy. A designer steel or concrete gully would have solved the problem. Unfortunately funding for the project was ended on the 31st of March 1994. Less than six months later the Royal Society awarded Whittaker with an award for contribution to energy conservation and led to the Inverness based company, Wavegen, showing an interest in the device. This was enough to satisfy the EU of it's potential and invest in it's future.

The original Islay plant was decommissioned in 1999 and a newer larger plant was built in its place. A different method of construction was utilised that allowed for quicker and safer assembly and in 2000 it was connected to the grid. The new device is rated at a maximum of 500 kW. Plans are being made at present by Wavegen for a LIMPET device to be installed in the Faroe Islands [110]. Also a new breakwater scheme on the Island of Lewis may include OWC units.

## B.10 K

### B.10.1 "Kaimei" (1977-early 80s)

Launched in 1977 Kaimei was an 80 m, 800 tonne (barge based) floating OWC, developed mainly by Japan but with some input from the UK, Canada, Ireland and the USA. Three holes were cut into the hull of the barge below the water line to create air columns and generator sets were placed over these holes. As this was an experimental setup a different turbine was used for each chamber. The ship sat bow-on to the incoming waves. The results from the ship testing were not that favourable but the project progressed on to the Mighty Whale.

## B.11 L

### B.11.1 Lancaster Flexible Bag (late 70s-1982)

This device was devised by French of The University of Lancaster. He had previously designed a system of flexible bags to be placed at the entrances of harbours that would absorb the energy of the waves and create a calm area of water. French had first looked at wave energy during the sixties but thought it uneconomical, a view which he maintained as he developed his own device. The design consisted of a concrete beam, 190 m long, lying offshore. It was to be submerged 13 m below the surface and floated by the use of air bags lined along the length of it. As the wave passed the bags would be squeezed by the pressure differential. The air in the bags would move through a series of chambers to turn a turbine before re-entering the air bag cells [72].

Although the air within the cells was self contained doubts over the device lay in the availability of a strong enough material to make the bags. In other respects it was ahead of the competition at the time. It was cheaper to construct and gave an equivalent amount of power for a smaller device footprint. The device was tested at $\frac{1}{100}$th scale and French was awarded £175,000 in 1979 to improve on his design. Unfortunately it was ended in 1982 with French himself claiming that it would inevitably be uneconomical [62].

## B.12 M

### B.12.1 Manchester Bobber (2004–present)

Conceived during a 12 month Carbon Trust funded scheme the Manchester Bobber consists of a grid of buoys hung beneath a sea bed mounted oil rig platform. The buoys are slung on a cable with a counterweight on the other end. The cable passes over a disc linked by a 1:20 gearbox to a flywheel which in turn drives an induction motor. Twenty-five such bobber units would be fitted to a platform giving a rating of 5 MW per rig.

Currently a 100th scale model has been tested in wave tanks and a 10th scale model has been in operation at the NaREC test facility. Further development is taking place on the optimisation of the 100th model. The device is backed by The University of Manchester, Royal Haskoning and Mowlem Plc [111].

### B.12.2 McCabe Wave Pump (1980-present)

The McCabe Wave Pump was conceived by McCabe in 1980, after which it was studied both theoretically and experimentally. The 400 kW prototype device consists of three steel pontoons, which are hinged together across their beam. The central pontoon is held stable by means of a plate attachment several metres below the surface, while the two end pontoons are free to move. The energy is extracted by hydraulic means, which can be tuned to allow the device to work more efficiently in a wider range of sea states. It is slack moored to allow it to turn into the dominant wave direction. The power output can either be fed back to shore or used to provide potable water by supplying pressurised sea water to a reverse osmosis plant. A 40 m prototype was tested in 1996 of the cost of Kilbaha, County Clare, Ireland [112]. Some academic studies continue [113] and the device was refloated in 2004 for continued testing.

### B.12.3 "The Mighty Whale" (1987-present)

The Mighty Whale is an OWC based device developed by JAMSTEC as a next step on from Kaimei. The design is similar to Kaimei but has three OWCs, utilising 1 m Wells turbines. Behind the OWCs is a buoyancy tank and a fin to restrict heave and pitch motion. The shape of the device serves to create a flat area of sea behind the device leading to its developers recommending its use in front of fish farms and recreational sports areas. Following tank tests a 120 kW prototype, of size 50 m in length, 30 m in breadth and 8 m in draft, has been

operating since 1998 at a site 1.5 km off Nansei Town at 40 m depth. The efficiency of the device can reach 70 % in optimum conditions of 6 sec wave periods. The mooring system has been designed to withstand 50 year storms [114]. Further research [115] is continuing on the optimisation of the OWC turbines and forms a significant part of Japanese research into wave energy.

### B.12.4 Multi-Resonant Oscillating Water Column (early 80s-1988)

This OWC was developed using research carried out by NEL in the development of the OWC and by Queen's University Belfast in the development of the Wells turbine. The CEGB (Central Electricity Generating Board) provided expertise on the hydrodynamics and offered data and the use of Cockerell's wave tank near Southampton.

The OWC was built into a cliff face on the island of Toftestallen, 35 miles from Bergen. The device consisted of a 19.6 m steel tower standing in 7 m of water with an opening 1 m below the mean sea level. Above this tower sat the turbine, similar to the Wells turbine but with guide vanes and a modified profile. As the wave peak hit the tower the air column rose and drove the turbine. As the trough approached the column fell and the air was sucked back into the device. It began generating on the 31st of October 1985 producing from 100 to 500 kW of output, about 1% of the local grid capacity. The device survived three winters but during Christmas of 1988 it was torn from the cliff as two storms passed by. The storms of that particular winter were powerful enough to halt production in the North Sea.

## B.13 N

### B.13.1 NEL Oscillating Water Column Devices (1975-early 80s)

In 1975 NEL (The National Engineering Laboratory) published a review of wave power development [73]. They found that the device pioneered by Masuda should be the one to be taken forward in design. The first thing they amended in the design was the shape of the buoy; prior designs had used a simple upturned can shape, they changed it to being based on a claw-like shape with a foot plate to improve the stability of the buoy raising it's efficiency from 30 to 70 %. At this point in time the device was still utilising a valve based system to rectify the air flow.

NEL were to provide two further designs based on the OWC principle. The first design was an evolution of the Japanese "Kaimei" project. A ship was to have holes cut in its hull

and moored broadside on to the incoming waves, the ship would have rows of OWC's above the holes to generate electricity.

The second design almost reached fruition in 1982, before running into funding problems and being discarded. The design was for a bottom mounted breakwater type device. By situating it on the bottom problems of mooring could be avoided. It was to measure 65 m by 32 m and to stand in 20 m of water at a distance of one kilometre off The Island of Lewis. Talks continued for a while during the early eighties concerning a floating version of the device but were to be unfruitful [72].

## B.14 O

### B.14.1 Ocean Motion International (1995–2004)

This was a floating oil rig like structure with buoys hung beneath the device. It is not clear if it proceeded beyond the drawing board stage and the website [116] has not been updated since April 2004. References to the company do not include any future plans so it is surmised that the device is no longer in active development.

### B.14.2 Ocean Wave Energy Company (1978–present)

Based on an architectural design for underwater living this device design is unusual [117]. The main components appear to have been developed during a US Coastguard funded project in 1982. The design is wrapped in patent applications and legal paranoia, little further information is available. The company is still active.

### B.14.3 Ocean Wave Master (2002–2004)

The is a large box like structure that uses the pressure field of a wave to force water into and out of chambers and through a turbine [118]. It received funding from the Carbon Trust and a proof of concept model was tested at the NaREC facilities in Northumberland during 2004. No further development information is available and the company is no longer thought to exist.

### B.14.4 Offshore Wave Energy Limited (1999–present)

The developers were the recipients of a DTI SMART award. The OWEL has been tank tested and verified by QinetiQ [119]. The device is a really a large box with a tapering funnel inside to force the air in a trapped wave trough into a pressure reservoir and through a turbine [120]. A Carbon trust grant was awarded for further testing in 2004.

### B.14.5 OPT WEC (1994–present)

Developed by Ocean Power Technology [121] in the USA, the OPT WEC consists of a 2.5 m diameter buoy type cylinder closed at the top and open to the seas at the bottom. A hydraulic ram is positioned between the top of the shell and a highly buoyant steel float contained within the shell. The relative motion of the shell to the float activates a hydraulic system to pump oil at high pressure to a generator. The system makes extensive use of existing technology in the design of the float and anchoring but also power electronics to extract the maximum usable electricity.

Testing has taken place in the Eastern Atlantic. A small 6-device farm has been deployed by the US navy in Hawaii [122] during 2004-2005 and a single 40 kW device has been operating off the cost of New Jersey since October 2005. The company are in discussions with Iberdrola for a 1.25 MW demonstration project on the North coast of Spain. A further deployment at the Wavehub facillity is expected in 2007-2008 for a 30 MW farm consisting of 150 kW and 250 kW devices.

### B.14.6 ORECon - MRC1000 (2002–present)

This device is the commercialisation of the SPERBUOY concept initially developed by the University of Plymouth. In essence it is a floating point absorber with multiple OWC chambers [123]. Each chamber is fed by a pipe of varying length which hangs beneath the buoy. The varying pipe lengths give a range of resonant frequencies to each OWC. The SPERBUOY device was tested in the open sea in 2002 at 10th scale but twice broke it's moorings resulting in damage to the buoy. Tank testing has continued funded by the Carbon Trust.

### B.14.7 Oregon State University Buoy (2003–present)

Developed at the Oregon State University in America this is a device that uses a magnetic direct drive power take-off [124]. The buoy consists of two elements. The floating canister which contains an electric coil and a magnetic shaft which passes through the coil and is anchored to the sea bed. As the wave passes, the shaft is held still and the wave causes the canister to oscillate. As part of the US government's push on wave energy a national research centre may be setup as part of this device's development. The device at present is being tested as a scale model.

### B.14.8 OSPREY (1990-present)

The main prototype device for nearshore deployment (less than 20 m in depth) in the early 1990s was the OSPREY (Ocean Swell-Powered Renewable Energy). This was a 2 MW device developed by Wavegen [110]. It's basic design was an OWC that sat on the seabed and acted at times like a point absorber being able to extract energy from all directions; this feature led it to having a capture conversion rate, with respect to it's width, of 115 %. The average energy extraction was expected to be 3.3 GWh per annum. In appearance it looked like two towers sitting on top of a sphere, with two splayed feet which held its ballast. The sphere section which contained the air column was 20 m in diameter and the full height was 28 m, which would be higher if an optional 1.5 MW wind turbine was installed.

The device was first developed in 1990 through private finance from a design by Wells. Testing and evaluation had taken place. The Joule funding scheme announced in 1993 gave the project the finance needed to advance. The design was fabricated from steel on the Clyde and launched on the 2nd August 1995. The device was floated to it's mooring site 300 m off of Dounreay. It was able to float as the steel ballast tanks had been partly filled. Upon reaching the site the tanks were to be filled and the device sunk to the sea bed. Unfortunately a heavy sea burst the steel ballast tanks and the device sank [62].

The turbines and electrical equipment were salvaged and lessons were learn for the design of a further device the OSPREY 2000 which has been redesigned to allow for easier installation and to probably be made in concrete rather than steel. In 2001 a loan of €2.7 million was received by Wavegen from the Scottish Executive to build a 2 MW device off the coast of Orkney, the loan would have covered 60 % of the cost of the device [125]. The device is not known to have been constructed.

### B.14.9 Oyster - OWSC (2001–present)

This device is an effective reworking of the Japanese pendulor system and focuses on hinged flaps [126]. For shoreline application the flap would be mounted in a gully and hinged above the device. For near shore application the device would be hinged at the seabed. The project is largely academic based at present with funding from the EPSRC and the Scottish Enterprise.

## B.15 P

### B.15.1 Pelamis (1998–present)

The Edinburgh based company [127] behind this design, OPD (Ocean Power Delivery), was created in the wave energy group at The University of Edinburgh where staff members were working on Post Doctoral research [64]. Founded in 1998 it aimed to create a device that took the lessons of all past devices and used them to design the best possible device that could be realisable. The two major criteria were to make it survivable and economical.

The first criterion was accomplished by designing a shape of device that would be able to weather any of the storm seas which exist off of the coasts of Scotland. The device is constructed of four long cylinders linked by hinged joints with three power conversion modules between the segments. A 750 kW unit has an overall length of 120 m and a diameter of 3.5 m. The device orientates itself in the waves so that it sits end on to the incoming waves. As the wave front passes the device the sections move with respect to each other. Hydraulic rams connect the sections and as they move, they pump hydraulic fluid into storage tanks where it is continuously discharged to run a hydraulic motor coupled to a hydraulic generator [128]. As storm waves grow larger their peaks grow further apart but they become steeper. At a certain point the Pelamis will de-reference itself and surf on top of the waves surface. However, as the wave fronts become ever steeper the movement in the hinged joint will grow too small and the device will duck under the steepest waves.

The second criterion of economical affordability is accomplished by drawing on the wealth of technology already implemented in the offshore industry. A major criticism during the projects of the 1980s was the cost of wave power. By making the devices more affordable it brings down the initial capital costs and in turn the cost of the electricity produced.

At this moment in time the Pelamis design has passed through scale model testing to the installation of a full-scale device at the European Marine Energy Centre in Orkney, where

it has been on trial since August 2004. A three device farm is in the process of installation in Portugal with a letter of intent signed for a further 28 machines. The Pelamis has also been selected as part of a 5 MW installation at the wavehub site in Cornwall.

### B.15.2 Pendulor (1981-present)

The Pendulor is a device that has been constructed in Japan by the Muroran Institute of Technology. It is essentially an box open to the sea at one end and with a hanging flap at the rear. The flap moves backwards and forwards as the waves come in creating a standing wave as they reflect from the rear wall of the box. The flap motion is used to power a hydraulic pump and then a generator. Two installations have been made at Muroran and Mashike harbour in Japan [65]. A recent proposal has been put forward for a 150–250 kW project in Sri Lanka [129].

### B.15.3 PS FROG (mid 80s-present)

An acronym for Pitching Surging French's Reactionless Oceanic Generator, this was a design taken up by French after he had dismissed his airbag device [130]. The PS FROG is shaped like a large paddle about 23 m wide and 15m high. The premise of the device is to extract energy from the surge of the waves since this is approximately twice that of the heave motion. At the base of the paddle is a mass that slides from side to side as the device moves. The mass is used to pump oil and drive a generator. Research is continuing at this time, this is focusing on small-scale model testing in The University of Lancaster's Wave Tank and computer-based simulations [131].

## B.16 S

### B.16.1 Salters Ducks (Winter 1973-present)

One of the first of the modern designs to evolve in the 1970s was the Duck designed by Salter of The University of Edinburgh [132]. He began experimenting in a tank of water with pieces of paper in order to discover a shape that would absorb waves without in turn creating them. The shape arrived at was pointed at the front and rounded at the rear.

In his seminal paper [133], the initial plans for a wave farm were set down. The paper also stated some of the fundamental design principles required in the design of wave capture

devices. The first being that offshore devices could not be rigidly fixed to the ocean floor and should be able to float and move with the waves. Secondly that all moveable components should be hidden from contact with the sea; in the case of the ducks the spline passed through the vane so that the vane protected the contacts. The third provision was to try and built the device from existing technology.

Prior to the seventies many of the previous patents had tried to utilise the bobbing motion of the waves which neglected the true motion of the wave. Movement occurs at the surface, this decreases exponentially. A straight vertical flap, hinged horizontally, would only absorb about 40 % of the wave energy. By having a rounded device with a point, more energy can be absorbed.

The length of the device was explained in that it needed something to react against. If a device is fixed to the sea bed then it has something solid to pull or push against. A free floating device has no such fixing. By making the ducks long then the forces of the waves against different sections would allow the device to remain relatively stable.

To assist in the design of the Duck, plans were made available to Coventry University to analyse the device using their analogue hybrid computer. A few months later, in Autumn 1977, Coventry put a modified version of the Duck into the waters of Loch Ness to test at 1/15th scale model. Although confirming wave energy, the response at Edinburgh was not very positive. They wanted the design to work well before going to further testing. The Coventry scale model did indeed fail and sink.

The Duck was far from being a simple wave conversion device. The next stage of evolution added to its complexity. The problem was in the power take-off. In the 1974 design, the motion of the Ducks was referenced to that of the spine, and as such the spine had to remain relatively stiff leading to problems in construction. The solution arrived at in 1978 [62] was to use gyroscopes to provide this reference allowing the spine to flex more freely.

The gyroscopes would be housed inside the vanes, as they moved the gyroscopes would spin, this motion then being transferred to hydraulic systems. The other added benefit in utilising gyroscopes was that they provided a means of flywheel storage. The storage in the flywheel motion of the gyroscopes would allow for 45 minutes of electricity to be stored as a backup to grid demands.

Further major modifications to the design came in 1992 after it had been shown to have certain weaknesses [79]. The gyroscope concept was set to one side and a ring-cam pump was to be used in its place. With the advent of digital technology it was possible to run complex systems of pumps and electronic poppet valves in order to have complex patterns of

sinks and sources of oil. This system would allow the Duck to run a generator at a constant 1500 rpm. The advent of this technology also led to the Duck absorbing the Scandinavian theory of "latching".

Plans were also made in the early nineties for a solo Duck. A single vane supported on tension leg moorings, similar to those used in North Sea oil platforms. The solo Duck would act in a similar way to a buoy system with different cluster sizes providing varying levels of power to the consuming country. Theoretical work on the duck continues.

### B.16.2 SARA WEC (1992-present)

This is a buoy system developed by a US company SARA [134]. The buoys are placed near shore and use the heave motion of the buoy reacting against a damper plate to cause a piston to move hydraulic fluid. The fluid is used in a magnetohydrodynamic process to generate electricity. A proof of concept device was funded by the US Office of Naval Research.

### B.16.3 SEADOG Pump (2002-present)

The SEADOG is a recent development from a Minnesota-based company [56]. It consists of a small offshore rig supporting a float. The heave motion of the float is used to pump sea water to a storage facility on shore where it will return to the sea through low-head turbines [135]. Trials have been completed in Texas and a further offshore demonstration rig is planned for Northern California.

### B.16.4 Searev (2001–present)

This is an unusually shaped device that has been optimised by genetic algorithm techniques for a moderate wave environment. The research is based at the École Centrale de Nantes and has been funded by European and French grants. Inside an enclosed shell a mass oscillates back and forth, similar to a pendulum, and drives a synchronous generator. The modelling of the device, at this stage, is at the scale tank level [136].

### B.16.5 SEAWAVE SSG (2003–present)

This device is funded through the EU and the Norwegian government. The Seawave Slotcone Generator (SSG) is a variation of the generic overtopping device. Instead of have a single reservoir into which the water is stored the SSG has three stacked one on top of each other.

If built as a breakwater the device will be wedge shaped with the sloping side to the wave field. As a wave runs up the slope channels will allow the water to fall into the reservoir chambers at different heights. As the wave recedes the water stored in the reservoirs runs out through a specially designed turbine [137].

The design is currently at a scale model stage. Plans are being made for both onshore and offshore designs. A demonstration shoreline plant is in discussion for a site at the island of Kwitsoy, Norway [138].

### B.16.6 SPERBOY (Late 90s-present)

This device is based on a patent taken out by Embley Energy Ltd. and developed by Plymouth University. It is essentially a floating oscillating water column device but with multiple water columns each tuned to different resonances. It is hoped that having these multiple tubes will allow the device to take advantage of a wide range of wave climates. A test device was deployed off of Plymouth in early 2002. The author strongly suspects that ORECon's MRC1000 device and Sperbuoy are identical devices [123].

### B.16.7 Sri Lanka OWC (2000)

This is a small 150 kW test station being funded by the Sri Lankan Ministry of Science and Technology following on from a prototype tested in February 2000. The station is mainly an R&D demonstration project.

### B.16.8 Swan DK3

An advance of the Backward Bent Duct Buoy this device was part of the Danish Wave Energy Development Programme.

## B.17 T

### B.17.1 TAPCHAN (early 80s-1996)

At the same time as the Norwegian OWC was being constructed another device was also built. This was the TAPCHAN (Tapered Channel). It was a development of Bott's early design for Mauritius but with a new adaption. A channel was built measuring 3 m wide at the sea and tapering over a distance of 90 m to 0.2 m. This channel lifted the waves 3

m up to a holding reservoir. As the waves were forced up the channel by the pressure of those behind them they overtopped the walls along it's length and created a spout at the terminating end. The water ran out of the reservoir through a low head Kaplan turbine. The dimensions of the design were governed by optimising the cost of the civil engineering over the conversion rate of the turbine. The installed capacity of the device was 350 kW and could produce 2 GWh per year. Recent discussions have taken place for the installation of a 1.1 MW scheme at Baron in Java [69] and on King Island, located just north of Tasmania, Australia [65]. Several other south pacific countries expressed an interest during the 90s but the last available reference was in 1996.

### B.17.2 Technocean Hosepump (1980-mid 90s)

The Technocean Hosepump was sea tested between 1983 and 1986. The device consisted of a large buoy 5 m wide, 16 m long and weighing 50 tonnes [139]. The buoy was attached to a horizontal plate hanging below the buoy. The plate in turn was attached to the sea bed. The advantage of the plate was that the buoy was unaffected by the tides because the plate was always the same distance below the buoy. The buoy was attached to the plate by a flexible hollow tube that contained water and a piston. As the buoy rose and fell the tube contracted and expanded sucking in water and pressurising it. The water was collected and used to power a turbine that averaged 3-5 kW [65]. The device was tested in Lake Lygnern and in the sea at Vigna. Work on this device was discontinued and incorporated into the AquaBuOY project.

## B.18 V

### B.18.1 Vickers' OWC Device (late 70s-early 80s)

This possible device design was devised by the Cumbrian firm Vickers. They were manufacturers of submarines and their device utilised that technology. An enclosed OWC system was to sit on the sea bed within a 196 m long shell. The pressure differential of the waves passing overhead were to produce oscillating changes within the shell causing the on board turbine to turn. Each device was rated at 3 MW [72].

## B.19 W

### B.19.1 Waveberg (1979–present)

This American device was designed by John Berg to mimic the motion of kelp [140]. The device consists of a central pontoon and three radiating arms which extend from the pontoon and rest on floats. As a wave passes the device the arms are moved in relation to the central pontoon and a pump is extended and contracted. The action of the pump pressurises sea water and this is fed back to shore to run a Pelton wheel generator.

The device has existed for many years but it is heavily patented and references in the scientific literature are very limited. The device has been tested at 30 foot scale in San Francisco bay, smaller scale models have been tested in the wave tank at the National Research Council Canada Institute for Ocean Technology and in real seas off the coast of Nova Scotia. Several scale deployments have also been made in Florida.

### B.19.2 WaveBob (late 90s–present)

This device has been developed in Ireland and invented by Dick. It is of the heaving point absorber type. The manufacturers claim that it can be adapted to any climate [141]. Two scale prototypes have been tested at HRMC Cork and FZK Hanover but details of the device structure and power take-off are not publicly available. Two of the devices main backers are Fred Olsen and the Marine Institute, Dublin.

### B.19.3 Waveblanket (2005–present)

This is an initial concept idea. It exploits the properties of future material strength to blanket a region of ocean with a flexible sheet. Built into the material will be pressure chambers through which air will be exchanged as the material is moved by the waves [142]. However the device would be appear to work in a similar manner to an oil slick effectively damping the waves and restricting the ultimate size of the blanket.

### B.19.4 Wave Dragon (1986-present)

The Wave Dragon is an offshore wave energy converter of the overtopping type, developed by a group of companies led by Löewenmark Consulting Engineers, Aps., Denmark [143]. It utilises a wave reflector designed to focus waves towards a ramp that fills a reservoir and

flows down to a low-head Kaplan turbine [144]. A 1:4.5 20 kW scale model was deployed at Nissum Bredning from March 2003 until mid 2006.

The Wave Dragon project has been funded by the Danish Energy Agency and the EU. In March 2006 £5m funding was set aside by the Welsh Assembly for a 7 MW device to be sited near Milford Haven. There are also possible plans for a 50 MW project in Portugal due for commissioning in 2008–2009.

### B.19.5 Wavemill (1993-present)

The Wavemill Energy company is located on the east coast of Canada in the province of Nova Scotia [145]. Their device appears to exist primarily as a desalination plant. Designed as a breakwater, the caisson consists of a surge ramp to force the waves upwards where it will act against a float. It is surmised that this float will drive a pump pressurising the desalination equipment.

A scale model of the device has been built and tested in conjunction with the National Research Council of Canada. Tests in real sea conditions were performed at Cape Breton Island, Nova Scotia. No further information on the device is available and the last news article posted on the developers website is dated 2002.

### B.19.6 Waveplane (1994-present)

This Scandinavian device uses an innovative technique to transform the slowly rotating ocean wave into a high speed motion [146]. Shaped like a triangular wedge, two sides of the device are taken up by the planes. These are vanes angled into the water. As the wave runs up the wedge the water is forced into several stacked chambers. The water exits these chambers into a circular void. The water in the uppermost chamber enters first followed by the preceding chamber. As each chamber empties the fluid in the void is imparted with a circular force causing the fluid to rotate at upwards of 800 rpm.

Much research has gone into developing a turbine to capture this energy. Additional work has taken place on the anchoring and stabilisation of the wedge platform. This is accomplished by a large damper plate situated 20–25 m below the device.

The developers of the Waveplane have positioned it in several different ways emphasising its possible use in desalination and oxygen production as well as for generating electricity [147]. Caley Systems, a Scottish based firm, were involved in commercialisation of the device in 2003 and the Carbon Trust made a £268,000 contribution to the development.

### B.19.7 Wave Rider (1997–present)

SeaVolt Technologies [148], an offshoot of University of California Berkley, is developing this offshore point absorber. Details on the device itself are limited. The buoy section of the device floats on the surface and follows the heave motion of the ocean. It would appear to be taught moored to the sea bed and that a hydraulic power take-off is utilised. It is unclear as to whether the power generation takes place onboard the buoy, on the seabed or onshore. It was recently part of the Carbon Trust's Marine Energy Challenge.

### B.19.8 WaveRoller (1999–present)

This Finnish design is a bottom-mounted flap for deployment in the near shore environment at depths of 7–15 m. The principle is to extract power from the wave energy that penetrates to the sea bed. With longer swell waves the water particles on the sea bed move backwards and forwards parallel to the ocean floor. The flap anchored to the sea bed is moved by this particle motion and in turn drives a hydraulic pump system.

The device has been tested in Ecuador and at the EMEC centre in Orkney at one third scale. Results from the Ecuador tests are unavailable but it is known that the EMEC device was washed ashore by a storm in 2005. The developers also appear not to have considered biofouling when deploying their device [149].

### B.19.9 Wave Rotor (2001-present)

The Wave Rotor is a hybrid design that aims to extract energy from both the heave and surge of the wave. This is accomplished by using a composite vertical and horizontal rotating blade. Looked at from above the rotor has three arms lying horizontally these are tilted upwards towards their ends. This design allows the rotor to generate lift as the wave passes and in turn rotation.

The design was tested at the NaREC facillity in 2004 as part of the Carbon Trust's Marine Energy Challenge [150].

# Appendix C

# Publications

The following conference publications have resulted from this thesis.

- J.R. Halliday & D.G. Dorrell, "Review of wave energy and wave generator development in the UK and the rest of the world", International Conference on Power and Energy Systems, IASTED, Rhodes, Greece, June 2004.
- D.G. Dorrell, J.R. Halliday, P. Miller & M. Findlater, "Review of wave energy resource and oscillating water column modelling", Universities Power Engineering Conference, UPEC, Bristol, UK, Sept 2004.
- J.R. Halliday, D.G. Dorrell, & A. Wood, "The application of short term deterministic wave prediction to offshore electricity generation", International Conference on Renewable Energy and Power Quality, ICREPQ, Zaragoza, Spain, March 2005.
- D.G. Dorrell, J.R. Halliday, S. MacLean, P. Miller & F. Santamaria Mosquera, "Development of small-scale facilities for initiating studies into sea wave energy generation", International Conference on Renewable Energy and Power Quality, ICREPQ, Zaragoza, Spain, March 2005.
- J.R. Halliday, D.G. Dorrell, & A. Wood, "A Fourier approach to short term prediction", 16th International Society of Offshore and Polar Engineers Conference, ISOPE, San Francisco, USA, July 2006.

# REVIEW OF WAVE ENERGY RESOURCE AND WAVE GENERATOR DEVELOPMENTS IN THE UK AND THE REST OF THE WORLD

J.R. Halliday and D.G. Dorrell
University of Glasgow, Glasgow, G12 8LT, UK

## ABSTRACT

Wave energy as a means of generating electricity has been the focus of study in the UK for over thirty years, albeit in a low-key manner and with little public support. Interest is now growing. This paper reviews the developments during this time period to put the work into context and briefly describes the different types of device that have been studied. It also discusses wave energy generation in a world-wide context.

## KEYWORDS

Renewable energy, wave generation, oscillating water column, Wells turbine

## 1. Introduction

With the drive to use more renewable energy sources for electric power generation more types of renewable energy sources are being investigated. Wind power is already reaching maturity for on-shore generating plants either as stand-alone turbines or wind farms with many turbines on exposed locations such as hill ridges. There are plans to move wind turbines to off-shore locations were they have less environmental impact and can take advantage of stronger and more steady off-shore winds, thus improving their duty cycle. Scotland has the highest wind resource in Europe. In conjunction with this Scotland also benefits from high sea waves since it is located on the Western edge of the north Atlantic. Fig 1 shows a world map of wave resource in terms of kW/m of wave front. Few other developed countries have this level of wave energy on its shores (South America and Australasia being two other locations). Briefly, the potential for wave generation in the UK is illustrated in Table 1. If the target wave/electrical energy conversion efficiency for a well-designed wave generator is 25 % then about 1000 km of wave generators could supply up to half of the current UK electricity requirement. The challenge now is to be able to produce such wave energy converters and harness the potential. The energy potential of the resource is discussed later.

Wave energy generation has, in fact, been the subject of research and study in the UK for over thirty years. The modern birth of interest in wave energy technology began in the UK in 1973 when Prof. S. Salter began a journey to find a reliable way to extract energy from the waves. 30 years on and wave energy is on the brink of breaking into the main stream. There are several test and demonstration installations either built or in the advanced stages of design. However, over this time the work has often been low key and with little public support in terms of funding. This paper will review the progress of this work in the UK, and in other parts of the world, and also briefly describes the different types of wave generator that have been the subject of initial investigation and development. Since it is relatively new technology, and not reached the level of maturity that on-shore wind power has, most of the electro-mechanical wave energy converters are still little more than first generation prototypes; with no system emerging as the dominant method for energy conversion. The opening of the EMEC test centre in Orkney for the testing of commercial wave energy conversion devices is seen as the latest step that will greatly aid the commercialisation of wave energy production.

**TABLE 1 Wave power values**

| | |
|---|---|
| Mean wave energy around the British Isles | 30-90kW/m |
| Annual average in North Atlantic | 50kW/m |
| Annual average around Japan* | 15kW/m |
| (*for comparison with a country that has done some notable testing of wave generators) | |

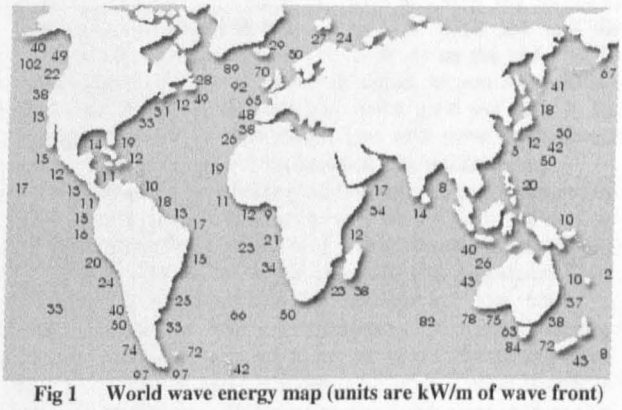

**Fig 1 World wave energy map (units are kW/m of wave front)**

## 2. Basic Facts about waves

Waves are in fact a very concentrated form of solar energy. The heat from the sun warms the earth at different rates causing air to flow from area to area depending on temperature differentials. The winds interact with the uppermost layers of the oceans; as the wind blows tangentially to the oceans surface it causes water particles to rotate in a circular motion. Over a large enough area this rotation penetrates deeper into the surface creating larger waves. The process can be seen on windy day if you look along the length of a loch with the wind blowing towards you. It will be observable that the waves rolling in towards you.

### *Terminology*

The most basic information about a wave is its height (trough to crest). The distance between successive crests is the wavelength and the time it takes between the crests is the wave period, which is typically 8 seconds in the North Atlantic. The term *Significant Wave Height* is used at times to describe the one-third highest waves. The *Fetch* is used to describe the uninterrupted distance over which the wind that is creating the waves has blown. In most cases the further the fetch the bigger

the waves will be. The power in a wave is roughly proportional to the square of the height; therefore higher waves give more power. The power is defined in terms of Watts per meter of wave front.

Some devices work on the principles of pressure changes as a wave passes over them. If a device is resting on the sea-bed and the sea is calm then a constant pressure will be experienced relative to the depth of water in which the device is sitting. If a wave of height 10m passes over the device then during the trough of the wave the pressure will decrease, as the crest passes the pressure will increase as more water is pushing down on the device.

There are four motions that an object will make whilst left to move freely in the ocean. *Pitching* describes a rocking back and forth movement; *Rolling* is the same rocking motion but from side to side; *Heave* is the up and down bobbing motion that an object will make; and *Surge* is used to describe the movement made by objects parallel to the oceans surface.

### *Possible Resources*

The resources available around the globe and in particular to the UK are impressive in size. Dr Johannes Falnes [4] made an estimate of worldwide resources of 1TW of onshore energy and 10TW of offshore potential. Many possible sites exist in the world with the main criterion being that they have a shoreline facing onto a prevailing wind that has been blowing over a considerable stretch of ocean. Much of the western coasts of Europe, South Africa, Australia, New Zealand, America and Chile all have high potential resources in excess of 40 kW/m. Many other countries without these resources have also been developing wave programs; Norway, Japan and India in particular are all at the forefront of research. Interest is also high in Pacific Island communities where diesel fuel generators are the staple energy provider; in some areas, imports of fuel oil are running at 500% of the islands total exports [5][7].

Recent studies [14] claim to show that the Atlantic resources are in the region of 290 GW. This is the area from the Iberian Peninsula to the Northern-most reaches of Norway. The power in these areas range from 25kW/m in the Canary Islands to a maximum of 75kW/m off the Irish and Scottish coasts; before decreasing to 30kW/m around the Arctic circle in Norwegian waters. Also included in this figure are the resources available in the North Sea, which range from 21kW/m in the best sites to 11.5kW/m in more sheltered areas. Although a smaller resource, the Mediterranean sea can add another 30GW of potential to this figure taking the total European resources to 320GW.

This resource is potentially vast but it is spread over the entire coastline. Many areas will be unreachable and so realistic resources are smaller. Our share of this total is roughly 50TWh per annum [28] after considerations of efficiency and transmission loses have been taken into consideration. Scotland's potential landable resource could be 14GW [1], more than enough to supply ourselves, but more importantly enough excess to supply some of the 80GW used in the UK as a whole.

In a recent estimate, the worldwide potential for recoverable energy was some 2000TW/h per annum, this would be equivalent to the current world installed capacity for hydro generation [27] and would represent 10% of world consumption at this time. Remember that only a small amount of the raw ocean wave energy could be practicably extracted. The cost of building this infrastructure would be around £500 billion (Euro 700 billion). The technology at this present moment is capable of delivering this energy at a cost of 5 p/kWh (7 Euro cent/kWh) which is twice the European average, but, as has been discussed in length in various papers and reports, this figure is based on developing technology and is estimated to be falling with every new generation of device. The high upfront costs would ultimately pay off in the long run as the fuel is essentially free.

In comparison with other alternative renewable energy resources wave energy has many factors in its favour. In terms of density, the energy of the ocean is roughly contained in the upper layer, 10-20m depth, whereas for wind it is dispersed over many kilometres, with the best resources located higher above the ground than a structure could physically survive. The average density for wind energy is rated as $1kW/m^2$; for the area off the western coast of the Hebrides islands in Scotland the average wave power, per metre of wave front averages between 40kW/m and 60kW/m. Solar energy also fairs badly in the northerly reaches of Europe with an average value of $0.1kW/m^2$.

### *The Case for Wave Energy*

Why should wave energy be favoured over other potential resources? As suggested by David Ross [2] it is a case of using the most appropriate technology for a given situation. Large-scale use of solar and geothermal energy is not a foreseeable possibility in the United Kingdom. Geothermal was investigated during the eighties but was abandoned by 1992, The United Kingdom not being in a particularly active geological region, unlike Iceland or New Zealand. Solar can be used in the UK and is mainly reserved for heating purposes in houses but, as stated previously, the power density of solar is rather low and the footprint of a viable solar station, 2GW, is on the order of 50 square miles. Solar is of course an option as you head further south and Mediterranean countries make good use of it in the heating or cooling of their homes and with some international assistance it would seem to be the ideal solution for Africa.

Wind has for the past ten years been seen as the renewable energy source. It is indeed hard to miss a wind farm, the average size of a turbine being in excess of 100m. The perennial problem with a wind farm is the visual intrusion and consequent legal difficulties in securing planning permissions. The UK is a crowded island and with a population of 56 million, finding agreeable locations for wind farms on land is becoming more contentious. This problem is mirrored in several other European counties. Early wind turbines were also quite noisy and people have complained about the noise pollution. The planners of farms arguing that if less than a certain number of people can see the farms then they should be built. Wind has recently gone offshore; the resources are higher and technology has allowed them to exploit it. But sites are again limited; and some maintain that there will be an affect on shipping, marine life and tourism in areas of natural beauty.

Wave energy would seem an appropriate renewable for the UK. The resources, about 14 GW, would make a sizeable dent in the 80GW our country needs at present, though this figure based on past trends will reach nearer 130GW by 2014. On a practical level, wave energy will make the least environmental impact; devices will be rarely seen from the shore, although the effects of energy extraction on coastal erosion and site selection on the behaviour of sea creatures cannot be ruled out and are difficult to assess until the plant is installed. A brief sojourn into the environmental impacts has been made in [15,18] concluding that the environmental impacts were of lesser concern than with other renewable sources.

Benefits of wave power schemes can be found in the fishing industry where the calm waters behind devices can be used for fish farming or the pursuit of recreational sports. Some of the largest devices of the past have ascertained that these farms could be implemented within the device reservoirs themselves,

the constant flow of fluid aerating the water. Other benefits may include a relatively cheep source of power for the production of hydrogen, an early deployment of Salter's Ducks talked of them being pushed back from their original mooring by the waves and storing this energy as hydrogen. The Ducks would then use this stored power to sail back to their starting point depositing the unused hydrogen on the shore.

## 3. Basic Device Designs

The wind energy industry, after many years of prototyping with different blade numbers and vertical-axis machines, has now settled on the basic design of a three-bladed horizontal-axis turbine with the generator in the cupola. The wave industry is still debating about the best design and in a recent count there were over 1000 patented ideas for wave energy conversion. They can be broken down into five basic technology groups after Thorpe [13].

- Oscillating Water Column (OWC)
- Overtopping device
- Point Absorbers (floating or mounted on the sea bed)
- Surging devices
- Mechanical Extraction

The best design will depend upon the situation in which it is to be utilised.

### *Oscillating water column*

One of the most studied devices is the Oscillating Water Column (OWC). As described in Thorpe [28], an OWC consists of a chamber for the oscillating water column, turbine (unidirectional of bidirectional) and generator. The basic topology is shown in Fig 2. There are a great many of these devices around the world. They are relatively simple to construct on land and as such whenever a government wants to get started on wave power development their first step is usually to commission the construction of an OWC type device.

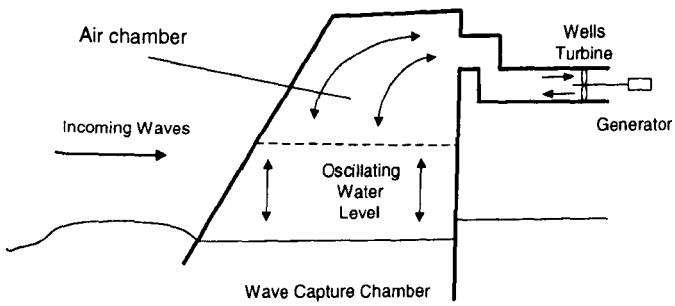


**Fig 2 Operation of Wells Turbine Showing Wave Capture Chamber and Bi-Directional Air Flow Through Turbine**

### *The Overtopping Device*

The first plant to develop electricity on a grid connection was a device of this type and it owes much of its design to the hydro-electric industry. In order to create electricity a reservoir needs to be situated a certain height above a turbine. This height is called the head. The higher the head the more potential energy the water will have and be able to turn the turbine faster. The concept of a raised reservoir is used in several device designs. Essentially the waves are forced into this reservoir by a variety of techniques where it will then fall through a small outlet to turn a Kaplan turbine.

### *The Point Absorber*

The classical example of point absorber is a buoy. The definition is made as a device being smaller in dimension than the wavelength of the waves it wishes to capture. The majority of these devices are based on systems involving a buoy or a float that moves in a heave, or bobbing, motion. This motion is used in reference to a fixed point, commonly the mooring point, on the seabed. This motion is then used to pump sea water or oil to drive a turbine or to directly engage with the power take-off.

### *Surge Devices*

These are Wave Energy Conversion devices that utilise the horizontal forces of the waves. Generally the surging motion of a device is twice that of the heaving motion. There are not many devices that go out of their way to capture this motion but some, in particular those of Sir Michael French, make use of this higher power level.

### *Mechanical Devices*

This is a category that Thorpe did not have but is included as a catch-all situation for the various mechanical devices that can't be comfortably placed in one of the above categories. In particular Salter's Ducks and Cockerell's Raft are two of the members of this category and more recently the Pelamis (Ocean Power Delivery Ltd, UK) [1].

### *Design for Survivability*

The greatest problem being faced by the designers of Wave Energy Converters (WEC) is how to balance capture efficiency, cost of construction and the survivability of the design. Many designs that look favourable on paper and have high capture efficiency would, if constructed, be destroyed by the largest storm waves. Although the west coast of Scotland has an average of 60-80 kW/m of wave front, under serve storm conditions this can rise to upwards of 10,000 kW/m. The parameter used by the designer of offshore structures in the oil industry is the 50-year design wave, i.e., the largest expected wave in a 50-year period; for the west coast of Scotland this is thought to be on the order of 30-40m (the size of a 5 storey building!).

### *Problem Areas*

Wave Energy is far from being without problems. Those that occur regularly concern the cabling required to transport the energy to shore and in turn how to transmit this energy to the customers. The cables have to be long and able to withstand the forces at their termination points at the device farms. A big problem faced by designers is scaling up models from tank testing at 1/4, 1/10, 1/25 scale models to full size. In many cases a doubling of scale can mean squaring of forces and with them new problems to solve. A further difficulty is that with wave energy you do not design to reach maximum conversion. A device that reaches 100% conversion at a definite wave period and height, will invariable have bad capture efficiency at other levels. What is required is a design that will cover the largest catchment area, where the most power is available for the most time during the year, thus allowing the device to generate for most of its lifetime.

## 4. Pre-1974 Designs/Patents [18]

The first recorded description of a wave powered device dates from a patent filed by the Girards in Paris in 1799. The device consisted of a lever attached at one end to a boat and at the other end to a pump sitting on the shore. The motion of the ship would cause the lever to work the pump. Some 340-350 patents have been filed to date in the United Kingdom. Many designs were wild and wonderful but all are based on the reality that the waves are ceaseless in their activity. The bulk of these patents were mostly filed prior to the First World War, the first British patent being filled in 1855. One of the most successful of these was an Oscillating Water Column device built by Bochaux-Praceique in 1910 [8]. The device was built into a cliff face at Royan, near to Bordeaux, and supplied his house with 1kW of energy.

*Masuda*

The next step forward came through the efforts of Commander Yoshio Masuda, a former Japanese naval commander, who designed the first wave power navigation buoy for use in the Sea of Japan during the years preceding the end of the Second World War. The ingenious step in his design was to change a violent slow moving force into something more controllable. This was down by transferring the energy of the waves into a column of air. The principle is best illustrating by thinking of an upturned can floating in the sea. As the waves move around the can the water level inside the can moves at the same time. If you put a hole in the top of the can the air inside will be alternately forced out then sucked back in. By the use of values this stream can be rectified so that it is moving in one direction and used to turn a turbine. This was in 1947 and was the first modern example of an Oscillating Water Column. These early buoys generated 30W in the relatively calm seas around Japan.

*Mauritius 1953-1966*

A.N. Bott arrived in Mauritius in 1953, the island is fringed by a broken ring of very tough coral and Bott proposed to use the coral as a base to build a basin into which waves would over-top, keeping it filled up. The water would then run out of the basin through low head turbines and generate electricity. The problem was to what height should the wall be built. Too high, and there would be times when the waves were not big enough to keep the basin filled; too small, and there would not be enough of a head to run the turbines. The solution was to use a low wall to keep the basin constantly topped up and to use the energy of the incoming waves to pump the water from the lower reservoir up to a higher one. A higher reservoir gave a greater head and reduced the turbine costs. Unfortunately the scheme was never built as oil prices fell during the 1960s and funding was withdrawn in 1966. The experience was however delivered in a paper to the Royal Society of Arts in 1975 [17].

*American Buoy 1960s*

A few devices were put forward and tested during the sixties. One of these came from the Avco Corporation [11], and foreshadowed some of the devices to follow during the late seventies. The device worked to exploit the pressure difference that occurs when a wave passes through a certain point. As the wave passes the submerged device the depth of water overhead caused a pressure difference between the outside water and air store in the device. This pressure was used to run a hydraulic motor. Initial tests conducted in Buzzard's Bay, Massachusetts, resulted in 0.25 of a watt being produced; a level just about powerful enough to run a navigational buoy.

## 5. Wave Energy in the UK

UK Government interest in wave energy began in 1974, with a letter to Prof. Stephen Salter of the University of Edinburgh concerning his device, known universally as the Duck. The oil crisis of the time provoked interest in alternative forms of energy. In 1976 there was an announcement of £1million [2] to fund research into wave energy, setting an ambitious goal of a 2GW power station to be situated off of the Hebrides.

The search for a wave power design began by falling back on research carried out on the wave regime of the UK waters. Initial investigations of wave power involved siting a Waverider Buoy at Benbecula in the Hebrides to record data. Funding increased in the second year to £2.5 million, but the small increase to £2.9 million for 1978 signalled the slackening of government interest in wave energy due to the perception that the technology was limiting progress.

Another sticking point was the price of electricity generated by the devices. It was estimated that the electricity from the devices ranged from 2 to 30 times the cost of domestic electricity at the time of reporting (1978). Wave Energy was killed off at this time in the UK in a series of government reports claiming uneconomical costs. Up to the point of the killing off of wave power in 1982 some £15 million had been invested in the programme, spending on the nuclear industry ran to orders of magnitude much greater than this.

The UK Wave Development Programme was abandoned in 1982 This disparaging of the UK scheme led the International Energy Authority and the European Community to hold back on wave energy as it was following the UK lead. The results of the UK Wave Programme were published in 1985, and were supposed to be the end of wave development in the UK [24].

The debate argued on for much of the eighties. Government support for the Islay project in 1987 came out of embarrassment that Norway had two working plants by 1985 which were built for less than the cost of the consultancy work carried out by RPT [23], roughly £1.1 million for two plants. The House of Lords published an inquiry in July 1988 [22] declaring that it was concerned in the scrapping of the wave programme. The government response was to conduct a study of wave energy that lasted over three years and was essentially conducted by one man. The report published in 1992 [20] was supposed to end speculation over wave power but in fact did the opposite and is one of the cornerstone publications for wave developers.

By the mid-90's the government's view was beginning to change. After several reports, in particular Thorpe's review [29], the recommendation was for the recommencement of funding for wave energy, the government announced that the wave program was to be resuscitated as part of a £43 million packaged for renewable development over three years. The commissions involved were the UK Marine Technology Foresight Panel, A Scottish commission to promote wave energy and a Royal commission on Environmental Pollution.

In 1999, three successfully bidding projects were chosen for development: a 400kW FWPV from Sea Power International, a Limpet 500 from Wavegen and two 375kW Pelamis from Ocean Power Delivery (OPD). All of these devices are being developed by private companies with the DTI (Department of Trade and Industry) allocating funding depending on which of those device were attracting the most industrial backing.

A pressing concern for potential private developers may be the institutional barriers that will need to be crossed in deploying devices. One of the most contentious is the planning stage, during which time many statutory bodies must be consulted and permissions granted. A second and very important consideration is for grid connection of the devices; the best sites in Scotland are at the ends of a very weak grid and any development will require it to be reinforced.

A very recent development has been the opening of the testing facility located near Stromness on Orkney, where near-production-ready devices can be tested in open water conditions.

## 6. European Projects

*Norway*

The researchers of Scandinavian institutes, in particular those from Trondheim, have provided some of the most insightful research into wave energy converters, with the first work appearing during 1968. In 1973 Kjell Budal and Johannes Falnes began their research and contributed theories which have become generally adopted by the wave energy community, these are termed "point absorber"[9] and "phase control"[10].

Phase Control refers to the artificial manipulation of an object's movement in order to effect maximum energy extraction. All devices have a natural frequency of oscillation. At wave frequencies near this natural resonance capture efficiency is highest but at frequencies elsewhere the device can have reduced efficiency. Different devices use different methods: some offshore devices can change their hydraulic systems resistance, OWCs can utilise valves to hold the water column in a high position. In essence the devices delay the movement of their mediums until sufficient pressure has built up.

A further three innovations were also contributed; the first being the building of harbour walls to collect more wave energy than would otherwise reach a device. By building angled harbour walls in front of the device they could capture twice as much power. Evan Mehlum, pioneered the technique of 'wave focussing'. It was found that the irregular formation of the sea floor causes certain areas to focus the incoming waves increasing their power and creating 'hot spots'. These places can be readily identified, as it is where the fisherman can find the largest concentration of fish. In order to capitalise on this discovery the Norwegians had planned to moor shaped plates on the seabed in order to copy this effect. It was not done in practice but was tested in tanks.

The government of Norway were also keen to support wave development and released government surveys in 1979 and 1980 [25] giving the resource available to Norway of 600TWh but due to it's gnarled coastline an estimated 0.5MWh could be harvested. The Norwegian government, working in partnership with its private companies, created two of the earliest successes in Wave Energy history. The 500kW Multi-Resonant Oscillating Water Column (Kvaener Brug A/S) and the 350kW TAPCHAN (Norwave A/R).

*Sweden*

Sweden fares relatively badly in the share of potential wave energy receiving only 5-10 TWh, but has been at the forefront of the implementation designs. Their involvement began in 1976 and in 1979 a Wave Energy research Group had been assembled bringing together Chalmers University and a private company, Technocean. By 1980 the first full scale point absorber buoy, "Elsking" was being tested by Interproject Service AB (IPS) [16].During the early eighties the Swedish government ran a National Wave Development Programme.

*Denmark*

Denmark did not become involved in wave power development until 1996 when the government announced 5.3 million euros over a four year period for the investigation of wave power. Bringing together it's most experienced development teams into an advisory body it was hoping to build on it's success in wind energy and be able to tap some of it's 30TWh of potential.

*Portugal*

The Portuguese have been active since 1978 and have largely been involved in the development of Oscillating Water Column technology, in particular designing and building the test facility on the island of Pico in the Azores.

*Ireland*

With perhaps the best resources in the world (187.5TWh) Ireland have been active in pushing forwards wave development with most of their Universities being involved in wave energy research. The government has put through legislation to encourage the implementation and development of wave energy; *A Foreshore Act for Licences and Leases for Offshore Development* was passed in July 2000. Disappointment did occur in 1997 when a planned Power Purchase Agreement fell through after funds from the European Union were withdrawn.

*Greece*

Greece is currently developing wave energy experience with the Daedlius, has hosted one of the European Wave Energy Conferences and was part of the European Thematic Network.

*Other European Countries*

Much of the rest of Europe has limited coastlines and as such interest from these countries has not been as strong. A Dutch company, Teamwork Technology BV, has built a device known as the Archimedes Wave Swing that is awaiting further funding. Other countries such as France, Germany and Italy are providing assistance with other EU projects, mainly the OWC installation in the Azores.

*European Commission Involvement*

The European commission has been monitoring wave energy development since 1985 when it commissioned a document to be prepared by Dr Tony Lewis of University College Cork [6]. In it he had produced a study of the European wave power potential and had made recommendations. The parliament had allocated 1.2 million ECU's to projects and announced a seminar to be held in Brussels in 1991. The EC were most enthusiastic about OWC plans. In 1993 the EC funding plans were given: A near-shore station, the OSPREY, rated at 2MW, was to be moored off Dounreay, Scotland and a new gully was to be built on Islay, Scotland. Also, a proposed 500kW device was to be built on the island of Pico. These planned devices were part of the Fourth Framework programme.

The series of EC sponsored conferences has continued with their taking place in: Lisbon, Portugal in 1995; Patras, Greece in 1998; Aalborg, Denmark in 2000 and Cork, Ireland in 2003. As well as providing financial support to demonstration projects the EU has also assisted in setting up a developers' network where information can be collated and made available to those involved. The network was set up in 1999 and consisted of 14 wave energy representatives from various countries. The network is there as a collation of information on wave energy and has been responsible for a concise and detailed report

published during 2003 [30]. The report covers several areas deemed to be relevant to wave energy developers: cooperation with the power industry; social, planning and environmental impact; financing and economic issues; R & D on wave energy devices; generic technologies; and promotion of wave energy. The Thematic Network has also been responsible for various publications and the establishment of the All Energy conferences held in 2001 and 2003.

## 7. Rest of World

With the potential for electricity production from the power of the waves other countries around the world have been conducting research programs. Australia with a potential of 120GW has awarded contracts to Energetech Australia Pty Ltd and to Ocean Power Technologies for commercial developments at Port Kembela and Bass Strait. Canada has no real plans for development but some research is being carried out at the University of British Columbia and at Powertech Labs Inc. China and Indian are currently involved with the development of OWC'S and the Backward Bent Duck Buoy (BBDB) converters, both have 100kW demonstration devices in operation.

Japan has been experimenting with wave energy for many years. Many different projects have been tested, the largest being the Mighty Whale, a floating OWC moored offshore, and Kaimei, a ship with OWC's built into it's hull. The OWC has also been deployed in Sri Lanka where a 150kW test facility has been built.

The Korean firm Baek Jae Engineering were developing a wind-wave energy scheme during the latter nineties. It is based on a lattice of small devices created from plastic. The company was aiming to develop a low cost device that will reduce the non-productive wave loading on its structure.

The USA is also involved with wave power but more at an entrepreneurial level with several companies exploiting the potential of mass-produced buoy systems.

## 9. European Wave Energy Thematic Network

A recent report from the European Wave Energy Thematic Network, published in March 2003 [30], examined in detail the progress being made in wave and tidal devices. It researched various areas of concern to developers and drew conclusions on areas where knowledge or technology was lacking. These gaps are described below.

*Onshore Fixed Devices*

- The forecasting of nearshore wave climate is critical to fixed shoreline devices. The effects of the seabed topography create hotspots of concentrated energy but also areas where all the energy is dissipated a method of forecasting this would prove beneficial.
- At the early stages of device design they are modelled with computer software; unfortunately this software can only model linear wave theory and cannot cope with the non-linear effects present in real waves. An R&D task would be to develop correction formulae to account for these non-linear effects.
- Although many papers have been written on the best type of turbine to use in fixed devices there is still more work to be done. In the case of the Wells turbine attention is needed as to the design of the blade profile; whether or not guide vanes are appropriate; and the design of variable pitch turbines should also be considered. For Impulse turbines, the other contender, the shape of the blades and the choice between fixed and variable pitched guide vanes is required. In both designs a systematic method for choosing the design parameters would be appreciated and also the noise created by the turbines and how it can be reduced has been requested.

*Nearshore Floating Devices*

- The forecasting of the short term to medium term wave climate is also a problem for floating devices, current methods of forecasting apply to larger areas than required and are based on probabilistic methods. Some research has been done in the motion of ships for the landing of helicopters.
- The design of compliant mooring and cabling structures is required. The cables and moorings must be strong enough to ensure survival but flexible enough to ensure that they do not affect their devices purpose. Again technology exists in the offshore industries that could be transfer with little R&D effort.

*Offshore Floating Devices*

The areas identified are generally analogous to those of the first two categories, but placing more emphasis on large-scale, shared test facilities. These test facilities would include a wind tunnel for testing air turbines, a 360-degree wave tank and a testing rig for durability of components in the open sea. Other items deal with the mechanical problems faced, some having been solved by the present offshore industry but needing a bit more work for them to survive in the wave industry.

Overall it would appear from the reports that the areas of wave prediction and further advancement of software modelling would be two areas that should be addressed

## 10. Conclusions

The paper has reviewed previous work and discussed the ongoing work in the UK and Europe on wave energy generation. It has highlighted the different types of device currently being developed and the appendix lists the relevant device types. The European Wave Energy Thematic Network has recently drawn conclusions for the relevant areas for technological improvement.

## 11. References


[1] Roger Dettmer, *Wave Energy Gets Seaworthy*, IEE Review, September 2000 pp 14-19

[2] David Ross, *Power From The Waves*, 1995, Oxford University Press ISBN 0 19 856511 9

[3] Ronald Shaw, *Wave Energy: A Design Challenge*, 1982, John Wiley & Sons, ISBN 0-470-27539-1

[4] Falnes, J. and Lovseth, J., *Ocean Wave Energy, Energy Policy*, 8, pp 768-775, 1991.

[5] Wave Energy Resource and Economic Assessment for the State of Hawaii http://www.hawaii.gov/dbedt/ert/wave92/wave92.pdf

[6] Lewis, T., *Wave Energy, evaluation for CEC*, 1985, Graham & Trotman, London

[7] Jafar, M., *Renewable Energy in the South Pacific- options and constraints*, Renewable Energy 19, pp 305-309, 2000
[8] Falnes, J., *Teaching on ocean-wave-energy conversion*, 4th European Wave Energy Conference, Aalborg, Denmark, 2000.
[9] Budal, K. and Falnes, J., *A Resonating Point Absorber of Ocean-Wave Power*, Nature, Vol 256, pp 478-479, 1975
[10] Budal, K. and Falnes, J., *Interacting Point Absorbers with Controlled Motion*, Power From Sea Waves (B. Count, ed.), pp 381-399, Academic Press, London, 1980. (ISBN 0-12-193550-7)
[11] Scott, K., *Electricity from Waves*, Sea Frontiers vol. 11 issue 4, pp 202-207, 1965
[12] Salter, S.H., *Wave Power*, Nature, Vol. 249, June 21st 1974, pp 720-724, 1974
[13] Thorpe, T et al., *Wave Energy in Europe: current status and perspectives*, Renewable and Sustainable Energy Reviews 6, pp 405-431, 2002.
[14] Pontes, M.T et al., The *European Wave Energy Resource*, 3rd European Wave Energy Conference, Patras, Greece, 1998.
[15] Thorpe, T.W., *An Overview of Wave Energy Technologies: status, performance and costs*, Wave Power – Moving Towards Commercial Viability. IMECHE seminar, London, 1999.
[16] Fredrikson G., IPS Wave Power Buoy Mark IV, Wave Energy R&D – Workshop, Cork, Ireland, 1993 EUR 15079 EN, 1992.
[17] Bott, A.N. Walton, *Power Plus Proteins from the Sea*, The Royal Society of Arts Journal, CXXIII, 486-503, 1975.
[18] Leishman, J.M. And Scobie, G., *The Development of Wave Power*, NEL, Glasgow, 1975.
[19] Salter, S.H., In Proceedings, wave energy conference, Heathrow Hotel, London, November 22-23, pp 20, HMSO, London, 1978.
[20] Thorpe, T., A Review of Wave Energy. ETSU R-72, 1992.
[21] Ogilvie, T.F., *First and second-order forces on a cylinder submerged under a free surface*, Journal of Fluid Mechanics. Vol 16, pp 451-472, 1963.
[22] *Alternative Energy Sources*, House of Lords (27 July), Select Committee on the European Communities, pp 178 et seq., 1988.
[23] *Alternative Energy Sources*, House of Lords Select Committee on the European Communities, Session 1987-88, pp 196, 1998.
[24] Davies, P.G., Cloke, M.S., Major, K.A., Page, D.I., and Taylor, R.J. (ed.) , *Wave Energy*, ETSU R-26, ETSU for the Department of Energy, Harwell, 1985.
[25] Royal Ministry of Petroleum and Energy, Oslo, White Paper no. 54, Chapters 5, 10 and 12, 1979-80.
[26] *R&D on Wave Power Device Mighty Whale*, Hitoshi, Hotta et al., WREC 1996.
[27] Thorpe, T., *The Wave Energy Programme in the UK and the European Wave Energy Network*, Fourth European Wave Energy Conference, Denmark, October 2000.
[28] Thorpe, T., *An Overview of Wave Energy Technologies: Status, Performance and Costs*, Wave Power: Moving towards Commercial Viability, 30 November, London, 1999.
[29] Thorpe, T., *A brief Review of Wave Energy*, ETSU Report Number R-120, May 1999.
[30] European Wave Energy Network., *Results from the work of the European Thematic Network on Wave Energy*, European Community ERK5-CT-1999-20001, March 2003.

# 12. Appendix – Device Index

**Salter's Ducks**

Developed by Prof Salter of Edinburgh University. In his seminal paper [12], heralding the first truly modern wave energy converter design, the initial plans for a wave farm are set down. This consists of a nodding float where the pivotal action is used to generate electrical energy. This is one of the best-known wave generators.

**Japan Kaimei**

Launched in 1977 Kaimei was a ship based floating OWC. Three holes were drilled in the hull of a ship below the water line to create the air columns and generator sets were placed over the holes. The ship sat bow on to the incoming waves.

**The Bristol Cylinder**

This device was based on a theoretical research paper produced in 1963 by Professor T.F. Ogilvie [21]. It consisted of a 100m by 16m cylinder floating on its side 3m below the surface and held to the seabed by moorings. At the base of the moorings are hydraulic pumps. As the cylinder moves it pulls on the moorings activating the pumps. The cost of a 2000MW station as per the UK 1978 government programme would have cost £5100 million, but the maintenance of undersea equipment would be prohibitively expensive.

**The HRS Rectifier**

The size of a large oil tanker it was to be built 5-10km from shore in 15-20m of water. The concept was to build storage reservoirs in the sea. The device was box shaped with a hinged flap that would only open inwards. As a wave came in the force of the water would cause the flap to swing open allowing the reservoir to fill. As the wave retreated the reservoir level was left sitting higher than the outside sea level. The reservoir was open to the sea by means of a pipe and turbine. As the wave pulled away the combined weight of the water in the reservoir and the suction of the wave was to cause the water to be drawn through the turbine and out into the sea.

**Cockerell's Raft**

Sir Christopher Cockerell was the inventor of the Hovercraft and the problems that he encountered with waves while trying to design it led to him designing a wave energy converter. The device consisted of three hinged pontoons and the motion of them caused a hydraulic system to move a turbine. A tenth scale model was built and tested on the Solent in April 1978, by Wavepower, and produced an average of 1kW.

**The Lancaster Flexible Bag**

This device was devised by Professor Michael French of Lancaster University. He had previously designed a system of flexible bags to be placed at the entrances of harbours that would absorb the energy of the waves and create a calm area of water. The design consisted of a concrete beam, 190m long, lying offshore. It was to be submerged 13m below the surface and floated by the use of air bags, cells, lined along the length of it. As the wave passed the bags would be squeezed by the pressure differential. The air in the bags would move through a series of chambers to turn a turbine before re-entering the air bag cells. The device was tested at 1/100th scale. Unfortunately it was ended in 1982 with Professor French claiming that it would inevitable be uneconomical.

**The Coventry Clams**

The Clam is a large box structure with one side having the flap attached to it and hinged at the base. As the bag expands the flap is pushed outwards and as it contracts the flap is pulled in. The air that was in the bag is passed through a Wells turbine. A 1/10th scale test had been successfully tested

**Falnes Point Absorbers**

This is a point absorber, a device that utilises the heaving motion (up and down) of the waves. In essence it is a large, 5m diameter buoy with a stick through the middle of it. The stick is anchored to the seabed and the buoy travels up and down the stick in sympathy with the waves. The device was rated at 500 kW and was to be deployed as a grid-like wave farm.

**Pendulor**

The Pendulor is a Japanese device. It is basically an open box open to the sea at one end and with a hanging flap. The flap moves backwards and forwards as the waves come in creating a standing wave as they reflect from the rear wall of the box, the motion is used to power a hydraulic pump and then a generator.

**IPS Hosepump**

The IPS Hosepump was sea tested between 1983 and 1986. The device consists of a large buoy 5m wide, 16m long and weighing 50 tonnes. The device was tested in Lake Lygnern and in the sea at Vigna.

**Multi-Resonant Oscillating Water Column**

This OWC was built into a cliff face on the island of Toftestallen, 35 miles from Bergen. It was not the best site but was close to an airport for visiting officials and potential customers to visit. The device consisted of a 19.6m steel tower standing in 7m of water with an opening 1m above and below the mean sea level. Above this tower sat the turbine, similar to a Wells turbine but with guide vanes and a modified blade profile. It began generating on the 31st of October 1985 producing from 100kW to 500kW of output, about 1% of the local grid capacity. The device survived three winters but during Christmas of 1988 it was torn from the cliff as two storms passed by. The storms being powerful enough to halt oil production in the North Sea and tear a tanker from it's mooring. The biggest lesson learned was to construct the chimney of concrete and to site the electrics and turbine on land.

**TAPCHAN**

Near to the Multi Resonant OWC at Bergen, Norway, a device called the TAPCHAN (A contraction of the words Tapered Channel) was built. It was an evolution of Bott's design for Mauritius. The installed capacity of the device was 350kW and could produce 2GWh per year. Recent discussions have taken place for the installation of a 1.1MW scheme at Baron in Java [28].

**The Islay 75kW Demonstration Project**

The wave regime of Islay was found to be very good with open sea all the way to Newfoundland giving 70 kW/m offshore reducing to 8kW/m onshore. The proposed gully, near Portnahaven increased this to 20-30kW/m as a result of its focussing effect. The device was to become an amalgamation of the OWC concept from Masuda of Japan and the TAPCHAN device developed in Norway. Construction began in April 1987 and lasted two years.

**Indian Oscillating Water Column Device**

The device the Indians have built is a 150kW test device situated 45m offshore at Vizhinjam, near Trivandrum. The device produces an average of 75kW from April to November and 25kW from December to March, showing the seasonal variability of the waves.

**"The Mighty Whale"**

The Mighty Whale is an OWC based device developed by JAMSTEC it is essentially a floating breakwater type device that has three OWC's, utilising 1m Wells turbines [26]. Following tank tests a 120kW prototype, of size 50m in length, 30m in breadth and 8m in draft, has been operating since 1998 at a site 1.5km off Nansei Town at 40m depth.

**Backward Bent Duck Buoy**

At a suggested from Masuda to point the air opening of an OWC away from the incoming waves its air output was greatly increased. The new design was tested at University College Cork and is backed by a Chinese consortium.

**Denmark Spring Box**

A combination of a point absorber and an OWC type device, the Danes have tested a 45kW model.

**PS FROG**

An acronym for Pitching Surging French's Reactionless Oceanic Generator, the PS FROG is shaped like a large paddle about 23m high. The premise of the device is to extract energy from the surge of the waves, as this is roughly twice that of the heave motion.

**The LIMPIT OWC, Islay**

This is a 500kW device situated on the Scottish island of Islay. The original installation of the 75kW device was decommissioning in 1999; the lessons learned from it testing life were used in making a larger version.

**European OWC Pico Plant**

The European Pilot Plant on the island of Pico in the Azores at Porto Cachorro and is a 400 kW OWC-type plant designed by the Insituto Superior Technico of Lisbon, Portugal. The wave regime on the island is around 20-40kW/m at the entrance to the gully in which the device is situated.

**Sri Lanka OWC**

This is a smaller 150 kW test station being funded by the Ministry of Science and Technology following on from a prototype tested in February 2000. The station is mainly an R&D demonstration project.

**OSPREY**

The main prototype device for nearshore deployment (<20m in depth) is the OSPREY (Ocean Swell-Powered Renewable Energy), which is a 2MW device developed by Wavegen. It is basically an OWC that sits on the seabed and acts at times like a point absorber being able to extract energy from all directions; this feature leads it to having a capture efficiency of 115%. The device was first developed in 1990. Testing and evaluation having taken place the design was fabricated from steel on the Clyde and launched on the 2nd August 1995. The device was floated to its mooring site 300m of Dounreay. It was able to float as the steel ballast tanks had been partly filled. Upon reaching the site the tanks were to be filled and the device sunk to the seabed. Unfortunately a heavy sea burst the steel ballast tanks and the device sank.

**Archimedes Wave Swing**

The Archimedes Wave Swing is developed by Teamwork Technology BV, Netherlands. The device consists of an air filled chamber, the 'Floater', which can move vertically with respect to the cylindrical 'Basement', which is anchored to the seabed. The 'floater' is neutrally buoyant so will remain at rest until a wave passes over the device. The wave causes a change in pressure and the floater to move. The relative movement is used to power some kind of take off system. A 2MW Prototype has been built but not yet commissioned.

**Floating Wave Power Vessel**

The Floating Wave Power Vessel is an overtopping device for offshore operation developed by Sea Power International, Sweden. It consists of a floating basin into which water is directed before being fed out through a low-head Kaplan turbine.

**McCabe Wave Pump**

The 400kW device consists of three steel pontoons, which are hinged together across their beam. The central pontoon is held stable by means of a plate attachment several metres below the surface, while the two end pontoons are free to move. The energy is extracted by hydraulic means, which can be tuned to allow the device to work more efficiently in a wider range of sea states. It is slacked moored to allow it to turn into the wave. A 40m prototype was tested is 1996 of the cost of Kilbaha, County Clare, Ireland.

**OPT WEC**

Developed by Ocean Power Technology in the USA, the OPT WEC consists of a 2.5m diameter buoy type cylinder closed at the top and open to the seas at the bottom. A hydraulic ram is positioned between the top of the shell and a highly buoyant steel float contained within the shell. The relative motion of the shell to the float activates a hydraulic system to pump oil at high pressure to a generator. The individual devices are rated at 20 to 50 kW and are to be deployed in arrays.

**Wave Dragon**

The Wave Dragon is an offshore wave energy converter of the overtopping type, developed by a group of companies led by Löewenmark Consulting Engineers, Aps., Denmark. It utilises a wave reflector designed to focus waves towards a ramp that fills a reservoir then falls down through to a low-head turbine. It has already passed through various model stages of design and is at present undergoing sea trials.

**SPERBOY**

A point absorber type buoy proposed by Starweld Ltd., UK. It received funding from the EU in 1997. Tank tests were successful but an open sea trial ended after the device broke its moorings.

**The Pelamis (Sea Snake) Device [1]**

The device is constructed of four long cylinders linked by hinged joints. A 375kW unit would have an overall length of 150m and a diameter of 3.5m. The device orientates itself perpendicular to the wavefront so that it's narrow end points into the oncoming waves. As the wave front passes the device the sections move with respect to each other. Hydraulic ram's connect the sections and as they move, they pump hydraulic fluid into storage tanks where it is continuously discharged to run a hydraulic motor coupled to a hydraulic generator.

**Energetech OWC**

This device was developed by Energetech in Australia. It incorporates a novel variable pitch turbine and a parabolic reflector wall used to focus the height of the incoming waves. It is subject to a power purchase scheme for a 500kW installation at Port Kembla, 80km south of Sydney.

# REVIEW OF WAVE ENERGY RESOURCE AND OSCILLATING WATER COLUMN MODELLING

D. G Dorrell, J. R. Halliday, P. Miller and M. Findlater
University of Glasgow, Glasgow, G12 8LT, UK

## ABSTRACT

Wave energy as a means of generating electricity has been the focus of study in the UK for over thirty years, albeit in a low key manner and with little public support. Interest is now growing. This paper is divided into two sections: it briefly reviews the developments during this time period to put the work into context and then describes a small oscillation water column system constructed within The University of Glasgow to aid understanding and in initiate a research program.

**Keywords:** Renewable energy, wave generation, oscillating water column

## INTRODUCTION

With the drive to use more renewable energy sources for electric power generation more types of renewable energy sources are being investigated. Wind power is already reaching maturity for on-shore generating plants. Scotland also benefits from high sea waves since it is located on the Western boarder of the north Atlantic. Few developed countries have this level of wave energy on its shores (South America and Australia being two locations). The potential for wave generation is illustrated in Table 1. If the target wave/electrical energy conversion efficiency for a well-designed wave generator is 25 % then about 1000 km of wave generators could supply up to half of the current UK electricity requirement. The challenge now is to be able to produce such wave energy converters and harness the potential.

Wave energy generation has been the subject of research and study in the UK for over thirty years when Prof. S. Salter of The University of Edinburgh began a quest to find a reliable way to extract energy from the waves. Thirty years on and wave energy is on the brink of breaking into the main stream; with several test and demonstration installations either built or in the advanced stages of design. However, over this time the work has often been low key and with little public support in terms of funding. This paper will briefly review some the progress of this work in the UK and Europe. Since it is relatively new technology, and not reached the level of maturity that on-shore wind power has, most of the electro-mechanical wave energy converters are still little more than first generation prototypes; with no system emerging as the obvious method for energy conversion. The opening of the EMEC test centre in Orkney for the testing of commercial wave energy conversion devices is seen as the latest step that will greatly aid the commercialisation of wave energy production.

**TABLE 1 Wave power values**

| | |
|---|---|
| Mean wave energy around the British Isles | 30-90kW/m |
| Annual average in North Atlantic | 50kW/m |
| Annual average around Japan | 15kW/m |

## ENERGY SOURCE IN WAVES

Waves are in fact a very concentrated form of solar energy. The heat from the sun warms the earth at different rates causing air to flow from area to area depending on temperature differentials. The winds interact with the uppermost layers of the oceans; as the wind blows tangentially to the oceans surface it causes the particles to rotate in a circular motion. Over a large enough area this rotation penetrates deeper into the surface creating larger waves. The rotating motion of the water particles is stored kinetic energy and the gradual phase shift in time and space over a length perpendicular to the wave front sets up the moving wave pattern, which are essentially progressing waves of potential energy. In some ways this is comparable to real and reactive power in an electrical power system with the reactive power being analogous to the stored kinetic energy (necessary to set up the wave motion) and the real power being the movement of the wave crests, which is the flow of potential energy. However it is not a totally analogous system, for instance, an electrical power system rarely spans even one wavelength, whereas a sea wave will travel thousands of wavelengths from source to termination.

The most basic information about a wave is its height (trough to crest). The distance between successive crests is the wavelength and the time it takes between the crests is the wave period and is typically 8 seconds in the North Atlantic. The term *Significant Wave Height* is used at times to describe the one-third highest waves. The *Fetch* is used to describe the uninterrupted distance over which the wind that is creating the waves has blown. In most cases the further the fetch the bigger the waves will be. The power in a wave is roughly proportional to the square of the height. The power is defined in terms of Watts per meter of wave front.

Some devices work on the principles of pressure changes as a wave passes over them. If a device is resting on the sea bed and the sea is calm then a constant pressure will be experienced relative to the depth of water in which the device is sitting. If a wave of height 10m passes over the device then during the trough of the wave the pressure will decrease, as the crest passes the pressure will increase as more water is pushing down on the device.

There are four motions that an object will make whilst left to move freely in the ocean. *Pitching* describes a rocking

back and forth movement; *Rolling* is the same rocking motion but from side to side; *Heave* is the up and down bobbing motion that an object will make; and *Surge* is used to describe the movement made by objects parallel to the oceans surface.

## POSSIBLE RESOURCES

The resources available around the globe and in particular to the UK are impressive in size. Falnes [1] made an estimate of worldwide resources of 1TW of onshore energy and 10TW of offshore potential. Many possible sites exist in the world with the main criterion being that they have a shoreline facing onto a prevailing wind that has been blowing over a considerable stretch of ocean. Much of the western coasts of Europe, South Africa, Australia, New Zealand, America and Chile all have high potential resources that are in excess of 40 kW/m. Interest is also high in Pacific Island communities, where imports of fuel oil is running at 500% of the islands total exports.

Recent studies [2] claim to show that the Atlantic resources are in the region of 290 GW. This is the area from the Iberian Peninsula to the Northern-most reaches of Norway. The power in these areas range from 25kW/m in the Canary Islands to a maximum of 75kW/m off the Irish and Scottish coasts; before decreasing to 30kW/m around the Arctic circle in Norwegian waters. Also included in this figure are the resources available in the North Sea, which range from 21kW/m in the best sites to 11.5kW/m in more sheltered areas. Although a smaller resource, the Mediterranean sea can add another 30GW of potential to this figure taking the total European resources to 320GW.

This resource is potentially vast but it is spread over the entire coastline. Many areas will be unreachable and so realistic resources are smaller. The UK share of this total is roughly 50TWh per annum [3] after considerations of efficiency and transmission loses have been taken into consideration. Scotland's potential landable resource could be 14GW [4], enough excess to supply some of the 80GW used in the UK as a whole.

In a recent estimate, the worldwide potential for recoverable energy was some 2000TW/h per annum, this would be equivalent to the current world installed capacity for hydro generation [5] and would represent 10% of world consumption at this time. Remember that only a small amount of the raw ocean wave energy can be practicably extracted. The cost of building this infrastructure would be around £500 billion (Euro 700 billion). The technology at this present moment is capable of delivering this energy at a cost of 5 p/kWh (7 Euro cent/kWh) which is twice the European average, but, as has been discussed in length in various papers and reports, this figure is based on developing technology and is estimated to be falling with every new generation of device.

## BASIC DESIGN TYPES

The wave industry is still debating about the best design for sea wave energy extraction and in a recent count there were over 1000 patented ideas for wave energy conversion. They were broken down into five basic technology groups by Thorpe [6].

- Oscillating Water Column (OWC)
- Overtopping device
- Point Absorbers (floating or mounted on the sea bed)
- Surging devices
- Mechanical Extraction

The best design will depend upon the situation in which it is to be utilised. A more detailed description of the different types can be found in [8].

### Oscillating water column

One of the most studied devices is the Oscillating Water Column (OWC). As described in Thorpe [7], an OWC consists of a chamber for the oscillating water column, turbine (unidirectional of bidirectional) and generator. The basic topology is shown in Fig 1. There are several of these devices around the world - the first commercial wave generator in the UK is of this type and located on the Isle of Islay. They are relatively simple to construct on land.

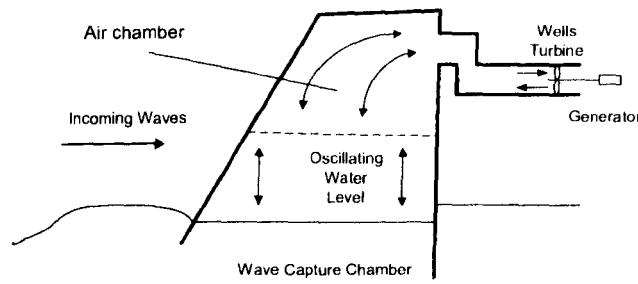


**Figure 1 Operation of Wells Turbine Showing Wave Capture Chamber and Bi-Directional Air Flow Through Turbine**

### The Overtopping Device

The first plant to develop electricity on a grid connection was a device of this type and it owes much of its design to the hydro-electric industry. In order to create electricity a reservoir needs to be situated a certain height above a turbine. This height is called the head. The higher the head the more potential energy the water will have and be able to turn the turbine faster. The concept of a raised reservoir is used in several device designs. Essentially the waves are forced into this reservoir by a variety of techniques where it will then fall through a small outlet to turn a Kaplan turbine.

### The Point Absorber

The classical example of point absorber is a buoy. This is a device that is smaller in dimension than the wavelength of the waves it wishes to capture. The majority of these devices are based on systems involving a buoy or a float that moves in a heave, or bobbing, motion. This motion is used in reference to a fixed point, commonly the mooring point, on the seabed. This motion is then used to pump sea water or oil to drive a turbine or to directly engage with the power take-off.

**Surge Devices**
These utilise the horizontal forces of the waves. Generally the surging motion of a device is twice that of the heaving motion.

**Mechanical Devices**
This is a category that Thorpe did not have but is included as a catch-all situation for the various mechanical devices that can't be comfortably placed in one of the above categories. In particular Salter's Ducks and Cockerell's Raft are two of the members of this category and more recently the Pelamis (Ocean Power Delivery Ltd, UK) [4]. The Pelamis (or "sea snake") is a tubular device of several sections (with similar dimensions to railway carriages) that is place perpendicular to the wave fronts. Hydraulic pumps at the hinges resist the movement between successive sections and so produce energy. An array of these (placed off-shore in a similar manner to a line of breakwaters on a breach) can be used are wave energy plant. This device looks very promising and has now entered sea trials.

## DESIGN FOR SURVIVABILITY

The greatest problem being faced by the designers of wave energy converters (WEC) is how to balance capture efficiency, cost of construction and the survivability of the design. Many designs that look favourable on paper and have high capture efficiency would, if constructed, be destroyed by the largest storm waves. Although the west coast of Scotland has an average of 60-80 kW/m of wave front, under serve storm conditions this can rise to upwards of 10,000 kW/m. The parameter used by the designer of offshore structures in the oil industry is the 50-year design wave, i.e., the largest expected wave in a 50-year period; for the west coast of Scotland this is thought to be on the order of 30-40 m.

Many problems concern the cabling required to transport the energy to shore and in turn how to transmit this energy to the customers. The cables have to be long and able to withstand the forces at their termination points at the device farms. A big problem faced by designers is scaling up models from tank testing at ¼ , 1/10, 1/25 scale models to full size. In many cases a doubling of scale can mean squaring of forces and with them new problems to solve. A further difficulty is that with wave energy you do not design to reach maximum conversion. A device that reaches 100% conversion at a definite wave period and height, will invariable have bad capture efficiency at other levels. What is required is a design that will cover the largest catchment area, where the most power is available for the most time during the year, thus allowing the device to generate for most of its lifetime.

## OSCILLATING WATER COLUMN OPERATION

The oscillation water column type of wave energy is currently in commercial operation in the Isle of Islay [9] and this represents still the sole commercial wave energy plant. It is rated at 250 kW and is a shoreline device. This device can also be located on floating platforms as was the case with the "Might whale" [10]. As water oscillates inside the chamber then ther is a pressure difference due to the difference in the external water level. This will cause air to blown and sucked through the turbine.

The turbine can be a standard type with valves to ensure that the airflow through the turbine is unidirectional, or it can be a more straightforward arrangement with a through-pipe and a bidirectional turbine (i.e. a turbine that produces torque in the same direction with airflow in either direction). Examples of the bidirectional turbines are the Wells turbine [11] and impulse turbine [12] Both the Islay plant and the Mighty Whale use Wells turbines. These turbines require a high Reynolds number for correct operation which means a diameter over 600 mm for reasonable. In the study reported in this section the diameter of the turbines is only 132 mm so that their performance is very poor. This is illustrated using computational fluid dynamics in [13]. However it represents an interesting study in scaled-down devices. In this paper we will report on some experimental results of the oscillation water column performance and a simple SIMULINK model that approximated the performance.

**Experimental Equipment**
The dimensions of the water column are shown in Fig 2 and the water column could operate with either all three sections or with simply the centre section. Because the torque produced by the turbine was very low, a dc motor was fitted and connected to a supply – this is shown in Fig 3. A wave tank that could produre waves up to 250 mm and down to a frequency of 0.45 Hz use used in the test (this facility was available with the University) and Fig 4 illustrates work during the testing stage.

The turbine was run up to speed and the input power measured. Waves were then produced and the power measured again so that the power difference represented the power generated. Care was taken to ensure that temperature variation of the motor did not affect the results. However, because the power differences were small, there was still considerable experimental error. The conversion factor for the turbine was of the order of less than 1 % in some instances.

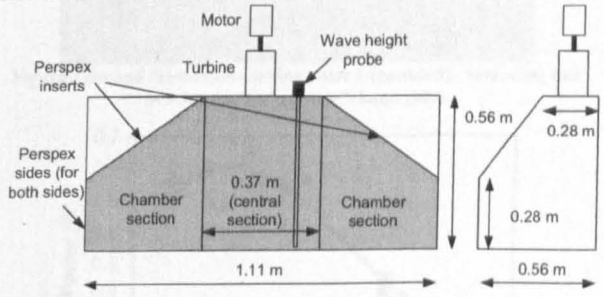


**Figure 2 Oscillating water column dimensions**

**Variation of Turbine Speed**
To find the most suitable speed to operate the turbine, the wave frequency was fixed at 0.56 Hz and the speed varied.

The results are shown in Fig 5 and these were obtained using only the centre section of the water column chamber and a wave height of 200 mm. They are compared to the calculated generated output power difference for a second turbine rotor that has been manufactured but so far only simulated using CFD [13]. The two rotor profiles can be compared in Figs 6 and 7. It can be seen that 1200 to 1500 rpm is the peak speed for the first turbine rotor whereas 1000 to 1250 rpm is calculated as the most suitable for the second turbine rotor. The power difference represents the difference at the turbine shaft in power if the turbine is rotating at that particular speed when there are waves and when there are no waves.

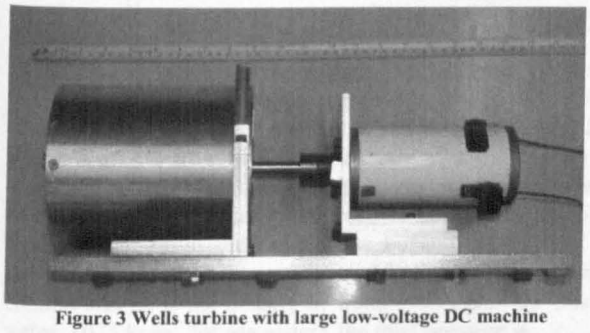

**Figure 3 Wells turbine with large low-voltage DC machine**

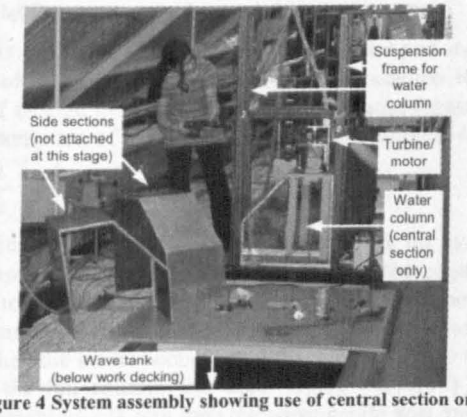


**Figure 4 System assembly showing use of central section only**

It was found that the output power for the first turbine was consistently higher than that calculated – it is assumed that the output power for the turbine simulations is so low that there is variation due to numerical error. However, consistent overestimation may be due to small variation in shape of the blade between the simulated and manufactured, which would affect the power significantly at these low power values. The actual oscillating water column and turbine arrangement will also produce more turbulence than simply modelling the turbine alone with constant inlet airflow velocity which could also produce higher output power.

### Variation of Wave Frequency

With the turbine speed fixed at 1500 rpm and a wave height of 200 mm, the wave frequency was varied and the results shown in Fig 8. These results were obtained with all three sections of the water column and at a different column height in the water from Fig 8. This illustrates that the most suitable frequency for the first turbine is 0.56 Hz. The wave tank could produce waves at 200 mm wave height down to 0.45 Hz (and higher wave heights at higher frequencies).

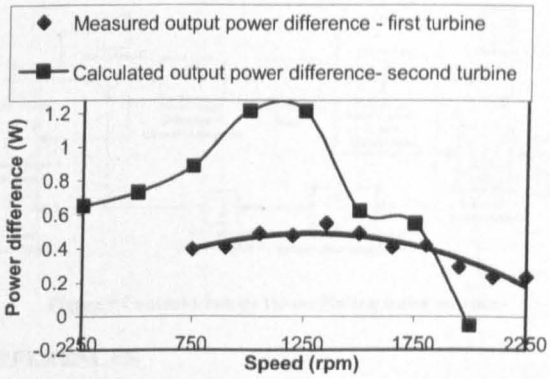


**Figure 5 Variation of output power difference for first turbine rotor (measured) and second turbine rotor (simulated using CFD)**

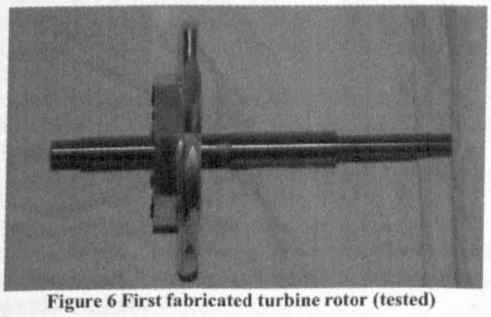

**Figure 6 First fabricated turbine rotor (tested)**

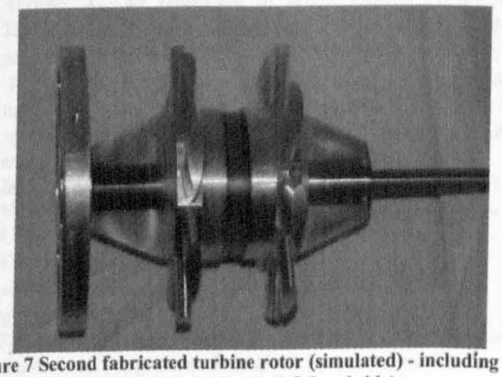

**Figure 7 Second fabricated turbine rotor (simulated) - including one bearing mounting on left hand side)**

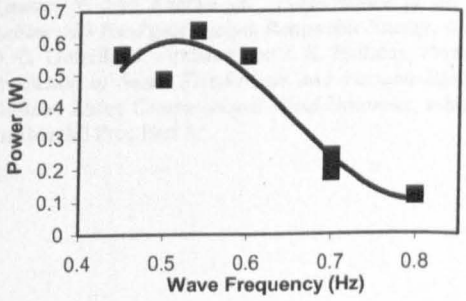


**Figure 8 Variation of wave frequency at 1500 rpm**

**Modelling of Water Column**

The complete system is a complex non-linear device. However, as an attempt to model the system in simple terms the SIMULINK system in Fig 9 was developed. The first turbine simulation look-up tables can be used for the transfer functions for the inlet pressure to airflow and also the pressure to output power. While the flow to pressure can be represented as a simple transfer function:

$$\text{Inlet Pressure} = 1.747 \times \text{flow}^3 + 39.71 \times \text{flow} \quad (1)$$

Inversion of this leads to a function with many terms – hence the use of look-up tables. The equations of the system are given below. The waves are assumed to be sinusoidal so that the driving function is:

$$h_s(t) = \frac{H_s}{2}\cos(2\pi f_s) \quad (2)$$

If we assume that the air density in the water column chamber is constant (which is probably one of the main sources of error in this model – at sea level, a change in pressure of ± 3 kPa produces a change of ± 2.4 % in air density – which will introduce a larger change in water height for a given change in column pressure and will change as air flows out through the turbine, introducing a phase lag) and, if $h_c(t)$ is the height of the water in the column and $\rho_w$ is the density of water (998 kgm$^{-3}$ for fresh water, 1025 kgm$^{-3}$ for sea water), the inlet pressure is

$$\text{Inlet Pressure} = \rho_w \left(h_s(t) - h_c(t)\right) \quad (3)$$

If $A_T$ is the cross section of the turbine inlet and $A_W$ is the cross section of the water surface in the column then the rate of change of height of the water column (again using the assumption of incompressible air in the column) is

$$\frac{dh_c}{dt} = \frac{A_T}{A_W} \times \text{flow} \quad (4)$$

An adjustment factor was also included since the system is very approximate. However, maintaining the adjustment factor to unity then the column height at a wave height of 201 mm was measured at 92.5 mm and simulated to be 68 mm when the centre section only was used ($A_T/A_W$ = 0.044). When the full column was used ($A_T/A_W$ = 0.0147) with a wave height of 221 mm then the wave height was measured at 77.6 mm and simulated to be 23.6 mm. Increasing the adjustment factor to 2 produces the correct oscillation for the centre section simulation however the full column still produces an underestimate (33.6 mm water height). The output power was underestimated however it has already been mentioned that the simulated power was low compared to that measured. Further work will be undertaken on the modelling of the water column.

## CONCLUSIONS

The paper has reviewed some of the different types of sea wave energy converters that have been studied. The different types are listed and consist of devices that can be shoreline or off-shore. Many of these devices are still in the process of development. The oscillating water column type is still the only type that has gone into commercial operation in the UK and this is more extensively described.

A small-scale model of an oscillating water column system that has been built and tested in the University of Glasgow and some of the work on this is put forward here in terms of the water column operation.

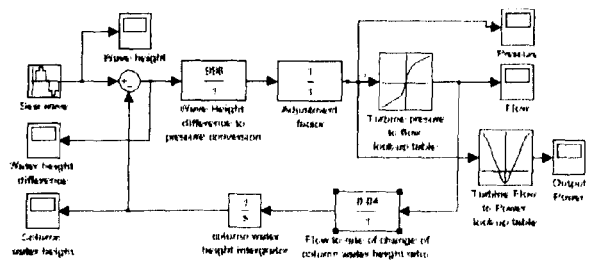

**Figure 9 Control strategy for oscillating water column**

## REFERENCES


1. Falnes, J. and Lovseth, J., *Ocean Wave Energy. Energy Policy*, 8, pp 768-775, 1991.
2. Pontes, M.T et al., The *European Wave Energy Resource*, 3rd European Wave Energy Conference, Patras, Greece, 1998.
3. Thorpe, T., *An Overview of Wave Energy Technologies: Status, Performance and Costs*, Wave Power: Moving towards Commercial Viability, 30 November, London, 1999.
4. Roger Dettmer, *Wave Energy Gets Seaworthy*, IEE Review, September 2000 pp 14-19
5. Thorpe, T., *The Wave Energy Programme in the UK and the European Wave Energy Network*, Fourth European Wave Energy Conference, Denmark, October 2000.
6. Thorpe, T et al., *Wave Energy in Europe: current status and perspectives*, Renewable and Sustainable Energy Reviews 6, pp 405-431, 2002.
7. Thorpe, T., *An Overview of Wave Energy Technologies: Status, Performance and Costs*, Wave Power: Moving towards Commercial Viability, 30 November, London, 1999.
8. Halliday, J. R. and D. G. Dorrell, *Review of wave energy resource and wave generator developments in the UK and the rest of the world*, IASTED International Conference on Power and Energy Systems, Rhodes, June 2004.
9. *Isay LIMPET Project Monitoring, Final Report*, ETSU V/06/00180/00/Rep. DTI Sustainable Energy Programme, UK.
10. Further details of "The Mighty Whale": www.jamstec.jp/jamstec/MTD/Whale/index.html www.jamstec.jp/jamstec/MTD/Whale/m-gal.gif
11. Raghunathan, S., *The wells air turbine for wave energy conversion*, Progress in Aerospace Sciences, Jan 1995.
12. Maeda, H., Santhakumar, S., Setoguchi, T., Takao, M., Kinoue, Y. and Kaneko, K., *Performance of an impulse turbine with fixed guide vanes*, Renewable Energy, Aug 1999.
13. D. G. Dorrell, M. Findlater and J. R. Halliday, *Performance Prediction of Small Fixed-Blade and Variable-Blade Wells Turbines Using Computational Fluid Dynamics*, submitted to the IMechE Proc Part A.

# The Application of Short-Term Deterministic Wave Prediction to Offshore Electricity Generation

J.R.Halliday[1], D.G. Dorrell[1] and A.R. Wood[2]

[1]Department of Electronics and Electrical Engineering
University of Glasgow, Oakfield Avenue, Glasgow, G12 8LT, UK
Tel: +44 141 330 2768, email: r.halliday@elec.gla.ac.uk, d.dorrell@elec.gla.ac.uk
[2]Dept of Electrical and Computer Engineering
University of Canterbury, Private Bag 4800, Christchurch, New Zealand
Tel: +64 (3) 3642-406 ext:6406, email: a.wood@elec.canterbury.ac.nz

**Abstract.** The field of wave energy extraction from the oceans is moving from the realm of drawing board dreams to the reality of device farms in the open ocean. Several devices are now at the stage of full scale testing and methods of increasing their economic potential are required. Maximum energy capture from a given sea state is one such way of increasing production and for devices to achieve this an accurate prediction of the sea surface elevation in the vicinity of these devices is required. The method proposed is based on the work of Belmont [1] and Zhang [2], extending from unidirectional modelling to directional. Preliminary simulations for a unidirectional buoy excited by a Pierson-Moskowitz spectrum are given and the proposed method for directional modelling is then set forth.

**Key words**
Wave Energy, Wave Prediction, Wave Modelling.

## 1. Introduction

For the past 30 years the field of wave energy has been gently progressing in the somewhat disjointed grouping of renewable energy research. The field was put into the spotlight during the oil crisis of the mid 1970's when Europe grew edgy over its dependence on Middle Eastern oil and looked for other means of generating electricity.

Before wind energy was given serious consideration the oceans, in particular the North Atlantic and to a lesser extent the Mediterranean Sea, were seen as a valuable resource. The energy off the West Coast of Scotland has some 50kW/m of wave front [3], with similar levels off the coasts of Ireland, France, Spain and Portugal. Many ideas proliferated during this time, but few went on to be developed and even fewer reached full scale implementation.

One of the greatest problems faced by the device teams was in making the devices strong enough to survive harsh offshore conditions while still being able to extract enough energy to make them economical. Of the devices developed in this era were Salter's Ducks, The Bristol Cylinder, The Cockerell Raft and many others which are described in [4].

The enthusiasm of the 1970's quickly waned as the price of oil fell and North Sea oil and gas came online. With a cheap and apparently plentiful supply of energy the plans of various governments for wave devices were dropped [5]. Interest has been renewed in the last decade with the rise of public interest in environmental concerns. Governments in Europe, recognising the political capital that could be gained from giving incentives to renewables, began funding various programs.

Incentives, such as the Kyoto agreement, have led to the setting of sweeping targets of renewable generation that some governments are committed to meet. For the UK the target varies between 15 and 40%, depending on which group the politician delivering their speech is addressing. The setting of the targets to be met has led an abundance of wind energy plants being erected. Wind energy is seen by the public as being green and the costs to the electricity companies are lower than for other devices. Whilst providing a suitably green image, the encroachment of windmills is beginning to be questioned by many concerned with the effects they will have on the countryside and particularly the tourism economy on which many rural areas depend. The dependence of large parts of the national grid on wind energy can also lead to shortfalls in supply with energy needing to be drawn from other countries.

Some of the money and incentives for renewable generation has trickled through to the field of wave energy and has been put to good use by the device teams based in Europe. Wavegen has developed the LIMPIT device and has plans for a redeployment of the OSPREY in the near future. The WaveDragon is undergoing sea trials, as is the Archimedes Wave Swing. The device on which the remainder of this paper will focus is the Pelamis (described in Section 2*C*).

Section 2 will give an overview of the short term wave prediction problem. Section 3 will give a basic description of the field of wave modelling. The proposed prediction method will be stated in Section 4 with a worked example and results in Section 5. The paper will finish with the conclusions of this initial research.

## 2. Short term wave prediction

*A. The European Wave Energy Network (EWEN)*
In 2003 a report was published by the European Wave Energy Network [6] described the work conducted on wave energy in the European Union. It covered areas such as farm siting, economic support for devices and future developments that would be required for wave energy to become profitable.

One of the areas which were recognised as requiring work was in the short term prediction of wave behaviour. Medium to Long term prediction is from 1hr to 1 week

ahead and is already a well developed field. The short term is from 10s to 1min ahead giving an accurate prediction of the surface elevation at a point on the sea surface.

Many of the devices which are being developed contain features which allow them to selectively change the frequency range over which they operate. A device such as an oscillating water column, on which much has been published, is essentially a large concrete box that operates at a fixed resonant frequency. Devices that float on the surface of the sea will also have a resonant frequency related to the specific dimensions of the device. For an oscillating water column this frequency can be changed by varying the pressure in the caisson by way of valves. For floating structures this is accomplished by varying fluid pressures in the mechanical connections of the device. In order to properly tune this resonance accurate information on the next expected wave is required. It is this information that is at present unavailable.

*B. Prior Work*

Work on short term prediction has taken place in the past with significant contributions from Zhang [2] and Belmont [1]. Zhang's 1997 paper demonstrated that a complex wave field can be decomposed into a specific set of wave trains using a maximum least likelihood approach. The resultant set of wave trains could then be used in making predictions of wave height in the vicinity of the measurements. The study showed that it was vitally important to retrieve the phase information for each wave train as well as the amplitude and frequency in order to make an accurate prediction of the surface elevation.

Belmont [1] went further with this method and has applied it to the prediction of wave elevation for use in the controlled landing of helicopters on ships. The main result of the paper is that a prediction can be made up to 30 seconds ahead from the point of data sampling. The method involved was based on the Discrete Fourier Transform and an adaptive windowing method of end fitting the raw sampled data.

*C. The Pelamis*

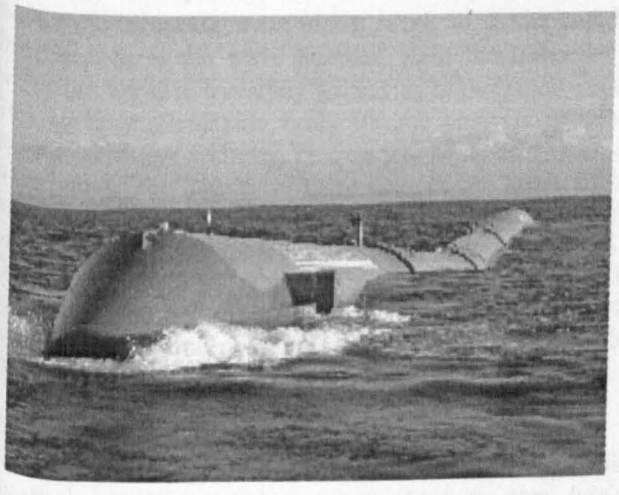

Fig. 1. A view of the Pelamis device

The Pelamis device has been developed by Ocean Power Delivery Ltd., a company based in Edinburgh and arose from the PhD theses of several students in the Wave Energy group at the University of Edinburgh. The device is shown in Fig. 1 and consists of four cylindrical sections joined at theirs ends by hydraulic rams. Its dimensions are 150m in length and 3.5m in diameter. The device was designed with survivability as its main goal and achieves this by being oriented lengthways into the prevailing wave direction and has the ability to de-reference itself in extreme wave conditions by its ability to duck underneath the highest of waves in a manner similar to a surfer getting out beyond the breakers on a beach. The resonance of the device can be varied by changing the resistance of the rams joining the sections. The resistance can be changed on a wave to wave basis and so that short term forecast will be of benefit.

Testing for the device has taken place of several small-scale models and at present a full-size test is ongoing at the EMEC test centre on the Orkney Islands. A possible farm design is planned for the Azores and it is at this stage of development that this research will focus on. Each device requires 150 m by 200 m of space in which to operate, so a 4-6 device farm would require 600-900 m by 200 m. The device has an optimum operating range for waves with a time period of 5 to 13 seconds, with a maximum output of 750 kW in seas of 5 m amplitude. It is envisaged that the device will be moored at the 50 m contour.

TABLE 1. Valid prediction distances at 30s

| Wavelength | Time Period | Wave Velocity | Valid Distance |
|---|---|---|---|
| 39m | 4.99s | 7.81m/s | 234m |
| 100m | 8.00s | 12.5m/s | 375m |
| 150m | 9.8s | 15.3m/s | 459m |
| 200m | 11.3s | 17.69m/s | 530m |
| 250m | 12.65s | 19.76m/s | 592m |

From Belmont [1] a valid prediction window of 30 sec ahead can be assumed for waves in the range in which the Pelamis is designed to operate. Using deep water wave equations and a range of 39-250 m, a valid prediction distance of 230 m from the point of sampling can be assumed for the shortest wavelength of interest to the device, given in Table 1. This should be a great enough distance to cover a device farm of 4-6 devices.

*D. Measurement*

Though the two methods used by Zhang and Belmont show that short term prediction is possible, the way in which the data was recorded in each of the papers is not economically viable for a wave farm.

In Zhang's experiments the data was recovered from an array of pressure sensors sited on an offshore platform. For a wave farm the cost of building an additional structure for the mounting of sensors is prohibitive. Pressure sensors are a possible alternative, but at a depth of 50 m will lose their accuracy at higher frequencies. The use of an array of wave rider buoys, recording the surface elevation is also an option but again the cost of sighting many buoys is expensive and

they would also pose a possible hazard if they were to break free.

Belmont's research uses a forward scanning LIDAR device. The LIDAR would be mounted onboard the ship on which a helicopter is to land and be orientated to face the direction of prevailing swell. At present the LIDAR device is able to distinguish a unidirectional wave train from a mixed sea and make a prediction. Unfortunately for an offshore wave farm there is no structure on which to mount a LIDAR and as with Zhang's method would prove uneconomical. This being said a LIDAR mounted on a shore-based device would be most useful.

In order to prove useful to the wave energy community this research focuses on existing measurement techniques using tried and tested equipment that is widely available. The goal is to make a prediction based on the readings of a directional wave buoy, which can be relatively cheaply moored and serviced.

## 3. Wave modelling

*A. The basics*

Interest in the modelling and prediction of the waves has existed since early civilisation but scientific study did not truly begin until after the Second World War when the landing of troops on the Normandy beaches was affected by the sea conditions. In the UK research took place at the National Institute of Oceanography, which was to become part of Southampton Institute of Oceanography.

A key realisation made by the scientists was that a complex sea can be approximated as the linear superposition of a large number of long crested periodic wave trains of low amplitude with different frequencies and directions of propagation all travelling independently of each other, A mathematical representation is given in Eqn. 1.

$$\zeta(x,y,t) = \sum_{n=1}^{\infty} a_n \sin(k_n x \cos\theta_n + k_n y \sin\theta_n - \omega_n t - \phi_n) \qquad (1)$$

where the subscript $n$ refers to the $n^{th}$ component, $\zeta$ is the surface elevation about mean sea level, $\omega_n$ is the angular frequency, $k_n$ is the wave number, $\theta_n$ is the direction in which the wave is travelling to and $\phi_n$ is the phase angle. This equation forms the basis for the analysis of wave records which are recorded by a variety of devices, such as wave buoys. The outputs of these devices can generally be transformed into a record of wave height and plotted against time. The records are then analysed, typically by means of a Discrete Fourier Transform, to give a spectral representation of a fixed time period, usually 1200 seconds. From these records various time period parameters are extracted to be used in further analysis.

*B. Deep water equations*

For small disturbances of the sea surface the hydrodynamic equations are linear and can be solved to give freely propagating, long-crested, sinusoidal wave trains.

In deep water (depth $h > \lambda/4$) the water particles travel in circular orbits with the particles moving forwards in the crests and backwards in the troughs. If the $x$ and $z$ displacements of a particle are $\chi$ and $\zeta$ from its rest position $x$ at a depth $z$ below the surface

$$\chi = ae^{kz}\cos(kx - \omega t - \phi) \qquad (2)$$

$$\zeta = ae^{kz}\sin(kx - \omega t - \phi) \qquad (3)$$

Where, $\omega^2 = gk$ is the dispersion relationship, $g$ is the acceleration due to gravity, $k$ is the wave number $k = 2\pi/\lambda$, $\lambda$ is the wavelength and $\phi$ is a random phase angle $= \pi < \phi < \pi$.

Equation 3 can be restated to include the effect of the direction of travel $\theta$

$$\zeta(x,y,z) = ae^{kz}\sin(lx + my - \omega t - \phi) \qquad (4)$$

where $l = k\cos\phi$ and $m = k\sin\phi$. An example showing a single wave train with $\lambda = 100m$ and $\theta = 0°$ is shown in the Fig. 2.

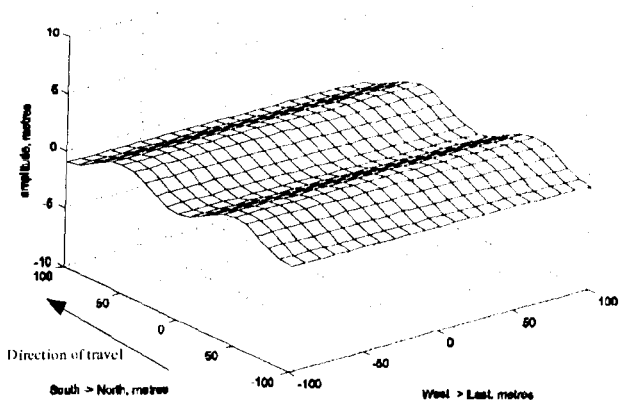


Fig. 2. A example of a wave train

*C Airy Equations*

In the case of the Pelamis device, which is to be situated in 50m depth the deep water equations will no longer strictly apply to the longer wavelengths and the Airy Equations must be used in predictions.

These equations were derived in 1845 by Sir G.B. Airy [7]. The equations for a small-amplitude sinusoidal wave in water of depth $h$ ($h$ is taken as positive, $z$ as negative: that is the point when $z + h = 0$ is the sea bed) are

$$\chi = a\frac{\cosh k(z+h)}{\sinh kh}\cos(kx - \omega t - \phi) \qquad (5)$$

$$\zeta = a\frac{\sinh k(z+h)}{\sinh kh}\sin(kx - \omega t - \phi) \qquad (6)$$

These basic equations are all in terms of the local wave number $k$, in practise the data available is usually the period

$T$ or the frequency $f$ as the phase velocity $cp = \lambda/T = \omega/k$, then

$$\omega^2 = gk \tanh kh \tag{7}$$

Figs. 3 and 4 show the difference in $k$ number between the deep water equations and the Airy formulation.

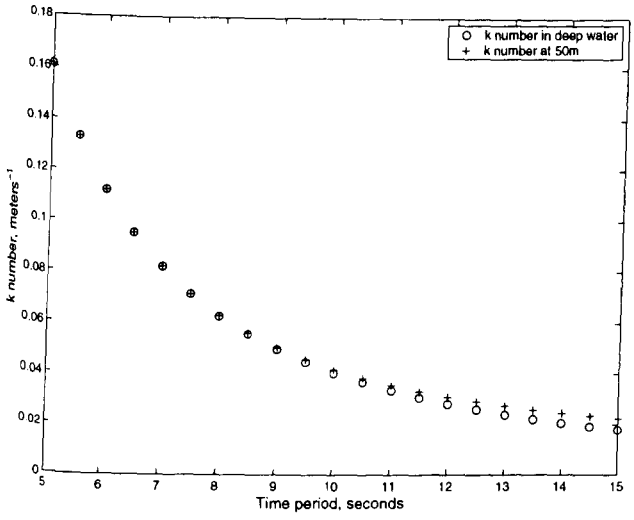


Fig. 3. $k$ number plotted against time period for deep water and airy equations at 50m

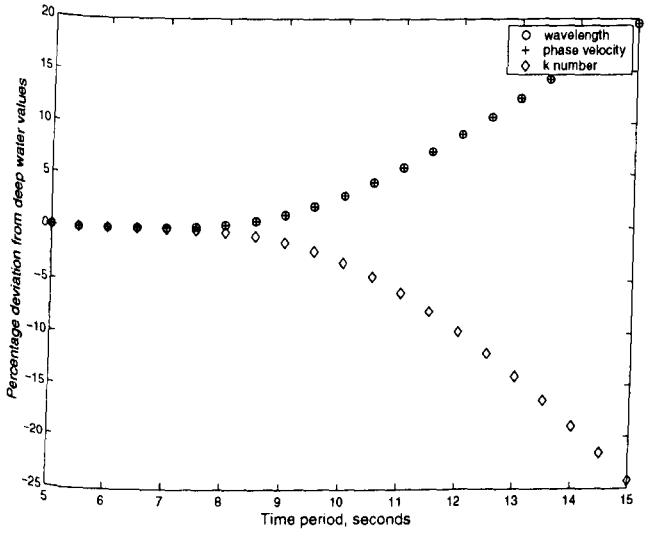


Fig. 4. Percentage deviation from deep water values of wavelength, phase velocity and $k$ plotted against time period

It can be seen that in deep water, where $\tanh(kh) \rightarrow 1$ the approximation $\omega^2 = gk$ is valid. As the water depth decreases the longer wavelengths will begin to feel the bottom. The effect of this is to slow down the phase velocity of the wave and to some extent cause the wave amplitude to increase. The effect of this is easily seen on any shallow sloping beach where the waves can be seen increasing in height as they approach the shore before eventually breaking.

For the Pelamis device we need to use the full Airy equations as for the longer wavelengths of interest the water in which the devices are situated is too shallow for the deep-water approximation to strictly hold true. As shown above the percentage deviations from the deep-water values increase for time periods greater than 7 sec. The most significant result from above is the change in phase velocity as the wave enters the shallower water. This is important in the prediction of waves as otherwise it would be assumed that the waves of a longer time period travel further that they actually would.

*D. The omni-directional spectral density function, S(f)*

$S(f)$ is called "the omnidirectional spectral density function" and has units of $m^2/Hz$. It is this function that is measured by a uni-directional wave buoy, such as Datawell's Waverider. This function forms the basis of wave measurement and prediction. The following gives the derivation of this function.

If the elevation of the sea surface is measured above a fixed point, (0,0), then Eqn. 4 loses its dependence on $x,y$ and reduces to

$$\zeta(t) = \sum_n a_n \sin(\omega_n t - \phi_n) \tag{8}$$

squaring this

$$\zeta^2(t) = \sum_n \sum_m a_n a_m \sin(\omega_n t - \phi_n)\sin(\omega_m t - \phi_m) \tag{9}$$

$$\zeta^2(t) = \sum_n \sum_m \frac{1}{2} a_n a_m \times \left\{ \begin{array}{l} \cos[(\omega_n - \omega_m)t + (\phi_n - \phi_m)] \\ -\cos[(\omega_n + \omega_m)t + (\phi_n + \phi_m)] \end{array} \right\} \tag{10}$$

Taking the long term average, components with $n \neq m$ become zero. Allowing $n = m$ and taking the long term average

$$E = \overline{\zeta^2(t)} = \sum_n \frac{1}{2} a_n^2 \tag{11}$$

That is, the variance of the sea-surface elevation equals the sum of the variances of its component wave trains. As the variance is proportional to the average energy per unit area of the sea surface, the total energy of the wave system is just the sum of the energies associated with individual wave trains.

If the output of a wave recording device is filtered to select only those frequencies in the range $f - \Delta f/2$ to $f + \Delta f/2$, giving a variance $\Delta E$, then a function $S(f)$ can be defined by

$$S(f) = \Delta E / \Delta f \tag{12}$$

$S(f)$ will remain finite as $\Delta f \rightarrow 1$ and from this it can be seen that

$$E = \int_0^\infty S(f)df \tag{13}$$

In practise it is not possible to continuously sample the sea surface elevation and an estimate has to be made for a finite

period of time/space, this is distinguished as $\hat{S}(f)$. An example of an omni-directional Pierson-Moskowitz spectrum [11] for a fully developed sea is given in Fig. 5.

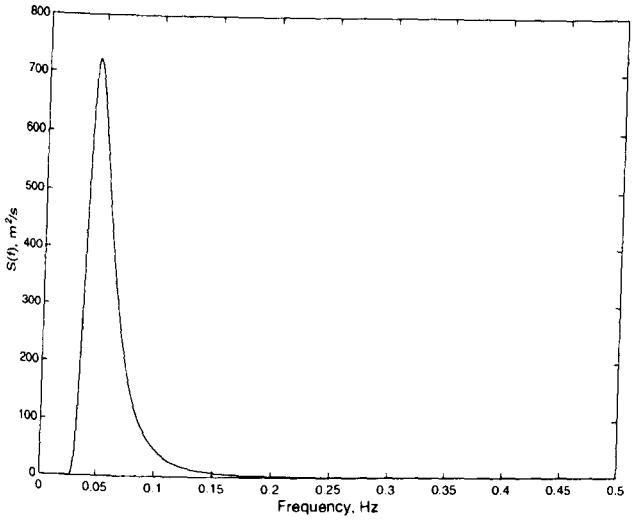


Fig. 5. Example of an omni-directional spectrum

Such spectra are derived from the Fourier transform of a recorded time series.

The estimate $\hat{S}(f)$ of the spectral density is obtained by summing the variances ("energies") of all the Fourier components within the chosen spectral resolution $\Delta f$

$$\hat{S}(f)\Delta f = \tfrac{1}{2}\sum_{\Delta f}(a_n^2 + b_n^2) \tag{14}$$

For example, if a record 1000 sec long were available, the harmonics would be spaced at 0.001 Hz intervals. If a spectral resolution of 0.01 Hz were required, then the harmonics would be summed in groups of 10 to give the spectral estimates.

*E. Spectral Moments*

Some definitions and statistical results, as used by the oceanographic community, are expressed in terms of the spectral moments of the spectral density function $S(f)$. The $n^{th}$ spectral moment is given by

$$m_n = \int_0^\infty f^n S(f)df \tag{15}$$

The spectral moment can be thought of as a frequency scaled version of the spectral density function, with the error associated with its calculation increasing with higher orders. The $0^{th}$ spectral moment is equivalent to the variance of the spectrum and is commonly used to calculate the expected significant wave height, $H_{m0} = 4\sqrt{m_0}$.

*F. The Directional Spectrum, $S(f,\theta)$*

Eqn. 11 can also be derived from Eqn. 1, incorporating wave direction, $\theta$. If you were now able to filter in the directional wave trains, those travelling between $\theta + \Delta\theta/2$ and $\theta - \Delta\theta/2$ as well as in frequency, then by analogy to Eqn. 12, a directional spectral density function $S(f, \theta)$ can be defined as

$$S(f,\theta) = \frac{\Delta E}{\Delta f \Delta\theta} \rightarrow \frac{d^2E}{df d\theta} \tag{16}$$

It is usual to define $S(f,\theta)$ as the product of the omnidirectional spectrum $S(f,\theta)$ and a normalised directional distribution $G(\theta)$, that is

$$S(f,\theta) = S(f)G(\theta) \tag{17}$$

So that

$$\int_0^\infty G(\theta)d\theta = 1 \tag{18}$$

In fact, $G(\theta)$ varies with frequency and will therefore be represented by $G(\theta f)$. Established methods of measurement do not give estimates of $G(\theta f)$ directly. In order to interpret such measurements usefully, it is usually necessary to make assumptions about the shape of the directional spread. The form that is most commonly used is

$$G(\theta, f) = F(s)\cos^{2s}\tfrac{1}{2}(\theta - \theta_1) \tag{19}$$

where $\theta_1$ is the predominant direction, and $s$ is known as the shape function. $s$ is a function of frequency according to Pierson-Moskowitz [11] and $\theta_1$ in this paper is not frequency dependent. An example of this function is shown in Fig. 6.

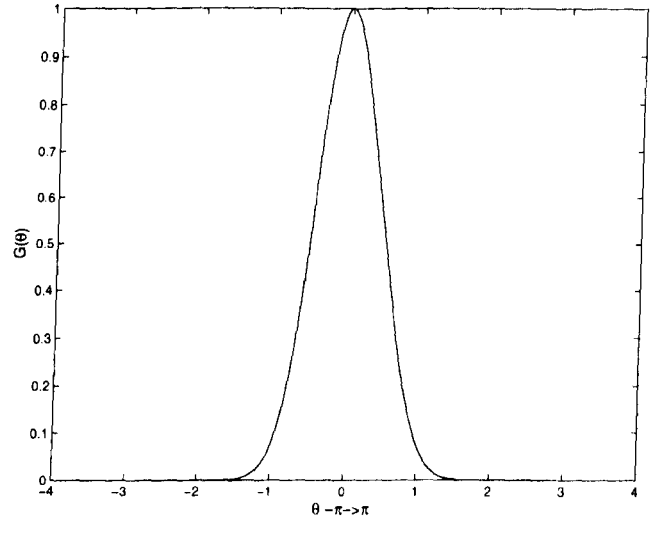


Fig. 6. Example of the directional spreading function with $s$ = 10

These equations were first used by D.E. Cartwright [8]. $s$ and $\theta_1$ are estimated from measurements. Usually two independent estimates can be obtained of each parameter at each frequency, which in principle allows a check as to whether the assumed form is correct or not.

## 4. Proposed method of prediction

The method of prediction is to record the wave elevation time history at a fixed point, (0,0). This time history is then Transformed to the frequency domain; an omni-directional spectrum created and the spectral moments stored.
The amplitudes and phases of this transform are then used to create a number of wave trains. These wave trains are then propagated to the prediction point (0,250) and the time history at that point recorded. Again the time history is transformed to the frequency domain and the omni-directional spectrum and spectral moments stored.
At the prediction point the time history and thus the spectrum and spectral moments should be available for comparison with the predicted results. Whilst having this information for two closely situated buoys would be desirable, none is available. Therefore, the data at the origin and prediction point will be derived from the same spectrum.

## 5. An omni-directional prediction example

It is proposed that a wave spectrum based on the Pierson Moskowitz [11] formulation for a fully developed sea at a wind speed of 30 m/s will be created. This spectrum will be broken down into a number of unidirectional wave trains. The wave trains will then be used to simulate the elevation of the sea a two points, one above the origin and representing the output of the wave rider buoy and the second taken at a distance of 250 m from the origin and will represent the target point of prediction.

The simulated wave record taken at the origin will be examined and spectral parameters recorded. This simulated spectrum will in turn be broken down into a number of wave trains and propagated to the prediction point. A new wave record will be recorded at the prediction point. The wave record will then be compared to the expected wave record.

*A. The input wave trains*

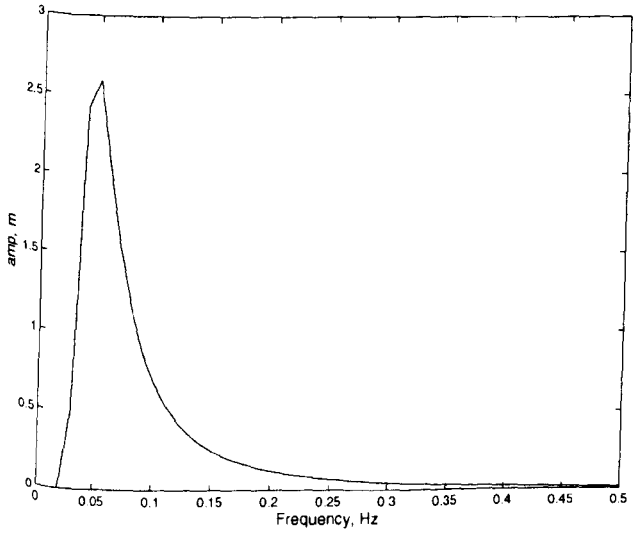


Fig. 7. Showing the amplitudes of the simulated wave trains

The spectra used to generate the input wave trains is the Pierson-Moskowitz formulation, given in Eqn. 30

$$S(f) = \alpha_{PM} g^2 (2\pi)^{-4} f^{-5} \exp\left[-\beta (f_0 / f)^4\right] \tag{30}$$

where

$\alpha_{PM} = 0.0081$ is empirically derived

$\beta = 0.74$ is empirically derived

$f$ = frequency

$f_0 = g/(2\pi U_{19.5})$ where $U_{19.5}$ is the wind speed recorded at 19.5 m.

The spectrum for $U_{19.5} = 30$ m/s is shown in Fig. 6 for 1000 wave vectors and $\Delta f$ = 0.0005 Hz and approximates to a continuous omni-directional spectrum $s(f)$.

In order to run the simulation the number of wave vectors must be reduced to 50 and $\Delta f$ increased to 0.01 Hz giving $\hat{S}(f)$. The equation to produce a list of amplitudes for each wave vector is:

$$C_j = \sqrt{\hat{S}(f_j)\Delta f} \tag{31}$$

This is shown graphically in Fig. 7.

From this list of amplitudes and frequencies the full Airy equations, Section 3.C, must be used in calculating the wavelengths, wave numbers and phase velocities of each component.

In addition to the spectra, the amplitudes, frequencies, spectral moments and derived time period parameters are also calculated for stored for later comparison. The discrete version of Equation 14 is

$$\hat{m}_p = 1/2 \sum_n f_n^p c_n^2 \tag{32}$$

*B. Data Generation*

Wave records taken in the field are often standardised to be 1200s in length and sampled at 3.4133 Hz to give 4096 samples. This is the pattern that will be used here.

The wave vector file generated in the previous section is opened and the parameters loaded in the MATLAB work space. A file containing the position of the sensors is also opened. For the sensor at (0,0), the recording point, and (250,0), the prediction point, the wave records are calculated using Eqn. 1.

The phase component $\phi_n$ is taken as being random and to some extent will simulate the random nature varying nature of the ocean, at a later time the effect of sea bed bathymetry and wave-wave interactions will also need to be modelled. The record for buoy 1 is generated from -1200 to 0 seconds, in order for it to have been a past record. The record at the prediction point is taken from 0 to 1200 seconds and will become the target wave record which we will be attempting to reproduce.

*C. Analysis and Prediction*

The first stage in processing a wave record is to filter out any low frequency components relating to tidal patterns. Filtering is also required to remove any high-frequency components of the wave record. In Scottish waters 0.5 Hz is a generally accepted cut-off frequency.

The time series is analysed using an FFT into 4096 frequency components at 0.0008333 Hz intervals. The negative frequencies are folded into the positive half of the spectrum reducing the number of frequency bins to 2048 with an upper frequency limit of 1.7 Hz.

The complex amplitude and phase data for the record taken at the origin is shown in Fig. 8.

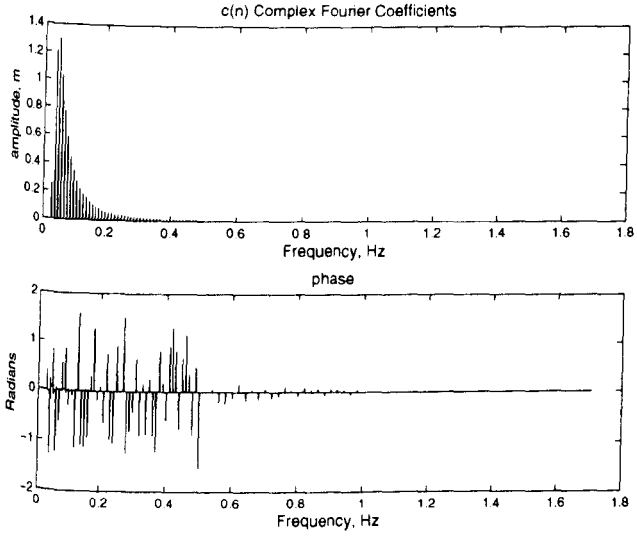


Fig. 8 The complex amplitude and phase information for the origin wave record

In the next stage of prediction the amplitude and phase information taken at the origin is used with the Airy wave equations, Section 3*C*, to create a sequence of wave trains. These wave trains are then used to calculate the time history for the prediction point. The spectra and spectral moments are then calculated with the resultant spectra shown in Fig. 9.

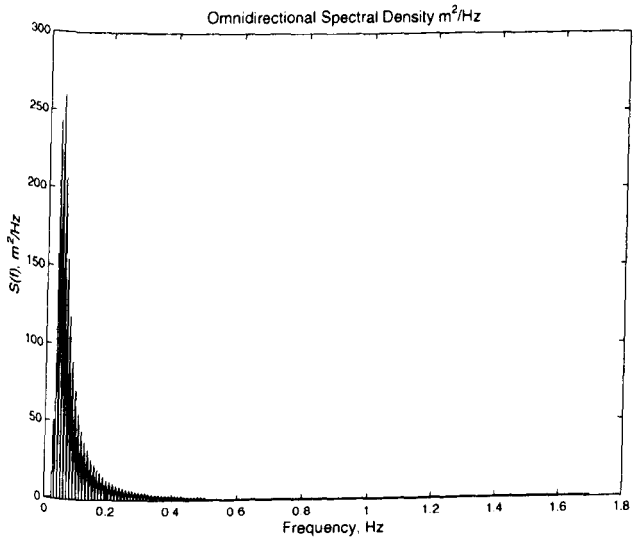


Fig. 9. Resultant omni-directional spectra for prediction point

*D. Results*

Tables 2 and 3 show the results for the comparison of various spectral parameters taken from the target spectrum and the one predicted using the previous method.

TABLE 2. Spectral moment comparisons

| | M0 | M1 | M2 | M3 |
|---|---|---|---|---|
| Target | 11.51 | 0.68 | 0.047 | 0.0041 |
| Prediction | 4.179 | 0.425 | 0.075 | 0.021 |
| Error % | 63.69 | 37.5 | -59.57 | -412.2 |

TABLE 3. Time period comparisons

| | Hm0 | Tz | T1 | TE | Tc |
|---|---|---|---|---|---|
| Target | 13.573 | 15.652 | 0.059 | 18.78 | 11.214 |
| Prediction | 8.177 | 7.443 | 0.102 | 15.09 | 3.603 |
| Error % | 39.75 | 52.45 | -72.88 | 19.65 | 67.87 |

As can be seen the results are not great. In [9] the errors associated with the discretizing of spectral moments were found to be great when compared to continuous spectra and this is possibly not the best of methods for comparing prediction results.

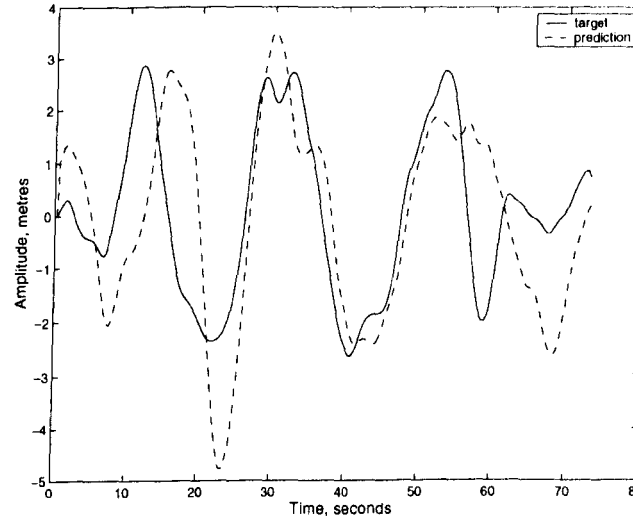


Fig. 10. Comparison of the time records for the target and prediction

Fig. 10 shows a comparison of the target wave record and the prediction made for the first 80 seconds. There would appear to be some identical features to the two records, in particular the average time period of the waves, but overall it is a poor match.

## 5. Further work

The problem with the prediction method as it stands may lie in the assumption that $\phi$ can take a random value. Zhang [2] takes a different approach using a maximum likelihood method to calculate the prediction parameters. Use of this method may lead to a better prediction.

The methods given in Tucker [9] also go further in eliminating spectral defects in the Fourier method which have as yet not been implemented.

Belmont [1] uses an adaptive windowing method to ensure that the wave record being processed by the FFT has no abrupt changes between the beginning and end of the record. This methodology would reduce some of the error in generating the phase information required for an accurate prediction.

When the omni-directional prediction has been made more accurate the problem of directional prediction will be tackled. The simulation of a directional wave buoy is already implemented with the analysis of the returned data yet to be completed but, it is expected that an omni-directional spectrum, $S(f)$, and a set of directional spectrums, $G(\theta,f)$, will be generated. From this data a sequence of wave trains can be produced and propagated to give a prediction at a point near to the origin.

A further avenue of exploration is in the use of data from the wave devices themselves. The devices will be able to record their orientation, relative motion between segments and various electro-mechanical data. From this information it is hoped that wave elevation and surface displacement in the vicinity of the device would be able to be calculated.

The prediction generated from a wave buoy situated near the wave devices could then be checked against the information from the devices, adjusted and then passed to other devices in the farm.

## 6. Conclusion

Initial research into the short term deterministic prediction of wave behaviour has been given and future paths have been laid out. While initial predictions are not great, with some more experimentation the methodology would appear to be useful and to be extendable to directional predictions.

A further course that may be followed if this methodology should fail would be to look closely at one of the third generation wave models [10] to see if they can be reduced to a scale small enough for a single wave farm. The output of a model of the North Western Atlantic at a large scale could then be used to drive this smaller model reinforced with data collected from a directional wave buoy moored in close proximity to the wave device farm. While not giving an accurate prediction of surface elevation, the spectral outputs of these models could be used to feed the devices general estimates of wavelength and wave height, which would then be used to self tune the devices to a prevailing sea state.

The usefulness of these predictions to wave energy devices would enable them to increase efficiency and thereby lower the cost of the electricity produced, hopefully to a level where it will be competitive with current thermal and renewable sources.

## References


[1] M.R. Belmont, E.L. Morris and H.K. Zienkiewicz, "Short term forecasting of the sea surface shape", Int. Shipbuild. Progr., **45**, no. 444 (1998) pp. 383-400.

[2] J. Zhang and I. Preslin, "Deterministic decomposition of deep water short-crested irregular waves", Journal of Geophysical Research, (1997) Vol. 102, No. C6, pp 12677-12688.

[3] S.H. Salter, "Wave power", (1974) Nature, Vol. 249, June 21st 1974, pp. 720-724.

[4] J.R. Halliday and D.G. Dorrell, "Review of wave energy and wave generator development in the UK and the rest of the world", IASTED International Conference on Power and Energy Systems, Rhodes, June 2004.

[5] P.G. Davis, M.S. Cloke, K.A. Major, D.I. Page and R.J. Taylor (ed), "Wave Energy", ETSU R-26, ETSU for the Department of Energy, Harwell, 1985.

[6] European Wave Energy Network, "Results from the work of the European Thematic Network on Wave Energy", European Community ERK5-CT-1999-20001, March 2003

[7] Sir G.B. Airy, "Tides and waves", Encyclopaedia Metropolitania, 1845

[8] D.E. Cartwright, *in* Ocean Wave Spectra, "The use of directional spectra in studying the output of a wave recorder on a moving ship", pp 203-218, Prentice-Hall, Englewood Cliffs, N.J., 1963

[9] M.J. Tucker and E.G. Pitt, "Waves in Ocean Engineering", volume 5 of Elsevier Ocean Engineering Book Series, Elsevier Science Ltd. 2001

[10] N. Booj, R.C. Ris and L.H. Holthuijsen, 1999, "A third-generation wave model for coastal regions, Part I, model description and validation", J. Geoph. Research, C4, 104, pp 7667-7681.

[11] W.J. Pierson and L. Moskowitz, 1964, "A proposed spectral form for fully developed wind seas based on the similarity theory of S.A. Kitaigorodskii", J. Geophysical Research, 69, pp 5181-5203.

# Development of Small-Scale Facilities for Initiating Studies into Sea Wave Energy Generation

D G Dorrell[1], R Halliday[1], S. McLean[2], P. Miller[1] and F. Santamaria Mosquera[1]

[1]Department of Electronics and Electrical Engineering
[2]Dept of Civil Engineering
University of Glasgow, Oakfield Avenue, Glasgow, G12 8LT, UK
Tel: +44 141 330 2768, email: d.dorrell@elec.gla.ac.uk

**Abstract.** This paper describes the preliminary work carried out within the Civil and Electronics and Electrical Engineering Departments of The University of Glasgow. Two experimental pieces of equipment are described; the first is a piston-type of device suitable for testing small turbines in an oscillating water column system. The second is the conversion of a water flume into a wave tank for use in tests of small wave generator models and wave prediction systems.

**Key words**
Wave energy, oscillating water column, wells turbine, flume, wave tank.

## 1. Introduction

Recently there has been new research projects instigated in the Electronics and Electrical Engineering Department of the University of Glasgow [1-4]. These have been aimed at investigating small wave generator models. The first set of results [1] were obtained from a small oscillating water column with a Wells turbine which was tested in a wave tank available in the Marine Engineering Department at Glasgow University (Fig 1). This has the problem that, even though the water column is small, the facility is large (tying up facilities) and steady-state operation is difficult since, even with a good beach, there are reflections, so that the maximum number of waves in any one run is about thirty.

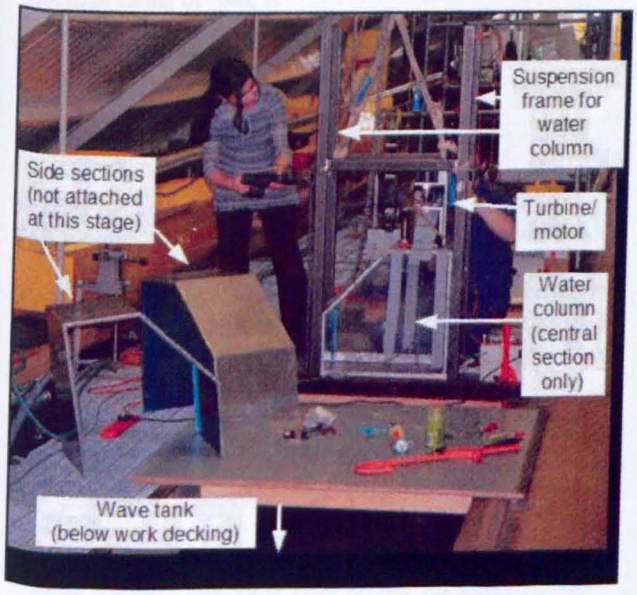


Fig 1 Initial oscillation water column testing in wave tank

It was decided to decouple the turbine from the water column and build a piston to test the turbines separately. Also it was decided to develop a flume, normally used in river flow and tidal studies, into a test bed for small wave generator models and for studies into short-term wave prediction methods. The advantages with the flume arrangement are that it was available locally in the adjoining Department of Civil Engineering and also the cost of developing the wave tank is relatively low and during testing there is no requirement to have technician assistance available – either for technical help or to satisfy health and safety requirements. These facilities, and initial experimental results, are described here.

## 2. Turbine test bed

This was designed to allow the testing of turbines of a diameter of up to about 200 mm. Fig 2 shows the basic dimensions of the test bed developed to test the turbines.

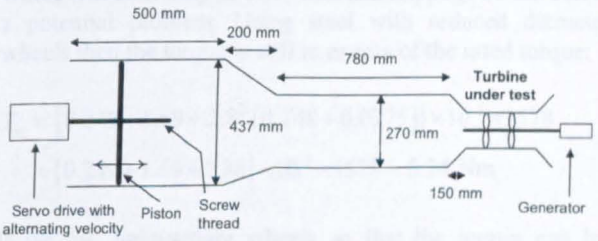


Fig 2 Dimensions of turbine piston test bed

The large piston has a diameter of 437 mm and a stroke of about 250 mm. The maximum frequency is designed to be about 0.5 Hz which requires the drive to be low inertia and high torque. Two photographs of the system during the manufacturing and initial testing are shown in Figs 3 and 4.

Fig 3 shows the turbine located on the left-hand side. The performance assessment of the initial Wells turbine designs (both using CFD and by measurement) are given elsewhere [2][4]. It was found that the Wells turbine had a Reynolds number that was far too low for this size. The performance could be improved using swivelling blades and there is also a program to investigate an impulse turbine.

The energy in the wave front in deep water is obtained from the equation

$$P = \frac{\sigma g^2 H^2}{32\pi f} = \frac{981.2H^2}{f} \quad \text{W/m} \qquad (1)$$

where $H$ is the wave height, $f$ is the frequency, $\sigma$ is the density of sea water (1025 kgm$^{-3}$) and $g$ is gravity. It can be seen that the power increase with wave height squared but is inversely proportional to the frequency. The Wells turbine under test operated well at a frequency of about 0.55 Hz. If oscillations inside the cylinder are about 250 mm then the external waves would have a minimum of about 111 W/m (though they are likely to be higher than this since the internal water level in a chamber may not oscillate at the same amplitude as the external water height in an actual column. Using the diameter of the cylinder as the width of water front then this would be a resource of 48.5 W. If we aim for a 50 % conversion factor then we wish to obtain about 24 W maximum out of the turbine. This is still to be achieved in the initial wave-tank tests since the turbine design is still being developed.

It can be seen in Fig 4 that the servo drive is connected by a belt; this was the initial design that utilised a servo drive already available in the laboratory. However this system is still under investigation since the load requirement for this system set-up is quite demanding. This is illustrated below. The thread of the piston screw is 2.5 mm so that for a 250 mm oscillation 100 turns are required which is 200π radians. Therefore, for a sinusoidally-oscillating system

$$\theta_{sh}(t) = 100\pi \sin(2\pi f_w t) \quad \text{rad} \qquad (2)$$

where $\theta_{sh}$ is the shaft angular position and $f_w$ is the wave frequency. The piston shaft rotational velocity is

$$\omega_{sh} = \frac{d\theta_{sh}(t)}{dt} = 200\pi^2 f_w \cos(2\pi f_w t) \quad \text{rad/sec} \qquad (3)$$

which, in terms of rpm, is

$$N_{sh} = \frac{60}{2\pi} \times 200\pi^2 f_w \cos(2\pi f_w t)$$

$$N_{sh} = 18850 f_w \cos(2\pi f_w t) \quad \text{rpm} \qquad (4)$$

At a frequency of 0.6 Hz (say to give some margin) then the peak speed is 11310 rpm. The maximum speed of the drive motor is 4000 rpm, hence gearing is required. The correct gearing should be at least 2.83. However the inertia of the system has to be considered. If we consider the solely the motor then the acceleration is

$$\frac{d\omega_m}{dt} = \frac{1}{K_{gear}} \frac{d\omega_{sh}}{dt} = -\frac{400\pi^3 f_w^2}{K_{gear}} \sin(2\pi f_w t) \quad \text{rad/s}^2 \qquad (5)$$

which gives a peak acceleration of 1578 rad/s$^2$. Ignoring friction, windage and other load losses, the equation for the torque is approximately

$$T_m = J \frac{d\omega_m}{dt} \quad \text{Nm} \qquad (6)$$

The motor inertia is quoted as $0.249 \times 10^{-4}$ Kg/m$^2$ so that the required torque is 0.39 Nm. However, the inertia of the steel shaft and the gearing has to be included. The shaft is 1.2 m long with a diameter of 20 mm. The mass is then $1.2 \times \pi D^2/4 \times \rho = 2.95$ Kg (where ρ is 7833 Kg/m$^3$), therefore the inertia = $0.5 \times 2.95 \times 0.01^2 = 0.148 \times 10^{-4}$ Kg/m$^2$. If the belt wheel of the motor is 22 mm wide and 200 mm in diameter then the mass is 5.41 Kg if made from steel giving an inertia of $0.5 \times 5.41 \times 0.1^2 = 27 \times 10^{-4}$ Kg/m$^2$. The belt wheel of the shaft will then be 71.4 mm to give the correct ratio so that the weight is 0.69 Kg giving an inertia of $0.44 \times 10^{-4}$ Kg/m$^2$.

The inertia is multiplied by the square of $K_{gear}$, i.e., the torque equation is modified to:

$$T_m = J_m + J_{g1} + K_{gear}^2 (J_{sh} + J_{g2}) \frac{d\omega_m}{dt} \quad \text{Nm} \qquad (7)$$

$$T_m = \{0.249 + 27 + 2.8^2 (0.148 + 0.44)\} \times 10^{-4} \times 1578$$
$$= \{0.249 + 27 + 4.6\} \times 10^{-3} \times 1578 = 50.2 \text{ Nm}$$

This clearly shows the problem with the system as being the diameter of the motor drive wheel. Its inertia clearly puts the torque beyond the 3.39 Nm rating of the motor. If the diameter is halved then the weight will decrease by 4 and the inertia by 4×4 = 16. However the diameter of the shaft wheel will then only be 35.7 mm and slippage of the belt is a potential problem. Using steel with reduced diameter wheels then the torque is still in excess of the rated torque:

$$T_m = \{0.249 + 1.69 + 2.8^2 (0.148 + 0.0275)\} \times 10^{-4} \times 1578$$
$$= \{0.249 + 1.69 + 1.38\} \times 10^{-3} \times 1578 = 5.24 \text{ Nm}$$

If we use light-weight wheels so that the inertia can be neglected then:

$$T_m = \{0.249 + 2.8^2 (0.148)\} \times 10^{-3} \times 1578$$
$$= \{0.249 + 1.16\} \times 10^{-3} \times 1578 = 2.22 \text{ Nm}$$

Therefore the rating of this motor is marginal. A chain drive would add too much inertia so that a belt drive with light-weight pulley wheels, or a lightweight gearing system, is required. In addition, there are friction and windage losses as well as the load of the piston due to the compression and vacuuming of the chamber. The piston itself is quite light. An alternative is to use a crank arrangement although this would cause problems if none-sinusoidal movement is required in order to put wave harmonics into the system. The correct drive is currently being investigated.

Fig 3 Turbine test bed in manufacture

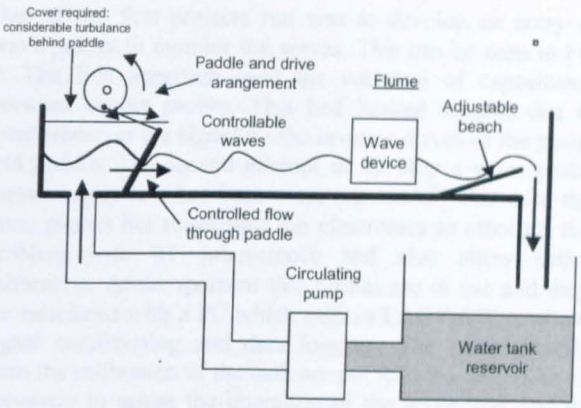


Fig 5 Flume arrangement with paddle

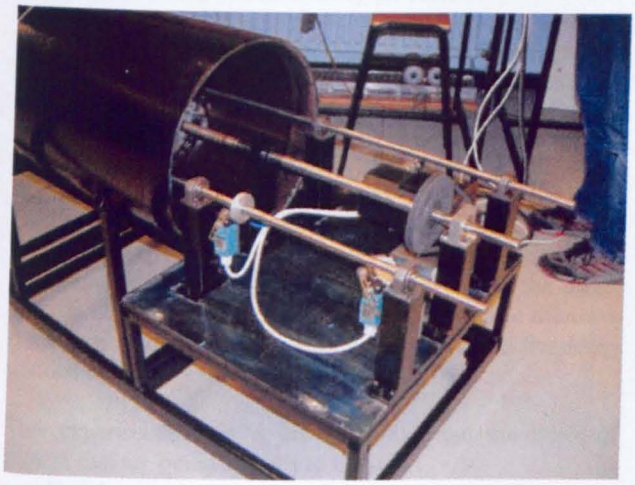

Fig 4 Turbine test bed with first drive fitted

Fig 6 Paddle arrangement of flume

The advantages of this system are that testing of the turbine can be conducted under controlled conditions and the piston fully calibrated and instrumented to measure chamber pressures and even flow rates. The resources required to use this equipment are also minimal.

## 3. Flume Wave Generator

*A. Practical arrangement*

A flume in the Department of Civil Engineering of the University of Glasgow has been modified to deliver waves under continuous conditions. The flume is usually used for experimental work into river and tidal flows. However, if a beach is located at the down-stream end and a paddle at the up-stream end then the flume can be used to produce waves with the beach being overtopped so that there is little wave reflection; a diagram is shown in Fig 5 for this arrangement.

Fig 6 shows photographs of the paddle arrangement. This is now totally enclosed due to water splashing and further modification is expected as described below. Fig 8 shows the flume when producing waves. Fig 9 shows a typical project with a student developing a wave measurement system using an array of wave probes.

*B. Dimensions of flume and paddle arrangement*

The flume is about 10 m in length with a width of 890 mm and a depth of about 300 mm to 400 mm depending on the height of the beach. A list of dimensions is given in Table I with a key in Fig 7.

Table I

| | | |
|---|---|---|
| Flume length for paddle to beach | Lt | 7.2 m |
| Back tank length | Bt | 3.2 m |
| Back tank width (not shown) | | 1.4 m |
| Fume height | Ht | 460 mm |
| Beach height | Bh | Adjustable (set to 275 mm in tests below) |
| Beach length | Bl | 350 mm |
| Paddle height | Ph | 450 mm |
| Paddle width (not shown) | | 830 mm(30 mm gaps either side) |
| Flume width (not shown) | | 890 mm |
| Paddle drive arm | Pa | 600mm (adjustable) |
| Drive wheel axis height | Wh | 710 mm |
| Horizontal distance between drive wheel axis and paddle hinge | Cl | 510 mm |
| Drive wheel torque arm length | Ta | Adjustable |

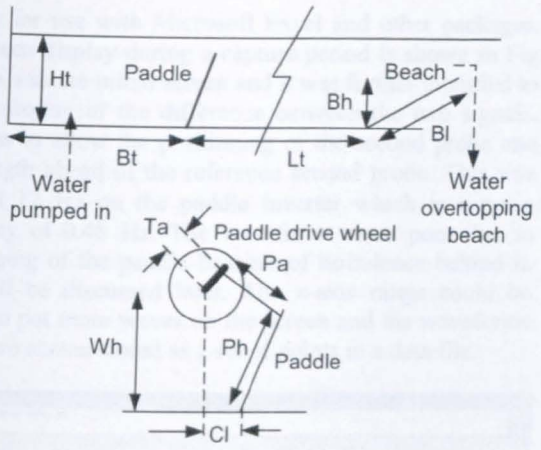


Fig 7 dimension key for Table I

Initially it was envisaged that the circulating pump could be pulsed to produce waves; however under test this was found to be impractical, therefore the paddle method of wave production was developed. The paddle drive wheel is driven by a 2-pole inverter-drive 0.75 kW induction motor with a step-down gearbox with a ratio of 25. At full load the speed drop of the motor is about 200 rpm however this would only be at a high drive wheel torque arm radius – in reality this is not normally used and at low torque arm length the motor will run close to the synchronous speed. Therefore the wave frequency will be approximately the inverter frequency divided by 25.

This experimental rig is cost effective and the types of project that are being applied to include:

- Development of wave probe array systems for use of short-term wave deterministic algorithms
- Small-scale wave generator models

This system is smaller in scale that a wave tank used in marine engineering departments for testing ship hulls etc and requires much less resourcing. The flume is shown working in Fig 8.

Fig 8 Waves in Flume

One of the first projects run was to develop an array of wave probes to monitor the waves. This can be seen in Fig 9. The first approach used the variation of capacitance between copper probes. This had limited success due to interference in the signal by the inverter drives of the pump and paddle. The second attempt to develop a wave probe measuring system has been more successful. This used the same probes but reassessed the electronics to alleviate the problem with RF interference and also allow better calibration. At the moment two probes are in use and they are interfaced with a PC which utilises LABVIEW to allow signal conditioning and data logging. The initial results from the calibration of the tank are put forward here. This is necessary to assess the operation of the wave tank and to find a good operating range of the system. Also some interesting problems were discovered.

Fig 9 Student developing wave probe arrays

## 4. Flume Calibration

*A. Initial settings*

The beach height was set to about 280 mm. With the flume pump running then the flat-calm water height was about 300 mm; the pump is adjusted during wave operation in order to keep the beach top at the level of the wave trough when the waves are overtopping, i.e., the top occasionally breaks the water surface. Two wave probes were used, these both being set one third the way across the flume at 330 mm from the tank side, One was kept at a constant position from the beach while the other was moved in order to find the wavelengths and also to assess the attenuation of the waves over one wavelength. The reference probe was located 1600 mm from the front hinge of the beach. It was decided to investigate waves at different drive wheel torque arm setting of 150 mm, 100mm and 50 mm. It was envisaged that the higher torque arm lengths would be suitable for the low frequency waves while short torque arm lengths would be suitable for the higher frequency waves. This was not found to be necessarily the case.

*B. Data acquisition*

The signals from the probes were conditioned and fed into a PC with the results illustrated using LABVIEW. The signals were digitized with a constant sampling rate. This also allowed the signals to be uploaded in the form of data files

suitable for use with Microsoft Excel and other packages. The screen display during a capture period is shown in Fig 10. This was the initial screen and it was further modified to gave a display of the difference between the two signals. This was to allow the positioning of the second probe one wavelength ahead of the reference second probe. This was taken at 12 Hz on the paddle inverter which is a wave frequency of 0.48 Hz. The waveforms were poor due to overtopping of the paddle because of turbulence behind it. This will be discussed later. The x-axis range could be altered to put more waves on the screen and the waveforms on the two screen stored as a set of points in a data file.

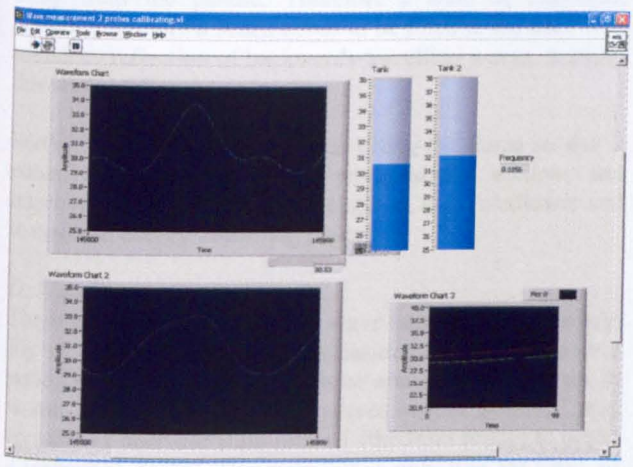

Fig 10 LABVIEW screen

*C. Investigation into wavelength and water depth*

The flume itself is not very deep and the range of wavelengths available may well fall into the category of "shallow" water, i.e., when the depth is less than a quarter of the wavelength. In deep water the wavelength is given by

$$L = \frac{g}{2\pi f^2} = \frac{1.56}{f^2} \quad \text{m} \tag{8}$$

and the velocity is

$$V = \frac{g}{2\pi f} = \frac{1.56}{f} \quad \text{m/sec} \tag{9}$$

As the waves get closer to shore the depth becomes shallower and the motion of the waves becomes more elliptical and poorer in quality. In shallow water, if the depth $D$ is less than a quarter of the wavelength $L$ then the velocity is

$$V = \sqrt{gD} = 3.13\sqrt{D} \quad \text{m/sec} \tag{10}$$

so that the wavelength in shallow water becomes

$$L = \frac{\sqrt{gD}}{f} = \frac{3.13\sqrt{D}}{f} \quad \text{m} \tag{11}$$

The best results were obtained when the torque arm length was 50 mm, some results were also obtained at 100 mm (larger waves) but it was found that at 150 mm the wave quality was low and there was overtopping of the paddle so that only one point was obtained. Fig 11 shows the wavelengths described by equations 8 and 11 for deep and shallow water and the wavelengths of waves measured for a torque arm length of 50 mm. It can be seen that the wavelength initially follows the shallow wavelength but as the frequency increases, and the wavelength shortens, the flume begins to act as a deep water channel. Discrepancies could be due to several reasons, firstly measuring the wavelengths by placement of wave probes one wavelength apart is not easy, especially when the waveforms are not pure sine waves. In addition, the wave frequency is obtained by assuming the paddle drive is operating at the synchronous speed. Obviously further work is needed here to measure the paddle frequency directly.

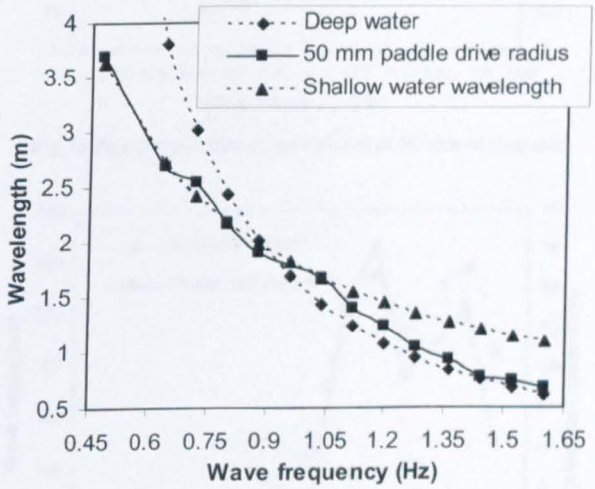


Fig 11 Comparison of measured wavelengths with deep and shallow wavelength predictions

Different wave heights can be obtained by altering the torque arm length. This does make a slight difference as shown in Fig 12 where the 50 mm and 100 mm measurements are shown for comparison; however these are small, with the waves tending to shorten in wavelength as the wave height increases.

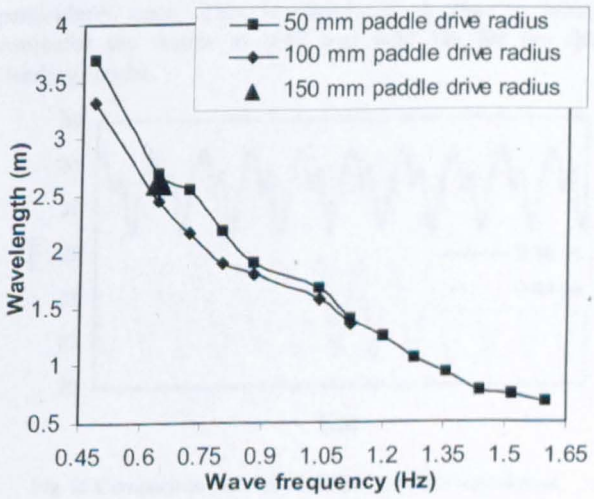


Fig 12 Comparison of wavelengths with different paddle torque arm lengths

The 100 mm torque arm length only goes up to 1.12 Hz because the wave quality was poor above this point and overtopping of the paddle occurred.

An interesting characteristic was when the paddle was operating with an inverter frequency of 12 Hz or multiples of this (24 and 36 Hz). It was found that there was considerable turbulence behind the paddle with overtopping and poor wave quality. This corresponds to 0.48 Hz which, if Fig 11 and Table 1 are inspected shows that the back wall of the flume back tank is approximately one wavelength away from the paddle. Therefore a state of resonance occurs. Therefore a beach needs to be fitted to the back wall to reduce reflection of backwards-travelling waves. Initially this was not thought necessary.

Further experiments will include tilting the flume so that it either deepens or becomes progressively shallow and improvements in the beach to lengthen, make shallower and to cover in energy-absorbing material.

*D. Wave height variation*

There is much variation of the wave height with frequency. Fig 13 shows the variation of measured wave height over a period of time. This is for a torque arm length of 50 mm. It would be expected that the waves would possibly stay constant or decrease from probe 1 (the front probe) to probe 2 (reference probe). However this is only true for some of the results – further work has to be done to produce more uniform waves. This includes putting a beach at the back of the paddle back tank and improvements in the beach.

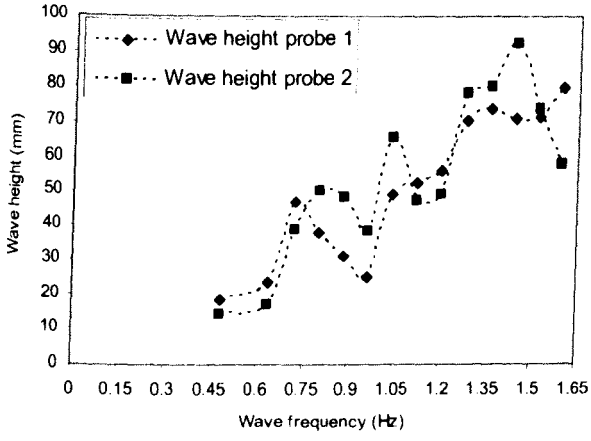


Fig 13 Variation of wave height with 50 mm torque arm length

If the wave heights are averaged and the power per metre of wave front calculated then the results are shown in Fig 14. Again the variation is large and also there are only a few watts per metre. At the lower frequencies the wave quality is quite good except at wave frequencies of 0.48 and 0.96 Hz. However above about 1.2 Hz the waves magnitudes begin to pulsate within an envelope – this is shown in the next section.

When the paddle torque arm length was set to 100 mm then the wave height and power per metre of wavelength are seen in Fig 15; again this shows some inconsistencies although the there was not the pulsating envelope – probably due to the fact the frequency was not increased to the same degree due to overtopping of the paddle. However the power stored in the waves is higher which is more suitable for use with wave energy generator models.

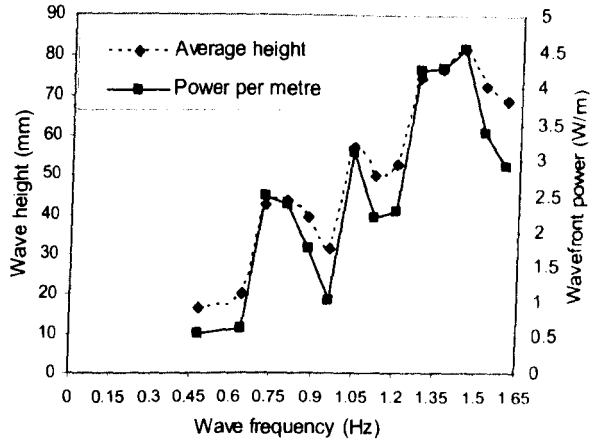


Fig 14 Power per metre of wave front at 50 mm torque arm

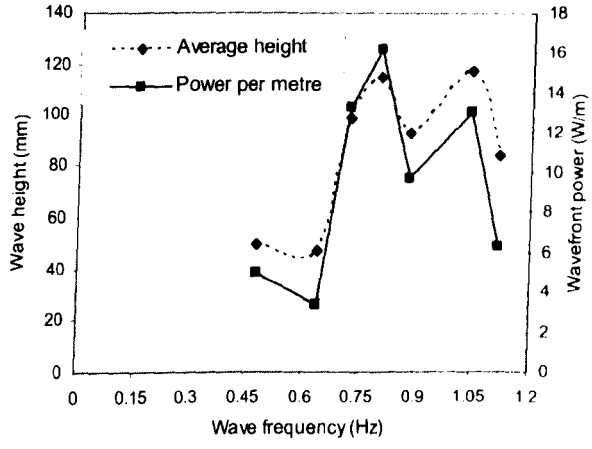


Fig 15 Power per metre of wave front at 100 mm torque arm

*E. Wave quality*

The quality of the waves varied considerably. The waves at resonant frequencies such as 0.48 and 0.96 Hz were particularly poor. This is illustrated in Fig 16 which compares the waves at 0.48 and 0.64 Hz for the first (leading) probe.

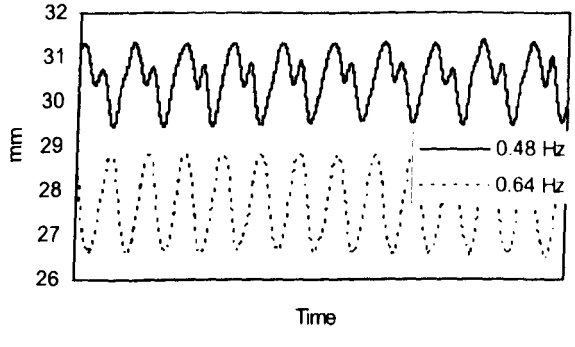


Fig 16 Comparison between 0.48 and 0.64 Hz waveforms

At higher frequency and 50 mm torque arm length then the waves begin to exhibit an envelope. This is illustrated in Fig 17. The waveforms, from top to bottom are for the front probe at frequencies of 1.04, 1.12, 1.28, 1.44 and 1.6 Hz showing the development of a pulsating envelope. The first two waveforms show a pretty constant magnitude but then a pulsation develops. Obviously this is the initial testing of the wave flume so that it is envisaged there will be further work required to smooth out some operational aspects of the system. For instance, the shape of the paddle and the inclination of it when paddling may make a difference. This could be adjusted using the connecting rod, positioning of the paddle hinges or movement of the torque wheel. Also the beach may be reflecting waves and the flume may need tilting and a back tank beach may make the water flow into the flume smoother.

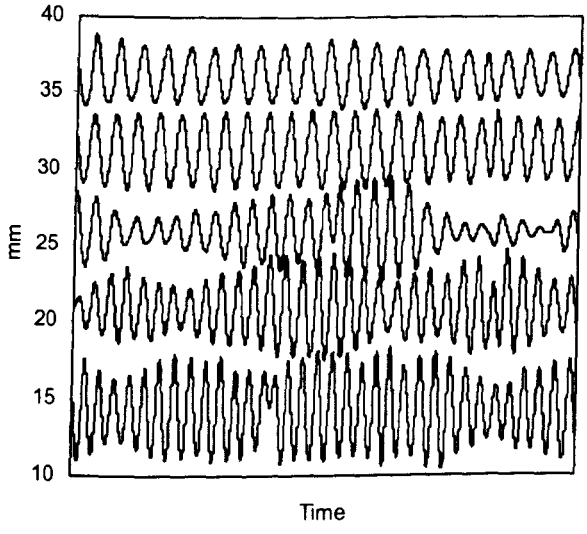


Fig 17 Development of wave envelope with increasing frequency. Wave frequency from top to bottom: 1.04, 1.12, 1.28, 1.44 and 1.6 Hz

## 5. Conclusions

This paper reports on some cost effective solutions to the development of simple systems aimed at investigating energy from sea waves. These can be used for studies ranging from undergraduate projects up to research projects. Further work is to use these systems to develop new models for different aspects of wave generators

## References


[1] *D. G. Dorrell, S. Kazi and M. Papadopoulos*, "Wave Generator Modelling using an Oscillating Water column and a Wells Turbine" Third IASTED International Conference on Power and Energy Systems 2003, Marbella, Spain, Sept 3-5 2003, pp 69-74.

[2] *D. G. Dorrell and M. Findlater*, "Computational Fluid Dynamic modelling of a Wells Turbine", IASTED EuroPES conference, Rhodes, Greece, 28-30 June 2004 (on CD).

[3] *J. R. Halliday and D. G. Dorrell*, "Review of Wave Energy Resource and Wave generator Developments in the UK and the Rest of the World", IASTED EuroPES conference, Rhodes, Greece, 28-30 June 2004 (on CD).

[4] *D. G Dorrell, J. R. Halliday, P. Miller and M. Findlater*, "Review of Wave Energy Resource and Oscillating water Column Modelling", Universities Power Engineering Conference, Bristol, 5-8 Sept 2004 (on CD).

# A Fourier approach to short term wave prediction

*J.R. Halliday*[1], *D.G. Dorrell*[1] *& A. Wood*[2]
[1]University of Glasgow, Dept. Electronics and Electrical Engineering
Glasgow, Scotland
[2]University of Canterbury, Dept of Electrical and Computer Engineering
Christchurch, New Zealand

## ABSTRACT.

This paper examines the appropriateness of the Fast Fourier Transform to the decomposition and representation of wave records taken at a fixed location. The prediction of wave behavior at any point on the sea surface should, theoretically, be realizable from this one record. The reality of this statement will be tested along with the use of harmonically generated wave records and the possible advantages of using non-harmonically generated records.

KEY WORDS: Fourier, wave prediction, dispersion relationship, non-harmonic modeling.

## INTRODUCTION

The goal of a short term deterministic prediction of wave behavior has been acknowledged for the past few years (EWEN, 2003; Salter, personal communication). To the offshore industries it would give information useful for the stabilization of ships and drilling platforms. For the wave energy industry a short term prediction would allow advanced control strategies for the maximum economical extraction of energy to be implemented. These control techniques (see Appendix B) are required in order to bring down the costs of electricity production and put offshore wave energy into the same costing bracket as other Renewables.

A few attempts have been made (Belmont et al, 1998; Zhang et al, 1999) to further this goal but they have left some doubts as to the range of their results. Belmont showed that a prediction on the order of 30 seconds ahead would be possible but, in producing his prediction results it appears that only 5 wave vectors were used to represent an omni-directional spectrum. Zhang went further in his prediction method by using real directional data and developing a directional hybrid wave model (DHWM) to produce an accurate prediction from a reference sensor to a point a few tens of meters distant. But, in his paper, he makes no mention as to whether this prediction was made in the time domain. Follow up work to this paper concerning prediction in time has not, to date, been found.

Additional papers and conversations with other researchers in this field have turned up examples of making the prediction over distance work. The Pealmis (Pizer et al, 2005) and Danish (Skourup and Sterndorf, 2002) experiments were conducted with a view to comparing linear and non-linear reconstruction and reported good prediction matches of 70m and 15m ahead using omni-directional wave spectra in both small, linear wave fields and larger non-linear fields. Experiments recently undertaken at Cork (Voronovich et al, 2005) also showed good prediction over distances to 12m with a spectrum of 5 to 6 frequencies, but at spectral densities greater than this the prediction began to wander.

In examining and recording time series data the Fast Fourier Transform (FFT) is used routinely and a prediction made using this technique would seem to offer the best and simplest avenue of attack; indeed all previous attempts appear to have been based, at some stage, on the FFT. This paper will show the difficulty of using such a method in both the time and spatial domains and will explore the relationship between discrete representation and the dispersal relationship of gravity waves. During the course of this we will hope to explain why previous efforts have begun to show breakdown in the prediction.

## WAVE DEVICES AND MEASUREMENT

In order for prediction techniques to be realizable a method of measurement must be in place in order to accurately record the surface elevation or other derivable property at a fixed location in the ocean. The most cost effective method is to utilize a directional wave rider buoy moored at a great enough distance from a wave energy device to avoid reflections. Other measurement techniques may be considered. For example, satellite or airborne measurement would provide a fixed measurement of the sea surface, but would be prohibitively expensive. A LIDAR device, such as that proposed by the University of Exeter (Belmont, personal communication), would also provide a fixed measurement but it would require to be mounted at a sufficient elevation above the maximum wave height in order to avoid wave shadowing effects. Wave devices which wish to survive North Atlantic sea conditions will on the whole tend to have a streamlined profile and be missing the elevated structure on which to mount this type of device.

The directional wave rider will not provide an absolutely fixed

reference point due to its motion with passing waves and reaction against its mooring. These errors in buoy measurement are given in (Tucker, 2000). The correction for these errors should theoretically be possible through signal processing to produce a best guess as to a record taken at a fixed point. The relatively new introduction of GPS based measurement buoys (Krogstad et al, 1999) would allow for accurate tracking of the point at which a record is being taken and assist in theoretical reconstruction of a fixed point record. For the moment it will be assumed that a record of surface elevation for a fixed point on the sea surface is realizable and available.

In the course of this study real wave records were unfortunately unavailable for use; however, the data collected during the WADIC experiment (Allender et al, 1989), where many records were taken in close proximity, would be ideal for this type of research. However, simulated records were created using a well known method as described by Tucker (2001) and Dean and Dalrymple (1991). The methodology for this is given in Appendix A. The method was modified to removed any harmonic trends in the resulting records.

## PREDICTION IN TIME

As one of the first steps in analyzing a time series of length $T$ seconds is to take its Fourier transform it would seem reasonable to explore this method as a means of making a prediction of wave behavior. The Fast Fourier Transform (FFT) resolves a time series $f(\Delta t \rightarrow T)$ into a summation of harmonically related sinusoids with unique amplitudes, $F_n$, and phases, $\phi_n$. This series of sinusoids could be used with the basic omni-directional linear wave equation for dispersive gravity waves. To recalculate the summation of sinusoids at an arbitrary time greater than $T$ seconds we can use

$$\zeta(x,t) = \sum_{n=1}^{N} F_n \cos(k_n x - \omega_n t - \phi_n) \qquad (1)$$

Where:

$F_n$ is the amplitude of the sinusoid

$k_n$ is the wave number

$\phi_n$ is the phase of the sinusoid

$\omega^2 = gk\tanh(kh)$; the dispersal relationship

## Experiment

The following experimental method was followed. A wave record of length 2400 sec was simulated for a 18.6 m/sec Pierson-Moskowitz spectra from 0-0.5 Hz using the non-harmonic method as described in Appendix A. An 18.6 m/sec wind speed (gale force 7-8) was chosen to allow for ease of identifying characteristics of the produced time series. This value of wind speed would be at the uppermost reaches of operation for winter sea conditions off of the west coast of Scotland. It is in this area where the devices will be working at their maximum, both in terms of their construction and the available market demand for their output. At wind speeds in excess of this the wave conditions will become too excessive and the devices will cease production and revert to a survival state (Yemm, 1999).

The model was run with a sampling frequency of 3.4133 Hz to produce 8192 samples. An FFT was applied to the first 4096 samples of this record and the real and imaginary components were retained. From this data, a wave vector file was generated using real and imaginary components to give amplitude and phase values for each wave vector. The frequency of these wave vectors were harmonically related to each other. This vector file was then used with Eq. 1 to produce a predicted wave record for the time period 1200 sec to 2400 sec. This was compared with the 2nd set of 4096 samples taken from the original record covering the same period.

## Results and discussion

Fig. 1 shows the results of this experiment. The upper graph shows the prediction compared to the original time series for the period $t = 1200 \rightarrow 1500$ sec. The time period and significant wave height would appear to be in good agreement but the phasing does not match. The lower graph shows the first 300 sec of the original record and the first 300 sec of the predicted series. They match almost perfectly. The explanation for this lies with the FFT itself.

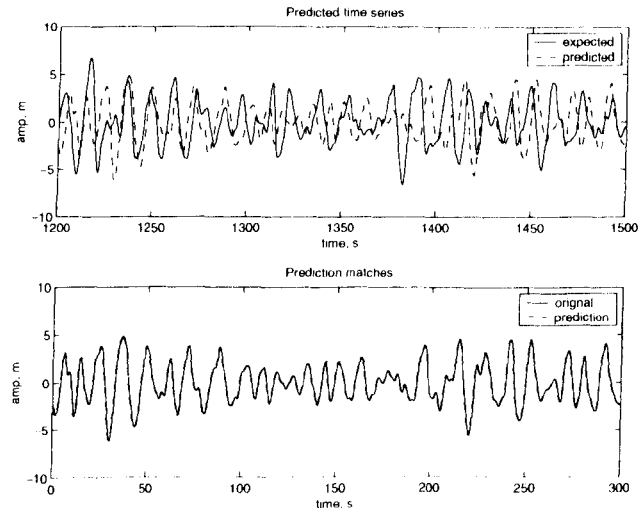


Fig. 1. Predicted time series using Fourier theorem

The FFT is designed to work with periodic time series for example $f(-T \rightarrow 0) = f(0 \rightarrow T) = f(T \rightarrow 2T)$ if the section from $t = 0 \rightarrow T$ is examined the wave vectors returned will exactly represent this series. Recalculating at any other time period will simply be a reproduction of a section of this original time series. As real gravity waves are known not to display periodicity then the Fourier method does not appear appropriate for the time prediction case.

Other institutes are working on alternate methods for prediction in time. For example, Heriot Watt University, Edinburgh, Scotland, is examining the zero-crossing period and amplitude of each wave (looking for a predictable pattern) while The University of Edinburgh, Scotland, is studying neural network prediction methods to determine if these techniques can be used to obtain a solution (personal communication, Price).

## PREDICTION IN SPACE

Following-on from results obtained by other researchers, using omni-directional spectra (which found good agreement up to 70m), it was proposed to see how far ahead in distance the prediction method would hold.

## Experiment

A reference sensor was positioned at 0 m. Wave records of length 1200 sec were generated for this sensor and at nine other positions at distances 50m, 100 m, 200 m, 300 m, 500 m, 1 km, 2 km and 5 km. Again, an 18.6m/sec Pierson-Moskowitz spectra, range 0-0.5 Hz, 256 vectors, was used as the input. The same process of taking the FFT of the record for each position was implemented to generate a sinusoidal series. In this instance a different equation for making the prediction was used as difficulties were found in obtaining the correct phase angles from the FFT routine available in the software used. This new equation is:

$$\zeta(x,t) = \sum_{n=1}^{N/2} a_n \cos(k_n x - \omega_n t) + b_n \sin(k_n x - \omega_n t) \qquad (2)$$

where

$$a_n = 2\,\mathrm{Re}\{\bar{F}_n(1:N/2)\} \qquad (3)$$

and

$$b_n = -2\,\mathrm{Im}\{\bar{F}_n(1:N/2)\} \qquad (4)$$

$\bar{F}_n$ is the raw imaginary-number set returned by the FFT routine. Eq.2 was then used to make the prediction at each sensor. The prediction used $t = 0 \rightarrow T$ so that the issue of temporal periodicity does not arise, but $x$ was selected to be at increasing intervals as used for the target records.

## Results

Figs. 2, 3, 4 and 5 show the results for the first four values of x of this experiment. At distances close to the reference sensor the prediction is reasonably accurate, especially in the 50 m and 100 m cases. At 200 m from the sensor the prediction is showing signs of weakness and at 300m distant the prediction becomes critically incorrect indicating troughs where there are peaks and vice versa. This sort of error could be detrimental to a wave energy device expecting a peak in the wave but hitting a trough. The range of prediction results that were achieved by Pizer et al (2005), Skourup and Sterndorf (2002), and Voronovich et al (2005), appear to be valid. In the light of the results shown in Fig. 4, prediction-over-distance, using omni-directional waves, appears to be valid up to at least 200 m.

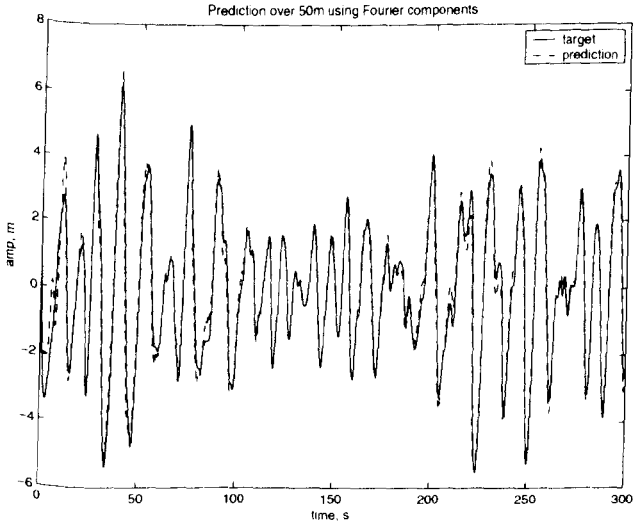


Fig. 2. Prediction made to 50 m

## Discussion

The results from the previous experiment showed promise within a 200m range but beyond this the prediction deteriorated. The explanation for this degradation with distance from source of the results lies in: a) the dispersion relationship; b) the manner in which energy is transported in a gravity wave; and c) how we choose to represent this in discrete time and space.

The most straightforward way to examine the manner in which wave energy is represented is to look at the spectra from which the wave vector files were derived. This is in turn related to the manner in which wave vectors are derived from the FFT of the reference time series. The common method of representing a mixed wave field is to create a plot of the energy density spectra. To the best of our ability this is the most concise manner in which to represent the data we have available.

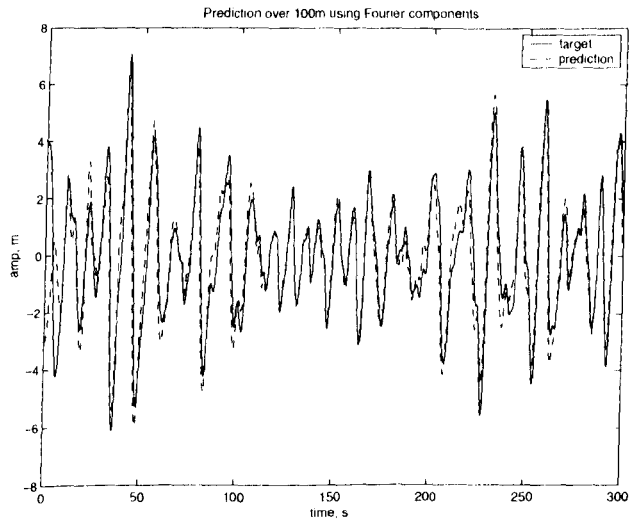


Fig. 3. Prediction made to 100 m

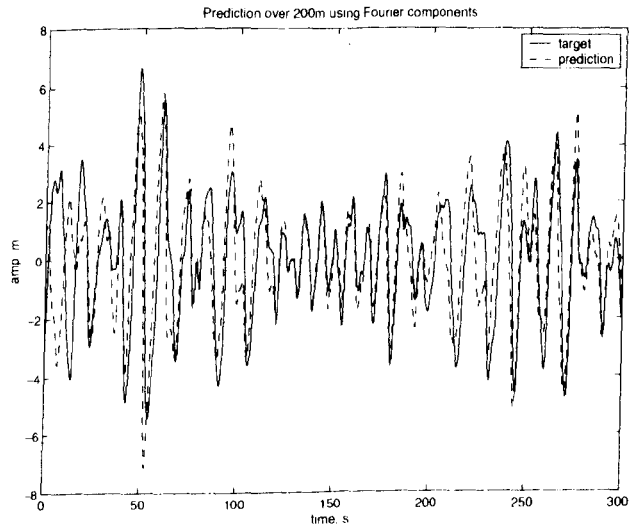


Fig. 4. Prediction made to 200 m

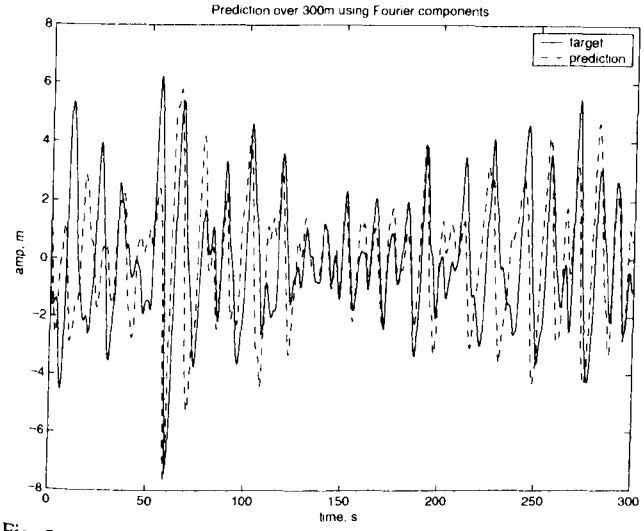


Fig. 5. Prediction made to 300 m

With the creation of wave vector files and with the IFFT we are effectively carving the continuous spectra into strips of energy of width $\Delta f$ . These strips are then represented as a discretely located sinusoid with its amplitude proportional to the energy bounded by $S(f)$ and $\Delta f$ given by Eq. A1. Fig. 6 shows this process with a 16 m/sec Pierson-Moskowitz spectra and the energy represented by a sinusoid placed at 0.125 Hz. With $\Delta f = 0.005$ Hz this delta function represents the continuous energy of the range 0.1225 Hz to 0.1275 Hz.

Using Eq. 1 an idealized wave vector can be easily propagated, but only if all the energy in the band taken from the original spectra can be exactly represented as single wave vector. In the case of real gravity waves and, to a certain extent, in wave tanks this will never be the case. The energy is spread continuously over the spectra. Looking at the modeling assumption made in the prior paragraph, the delta function at 0.125 Hz is taken to represent the range from 0.1225 Hz to 0.1275 Hz. Restating this in terms of wavelength; a 99.8 m wave is to represent the range from 95.9 m to 103.9 m. The difference here is 8 m, which in terms of cumulative wave vector behavior can change a trough to a peak.

The dispersion relationship also plays a role here as a wave of longer wavelength will travel faster than a wave of a shorter wavelength. Considering the range of $\Delta f$ the energy at the lower end of the range will tend to overtake the energy at the higher end.

A further experiment was conducted to show how energy can be represented in many different ways, with vastly varying effects on the surface displacement but still retaining the original energy. To model the situation the band of energy $\Delta f$ can be subdivided and modeled by an infinite number of idealized wave vectors; so long as the sum of the energy of these wave vectors equals the energy in the band $\Delta f$ . To show this imagine we split the band, $\Delta f$ , into two new bands and model each of the new energy bands by idealized wave vectors located at 0.12375 Hz and 0.12625 Hz, the amplitudes of which being proportional to the newly subdivided energy bands. Squaring and summing these amplitudes gives the same energy as was present in the original band $\Delta f$ . The process can be continued *ad. infinitum*, Table 1 shows the first 4 levels of subdivision, the energy in each sub-band and the summation of these energies are equal to the original.

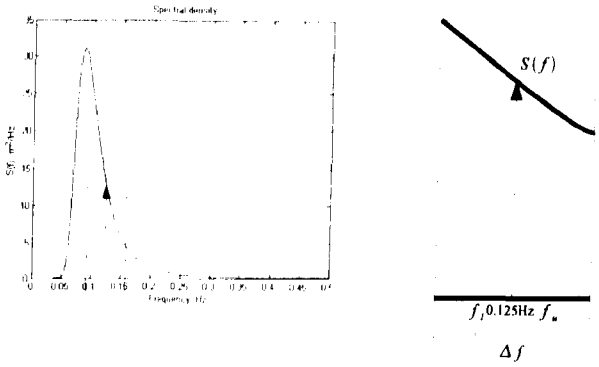


Fig. 6. Discrete representation of continuous energy spectrum

Simulating each of these representations for 1200 sec and the taking the FFT of each result gives the same general spectral shape and magnitude but, if the time series are compared the differences between each become apparent.

Fig. 7 shows the same energy band centered on 0.125 Hz represented as 1, 2, 4 and 8 discrete wave vectors. In the second graph the classic phenomenon of beating between two closely spaced frequencies is seen. The usual method of explaining the lower two time series is to proceed with a description of group velocity. Most definitions of group velocity are taken using two frequencies and idealized graphical methodologies and they arrive at the guideline that the group velocity of wave energy is roughly half that of the individual waves phase velocity.

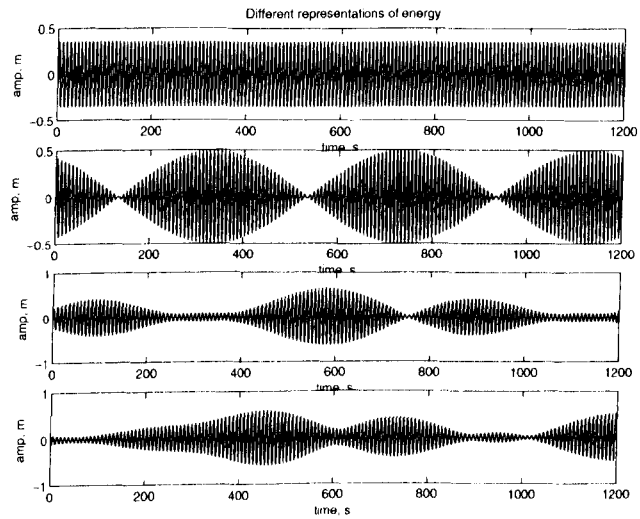


Fig. 7. Equivalent energy time series for 1, 2, 4 and 8 discrete wave vectors (top to bottom)

Repeatedly breaking down the representation of the energy into finer graduations will likely have little effect on producing an accurate representation of the continuous spectra. The first reason is that no matter how small you take the band over which a single vector is representing, it can be made into infinitely more smaller ones and the

time representation you have at one gradation will not generally correspond to those at finer ones. Fig. 7 showed this to a level of 4 orders smaller. It is presumed that if you take line 10 of Table I (a wave vector of frequency 0.124062 Hz) and break this down into finer representations of the same energy they will not reconstruct to give the same time series as the original.

Table 1. Different representations of an energy band

| $\Delta f$ | F | wavelength | Amplitude | Energy = $\sum$(amplitude) |
|---|---|---|---|---|
| 0.005 | 0.125 | 99.9238 | 0.3528 | 0.1246 |
| 0.0025 | 0.12375 | 101.9526 | 0.1118 | |
| | 0.12625 | 97.9549 | 0.0821 | 0.1246 |
| 0.00125 | 0.123125 | 102.9903 | 0.0629 | |
| | 0.124375 | 100.9306 | 0.0497 | |
| | 0.125625 | 98.9320 | 0.0402 | |
| | 0.126875 | 96.9922 | 0.0333 | 0.1246 |
| 0.000625 | 0.122812 | 103.5151 | 0.0629 | |
| | 0.123437 | 102.4695 | 0.0497 | |
| | 0.124062 | 101.4397 | 0.0402 | |
| | 0.124687 | 100.4253 | 0.0333 | |
| | 0.125312 | 99.4260 | 0.0629 | |
| | 0.125937 | 98.4416 | 0.0497 | |
| | 0.126562 | 97.4718 | 0.0402 | |
| | 0.127187 | 96.5162 | 0.0333 | 0.1246 |

A further problem occurs in that the energy banding imposed on the spectra is for purely mathematical purposes and the wave vectors in the band centered on 0.125 Hz will certainly interact with the frequencies above and below this. The classical explanation of group velocity with two frequencies is too simple to apply to the continuous case.

It may be argued that in taking an FFT of 4096 points then surely this would describe the continuous spectra in fine enough detail with a great enough number of wave vectors to be able to carry the prediction over a distance. The problem here is that the same time series can be represented by a 128, 512, or indeed a 65536 point FFT and the reconstruction of each will not yield the same time series if displaced by a distance $x$ m from the reference sensor.

## CONCLUSION

This paper has explored the use of the FFT in making predictions of surface elevation. A general misconception of many proposing wave energy projects is that the prediction of surface elevation is a simple problem. Just by visual observation of sea waves, it is very difficult to track a sea wave since the wave will grow then disappear as different frequencies of the continuous spectra come into phase with each then drift apart.

The inherent discrete properties of the FFT are not adequate to deal with the dispersal nature of gravity waves. In terms of prediction in time the periodic nature of the FFT does not fit comfortably with the continuous a-periodic signal it is being fed with. Extending the wave vectors, derived from the Fourier components, results in a repetition of the series from which the components came. For signal processing, communications technology and the extraction of periodic signals the FFT cannot be faulted but it has been found to be inappropriate for use with a-periodic signals.

The prediction of time series is overall a complex problem and has attracted much investigation but it is still, to some extent, a black art. At present, time series prediction based on neural network processing and genetic algorithms are being developed (personal communication, Price) and it will be interesting to note their effectiveness. Scope exists for the examination of other transforms and data processing methods: namely the Kalman filter currently in use in Trondheim, Norway (personal communication, Torkel Bjarte Larsson) or through the use of the Hilber Huang transforms which have recently been suggested as an alternative to the FFT (Hwang et al, 2003).

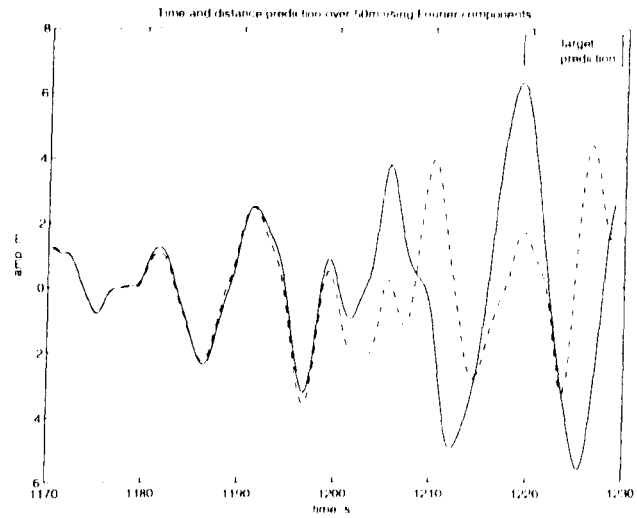


Fig. 8. Prediction for 50 m ahead and 30 s into the future

As a point of interest, the two Fourier methods for predicting wave records over of distance and time were combined for the case of predicting 50 m ahead and 30 sec into the future. As shown in Fig. 8, the results obtained were as expected, with the penultimate 30 sec section of the source record found to be a good match, but when extended past this the prediction fails.

Predicting over distance, while working well over short distances, has been shown to be complicated by the differing speeds at which the waves travel. Since the spectrum is continuous there is continual reinforcement of amplitude at some points and near cancellation at others. The simulations reported in the papers mentioned in the introduction, and the experiments presented, succeeded in generating predictions over distance; the possibility of these models producing poor results with real sea states is quite possible as they were only tested with restricted wave tank or simulated data. Further work is needed to test these modeling techniques when subjected to real wave measurements.

Further work, using a new formulation which is a development from that presented here, suggests that predictions based upon an omni directional approximation of a full directional sea state could be accurate up to 150m. This work, at the time of submission, is in the very early stages and full testing has yet to be carried out. It will be reported in due course.

In real sea conditions a swell sea and local sea are likely to exist; as long as the local sea is not being powered by a strong wind the spectra should contain a double peak. Analytical methods should exist to separate the two sea states. It is also likely that the swell and local seas will be traveling in independent directions. In separating the spectra into two

parts, an omni-directional approximation of both should be possible. In local seas with a high wind speed, the swell will become absorbed into the omni-spectra and local conditions will dominate, thereby leaving only one spectral peak to fit. Additional work looking at Zhang's DHWM may turn up other information, as would closer examination of the WAM (Komen et al, 1994) and SWAN (Booij et al, 1999) models. At present the WAM and SWAN models operate on much larger time and dimensional scales than are appropriate for the short-term problem, but the physics and computational routines on which they are based may prove useful.

AKNOWLEDGEMENTS

Mr. Halliday would like to thank the University of Canterbury, Christchurch, for the use of their facilities during his stay in New Zealand. He would also like to thank the EPSRC, UK for their financial support during his studies.

REFERENCES

Allender, J., Audunson, T., Barstow, S.F., Bjerken S., Krogstadm H.E., Steinbakke, P., Vartdal, L., Borgman, L.E. and Graham, C. (1989), "The WADIC project: a comprehensive field evaluation of directional wave instrumentation", *Journal of Ocean Engineering*, Vol. 16, No. 5/6, pp. 505-536.

Belmont, MR, Morris, EL and Zienkiewicz, HK (1998), "Short term forecasting of the sea surface shape," *Journal of International Shipbuilding Progress*, Vol. 45, No. 444, pp 383-400.

Booij, N., Ris, C. and Holthuijsen, L.H. (1999), "A third-generation wave model for coastal regions", *Journal of Geophysical Research*, Vol. 104, No. C4, pp. 7649-7666.

Dean, RG and Dalrymple, RA (1991), "Water wave mechanics for scientists and engineers", *World Scientific*, ISBN 9-81020-421-3.

EWEN (2003), "Results from the work of the European Thematic Network on Wave Energy," *European Community*, Report No. ERK5-CT-199-200001.

Falnes (2002), "Ocean Waves and Oscillating Systems", *Cambridge University Press*, ISBN 0-521-01749-1.

Hwang, P.A, Huang, N.E. and Wang, D.W. (2003), "A note on analyzing nonlinear and nonstationary ocean wave data", *Applied Ocean Research*, No. 25, pp. 187-193.

Komen, G.J., Calvaleri, L., Donelan, M., Hasselmann, K., Hasselmann, S. and Janssen, P.A.E.M. (1994), "Dynamics and Modelling of Ocean Waves", *Cambridge University Press*, ISBN 0-521-57781-0.

Krogstad, H.E., Barstow S.F., Aasen S.E. and Rodriguez, I. (1999), "Some recent developments inwave buoy measurement technology", *Coastal Engineering*, No. 37, pp. 309-329.

Pizer, D.J., Retzler, C, Henderson, R.M., Cowieson, F.L., Shaw, M.G., Dickens, B. and Hart, R. (2005), "Pelamis WEC- recent advances in the numerical and experimental modeling programme", *6th European Wave and Tidal Energy Conference*, 30th Aug-2nd Sep 2005, Glasgow, Scotland.

Skourup, J and Sterndorff M.J. (2002), "Deterministic reproduction of nonlinear waves", *Proceedings of OMAE'02*, 23-28 June 2002, Oslo, Norway.

Tucker, MJ and Pitt, EG (2001), "Waves in Ocean Engineering", *Elsevier*, ISBN 0-08-043566-1.

Voronovich V., Holmes B, and Thomas, G. (2005), "A preliminary numerical and experimental study of wave prediction.", *6th European Wave and Tidal Energy Conference*, 30th Aug-2nd Sep 2005, Glasgow, Scotland.

Yemm, RW (2000), "The history and status of the Pelamis wave energy converter", *Wave Power: Moving Towards Commercial Viability*, IMechE, ISBN 1-86058-305-9.

Zhang, J, Yang, J, Wen, J, Preslin,I and Hong, K (1999), "Deterministic wave model for short-crested ocean waves: Part I. Theory and numerical scheme," *Applied Ocean Research*, No. 21 pp. 167-188.

APPENDIXES

## A. Non-harmonic modeling approach

In lieu of available wave data taken from real sources, all records utilized were simulated. The method of simulating wave records, as suggested by both Tucker (2001) and Dean & Dalrymple (1991), was found to have undesired results, namely the presence of periodicity.

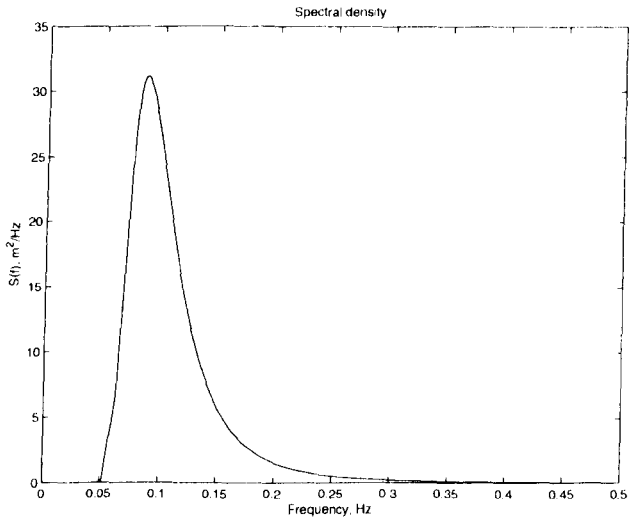


Fig. 9. An energy density spectrum for 16 m/sec wind speed

This method is based on the Inverse Fast Fourier Transform (IFFT). A wave spectra $S(f)$ (Fig. 9), is created for the desired situation: wind speed; mean direction; fetch, etc. The limits of the IFFT are then decided upon. First of all the spectral resolution $\Delta f$ is fixed. This will determine the lowest possible frequency to be simulated. It will also limit the possible duration of the record in time once it has been transformed to be the time period of one oscillation of a sinusoid with frequency $\Delta f$. For example a $\Delta f$ of 0.01 Hz limits the transformed record to 100 sec. The second variable to be selected is the number of elements in the IFFT $N$. This determines the highest frequency of the record. As the wave spectra is real then the highest simulated frequency will be $\Delta f(N/2)$.

The energy density spectrum $S(f)$ is then calculated for these $N/2$ values from the lowest to the highest frequency. The amplitude of each wave vector is then determined by using

$$a(n\Delta f) = \sqrt{S(n\Delta f)2\Delta f} \qquad (A.1)$$

This is plotted in Fig. 10. For the IFFT the phase information for each vector is also required. If this is set to zero then as each vector is harmonically related to each other and they will all be in phase at the beginning of the record. This results in every vector summing positively and creating a time series that has a very large spike of energy for the first few oscillations before dying away as the vectors move out of phase. To counteract this and induce some variability into the record the phase is chosen to be a random number between 0 and $2\pi$. This eliminates the energy spike.

The amplitude and phase values for each real wave vector are then used to create the real and imaginary data required by the IFFT. The IFFT is then performed resulting in the time series.

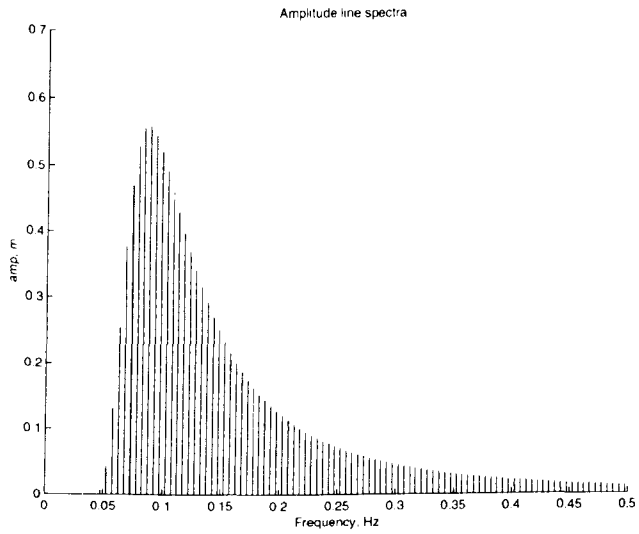


Fig. 10. Amplitude spectrum for 16 m/sec wind speed

For this study, it was the ability to visualize the wave field as it moved over an area of ocean, and the need to extract wave records of arbitrary length at various points, which were desired. The ability to simulate directional wave spectra was also desired. To this end the IFFT method was not practicable as it produced a fixed length record for a fixed point. The method of breaking the wave spectra down into harmonically related wave vectors was retained but was also simulated using

$$\zeta(x,y,t) = \sum_{n=1}^{N=100} a_n \cos(k_n \sin\theta_n x + k_n \cos\theta_n y - \omega_n t - \phi_n) \qquad \text{(A.2)}$$

Where

$\zeta$ is surface elevation

$n$ is the wave vector index

$a$ is the wave vector amplitude

$k$ is the wave number

$\omega$ is the frequency related to $k$ by $\omega^2 = gk\tanh(kh)$

$\phi$ is the phase shift

Once the spectra had been broken down into a series of wave vectors these details were stored in a file. A separate MATLAB routine read in this file and one which contained the x-y position of the desired records. The length of a record and sampling frequency were passed to the routine and Eq. A.2 was iteratively calculated at each time step for all of the input vectors. While this process lacked the speed of the IFFT it makes up for this in terms of the flexible of input wave vectors, the unlimited length of wave record produced and if applied to a grid of x-y co-ordinates, the ability to visualize the simulated sea state.

The IFFT and the iterative method have both shown drawbacks due to being based on harmonically derived wave vectors. The output of both methods will tend to show periodicity as displayed in Fig. 11; the series around 100 sec and 500 sec appear to be similar. This periodicity results from the wave vectors being all derived from multiples of $\Delta f$ .

The correction to this lies in realizing that the amplitude of each wave vector represents the energy in the area bounded by $n\Delta f$ and $S(n\Delta f)$. If the selection of the wave vectors to be simulated were based on a random distribution of frequencies from zero to the upper frequency limit instead of harmonic multiples of fundamental frequency spacing $\Delta f$ then the periodic tendency of records should be eliminated.

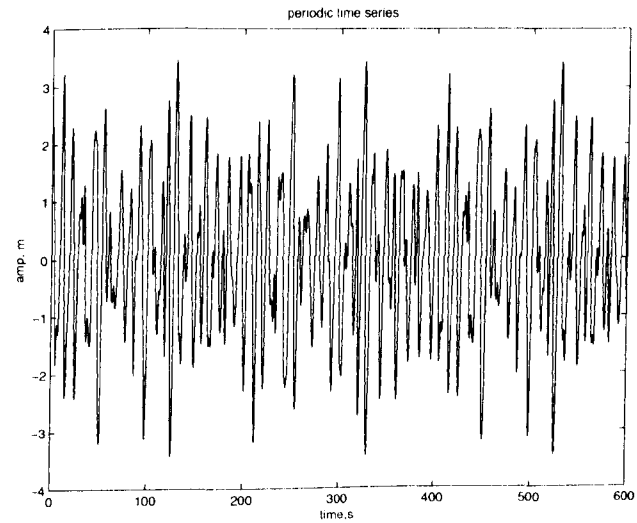


Fig. 11. Time series from harmonically related wave vectors

As before, an upper frequency limit $f_{upper}$ and the desired number of wave vectors $N$ are selected. $N$ randomly distributed numbers between 0 and $f_{upper}$ are generated; $f_{upper}$ is added to this series to ensure the upper limit is reached. The series is then sorted into ascending numerical order and the difference between each frequency is calculated to give a second series of $N$ frequency spacings $\Delta f(n)$. The centre of each frequency-spacing can then be found and this will be the frequency of the simulated wave vector $f(n)$.

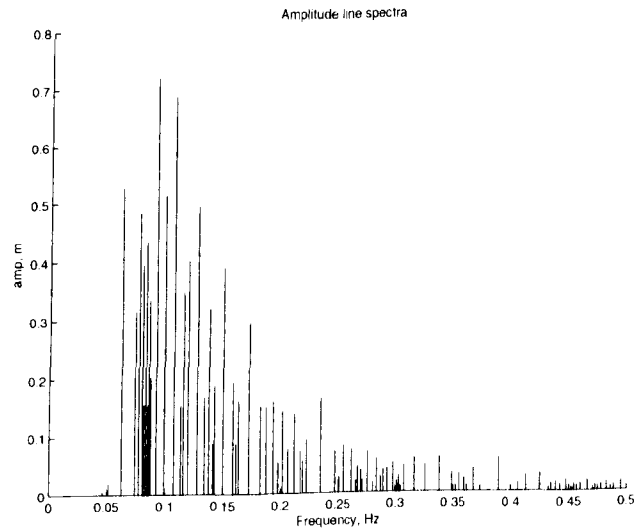


Fig. 12. Non-harmonic amplitude spectra for 16m/s wind speed

The energy spectral density function $S(f(n))$ is calculated at each desired frequency and Eq. A.1 is used to determine the amplitude of each vector using $\Delta f(n)$ in place of $\Delta f$. The resulting amplitude spectrum is shown in Fig. 12. If can be observed that some frequencies are more densely spaced than others. In these densely packed areas the individual amplitudes of each wave vector has been reduced to preserve the energy that it represents. Correspondingly, sparsely spaced vectors have greater amplitude. These amplitudes are then use to construct a wave vector file, the need to have random phase shifts is now not required as the harmonic reinforcement at the beginning of the record should not be present.

Figs. 10 and 12 both represent the same energy spectral density function but in two different ways. The harmonic approach has the advantage of quick execution through the IFFT but has the drawback of being inherently periodic. The non-harmonic approach with the iterative implementation does not limit the length of records or show signs of periodicity which more accurately reflects a real wave record.

## B. Wave device control methods

**Latching** is a method commonly utilized with devices employing a float that moves relative to a fixed element (Falnes, 2002). An example of this is the AWS, where a float is held within a sub-surface cage, and rises and falls with the passing waves. If the float is held at the bottom of its travel until the wave above is at maximum steepness then the float will experience a greater acceleration into the crest than if it is allowed to freely follow the wave. Similarly the float can be held at its maximum position to obtain maximum acceleration into the trough. A prediction of wave behavior at the device would allow for the forward planning of this latching behavior. Measurements must be remote from the device since in the near vicinity, the mass of the float distorts measurements (Prado, 2005).

**Complex Conjugate** control is utilized in the Pelamis device to allow the onboard hydraulic system that controls the reactance of the joints between each section to match the incoming wave. The device consists of several hinged tubular sections joined by hydraulic rams. The device has an effective resistance and reactance supplied by the mass, spring, damper system of these joints. With a prediction of incoming wave behavior the hydraulics can actively change the reactance of the device to allow for maximum power capture in low amplitude seas. A similar hydraulic approach could be made in the design of Bristol Cylinder devices.

**Valves** can be used by oscillating water column devices to artificially hold the water level inside the caisson at a high level to be released when maximum acceleration of the column is possible (EWEN, 2003). This method is similar to latching and, due to the positioning of the devices on the shore line, a LIDAR mounted on the caisson may be used in this case to provide the prediction data.